DEVELOPMENT OF TEST EQUIPMENT AND PROCEDURES FOR DETERMINATION OF THE GAS-BREAKTHROUGH PRESSURE OF COMPACTED CLAY MATERIALS WITH PRELIMINARY RESULTS

by

TIM KIRKHAM

A Thesis

Submitted to the Faculty of Graduate Studies

in Partial Fulfillment of the Requirements for the Degree of

MASTER OF SCIENCE

Department of Civil and Geological Engineering

University of Manitoba

Winnipeg, Manitoba

August, 1995

National Library
of Canada

Acquisitions and
Bibliographic Services Branch

395 Wellington Street
Ottawa, Ontario
K1A 0N4

Bibliothèque nationale
du Canada

Direction des acquisitions et
des services bibliographiques

395, rue Wellington
Ottawa (Ontario)
K1A 0N4

Your file *Votre référence*

Our file *Notre référence*

ISBN 0-612-13253-6

Canada

Name _____

Dissertation Abstracts International is arranged by broad, general subject categories. Please select the one subject which most nearly describes the content of your dissertation. Enter the corresponding four-digit code in the spaces provided.

Geotechnology
SUBJECT TERM

0428
SUBJECT CODE

U·M·I

Subject Categories

THE HUMANITIES AND SOCIAL SCIENCES

COMMUNICATIONS AND THE ARTS
Architecture 0729
Art History 0377
Cinema 0900
Dance 0378
Fine Arts 0357
Information Science 0723
Journalism 0391
Library Science 0399
Mass Communications 0708
Music 0413
Speech Communication 0459
Theater 0465

EDUCATION
General 0515
Administration 0514
Adult and Continuing 0516
Agricultural 0517
Art 0273
Bilingual and Multicultural 0282
Business 0688
Community College 0275
Curriculum and Instruction 0727
Early Childhood 0518
Elementary 0524
Finance 0277
Guidance and Counseling 0519
Health 0680
Higher 0745
History of 0520
Home Economics 0278
Industrial 0521
Language and Literature 0279
Mathematics 0280
Music 0522
Philosophy of 0998
Physical 0523
Psychology 0525
Reading 0535
Religious 0527
Sciences 0714
Secondary 0533
Social Sciences 0534
Sociology of 0340
Special 0529
Teacher Training 0530
Technology 0710
Tests and Measurements 0288
Vocational 0747

LANGUAGE, LITERATURE AND LINGUISTICS
Language
- General 0679
- Ancient 0289
- Linguistics 0290
- Modern 0291

Literature
- General 0401
- Classical 0294
- Comparative 0295
- Medieval 0297
- Modern 0298
- African 0316
- American 0591
- Asian 0305
- Canadian (English) 0352
- Canadian (French) 0355
- English 0593
- Germanic 0311
- Latin American 0312
- Middle Eastern 0315
- Romance 0313
- Slavic and East European 0314

PHILOSOPHY, RELIGION AND THEOLOGY
Philosophy 0422
Religion
- General 0318
- Biblical Studies 0321
- Clergy 0319
- History of 0320
- Philosophy of 0322

Theology 0469

SOCIAL SCIENCES
American Studies 0323
Anthropology
- Archaeology 0324
- Cultural 0326
- Physical 0327

Business Administration
- General 0310
- Accounting 0272
- Banking 0770
- Management 0454
- Marketing 0338

Canadian Studies 0385
Economics
- General 0501
- Agricultural 0503
- Commerce-Business 0505
- Finance 0508
- History 0509
- Labor 0510
- Theory 0511

Folklore 0358
Geography 0366
Gerontology 0351
History
- General 0578
- Ancient 0579
- Medieval 0581
- Modern 0582
- Black 0328
- African 0331
- Asia, Australia and Oceania 0332
- Canadian 0334
- European 0335
- Latin American 0336
- Middle Eastern 0333
- United States 0337

History of Science 0585
Law 0398
Political Science
- General 0615
- International Law and Relations 0616
- Public Administration 0617

Recreation 0814
Social Work 0452
Sociology
- General 0626
- Criminology and Penology 0627
- Demography 0938
- Ethnic and Racial Studies 0631
- Individual and Family Studies 0628
- Industrial and Labor Relations 0629
- Public and Social Welfare 0630
- Social Structure and Development 0700
- Theory and Methods 0344

Transportation 0709
Urban and Regional Planning 0999
Women's Studies 0453

THE SCIENCES AND ENGINEERING

BIOLOGICAL SCIENCES
Agriculture
- General 0473
- Agronomy 0285
- Animal Culture and Nutrition 0475
- Animal Pathology 0476
- Food Science and Technology 0359
- Forestry and Wildlife 0478
- Plant Culture 0479
- Plant Pathology 0480
- Plant Physiology 0817
- Range Management 0777
- Wood Technology 0746

Biology
- General 0306
- Anatomy 0287
- Biostatistics 0308
- Botany 0309
- Cell 0379
- Ecology 0329
- Entomology 0353
- Genetics 0369
- Limnology 0793
- Microbiology 0410
- Molecular 0307
- Neuroscience 0317
- Oceanography 0416
- Physiology 0433
- Radiation 0821
- Veterinary Science 0778
- Zoology 0472

Biophysics
- General 0786
- Medical 0760

EARTH SCIENCES
Biogeochemistry 0425
Geochemistry 0996
Geodesy 0370
Geology 0372
Geophysics 0373
Hydrology 0388
Mineralogy 0411
Paleobotany 0345
Paleoecology 0426
Paleontology 0418
Paleozoology 0985
Palynology 0427
Physical Geography 0368
Physical Oceanography 0415

HEALTH AND ENVIRONMENTAL SCIENCES
Environmental Sciences 0768
Health Sciences
- General 0566
- Audiology 0300
- Chemotherapy 0992
- Dentistry 0567
- Education 0350
- Hospital Management 0769
- Human Development 0758
- Immunology 0982
- Medicine and Surgery 0564
- Mental Health 0347
- Nursing 0569
- Nutrition 0570
- Obstetrics and Gynecology 0380
- Occupational Health and Therapy 0354
- Ophthalmology 0381
- Pathology 0571
- Pharmacology 0419
- Pharmacy 0572
- Physical Therapy 0382
- Public Health 0573
- Radiology 0574
- Recreation 0575
- Speech Pathology 0460
- Toxicology 0383

Home Economics 0386

PHYSICAL SCIENCES
Pure Sciences
Chemistry
- General 0485
- Agricultural 0749
- Analytical 0486
- Biochemistry 0487
- Inorganic 0488
- Nuclear 0738
- Organic 0490
- Pharmaceutical 0491
- Physical 0494
- Polymer 0495
- Radiation 0754

Mathematics 0405
Physics
- General 0605
- Acoustics 0986
- Astronomy and Astrophysics 0606
- Atmospheric Science 0608
- Atomic 0748
- Electronics and Electricity 0607
- Elementary Particles and High Energy 0798
- Fluid and Plasma 0759
- Molecular 0609
- Nuclear 0610
- Optics 0752
- Radiation 0756
- Solid State 0611

Statistics 0463

Applied Sciences
Applied Mechanics 0346
Computer Science 0984
Engineering
- General 0537
- Aerospace 0538
- Agricultural 0539
- Automotive 0540
- Biomedical 0541
- Chemical 0542
- Civil 0543
- Electronics and Electrical 0544
- Heat and Thermodynamics 0348
- Hydraulic 0545
- Industrial 0546
- Marine 0547
- Materials Science 0794
- Mechanical 0548
- Metallurgy 0743
- Mining 0551
- Nuclear 0552
- Packaging 0549
- Petroleum 0765
- Sanitary and Municipal 0554
- System Science 0790

Geotechnology 0428
Operations Research 0796
Plastics Technology 0795
Textile Technology 0994

PSYCHOLOGY
General 0621
Behavioral 0384
Clinical 0622
Developmental 0620
Experimental 0623
Industrial 0624
Personality 0625
Physiological 0989
Psychobiology 0349
Psychometrics 0632
Social 0451

DEVELOPMENT OF TEST EQUIPMENT AND PROCEDURES FOR DETERMINATION OF THE GAS-BREAKTHROUGH PRESSURE OF COMPACTED CLAY MATERIALS WITH PRELIMINARY RESULTS

BY

TIM KIRKHAM

A Thesis submitted to the Faculty of Graduate Studies of the University of Manitoba in partial fulfillment of the requirements of the degree of

MASTER OF SCIENCE

ABSTRACT

Clays and clay-sand mixtures have been used to isolate contaminants from the biota in schemes such as that proposed by AECL for the disposal of heat-generating nuclear fuel wastes. This study focusses on the effects that gas generation and release in a repository may have on its engineered clay barriers. The results are not specific to a repository for nuclear waste and may apply wherever engineered clay barrier properties may be affected by gas migration.

Equipment and test procedures were developed to determine the resistance specimens would have against penetration of gas due to an increasing gas pressure gradient. Forty-six tests on illitic clay compacted at moisture contents (w) from 10-17% to dry densities (ρ_d) from 1.85-2.10 Mg/m^3 showed gas-breakthrough resistance ranging from 0.2-6.4 MPa. Six specimens of bentonite and sand mixed in equal portions by dry mass (buffer) were compacted to 1.67 Mg/m^3 ρ_d with w from 11-21% and were tested for their gas-breakthrough resistance. Only one showed signs of gas-breakthrough (at 9.4 MPa) before the limiting pressure of the equipment of 10 MPa was reached. The equipment developed did not have adequate capacity to detect gas-breakthrough in buffer.

For the illitic clay, gas-breakthrough generally decreased with decreasing w, ρ_d and degree of saturation (S). Gas-breakthrough decreased with decreasing S and decreased step-wise and markedly with S<80%. At S>80% it is likely that the gas phase within soil pore-space is occluded and at S<80% the gas phase is continuous. Gas-breakthrough pressures for illitic clay were closely related to expected values, based on capillary theory and pore-size. This relationship was not observed in the buffer materials where microstructural differences likely account for observed differences in material behaviour.

ACKNOWLEDGEMENTS

The author would like to take this opportunity to express thanks to his advisor, Dr. Malcolm N. Gray, of AECL at Pinawa and an Adjunct Professor in Civil and Geological Engineering at the University of Manitoba, for his technical input and personal guidance throughout the research program and preparation of this thesis.

The author would also like to thank the members of his review committee: Professor Doug Ruth, of the Department of Mechanical Engineering at the University of Manitoba, Dr. Dennis Oscarson, of AECL at Pinawa and an Adjunct Professor in Soil Sciences at the University of Manitoba, and Professor James Graham, of the Department of Civil and Geological Engineering at the University of Manitoba, who also acted as co-advisor during the research program.

Meaningful discussion with fellow students Dr. D. Dixon, A. W.-L. Wan, N. Tanaka, T. Crilly, and the entire geotechnical group at the University of Manitoba is gratefully acknowledged, along with the technical support provided by K. Gelmich, N. (Tai) Piamasalee and K. Majury.

Financial support provided by AECL Research and the National Science and Engineering Research Council, through Mac Gray, is also acknowledged.

Finally, the author is greatly indebted to his family, friends and Vanessa, who provided encouragement, guidance and comic relief throughout the course of this graduate study.

TABLE OF CONTENTS

Page

LIST OF TABLES

Table Page

LIST OF FIGURES

Figure

LIST OF SYMBOLS AND ABBREVIATIONS

Å - Angstrom (10^{-10} m)

AECL - Atomic Energy of Canada, Limited

AEV - Air entry value

CANDU - Canada Deuterium Uranium reactor

CEC - Cation exchange capacity

D - Diffusion coefficient

D_a - Apparent diffusion coefficient

D_o - Free-solution diffusion coefficient

DDL - Diffuse double layer

DDW - De-aired, distilled water

DL - Diffuse ion layer

EDL - Electric double layer

EIS - Environmental impact statement

h_s - Capillary rise, pertaining to the capillary pressure equation

i - Hydraulic gradient, $\partial h/\partial l$

J - Mass flux

K - Hydraulic conductivity

k - Permeability

L - Capillary length

MIP - Mercury intrusion porosimetry

p - Triaxial mean confining pressure

PSD - Pore-size distribution

P_A-P_B - Pressure gradient across meniscus

Q - Flow volume

q - Triaxial deviator stress

QC - Quality control

r - Pore radius

R_s - Radius of curvature of the meniscus in a capillary tube

S - Degree of saturation

s - Suction

SSA - Specific surface area

T_s - Surface tension in a capillary tube

u_a - Pore-air pressure

u_w - Pore-water pressure

u_g - Gas flow rate

V - Specific volume

w - Moisture content

α - Contact angle at the gas-water interface in a capillary tube

α - Soil compressibility factor

ζ - Aereosity

η - Porosity

η_{eff} - Effective porosity

τ - Tortuosity

τ' - Tortuosity factor

μ - Fluid viscosity

μ_g - Gas viscosity

π - Osmotic suction

ρ_b - Bulk density

ρ_d, ρ_{dry} - Dry density

σ - Total stress

σ' - Effective stress

Ψ - Total suction

$\Psi_{m\sigma}$ - Matric potential under loading

Ψ_{mo} - Matric potential without loading

χ - Constant referring to the degree of saturation in effective stress principle proposed by Bishop (1959)

1. INTRODUCTION

Clays and clay-sand mixtures are being used increasingly as barriers between contaminants and the biosphere in storage and disposal systems in several fields of the waste management industry. In Canada, for example, the present concept for disposal of nuclear fuel waste incorporates a mixture of silica sand and sodium bentonite into its engineered barrier design. Extensive research of the geotechnical behaviour of this material, referred to as buffer, is ongoing at AECL and several Canadian universities. One aspect of buffer research that Canadian researchers have yet to focus on is the study of gas migration. Models of contaminant transport in porous media usually do not consider gas flow as a parameter (Cheung and Chan, 1983; and Hensley and Schofield, 1991, for example). Scientific awareness of the significance of gas evolution in a disposal repository environment is increasing, therefore studies of gas migration through the buffer are timely. This chapter initially gives a brief overview of the Canadian repository design, describing the role of each of its various engineered and natural barriers in minimizing migration of contaminants. In particular, the function of the buffer material is fully explained. Next, the importance of gas migration studies is highlighted by a discussion of several aspects of gas generation within a repository, including gas sources, gas generation rates, and implications of the presence of gases. Finally, the format of the ensuing text presented in this report is described.

1.1 CANADIAN DISPOSAL CONCEPT

The Canadian nuclear fuel waste disposal concept involves disposal of CANDU reactor fuel or solidified high-level waste from reprocessing in a repository within the granitic rock mass of the Canadian Shield. Key to the design concept is a high degree of safety for repository workers, the public, and the environment at present and into the future. Risk assessment for the repository concept involves modelling of safety for tens of thousands of years, taking into account minimization of the burden of repository maintenance for future generations.

1.1.1 Repository Design

The Canadian nuclear fuel waste disposal concept, presently in the environmental review stages, relies on a system of multiple natural and engineered barriers to inhibit the migration of contaminants to the biosphere. Shown in Figure 1.1 (from Johnson et. al., 1994a) is the design concept for repository disposal of CANDU fuel using in-borehole emplacement which has been modelled full-scale at the AECL Research Underground Research Laboratory facilities. In order of relative distance from the actual nuclear fuel waste, the barriers for isolating contamination from the biosphere include the waste container, buffer material, and host rock. The upper and lower backfill material inhibit contaminant migration into the tunnels and lifts of the repository, aided by grout, plugs and seals. The multi-barrier system is described in full in the AECL Environmental Impact Statement (AECL EIS, 1994).

In simplified terms, the most likely scenario for radionuclides to reach the biosphere is for them to be introduced into groundwater at a breach in the waste containers. They would travel as part of the groundwater through the buffer and into the slightly permeable granitic host rock. Radionuclides may enter the host rock directly from the buffer, or they may first travel through repository mine shafts and tunnels. Groundwater flow through fissures and faults in the host rock will disperse radionuclides away from the repository until they eventually reach the surface where they can freely interact with the biosphere, primarily as part of the water cycle.

1.2 BUFFER PROPERTIES

Of the barriers incorporated into the repository design, the sand-clay buffer material is the focus of this research program. The buffer has many properties that make it attractive as a sealant in the Canadian repository design (Johnson et. al., 1994b). These properties are discussed in this Section.

The low diffusion coefficient ($D_a \sim 10^{-10}$ m^2/s) and hydraulic conductivity ($K \sim 10^{-11}$ m/s) of the buffer at the design clay dry density provide little opportunity for contaminant migration of appreciable volumes or flow rates, particularly because the most likely mechanisms for contaminant migration involve flow within the groundwater regime.

The high swelling potential exhibited by the buffer is another major benefit of the material as a sealant. The ability of the buffer to swell when in contact with water

allows it to close off cracks and fissures created by thermal- or moisture-induced drying. If not for this 'self-healing' ability of the buffer, such damage would allow contaminated groundwater to flow at rates much higher than permitted in unaltered buffer.

The buffer chemically maintains the pH of the pore-water at neutral or slightly alkaline conditions which minimizes corrosion, thus extending the life of the waste containers. The high thermal conductivity of the buffer allows for relatively fast dissipation of heat generated by the fuel waste radially outwards towards the host rock, minimizing thermally induced shrinkage and deformation within the buffer mass. Moreover, the drying shrinkage of the buffer material is relatively low so that fissuring should be minimal. The buffer has relatively strong ability to sorb radionuclides from the groundwater, thus further inhibiting the migration of radioactive waste through the buffer and into the host rock.

The stress-strain behaviour of the buffer material is well-suited to the repository environment. As well, the buffer has adequate bearing capacity to carry the weight of a waste container without appreciable deformation due to the loading (AECL EIS, 1994).

1.3 REPOSITORY GAS GENERATION ISSUES

There is potential for the formation of appreciable volumes of gas within a repository

environment from several sources. It is widely accepted that the rate of gas generation near the waste containers could be significantly greater than the rate that gas could migrate away from the waste containers in solution by diffusion and advection within the buffer. Work by Pusch and Forsberg (1983), Pusch et. al. (1987), Grogan et. al. (1992) and Wikramaratna et. al. (1993) suggest that gas pressure at the waste containers would mount as a growing potential until free gas is permitted to flow into the buffer, thus dropping the local gas pressure at the waste container. This section describes the gas sources within a repository environment and the potential effects of the presence of gases on repository performance.

1.3.1 Gas sources

Various gases could form in a repository environment, but hydrogen (H_2), methane (CH_4) and carbon dioxide (CO_2) would likely dominate. The key mechanism for gas formation is degradation of barrier materials and the waste within the repository (Grogan et. al., 1992). The presence of gases in a repository will therefore be a function of the containment system design and the nature of the wastes present.

According to Jeffries et. al. (1991) the formation of CO_2 or CH_4 due to microbial degradation of organic material will dominate in the short-term (up to a few hundred years). As well, a significant quantity of steam could form at the heat-generating wasteform in the short-term. Formation of H_2 gas due primarily to corrosion of the waste containers will dominate in the long-term (hundreds or thousands of years). Generation of other gases from radiolysis could also affect long-term gas generation

rates. In a paper presented at the International Workshop on Research and Development of Geological Disposal (PNC Tokai, Japan, 1993), Sharland et. al. catalogue reactions involved with the formation of several typical repository gases.

1.3.2 Gas generation implications

The formation of repository gases is associated with several hazards and could affect repository integrity in various ways.

The first such hazard involves the formation of the main repository gases (H_2, CH_4, and CO_2). The formation of these gases in the presence of radionuclides could involve ionic substitution of radionuclides, resulting in radioactive gases. As well, decay of waste over time and radiolysis is associated with direct formation of several radioactive gases (Jeffries et. al., 1991) which could also lead to dispersion of radioactive material.

Jeffries et. al. (1991) and Grogan et. al. (1992) recognize the explosive and flammable behaviour of several repository gases as a second danger. Accumulation of gases including H_2 and CH_4 in surface facilities even after a repository is closed could eventually lead to explosion or fire. Moreover, an explosion due to accumulation of such gases within an underground structure could cause considerable damage to the repository barrier system, leading to accelerated contaminant migration.

A third effect of repository gases involves the formation of steam from groundwater in the buffer when it is heated by the elevated temperature of the fuel waste. Studies by

Oscarson and Dixon (1989) and Couture (1985) show strong evidence that swelling potential of montmorillonite-based buffer materials is decreased by the formation of steam, thus decreasing its 'self-healing' abilities.

A fourth effect of repository gases involves their pressure effects on repository barriers. As described earlier, the low diffusion rate and hydraulic conductivity of buffer could cause accumulation of gases generated at the waste containers under continuously increased pressure. Local gas pressures may become sufficiently high that the gas could penetrate into the buffer material by a 'piping' or 'breakthrough' process which would promote contaminant migration in two ways. Firstly, gas-breakthrough could involve de-saturation of the buffer as gas pushed water through invaded pores, aiding migration of contaminants by means of the displaced water and gas. Secondly, de-saturation and drying could cause the formation of cracks in the buffer which could lead to increased hydraulic conductivity and accelerated contaminant migration. It is possible that gas-breakthrough at very high pressures could even cause permanent structural damage to the buffer by creating new pores by tensile fracturing (preferential pathways) or by enlarging existing pores to accommodate permeating materials (pathway dilation).

1.4 OVERVIEW

These pressure-related implications of repository gas generation are the focus of this research program. Chapter 2 reviews literature relevant to the engineering problem

presented and leads up to a formal statement of the scope of the research program. The test equipment and tested clay types are then described in Chapter 3, followed by a complete description of the test procedures in Chapter 4. Chapter 5 provides a presentation of test results with supporting discussion. Finally, conclusions drawn from the testing program and recommendations for further testing are discussed in Chapter 6.

2. REVIEW OF LITERATURE

2.1 INTRODUCTION

The research program that forms the basis of this thesis is concerned with the migration of gases through compacted clay material. It will be shown that an understanding of clay mineralogy and structure is required before the mechanisms involved in this process can be appreciated. This chapter discusses clay mineralogy and structure; the interaction of gases, liquids and solids within compacted clays; and a brief discussion of unsaturated soil mechanics. It then describes the theory behind capillary pressure and transport phenomena in clays, in particular ionic, liquid and gas migration. It goes on to describe what research has been done on gas migration in compacted clays, particularly in the nuclear fuel waste disposal industry, and explains where our present knowledge. Finally, the preceding information leads to a statement of the scope of the research program.

2.2 CLAY STRUCTURE

Clay behaviour depends on the physical interactions between the particles, liquids and gases that comprise the material. Clay mineral particles are very small , often of the order of 0.01 to 1 μm, and have large surface areas in relation to their mass. They are also quite active chemically, and all physical properties of clay soils can be related to

the interactions between the particles and the pore fluids (Mitchell, 1976; Yong et. al., 1992). For this reason, it is essential to develop at least a working understanding of clay behaviour.

Soil, whether it is a clay, silt, sand, gravel or peat, is a combination of gases, liquids and solids. The liquid and gaseous phases occur in pockets, pores or voids between and around particles of solids which can be inorganic or organic, including organisms in any state of decomposition. Peat is comprised of organic solids, while clays, silts, sands and gravels predominantly contain particles of inorganic solids that possess well-defined crystalline structure. These inorganic soils can be differentiated on the basis of particle size, with clays containing the smallest particles, followed by silts, sands and then gravels. It is widely accepted by definition that most clay particles are of colloidal size, with an equivalent diameter of less than $2x10^{-6}$ m (2 μm). In passing, it is noted that some clay minerals may exist at sizes larger than 2 μm, while non-clay minerals may be smaller than 2 μm. It is therefore important to distinguish between 'clay minerals' and 'clay size particles'. Clays exhibit cohesive properties (that is, they exhibit intrinsic strength), while silts, sands and gravels are considered cohesionless materials with strengths that depend on stress level. While silts, sands and gravels consist mainly of primary minerals, formed from high temperature processes such as metamorphosis, clay minerals are mainly of secondary minerals, formed from low temperature processes such as weathering (Bohn et. al., 1985). Clay minerals typically form in rock veins, fracture zones and depressions, around springs and geysers. Following erosion, transportation and deposition, they form in sedimentary fields such as lake bottoms and alluvial plains (Mitchell, 1976).

2.2.1 Structure levels

Yong and Warkentin (1975) divide soil structures, or soil fabric, into three classifications, namely; (1) ultra-microscopic structure where single clay 'particles' (< 0.001 mm) or groups of clay particles called 'domains' (< 0.01 mm) can only be seen under an electron microscope, (2) microscopic structure with fabric that forms units known as 'clusters' (< 0.1 mm) which are visible under a light microscope, and (3) macroscopic structure with fabric units that are visible to the naked eye and are called peds (< 1 mm) or aggregates (< 10 mm). The structural levels are more fully described in this Section in order of increasing size, starting at the atomic level.

As in all matter, the atoms that make up clay particles are held together by interatomic forces that govern clay behaviour. At the most basic structural level, the majority of clays form a crystalline lattice known as phyllosilicate, or layer silicate structure. The phyllosilicate lattice consists of a 'basic structural unit' of atoms which is repeated in an orderly manner throughout the lattice. The two most common structural units in clays are the silicon tetrahedron and the aluminum octahedron, shown in Figure 2.1. Silica tetrahedra consist of a silicon atom surrounded by four equidistant oxygen atoms while alumina octahedra consist of an aluminum atom surrounded by six hydroxyls (OH^-). Each structural unit is bound together by very strong primary interatomic forces which include combinations of ionic, covalent and metallic bonding. Adjacent structural cells are also held together by primary bonds to form a two-dimensional structural unit sheet, chain, or ring, although in phyllosilicates, the predominant structural unit is the sheet. Similarly, adjacent sheets are held together face-to-face by primary bonds to

form two-, three-, or (less-frequently) four-sheet thick layers or 'particles' (Yong and Warkentin, 1975).

Three of the most naturally abundant clays are kaolins (kaolinite), illite (hydrous mica) and montmorillonite (a sub-group of smectites which includes bentonite). Bohn et. al. (1985) suggest that these clays can be differentiated on the basis of (1) how the structural units are stacked to form a particle, (2) the particle charge per unit cell, (3) the type of bonding and the cations present between adjacent particles, and (4) the cations present within the layers that form a particle.

Silica tetrahedra and alumina octahedra layers are stacked to form particles with dimensions on the order of 1 μm in fixed arrangements for specific clays, as shown in Figure 2.1. Kaolinite has unit cells in a 1:1 stacking arrangement, meaning that a particle consists of 1 sheet of silica tetrahedra and 1 sheet of alumina octahedra bound by primary bonds. Illite and montmorillonite both have a 2:1 stacking arrangement where unit cells consist of 1 sheet of silica tetrahedra stacked between 2 sheets of alumina octahedra. Because of differences in the way the sheets are arranged, kaolinite, illite and montmorillonite form particles of different thicknesses and sizes. For example, a typical kaolinite crystal may be 70 to 100 layers thick (Yong and Warkentin, 1975) for a total particle thickness of approximately 0.05×10^{-6} m to 0.10×10^{-6} m (500 to 1000 angstroms). Illite clay particles are typically 0.03×10^{-6} m (300 angstroms) thick and montmorillonite particles are typically 0.003×10^{-6} m (30 angstroms) thick. Particles of this size can only be seen using electron microscopy (Mitchell, 1976).

Figure 2.2 describes the size of the various structural entities of clay. Most commonly,

several particles will stack upon each other to form a crystalline clay 'domain' with dimensions on the order of $10x10^{-6}$ m (0.01 mm). When several domains are grouped together to form a structural unit with dimensions up to $100x10^{-6}$ m (0.1 mm), the structure is referred to as a 'cluster'. Several clusters will group together to form a 'ped' with dimensions up to $1000x10^{-6}$ m (1 mm), and peds will group to form 'aggregates' of up to $10\,000x10^{-6}$ m (10 mm).

The net charge per unit cell depends on the type and degree of isomorphous substitution within the unit cell. This refers to the situation where a silicon or aluminum cation in a unit cell is replaced by another cation such as iron, magnesium, lithium, or calcium. Very little isomorphous substitution occurs in kaolinite. Isomorphous substitution in illite mainly consists of replacement of aluminum for silicon in the tetrahedra sheets, whereas in montmorillonite, most isomorphous substitution occurs in the octahedra sheets where magnesium and iron, for example, replace aluminum. The nature and extent of isomorphic substitution can greatly affect clay properties (Mitchell, 1976; Yong et. al., 1992).

2.2.2 **Pore-Structure**

Liquids, gases and matter in solution exist between separate structural features of clay fabric, such as between adjacent peds or between several peds and an aggregate. Similar to the size distribution of solid fabric structures, pore-size distribution (PSD) also ranges from ultra-microscopic to macroscopic. As with fabric size distribution, the type of clay and its origin also affect PSD. Other factors affecting PSD in compacted

clays include clay dry density, moisture content and method of formation (for example, reconstituted, dynamically compacted, statically compacted or taken from an in-situ specimen) (Lambe, 1958).

2.2.2.1 *Structured pore-space*

Pore-water occurs as either free (interstitial) water in pores or as bound (adsorbed) water on soil fabric surfaces. The bulk of the pore-water exists in many clays as interstitial water with typical liquid water properties. Yong et. al. (1992) describe a microstructural model of structured pore-water known as the diffuse double layer (DDL). The DDL is partially made up of a micro-thin layer of water adsorbed on the surface of clay particles. This electric double layer (EDL) makes up part of the Stern layer and exhibits behaviour similar to that of ice. A layer of partially hydrated cations and adsorbed water is held in close contact with negatively charged soil particles via relatively strong hydrogen bonds due to the dipolar configuration of water molecules. The bonding is so strong that the water molecules are packed to an abnormally high density, thus leading to their unique characteristics. The EDL is typically two to three water molecules thick (approximately $5x10^{-4}$ μm).

In addition to the EDL is a region of closely arranged cations known as the diffuse ion-layer (DL). The DL exists between the EDL and interstitial pore-water and is caused by attraction of cations originating in the interstitial pore-water to the negatively charged clay particles. The attraction results in formation of a dense 'cloud' of cations around clay fabric particles which lessens in density with distance away from the solid surface. Together, the EDL and the DL form a 'gel' (van Olphen, 1963) around the

clay fabric particles known as the diffuse double layer (DDL). The gel between adjacent soil particles interact, affecting pore-structure and related clay behaviour by restricting the size, shape and direction of free pore-space, thus altering clay properties such as mass transport. A thorough discussion of the theory, causes and effects of the DDL and adsorbed water is given by Mitchell (1991, 1976), Yong and Warkentin (1975), and van Olphen (1963).

The thickness of the DDL is governed by several factors and greatly affects many clay properties. It can have considerable influence up to $1x10^{-2}$ μm from particle surfaces (Yong et. al., 1992). The DDL is intimately related to electric charge within the pore-water and on particle surfaces. The degree of isomorphous substitution, the composition of the pore-water, and temperature all contribute to the size of the DDL (Mitchell, 1976). The nature of the DDL is directly related to the surface charge density of solid particles.

2.2.2.2 *Swelling pressure*

Clay swelling pressure is closely linked to DDL theory and related properties such as SSA and CEC. Swelling occurs because the DDL water has osmotic potential much lower than interstitial water, as explained by Dixon et. al., 1992. Water will flow from regions of high potential to low potential in order to balance the potential difference and achieve an equilibrium between the bound water, the free water and the externally applied stresses. Under low external stresses, flow of water leads to a decrease in local effective stress and hydration of soil fabric. On a macroscopic scale, this is seen as swelling or soil expansion.

2.2.2.3 *Free pore-space*

The portion of pore-space that contains fluids with properties that are not significantly affected by the electrical charges of the nearby soil particles is known as 'free pore-space'. As mentioned earlier, most of the pore-space in low-to-medium density clays is filled with interstitial water with its dissolved salts. This water is not influenced by soil particle surfaces and is therefore free to flow with typical liquid behaviour. It is consequently known as 'free' pore-water. In the case of unsaturated clays, free pore-space also contains a gas phase. Usually, discussion of pore-space refers to the free pore-space, except when the DDL is directly referred to. The term 'pore-space' is used, hereafter, to mean 'free pore-space'. While some coupled and direct flow phenomena can occur in the DDL, mass transport occurs almost entirely in free pore-space. The pore-space can be classified on a basis of relative pore-size, degree of interconnection between pores, and degree of order and homogeneity (Yong and Warkentin, 1975; Mitchell, 1976). Porosity (η) is a measure of the volume of pore-space in a unit volume of the soil as a ratio to the total volume. Void ratio (e) is the ratio of the volume of voids to the volume of soil solids in a unit volume of soil. In general, in a soil with fixed particle size distribution, high porosities and void ratios are associated with soils with low density and with more and larger pores.

The degree of interconnection between pores is important because it generally governs mass flow through a soil (Mitchell, 1976). If pores are occluded, or not connected to adjacent pores, then mass flow cannot occur, no matter how large or numerous the pores. The term effective porosity (η_{eff}) refers to that portion of porosity that contributes to flow through interconnectability and typically excludes pore-space

within the DDL. Paths connecting pores throughout a unit volume of soil are always non-linear, or tortuous. Tortuosity (τ) can be defined as the ratio between the actual distance mass will travel through a non-linear path between two points in a unit volume of soil to the straight line distance between those two points. Aereosity (ζ) (Ruth, 1993) is a parameter that relates the average microscopic speed of a particle being transported in a unit volume of soil to the net macroscopic speed of flow through that unit volume.

The DDL's of adjacent fabric structures can interact in such a way that their effects superimpose, leaving little or no free pore-space and reducing n_{eff} towards zero. Dixon et. al. (1992) and Dixon (1995) studied saturated swelling clays where this was the case. In some situations, adsorption of cations on particle surfaces can neutralize local electric charges so that a DL will not develop, and thus porosity will remain unaffected.

2.2.2.4 *Pore-size distribution*

The pore-structure of a soil can be modelled using a statistical network approach. Ruth (1993) defines two models for pore-structure networks, shown in Figure 2.3. Figure 2.3(a) shows a parallel network where tubular pores, each with a given uniform diameter, penetrate a unit volume of soil. Figure 2.3(b) shows a serial network where a series of tubular pores, each of varying diameter, penetrate a unit volume of soil. In each case, the pores are sized using statistical distributions, typically normal distributions. Ruth (1993) further models pores as being a series of large pores (vugs)

connected by pore-throats that are many orders of magnitude smaller (tubes), shown in Figure 2.3(c). The vugs are analogous to the macroscopic inter-ped and inter-aggregate pore-spaces and the tubes are analogous to microscopic voids directly between clusters, domains or particles.

Soils can have more than one level of porosity where there are concentrations of pores with more than one average diameter. For example, a specimen of soil with discrete grains will have a porosity controlled by the inter-grain pore-spaces, but the individual grains may also be porous with the intra-grain pores being much smaller than the inter-grain pores. In such a soil, the intra-grain and inter-grain porosities are greatly different, but both may contribute to the net porosity of the soil. Inter-aggregate (between aggregates) and intra-aggregate (within aggregates) pores can similarly lead to dual porosity, often described as macropores (large pore mode) and micropores (small pore mode). Such evidence has been seen in mercury intrusion porosimetry (MIP) measurements collected by Wan at AECL in current studies on various clays (such as calcium bentonite) and clay-sand materials (such as buffer) and by Garcia-Bengochea et. al. (1979) on silty clays. MIP is a frequently-used laboratory technique for investigating pore-size distribution (PSD) in soils and other porous media. It is based on the relationship between capillary pressure and pore-size.

Basically, MIP involves injecting mercury at numerous pressure increments into a small, dry porous specimen. The volume of mercury injected and the pressure at each increment is used to determine the PSD of the dry porous specimen. The procedures are described in full by Diamond (1970) who points out the significance and extent of specimen alteration due to drying during the preparation stage. Basically, drying can

decrease the typical size of pores through shrinkage but can also induce larger pores in the form of fissures and shrinkage cracks. To get meaningful results from MIP, it is essential that specimens are fully dried by a procedure such as accelerated freeze-drying that minimizes specimen shrinkage and other effects.

Another consideration in analyzing MIP data is the distinction between pore-spaces that were formerly filled with free water and those filled with structured water. MIP testing usually involves completely dry specimens, thus pore-diameter measurement pertains to the full distance between adjacent structural features, including the DDL and interstitial pore-space. The 'structured' pore-space of the DDL, which does not contribute to transport phenomena, cannot be distinguished directly from total pore-space based on MIP and must be inferred. An approximation of effective porosity is required for this type of comparison.

The effects of moisture content at the time of compaction on the pore-size distribution in dynamically compacted clays is well-documented and explained, for example by Diamond (1971), Juang and Holtz (1986) and Garcia-Bengochea et. al. (1979). Soil fabric in specimens compacted dry of optimum (the moisture content that produces the maximum dry density for a given compactive effort) have high strength and can resist compaction and remoulding forces, so that large inter-aggregate pores remain. As the compaction moisture content approaches the optimum value, effective strength decreases, so smaller and smaller inter-aggregate pores remain. Specimens compacted at or above the optimum moisture content have relatively little resistance to compaction forces and become distorted and re-orientated. Soils become so well-packed or ordered that the pore-structure becomes discontinuous and develops very

low permeability. In general, only small changes in pore-size distribution were found between soils compacted at and above the optimum dry density. Diamond (1971) described the particle structure of soils compacted below the optimum moisture content as flocculated (random, edge-to-face orientation); while that in soils compacted at or above the optimum moisture content was dispersed (parallel, face-to-face orientation). Barden and Sides (1970) pointed out that unsaturated clays of appreciable plasticity that are compacted below the optimum moisture content are highly unstable and can either swell or collapse upon wetting, depending on the confining pressure. These effects are likely much less marked in clays compacted with shearing strain, for example, by static compaction. The soil fabric will therefore not become re-oriented to the same extent.

2.3 UNSATURATED SOIL MECHANICS

When discussing gas migration through compacted clays, it is understood that the soil system is not fully saturated. Some knowledge of unsaturated soil mechanics is therefore needed for an understanding of gas flow within such soils.

2.3.1 Effective stress concept

The most basic form of the stress equilibrium equation for soils was proposed by Terzaghi (Terzaghi and Peck, 1948). It states that the total stress on a given plane within a fully saturated soil equals the sum of the pore-water pressure and

intergranular (effective) stresses at mineral-mineral interfaces along that plane. In other words,

$$\sigma = \sigma' + u_w$$

where σ = total stress
σ' = effective stress, and
u_w = pore-water pressure.

This form of the effective stress principle only holds true for fully saturated granular silts, sands and gravels, or low plasticity clays. For medium- to high-plastic clays where the DDL significantly interferes with direct mineral-mineral interfaces, an (R-A) term that accounts for the physico-chemical repulsive (R) and attractive (A) forces is incorporated into the equation. For unsaturated soils, a more complicated principle of effective stress is required to model the stress regime. In such soils, physico-chemical effects including soil suction become a contributing factor in stress analysis, and so stresses cannot be explained in terms of mineral-mineral contact stresses and pore-water pressures alone. A good definition of soil suction is provided by Richards (1974). He describes an unsaturated soil coming in contact with a quantity of free water, and adsorbing water by asserting a suction on it. Soil suction, therefore, is associated with negative pore-water pressures (below atmospheric) and is made up of two components, namely osmotic and matric suction. Osmotic suction (π) arises from the difference in cation concentrations between the DDL and free water whereby negative pressure is created in the free water in an attempt to increase its cation concentration and come to an equilibrium with the DDL cation concentration (Mitchell, 1976). Matric suction (u_a-u_w) refers to the suction created due to the difference in

water pressure and gas pressure at the interface between water and gas phases in an unsaturated soil (Fredlund and Rahardjo, 1993). Matric suction is synonymous with the terms 'surface tension' and 'capillary pressure'. Total suction, Ψ, is simply the sum of the osmotic and matric suction:

$$\Psi = (u_a - u_w) + \pi.$$

Fredlund and Rahardjo (1993) note that osmotic suction is not very sensitive to moisture content changes. Moreover, Barden and Sides (1970) note that osmotic suction is typically much less than matric suction, especially with nearly pure water, and so matric suction is often used to approximate total suction. In any case there is a close relationship between π and (R-A), so the osmotic suction is taken into account in the modified effective stress term.

Bishop (1959) proposed an equation for the effective stress principle for unsaturated soils which ignores osmotic suction and includes a χ parameter which refers to the degree of saturation:

$$\sigma' = (\sigma - u_a) + \chi(u_a - u_w).$$

Later, Mitchell (1976) described the χ parameter as the ratio of planar area taken up by water to the total planar area for a given imaginary plane of study within a soil. In the case of a fully saturated clay ($\chi = 0$) or a completely dry clay ($\chi = 1$) the equation reduces to the effective stress principle proposed by Terzaghi ($\sigma = \sigma' + u_w$). The relationship between χ and saturation S is strongly non-linear, and varies considerably

with many test variables (Fredlund and Rahardjo, 1993). It currently receives little attention.

Many similar single-valued effective stress equations have been proposed. However, Fredlund and Rahardjo (1993) pointed out that stress - void ratio states in unsaturated soils are stress path-dependent and the relationships are thus not single-valued. On the basis of Matyas and Radhakrishna (1968) and Fredlund and Morgenstern (1977), they separated the applied stress, $(\sigma - u_a)$, and suction, $(u_a - u_w)$, into two separate stress state variables, and modelled unsaturated soils as a 4-phase system, adding the contractile skin at the gas-water interface to the 3 previously understood solid, liquid and gas phases.

In studying gas bubble formations in offshore soils, Wheeler (1988) and Wheeler et. al. (1990) found that, in terms of pore-fluids, there are three modes of unsaturated soils, namely soils with; (1) a continuous gas phase and a discontinuous water phase, (2) a continuous gas phase and a continuous water phase, and (3) a discontinuous gas phase and a continuous water phase. Wheeler (1988) noted a critical degree of saturation at approximately S=85%, above which the gas phase broke up into discrete (occluded) bubbles resulting in a discontinuous gas phase. Wheeler et. al. (1990) suggest that the approach discussed by Fredlund and Rahardjo (1993) is invalid for such soils.

2.3.2 Stress-strain behaviour

Although the stress-strain behaviour of compacted clays is not a focus of this research program, it merits mention due to its relative importance in the field of unsaturated soil mechanics. Using the terms of critical state soil mechanics, the stress-strain behaviour of saturated soils is commonly described in (p':q:V) space, where p' is the mean effective stress, q is deviator stress, and V is specific volume (Wood, 1990). Alonso et. al. (1990) developed a basic critical state model for unsaturated soils which describes the soil in (p:s) space where p is the net mean stress and s the suction. Their model was primarily valid for granular and low plasticity cohesive soils, and was later extended for use with highly plastic clays by Gens and Alonso (1992). Wheeler and Shivakumar (1993) more recently developed a model which involved (p':q:s:V:w) space, where w is moisture content.

2.4 CAPILLARITY

Capillary pressure, described in passing in Section 2.3.1 as matric suction, is of paramount concern to studies of gas transportation in soils because basic theory and studies by numerous researchers (for example, Volckaert et. al., 1993; Wikramaratna et. al., 1993; Pusch, 1993) suggest that capillarity is a controlling mechanism for the migration of gases through the pores of a soil. The relationship between capillarity and gas migration will be discussed in Section 2.5.3 following the description of capillary pressure presented in this Section.

Capillarity is the phenomenon whereby fluid is held in tension under the influence of a contractile skin (surface tension). The basic theory for capillary pressure is usually derived using a model of an elemental point in hydrostatic equilibrium on the gas-water interface (meniscus) in a capillary tube. Figure 2.4 shows the model, a capillary tube submerged in a water bath. The height that the water rises above the bath in the capillary tube, h_c, is a function of the wetting nature of the gas-water interface (with contact angle, α) and its interaction with the walls of the capillary tube (surface tension of water, T_s). The contact angle, α, is often taken as zero at a gas-water interface within soils (Yong and Warkentin, 1975) and so the pore-radius, r, can be equated to the radius of curvature of the gas-water interface meniscus, R_s. The model is fully described by Fredlund and Rahardjo (1993) who derive the generally accepted capillary pressure equation, often called the Washburn or Laplace equation:

$$(u_a - u_w) = \frac{2\ T_s}{r}$$

The model shows that capillary pressure, here equal to the matric suction ($u_a - u_w$), will increase with decreased pore-size. Because capillary pressure (suction) is inversely proportional to pore-radius, it is evident that the largest pores will de-saturate first, followed by successively smaller pores. While the upper limit of R_s is r (when α=0), Wheeler et. al. (1990) suggest the lower limit for R_s in clays would be approximately 0.5×10^{-6} m (0.5 microns). Several researchers (Wheeler et al., 1990; Corey, 1990; and, Fredlund and Rahardjo, 1993, for example) estimate surface tension involving water and various gases at room temperature (approximately 22°C) as approximately T_s=0.073 N/m. It appears reasonable to assume that surface tension at the interface between water and inert gases such as argon is similar.

Capillary behaviour of porous media is often shown as graphs of degree of saturation versus capillary pressure (Figure 2.5; from Ruth, 1993). Ruth (1993) explains that a fully saturated specimen will initially drain along the primary drainage curve. An initial threshold capillary pressure is required before the gaseous phase enters even the largest pore-spaces. Drainage will then occur with increased capillary pressure until the pore-fluid becomes discontinuous at the point where the soil is at the point of 'irreducible' saturation (where the saturation and moisture content cannot reduce further without external drying) and the corresponding 'pendular' capillary pressure. If the capillary pressure is then decreased and the medium is allowed to re-saturate, it will follow the imbibition (sorption) curve to a point near full saturation. When de-saturation is again undertaken, the secondary drainage curve is followed back to the point of pendular capillary pressure and irreducible saturation.

Two explanations exist for the hysteresis between the imbibition curve and the secondary drainage curve. Several investigators (for example, Freeze and Cherry, 1979) suggest that the hysteresis is due to alteration of the soil fabric. Ruth (1993) concludes that it is partly caused by variability of the diameter of individual pores within the medium. This 'bottleneck' effect is described in Figure 2.6. In the initially dry system in Figure 2.6(a) capillary pressure begins at P=0 and increases to P_1, P_2 and finally P_3, which are actually increasingly negative pressures. P_1 in this model coincides with the capillary pressure required to invade pores with diameter d. Similarly, P_2 and P_3 are the capillary pressures required to invade pores with diameter 2d and 3d, respectively. Figure 2.6(b) shows the same pore-system initially saturated with $P=P_3$. The system in Figure 2.6(b) is de-saturated by a drop in capillary pressure from P_3 to P_2, P_1 and finally to P=0. Notice that at the intermediate stages (at P_1 and

P_2) the saturation state within the system differs between the wetting and drying processes. Water is retained longer in certain pores in the drying process, thus giving the system higher net saturations at the intermediate pressures - marked as hysteresis in capillary pressure versus saturation space.

Hysteresis is also evident in the 'characteristic' or 'water retention' curves shown in Figure 2.7 (from Freeze and Cherry, 1979). The negative pressure shown on the horizontal axis is the same as suction or capillary pressure. Notice that the soil remains saturated for small negative pressures until a point known as the air entry value, AEV, is reached. The AEV refers to the point at which soil suction has increased such that gas will invade the largest saturated pores - it is the point at which a soil will begin to de-saturate. Soils with suction less than the AEV are referred to as tension-saturated because the soil is still fully saturated, but the pore-water is in tension. At points of positive pressure head, the soil is fully saturated and pore-water is in compression.

2.5 FLOW PHENOMENA

Under the influence of potential gradients, physical mass (water and gas), heat and electricity flow through porous media. Figure 2.8 (after Mitchell, 1976) shows a summary of flow phenomena that occur in soils and the relevant driving gradients (Mitchell, 1991). Such flow can occur in a soil through the inter-connected pore-spaces given certain conditions. Direct flow occurs when flow of a certain type is

initiated by its own potential gradient. For instance, the flow of fluid under a hydraulic potential gradient is a direct flow phenomenon known as hydraulic conductivity, governed by Darcy's Law. Coupled flow occurs when a flow mechanism is initiated by some other potential gradient. For instance, the flow of fluid under a chemical potential gradient is the coupled flow phenomenon known as osmosis. Flow of gaseous matter belongs to the category of 'fluid flux' in Figure 2.8.

As discussed in the Chapter 1, the primary purpose of the buffer in the Canadian nuclear fuel waste disposal scheme is to minimize transport of radioactive material from corroded fuel canisters to the surrounding host rock. Transport of the radioactive material will result from a combination of the mechanisms shown in Figure 2.8.

The buffer is to be placed in an unsaturated state at approximately S=85% (Dixon et. al., 1992) and will slowly take on water from the surrounding host granitic rock. While the wasteform is generating heat, thermal gradients will cause moisture to move from the region close to the container towards the buffer-rock interface. Hence, it is certain that the water regime within the buffer will change over time and that permeability will be an important factor involving gas migration and transport of radioactive materials through the buffer. Furthermore, modelling simultaneous migration of water, gas and ionic material will prove to be highly complex.

The most prominent mechanisms involved with the transportation of radioactive contaminants within the buffer material are discussed in the following Sections.

2.5.1 Hydraulic conductivity and permeability

The direct flow of fluid in saturated soils is governed by the empirically-based Darcy's Law which states that the superficial velocity of flow through a volume of soil is directly proportional to the hydraulic gradient, $\partial h/\partial l$. The constant of proportionality is termed hydraulic conductivity. This leads to:

$$Q = - K A i$$

where Q = flow volume [m^3/s]
K = hydraulic conductivity [m/s]
A = cross-sectional area of the soil volume [m^2], and
$i = (\partial h/\partial l)$ = change in hydraulic head, ∂h,
over the length, ∂l, of a soil element (hydraulic gradient).
The negative sign indicates that flow occurs from high to low head.

Hydraulic conductivity is a function of both the porous medium and the pore-fluid. For soil studies, it is often desirable to describe the transport characteristics of the soil and the pore-fluid independently. For this reason permeability, k, is often used rather than hydraulic conductivity, K, where k is defined as a function of the porous medium alone. The relationship between permeability and hydraulic conductivity is described extensively by Freeze and Cherry (1979). It can be summarized as:

$$k = (\mu/\rho g)K$$

where k = permeability (m^2)
μ = pore-fluid dynamic viscosity (kg/m/s)
ρ = pore-fluid density (kg/m^3)
g = gravitational acceleration (m/s^2)
K = hydraulic conductivity (m/s).

Darcy's Law does not always accurately model fluid transport, however, and has been shown to have upper and lower limits of validity (Freeze and Cherry, 1979). The upper limit to Darcy's Law, in terms of flow rates, is reached when the pore-fluid flows in a turbulent manner. Ruth (1993) points out that the flow in this situation is not truly 'turbulent' and that the deviation from Darcian flow is actually a result of Forcheimer effects which involve laminar inertial losses due to tortuosity. The lower limit is reached when the hydraulic gradient decreases below a threshold value, below which no flow will occur. A threshold or critical gradient often occurs in fine-grained, low permeability materials such as highly compacted clays. Dixon et. al. (1992) suggest that the lower limit of validity for Darcy's Law occurs when the effects of the coupling influences from electrical, thermal and osmotic potential become significant compared to the direct influence of hydraulic potential, and the assumption of direct flow is no longer valid. These effects are more prominent in clays such as montmorillonite with high surface activities than in clays of lower activity, such as illite.

2.5.2 **Chemical diffusion**

The direct flow of ionic matter due to a chemical potential gradient is known as chemical diffusion, or simply diffusion, and is governed by Fick's Law. Diffusion becomes an important mechanism for ionic transportation at the permeabilities predicted for highly-compacted clays such as those tested in this program, and those used in the proposed buffer design.

Cheung (1989) makes several important generalizations concerning diffusion, including the following: (1) diffusion of ionic matter from regions of high concentration to regions of lower concentration can occur either in the free pore-water or the bound water of the DDL, although diffusion rates are higher in the free pore-water, (2) cations migrate through free pore-water and bound water whereas anions tend to migrate only through free water, and (3) diffusion depends on physico-chemical parameters such as sorption, ion exchange and precipitation as well as porous medium characteristics such as porosity and tortuosity.

Two types of diffusion tests are commonly performed. The first type, in-diffusion testing, measures transient diffusion within a soil specimen. The second type, through-diffusion testing, measures the steady-state diffusion rates through a soil specimen. In-diffusion tests are based on Fick's Second Law given as:

$$\partial c/\partial t = D_a(\partial^2 c/\partial x^2)$$

where c = concentration of diffusant
t = time
D_a = apparent diffusion coefficient
x = position.

For a nonsorbing diffusant, D_a can be related to the free-solution diffusion coefficient, D_o, by:

$$D_a = D_o\tau'$$

where τ' = tortuosity factor = $(L/Le)^2$
with specimen length, L, and actual pore length, Le.

Through-diffusion testing is governed by Fick's First Law given as:

$$J = -D\,(\partial c/\partial x)$$

where J = mass flux
D = diffusion coefficient.

Nearly all efforts in diffusion studies for the Canadian nuclear fuel waste disposal concept have focussed on the diffusion of relevant cationic radioisotopes through saturated clays and buffer (Cheung and Chan, 1983; Cheung, 1989, for example). Few studies of diffusion in unsaturated materials have been completed to date, because, in the case of a repository environment, the buffer density and saturation are such that a continuous gas phase does not exist. The mechanism of diffusion within pore-space with an occluded gas phase seems to be similar to that in water-saturated pore-space. Rolston (1986) and Troeh et. al. (1982), for instance, similarly describe gas diffusivity within dry soils in terms of Fick's Law when discussing agricultural implications of gas migration such as soil aeration and the role of degree of saturation.

2.5.3 **Gas migration**

European researchers such as Volckaert et. al. (1993) and Horseman and Harrington (1994) suggest that there are four scenarios for gas transport, namely:

(1) transport of gas in solution (diffusion),

(2) 2-phase flow,

(3) transport by pathway dilatancy, and

(4) transport by tensile fracturing (Figure 2.9).

In an alternative classification, Jeffries et. al. (1991) refer to the three mechanisms as (1) biochemistry, (2) multi-phase flow, and (3) geomechanics. Horseman and Harrington (1994) describe the difference between the three modes of transport in terms of the principle of effective stress which states that total stress in a soil is a function of direct mineral-mineral contacts, pore-water pressure and physico-chemical forces of repulsion and attraction between particles and their DDL's. They recognize that gas cannot transmit stress or work against these physico-chemical forces, and thus cannot occupy local pore-space, until the gas pressures can overcome these forces. Until this occurs, gas can only enter pore-spaces and migrate through the processes of diffusion and advection, based on Fick's and Darcy's Laws. A gas phase will enter pore-spaces when the difference between the gas pressure and water pressure at the gas-water interface at the largest pore-throats is greater than the capillary pressure (air entry value, AEV) at that pore-throat. Gas will enter successively smaller pores as its pressure increases relative to water pressure and overcomes the capillary pressure in successively smaller pores. Water will be displaced and pushed ahead of the gas front as the gas migrates into these pores (de-saturation). If the pores in a given host medium are so small that capillary pressures are greater than the total pressure within the host medium, then invading gas will have to disturb the existing pore-structure. This can be done either by dilating existing pore-throats or by creating new pore-spaces through tensile fracturing (fissuring) to

accommodate further gas entry at pressures lower than would be allowed by capillarity in the original pore-structure.

Volckaert et. al (1993) suggest that for a saturated clay specimen, the pore-water pressure for a clay under loading equals the matric potential under the same loading conditions. In other words, pore-water pressure equals the sum of the matric potential before loading plus a compressibility factor multiplied by the total stress in the clay. Although not specifically stated, this theory is valid only for drained conditions. The relationship can be expressed as:

$$u_w = \Psi_{m\sigma} = (\Psi_{mo} + \alpha\sigma)$$

where u_w = pore-water pressure
$\Psi_{m\sigma}$ = matric potential under loading
Ψ_{mo} = matric potential without loading
α = compressibility factor (0.3 for silty clay, 1 for pure clay)
σ = total stress.

For gas to be transported by diffusion, the gas pressure, P_g, must be such that $P_g < (P_w - \Psi_{mo})$, or $P_g < \alpha\sigma$. Gas will remain in the gaseous state and push water through existing pores as 2-phase flow once $P_g \geq (P_w - \Psi_{mo})$, or $P_g \geq \alpha\sigma$. Finally, when $P_g = \sigma$, the gas will deform existing pores and will induce the formation of new pores at weak points in the clay. Therefore, for a pure clay with $\alpha = 1$, no 2-phase flow will occur. These flow mechanisms are depicted in Figure 2.9.

Volckaert et. al (1993) and Horseman and Harrington (1994) relate gas flow most intimately to the total stress in the clay and to a compressibility factor which they leave

relatively unexplained. Although a general trend in compacted clays is for decreased pore-size with increased total stress, the two parameters are not directly related. However, the trend in gas flow mechanisms with increased gas pressure from diffusivity at low pressure; to 2-phase flow; to flow due to alteration of the pore-structure presented by these researchers is conceptually attractive. However, explaining gas transport in terms of total stress without taking proper account of degree of saturation or pore-structure geometry seems to be an oversimplification of the process.

The following text describes some additional observations and deviations from the theory of Volckaert et. al. (1993) and his colleagues.

Horseman and Harrington (1994) noticed that when local capillary pressures were overcome and pathway dilatancy occurred, the local pore-structure became very unstable. Pathway dilatancy would reverse so that pores were intermittently closed off even under slight changes in pressure or temperature, resulting in 'burst-like' or fluttering flow.

Jeffries et. al. (1991) recognized the importance and complexity of understanding the simultaneous migration of gas and water within the host material and the importance of the validity of Darcy's Law. They also described processes within a repository that enhance and retard gas migration. Enhancement of gas flow will arise from expansion of pores and creation of new pores as previously mentioned. Flow enhancement also occurs due to factors related to repository design, such as repository construction methods, repository geometry, engineering specifications, and tectonic movement.

This research emphasized the importance of degree of saturation in the gas migration process. This is apparent in the flow chart of gas flow scenarios presented in Figure 2.10 (from Jeffries et. al., 1991). The complexity of the mechanism of gas flow becomes obvious in this figure. These researchers present other phenomena related to gas flow, including increased mobility of gas due to viscous fingering. This refers to the tendency for gas to extend into the water phase across gas-water interfaces in pores in discrete finger-like formations. Another phenomenon discussed is the effect of kinetic energy of flowing gas on assisting passage through small pore-throats.

Lineham (1989) defines a critical gas pressure or AEV as the minimum pressure required to overcome capillarity in pore-spaces. He goes on to explain that the critical gas pressure, primarily a function of surface tension between the pore-fluid and pore-walls, is that pressure above which a gaseous phase will flow through a porous medium, much like the 2-phase flow described earlier by the Volckaert et. al (1993) and Horseman and Harrington (1994). Lineham (1989) states that diffusion will occur below this critical gas pressure (or critical gas saturation; Ruth, 1993), but does not make reference to the third gas flow mechanism involving the deformation of pores.

Wikramaratna and Goodfield (1994) give the following equation, based on Darcy's Law with several generalizations, for determining the gas flow rate in soils with a continuous pore-structure:

$$u_g = \frac{r^2}{8\mu_g} \frac{(P_A - P_B)}{L}$$

where u_g = gas flow rate,
r = pore radius,

μ_g = gas viscosity
$(P_A - P_B)$ = pressure gradient along capillary, and
L = capillary length.

This equation is valid for 2-phase gas flow. If the gas generation rate is greater than the gas flow rate, then pore dilatancy or fissuring could accompany 2-phase gas flow to increase the rate of dispersion of the gas and minimize gas pressure increases.

Most Swedish work (Pusch and Forsberg, 1983; Pusch et. al. 1985; Pusch et. al. 1987; Pusch 1993; and Wikramaratna et. al., 1993) relates gas conductivity to capillary pressure. In a review of earlier work, Pusch (1993) suggests that clay microstructure is even more important to the gas migration mechanism than it is to the mechanism of water migration and suggests that there is a critical gas pressure, which can be understood as capillary pressure, that, when surpassed, will allow gas to penetrate into a porous medium. He describes this gas pressure as the sum of the piezometric pressure and a 'true' critical gas pressure. Pusch et. al. (1985) and Pusch (1993) state that empirical evidence indicates that the critical gas pressure is 50% to 90% of the swelling pressure in montmorillonite clay. Much like the relationship between gas conduction and total pressure suggested by Volckaert et. al. (1993), the suggestion that gas conduction and swelling pressure are related appears unlikely since the two parameters are not closely linked through theory. This point will be returned to later in discussing the experimental data in this project.

In light of the above theories and research, one concludes that the mechanism of gas transport in compacted clays is complex and appears to be closely related to clay structure and degree of saturation. Fick's Law and theories of diffusivity, theories of

capillarity and soil suction, geomechanical properties, and pore-structure are all contributing factors to understanding gas flow. With a relatively low gas pressure gradient, if soil suction is sufficiently low, then dissolution of gas across the gas-water meniscus in existing pores may occur and gas will only migrate in solution by diffusion or advection. Once soil suction develops such that it can overcome the capillary pressure in pores by way of increased gas pressure, then the gas-water meniscus may displace and initiate 2-phase gas flow. If capillary pressures are excessively large, then pore dilatancy and tensile fracturing may occur. The latter mechanism is probably the least understood process involved with gas flow in terms of its causes, effects and relative importance to the general phenomenon of gas migration.

2.6 GAS MIGRATION RESEARCH

The previous Section described the basic theory of gas migration adopted by several researchers. This Section expands on this discussion, making more detailed reference to test procedures, and how the theory relates to compacted clay barriers associated with fuel waste repository designs. The value of this comparison of different research programs is unfortunately limited because each program uses unique test equipment, conditions, materials and procedures, depending on the nature of the relevant repository design being studied.

Gas migration in compacted clay, with the exception of diffusivity, has generally been given relatively little attention in the research community in the past. The most likely

reason for this is that in most fields of study involving gas transport in compacted clays, the supply rate of gas is sufficiently low that gas can be dissolved in the pore-fluids and transported via diffusion processes. In agricultural applications, for example, gas flow is usually by diffusion and soils involved are generally very loose and exhibit behaviour very dissimilar to compacted clays. In the oil and gas industry, clays are typically treated as impervious, and gas conductivity is only an issue within the reservoir which is typically a granular soil. Clay liners for surface waste disposal systems are relatively low in clay content and density, and gases generated in the waste usually escape by diffusion or are re-routed and collected before entering the clay liner. On the other hand, nuclear fuel waste disposal technology often involves a system where the amount of gas generated at the waste will be much greater than the amount that could escape through the surrounding buffer material by diffusion without mounting gas pressure (for example, Wikramaratna et. al., 1993; Grogan et. al., 1992). Migration of a gaseous phase in a repository environment is, therefore, of considerable importance .

2.6.1 Gas migration in a repository

Lineham (1989) completed several low pressure (diffusion) and high pressure (breakthrough) laboratory tests on saturated specimens of London and Kimmeridge clay using nitrogen gas. In his low pressure tests, specimens were initially saturated and backpressured. A gas pressure was then introduced at one end in increments up to 1 MPa. Results showed slow formation of a gas bubble in a collection system that suggested the occurrence of diffusion of gas through the specimen. The high pressure

tests involved similar procedures, but the gas increments were much greater. Results showed that a sudden passage of gas through the specimens occurred between 3.4 MPa and 6.2 MPa. Based on capillarity, these critical pressures relate to pore diameters between 0.85 nm and 0.47 nm. These pore-sizes are much smaller than those expected in these clays. High pressure tests were completed on cylindrical specimens with 10 mm diameter and 10 mm height, dimensions that are typically unacceptably small for laboratory testing.

Laboratory testing has been completed by several researchers in the international nuclear fuel waste disposal industry. Laboratory work completed by Volckaert et. al. (1993) involved through-diffusion, one-dimensional oedometer testing and triaxial testing of natural Boom clay specimens using nitrogen and hydrogen as permeating gases. Hydraulic conductivities and breakthrough pressures were calculated in the oedometer tests. Repeatable results were achieved for hydraulic conductivity and gas-breakthrough, but associated gas flow rates were less repeatable. Specimens were initially saturated, but by the completion of tests, degree of saturation dropped to values as low as 86%, but were generally greater than 90%. Degree of saturation at the gas inlet side was generally lower than at the outlet side. The researchers concluded that the relatively small changes in degree of saturation indicated the gas flowed through only a few individual paths rather than as an advancing face. Triaxial tests were used to generate water retention curves for the specimens. The researchers give a complete description of a conceptual and physical model for gas flow and describe in situ tests and mathematical modelling underway in conjunction with MEGAS (Modelling and Experiments on Gas Migration in Repository Host Rocks).

Horseman and Harrington (1994) completed similar hydraulic conductivity and gas-injection tests on Boom clay. Their specimens were significantly larger than those tested by Lineham (1989). Specimens were oriented parallel and perpendicular to the natural layering of the Boom clay to study the effects of anisotropy. In the gas-injection tests, the gas pressure was increased at a constant rate until gas-breakthrough occurred, usually at a distinct pressure peak. Degrees of saturation after the tests remained relatively high (S > 95%) showing that the gas travelled through only a few pathways, much like specimens tested by Volckaert et. al. (1993). Interpretation of the results was enhanced by microstructural analysis. The main focus of this paper was not the tests and test results, however, but rather the development of a conceptual model for gas flow.

Theories regarding gas flow presented by Swedish researchers seem to have changed over time. Pusch and Forsberg (1983) studied gas-breakthrough of nitrogen and hydrogen through bentonite specimens. Relative permeabilities of water and gas were calculated. As with other researchers, S did not significantly decrease during the tests, indicating that the gas passed through only a few discrete passages. Some microstructural analysis was completed to relate the test results to capillary theory, and the breakthrough pressures were also related to swelling pressures. Assuming a theoretical pore diameter in the bentonite of 50 nm, the clay would resist pressures up to 11 MPa before gas could enter due to capillary action, and below 5 MPa the gas would only enter the bentonite due to diffusion. Studies by Pusch et. al. (1985) similarly showed sudden breakthrough of gas at pressures of the same order of magnitude as the swelling pressure. The relationship was explained on the basis that resistance to gas flow at relatively low density is generated by negative pore-pressure

(suction, capillary pressure) in the pore-space of the clay. At higher pressures, on the other hand, the gas pressure would become sufficiently high that soil aggregates could be displaced to allow gas migration. Pusch and his colleagues claim that the change from a controlling mechanism based on capillarity to one controlled by aggregate displacement is a function of the swelling pressure. Although their general gas flow mechanism is similar to that described by others, the way in which it is described in terms of swelling pressure is unique. Pusch et. al. (1987) relate capillarity to clay density through the associated mechanical strength of the clay gel. Syntheses of the Swedish work, presented by Wikramaratna et. al., (1993) and Pusch (1993) bring much of the Swedish conceptual and laboratory work together into a physical model for gas migration from their copper/steel canister system. Wikramaratna et. al., (1993) again describe the conceptual model for gas flow, including its relationship to Fick's Law, swelling pressure, capillary pressure and pore-structure alteration. This paper also presents a study of the causes, quantities, consequences and long-term fate of repository gases with respect to the Swedish KBS-3 repository design. A model for gas flow rates due to capillary action is presented.

Grogan et. al. (1992) present a physical model for gas migration in a low- or medium-level waste repository based on the Swiss Nagra design. Unlike most other papers on the subject, the main focus of this paper was the gases involved (sources, volumes, time dependency, dangers involved) rather than the conceptual model of gas flow.

A report by Jeffries et. al. (1991) gives a general summary of gas migration knowledge based on international technologies for nuclear fuel waste as well as other industries including oil and gas and coal mining. The conceptual model for gas flow was

described meticulously by the researchers and is very similar to the concept described by most other researchers. Nearly all aspects of repository design as related to gas conductivity are discussed in this paper, from workmanship in repository construction to the reaction of a repository to long-term tectonic movement. Wikramaratna and Goodfield (1994) give a similar review of work completed in the UK and Switzerland with an overview of proposed studies at their facilities.

2.6.2 Summary of research

Although it is difficult to give a detailed synopsis of existing gas migration test results because of the variability in test equipment, procedures, conditions, and materials, some general inadequacies can be identified in the research to date. Most studies have given insufficient attention to the effects of saturation state of test materials on gas-breakthrough pressures and gas diffusivity. Testing at elevated backpressures to ensure initial specimen saturation has not been fully investigated, and quality control for saturation in test specimens is not well documented. Of the literature reviewed, no study of the effects of specimen size has been completed. Related to this, a study of the effects of pressure gradient, based on varied specimen height, also has not been investigated. Only a narrow set of materials has been studied as most institutions opt to study only the clay materials relevant to their specific repository design. Apart from one test series by Lineham (1989), limited gas diffusion testing has been completed to date to confirm predictions related to this mechanism. As well, the transition between true 2-phase flow and flow due to pore-structure alteration has not yet been investigated, as recognized by Volckaert et. al. (1993). Such a study would likely

involve extensive microstructural analysis. Furthermore, no study of the effects of temperature or clay content (in sand-clay mixtures) has been completed.

2.7 SCOPE OF RESEARCH

The deficiencies in our present knowledge of gas migration in compacted buffer materials discussed in Section 2.6 contribute to the basic need for this research project. The level of understanding of the issue of gas migration in the Canadian nuclear fuel waste industry is not well advanced at present, and so initiation of relevant studies in Canada is timely.

The scope of the research program being reported is as follows:

(1) to review and explain the mechanism for gas migration through porous media such as the buffer materials incorporated in the Canadian nuclear fuel waste design,

(2) to design and fabricate laboratory equipment and procedures for studying gas-breakthrough pressure in compacted clay materials, and

(3) to generate initial test results to confirm the test methodology and to provide a basis for more extensive materials testing programs.

The test parameters chosen for this initial study were limited to specimen material type, and to density and moisture content (or degree of saturation) ranges. Other parameters such as test duration and effects of repeated gas pressure loading were investigated in an introductory manner. The majority of tests have been conducted on illitic clay as its non-swelling behaviour simplifies analysis and understanding of results. Some tests were conducted on sand-bentonite buffer specimens to quantify the suitability of the test methodology to testing this material.

3. EQUIPMENT

3.1 INTRODUCTION

A major objective of this project was to develop equipment and procedures for studying the pressure at which gas at elevated pressure will pass through compacted clay specimens. This equipment was subsequently used for a series of tests on compacted clays. Because no standard procedures or equipment for such testing were available, the equipment design was based on the specific requirements of the testing program. Briefly, the testing program consisted of a series of one-dimensional bench scale tests on clay specimens of approximately 50 mm diameter and 24 mm height with varying moisture contents and dry densities. Specimens were compacted in a rigid test cell and brought to a pre-determined degree of saturation by uptake of water. A gas pressure was then applied at one end of the specimen and was incrementally increased until the membrane action of the clay specimen was overcome and gas flowed freely through the specimen. This was indicated by a pressure response at the downstream end of the specimen. The gas pressure at which free flow of gas occurred was taken as the 'gas-breakthrough' pressure for the specimen.

This chapter describes the developed equipment under three headings which define the three major elements of the test system. Sequentially, these are the test cell, the pressure supply and flow metering systems, and the data acquisition system. The applicable jurisdictional safety standards governing the design of the test system are

discussed. The performance of individual hardware components are described and alternative ideas for equipment design are examined.

3.2 TEST CELL

The gas-breakthrough specimen test cells were designed to meet a number of gas-breakthrough test criteria which were, in turn, designed to simulate the possible geotechnical conditions that may be encountered in the vault proposed for disposal of heat-generating radioactive wastes in Canada (AECL EIS, 1994).

Resistance to gas-breakthrough exhibited by the reference bentonite-sand buffer material proposed for application in the Canadian nuclear fuel waste disposal vaults is expected to be quite high (AECL EIS, 1994). Pusch (1993) has measured gas-breakthrough pressures in bentonite clay on the order of 50% to 90% of the clay swelling pressure. This would suggest that gas-breakthrough pressures of up to 1.0 or 1.5 MPa could be expected for buffer material in the proposed Canadian nuclear fuel waste repository design. Other researchers (Horseman and Harrington, 1994, for example) suggest that gas-breakthrough pressure is controlled by pore-size and capillarity. Based on available information on compacted clay pore-size, gas-breakthrough could occur at pressures as low as a few kPa. Taking into consideration the effects of structured water within compacted clays on pore-size and alteration of specimens used for pore-size distribution studies, this would likely be an underestimate of the resistance of compacted clays to gas-breakthrough. Hence, for safety and

allowing for variation in a number of test variables, such as clay density and pressure gradient, the cells and secondary hardware were designed to contain a maximum gas pressure of 10 MPa.

The newly designed test cells were manufactured by AECL Research as per ASME VIII and were registered with the Manitoba Department of Labour as per CSA B51, as discussed in Appendix A. Design drawings of the cells are included in Appendix B. Because the focus of this research was non-swelling illite clay, only the constant volume cell design was used. A simplified schematic of the constant volume cell is shown in Figure 3.1 for reference and a drawing of the flange detail and a photograph of a partially assembled cell are included in Figure 3.2.

Cells were made of stainless steel, because of its high strength and corrosion resistance. Cells had to be sufficiently rigid to withstand the cell pressures expected without significant deformation which could alter the stress state in specimens or lead to cell leakage. Moreover, stainless steel is a relatively robust material that resists scarification caused by in-cell specimen compaction and specimen extrusion. Specimens were compacted directly in the cell to facilitate the specimen preparation stage and to maximize the adhesion between specimens and the inner-wall of the sleeve. The corrosion resistance of stainless steel makes the cells suitable for long term testing and the use of permeating fluids and gases with varied corrosiveness.

Temperatures in a repository for heat-generating radioactive waste could increase to about 100°C (AECL EIS, 1994), and so features such as thermo-wells to allow for thermal expansion of the cells were included in the cell design to accommodate testing

at elevated temperatures. The materials used for the O-ring seals in the cell were chosen to permit tests at elevated temperatures.

The swelling behaviour of bentonite-based material is important to the performance of engineered barriers. In light of this and the suggestion that gas-breakthrough and swelling pressure are directly related (Pusch, 1993), the cells were designed to measure the swelling pressure exerted by the clay specimens being tested. Two separate cell designs were made. One had an independent piston to accommodate development and measurement of swelling pressure (piston-type cell), and one was of fixed volume to simplify testing of non-swelling clays (constant volume cell). Two constant volume cells and two piston-type cells were constructed.

The constant volume cells were designed with two identical flanges separated by a thick-walled cylindrical sleeve which housed the specimen. Each flange was equipped with three separate ports for gas flow, water flow, and flushing. This allowed the cell leads, filter stones and filter papers (filter stones and filter papers are collectively referred to as 'filters', hereafter) located at each end of a specimen to be either flooded or de-watered, depending on the stage of testing at hand, without dismantling the cell and disturbing the specimen. For example, after the saturation stage of testing was completed and before the gas-breakthrough stage of testing commenced, the leads and filters had to be de-watered to allow non-restricted flow of gas in to and out of a specimen. The piston-type cells consisted of a similar end flange on one end and an independent piston on the other end, free to move in the axial direction with respect to specimen volumetric strain. The flange and piston were similarly separated by a thick-walled cylindrical sleeve. The piston was designed to house a load cell next to

a fixed plate to detect specimen swelling pressure. Ports on the flange and piston on the piston-type cell were similarly designed so that water and gas could interchangeably be introduced into the cell leads and filters. In both cell designs, the sleeve encompassing the 50 mm diameter specimen chamber was 38 mm thick. The constant volume cell sleeves were 90 mm long while the piston-type cell sleeves were 135 mm long.

The cells were designed so that sleeves of varying height could be fitted between the flanges so that specimens of different height could be tested. This allows for the effects of gas pressure gradient to be discriminated from those of gas pressure difference.

Because sealing systems used in similar studies in the past have proven to be problematic (Pusch and Forsberg, 1983, for example), design of the sealing system for the test cells was given special consideration. The sealing system consisted of three rubber O-rings seated on each flange or the piston to seal the space between the flange or piston and the sleeve. The seals were tested over the entire test range to ensure their suitability to both high and low pressure conditions. As well, gas was used as a test medium because the cell would more likely leak gas than water during operation. Preliminary leak tests performed on the cells at room temperature (approximately 22°C) showed that the O-rings prevented gas and water leakage over the designed pressure range of the test cell (i.e. up to 10 MPa). Although not specifically investigated, the seals are expected to perform well at temperatures to 100°C.

3.2.1 Filters

The dimensions of the flanges and pistons were selected so that a filter stone and a filter paper could be installed on both end faces of the specimens. The purpose of the filters was to improve the uniformity of the flow of gas and water over the specimen faces and to minimize the movement of material from the clay specimen into the cell leads under the influence of flowing gas or liquid. Sintered stainless steel filter stones were used because of their corrosion resistance and low air entry value, meaning that they freely allow the flow of liquids and gases. Whatman number 54 filter papers were also chosen because of their low air entry value. Furthermore, these filter materials were readily available and have been successfully used in similar laboratory programs. A gas-breakthrough pressure of 30 kPa was experimentally determined for the filters, indicating that they should not affect the gas-breakthrough data obtained for clay specimens. A network of grooves in the flanges and pistons connected the leads next to the filter to further improve the uniformity of flow entering specimens and to aid in the flushing process. This feature is evident in Figure 3.2.

3.3 PRESSURE SUPPLY AND FLOW METERING SYSTEM

Hardware components were attached to a 152 x 76 x 2 cm (5' x $2^1/_2$' x $^3/_4$") plywood board which was fastened upright to a table (Figure 3.3). A schematic layout of the test board is shown in Figure 3.4 and the various components are discussed in the following Sections.

3.3.1 Flow meter

The flow meter shown in Figure 3.4 was designed and has been commonly used at the AECL Research - Whiteshell Laboratories. A more detailed drawing of the flow meter used on the test boards is shown in Figure 3.5. The flow meter was designed to measure relatively small flow volumes (graduated in hundredths of mL) and is thus well-suited to applications such as hydraulic conductivity testing and the saturation stage in this test program. It was designed to measure flow of liquids and works on the principle of conservation of mass assuming all permeating liquids are incompressible. Basically, the flow meter consists of an upper and lower reservoir connected by a sight buret and is positioned in-line with the system lines. An interface between a coloured column of paraffin oil and a column of water in the sight buret is used to visibly detect and register flow in the test system. A 4-way null valve positioned just below the sight buret allows the reversal of the direction of flow of the oil column within the sight buret, as shown in Figure 3.6. Without this feature, the entire oil column would eventually travel into one of the reservoirs and out of the range of the sight buret, thus making it necessary to stop flow and to disrupt a test to continue measurement. The 4-way valve allows for continual measurement without having to stop and re-position the oil column.

As previously mentioned, the flow meter is best-suited for the measurement of relatively low rates of liquid flow. For example, the hydraulic conductivity of illite and buffer for the dry density ranges tested could be less than 10^{-8} m/s and 10^{-11} m/s, respectively. For the basic task of measuring inflow volumes of water during the

saturation stage of testing, therefore, the present flow meter design was adequate. A complete mass balance of the gas phase was not included as part of the analysis in this research program. This would require a gas flow measurement device capable of measuring both small and large gas flow rates because of the expected nature of the gas migration mechanism in compacted clays. In short, gas migration in a compacted clay specimen could progress by 2-phase gas flow with relatively low flow rates, or even by slower diffusion processes, but the flow rates could increase suddenly due to alteration of the soil fabric and creation of preferential pathways for gas flow through the clay. These processes are more thoroughly discussed in later chapters. A specialized flow meter device would be required to detect both ranges of flow rates. The author is not aware of any commercially available technology for measurement of such ranges in gas flow rate.

Initially, a system for measuring the volume of gas flow into specimens was incorporated into the test board design. The proposed system used the present flow meter with bladder-type accumulators just upstream and downstream of the flow meter in the gas lines (Figure 3.7). In this system the upstream bladder-type accumulator would separate the supply of gas from the water within the flow meter, but would transfer the gas pressure to a water pressure through the flow meter. The downstream bladder-type accumulator would then similarly convert the water pressure back to gas pressure so that the volume of gas flow into a specimen could be detected by the flow meter. Hence, volumes of gas flowing into a specimen could be determined and compared to volumes of gas collected on the outflow side of the specimen so that a mass balance of gases could be determined. Parker Fluidpower Model AB10B3T1W1 bladder-type accumulators were to be used in this initial design. However, this scheme

would not directly solve the problem of having to measure gas flow with a sudden increase in flow rate associated with gas-breakthrough. Moreover, when this flow measuring system was initially tested, the bladder-type accumulators showed resistance to the transfer between gas pressure and water pressure across the rubber membrane housed within the accumulator so that gas flow into the specimen could not be properly controlled or maintained. In light of these operational limitations, and because of the complexity of the gas flow mechanism in compacted clays and the associated range of flow rates, a simplified system that did not include a mass balance of the gas was used. Only absolute gas pressures were calculated for gas inflow and gas collection.

3.3.2 Accumulators

Two accumulators were used on the test board for two separate applications. The larger accumulator, a 1000 mL Whitey sample cylinder, was used as a supply of water for specimen saturation. This accumulator is shown as the 'gas-water interface accumulator' in Figure 3.4 and was simply a hollow stainless steel cylinder. This particular model was chosen because of its availability and low cost and because it met the relevant safety requirements for the system. Its capacity had no effect on test procedures or results except that it was sized so that several tests could be completed without requiring accumulator recharge. Because it served as a gas-water interface, a longer bottle with a smaller diameter may have been more suitable to this application by reducing the area of contact between the gas and water phases, thus minimizing the amount of interaction between the two phases. As an alternative, a thin film of oil

could have been placed on the water to reduce the interaction. Minimal interaction between the phases is desirable because the water from the accumulator is being used to saturate specimens and gas dissolved in water could come out of solution once within the pore-space of a compacted clay specimen, leaving the specimen only partially saturated.

The smaller accumulator in Figure 3.4, a 300 mL Whitey sample cylinder, was used as a 'gas collection accumulator' in the gas collection circuit. This accumulator was used to increase the total volume of the outflow lines so that several pore-volumes of gas could flow through a specimen in a test without being interrupted by a venting procedure. It was sized sufficiently small that a reasonable amount of gas passing through a specimen would show the full pressure response with the instrumentation used. Its exact capacity and dimensions had no effect on testing, and it was chosen primarily based on its availability and low cost and because it met the relevant safety requirements.

Several related studies (Lineham, 1989, for example) used an accumulator to bubble the gas source through water before it entered the specimen so that a water-saturated gas source could be used for gas-breakthrough testing. This would reduce the tendency of the permeating gas to dry its host clay specimen and would minimize the amount of gas going into solution when in contact with pore-water. For the sake of simplicity, these effects were not considered in this research program, although this issue may merit future investigation.

3.3.3 Pressure regulators

The pressure regulator fitted to the gas source tank (regulator RA in Figure 3.4) was a type commonly used with commercially available argon gas source cylinders.

A Matheson Model 3030-580 pressure regulator was used for the inflow circuit on the test board (regulator RB) while a Matheson Model 8-250 pressure regulator was used for the gas collection circuit (regulator RC). These two particular models were chosen based on their availability. Both of these regulator types had a maximum allowable inlet pressure of 3000 psi (approximately 20 MPa). The regulators were a single-stage type where the pressures were dropped from inlet to outlet pressure in one step; a two-stage regulator would drop the inlet pressure to near the outlet pressure in a first step and would then drop the remaining pressure down to the outlet pressure in a second step, thus offering better control of outlet pressures. It was difficult to set the outflow pressures using the one-stage regulator type, and as a result the targeted pressures were often exceeded, temporarily. The regulators had to be adjusted several times before the target pressure was achieved. With some care, however, the pressures could be controlled sufficiently well that the quality of testing was not affected. Target pressures were maintained within 1 percent of the test value. This degree of accuracy was acceptable. Of the two regulator models chosen, the Model 8-250 provided better control.

When sudden, high gas-breakthrough pressures were reached and a large volume of gas surged through a specimen into the collection circuit, the regulator often did not

reset the inflow pressure to its preset value. While this did not compromise the results in this testing program, it may affect results in future studies and should be considered during the design of those studies. Because the regulators did not have self-bleeding capability, a venting valve was designed and fitted into the system just downstream of each regulator (valves 23 and 24) so that inbuilt pressures could be relieved.

In general, the regulators proved adequate for the purpose of the tests described in this report. However, it may be advantageous in future endeavours to use a self-bleeding regulator that can more easily be set at a given pressure and will hold its set pressure during flow rate changes.

3.3.4 **Bourdon gauges**

A Bourdon dial gauge was placed alongside the pressure transducers in the gas inflow circuit (at pressure transducer TA in Figure 3.4) and in the gas collection circuit (at pressure transducer TC) as a backup to the electronic pressure transducers for measuring gas inflow pressure and gas outflow pressure, respectively. For safety, the dial gauges offered a direct measurement of line pressures and could be relied on if the electronic system failed. Dial gauges were included in the present design because the electronic measuring system used had been newly implemented. Solfrunt (USG) 0-10000 kPa dial gauges were chosen for this application. As long as a reliable electronic system is used, the dial gauges can be removed from future test board designs.

3.3.5 Valves

Three types of valves were used in the test board design. All valves were stainless steel for corrosion resistance and adhered to the safety requirements of the system. The majority of in-line valves used were constant volume (null) valves manufactured by NUPRO (Model SS-2P4T). Other in-line valves used were needle valves manufactured by Whitey (Model SS-ORS2). A third type of valve used was a 4-way (null) valve that changed flow directions through the flow meter. Null valves were selected with water and gas flow measurement in mind. Adjustment of the null valves did not involve any inherent volume change in the system, and thus facilitated the measurement of small volume changes in the tests. Needle valves were used where a controlled flow rate was required or where valve adjustment would not affect volume measurements. For example, valve 7 was only adjusted between tests, when volume measurements were not being recorded. Moreover, operations involving valve 7 required a controlled flow rate through the valve, and so a needle valve was suitable at this location.

The procedures adopted for this research program did not include measurement of the volume of gas flowing into specimens during the gas-breakthrough stage of testing, and, so, many of the constant volume valves could have been replaced by less-expensive needle valves. As well, during the saturation stage of testing once the lines including the cell leads were set at the backpressure and a flow meter base reading was taken, only the final valve opened between the specimen and the flow meter (valve 9) was required to be a constant volume valve. Needle valves could not be

adjusted during testing that included flow measurement, as this would affect the flow readings.

Operation of the 4-way valve to control the direction of flow through the flow meter is explained in Section 3.3.1. There was no volume change in the lines associated with the adjustment of the 4-way valve, and thus its operation did not alter flow meter readings.

3.3.6 **Gas supply**

A standard, readily available argon gas cylinder was used as a source of gas pressure. Argon gas was chosen for its inert behaviour. Furthermore, argon is relatively less soluble in water than other readily available gases such as nitrogen so that the gas and liquid phases could be better separated in the system lines and specimen. This would minimize the quantity of gas dissolved in the water so that specimens could be fully saturated.

3.3.7 **Water supply**

Distilled, de-aired water (DDW) was chosen as the permeating fluid to simplify the analysis of physico-chemical processes acting in a specimen. The DDW was assumed to be pure, although it likely took on salinity from dissolved salts within the clay. Barden and Sides (1970) explain that osmotic suction can be neglected when the pore-water is DDW, and so the matrix suction can be equated to the total suction

of a specimen.

3.3.8 Safety features

Technical support was provided by AECL Research to ensure that the designed apparatus met all jurisdictional safety requirements. A summary of the safety requirements for the system are listed as notes 1 to 9 on AECL drawing A1-61W08-F1 in Figure 3.8. Based on design requirements of the relief valve implemented, the maximum operating pressure of the system was 10 MPa and must operate between 15°C and 35°C. For tests at higher temperatures, this range will need to be modified. Distilled water, nitrogen or argon gas were the only flow media allowed in the system lines and fittings. All tubing and fittings were to be stainless steel for corrosion resistance and were rated for the design pressure of the system. Connections were to be commercially available Swagelok fittings with ferruled threads where possible. All pipe threads required sealant tape (Teflon tape) and all equipment was to be properly fastened to the test board. Each component on the test board required a Canadian Registration Number (CRN) for the Province of Manitoba as per Canadian Standards Association specifications (CSA B51).

Design specifications required the test board to be subjected to a pressure test for leaks before use. Appendix C shows the documentation and results for the leak tests performed on the test boards by personnel in the AECL Research Quality Assurance Branch at the Whiteshell Laboratories. The leak tests were initially to use distilled water as a pressurizing medium. An amendment was made to this requirement so that

gas could be used to pressurize the system as it would be difficult to remove the moisture from the system after completion of a fluid leak test and the use of gas during testing would represent a more hazardous situation. The leak tests were performed at gas pressures up to 12.5 MPa. The flow meter was bypassed during the leak tests because of the brittle nature of the sight buret. Flow meters of this design had passed hydrostatic leak tests above 10 MPa in the past at AECL Research (Dixon, D.A, personal communication). The flow meter was pressure tested separately to 10 MPa. This amendment, as discussed in note 4 of Figure 3.8, was permitted on condition that the standard practice of positioning a plexiglass shield over the flow meter sight buret was continued.

The primary safety feature on the test board was the safety relief valve. The purpose of the relief valve was to vent gas to the atmosphere if the source tank delivered gas above the maximum design pressure. The relief valve, a Teledyne Farris Engineering Model 274OUL, was factory pre-set to vent at 10 MPa. Note 9 of Figure 3.8 states that any portion of the system downstream of the relief valve could be modified, as long as modifications did not violate other design specifications, which they did not.

A final safety feature of the test boards was a plexiglass shield which was suspended in front of the equipment to cover all fittings and tubing and to stop the travel of any loose fittings in the case of a sudden pressure leak.

3.4 DATA ACQUISITION

Water flow information was collected and recorded through periodic readings of the oil column position as shown by the flow meter sight buret. Pressure values were collected automatically using a software package and an analog-digital converter. The software package used was LabTech Notebook DOS Version 7.3.0 which was loaded on a 386 DX IBM-compatible personal computer. A PC-LabCard Model PCL-818 analog-digital converter card with programmable gain was used to convert analog signals from the pressure transducers to digital signals which could be processed by the computer. LabTech software was chosen because it was currently used and immediately available at the University of Manitoba and at AECL Research and technical support could be provided by other laboratories on site. A switch board from PC-LabCard was used to help to organize the data acquisition wiring. A 2 ampere, 10 volt DC power supply was used as an excitation voltage supply in accordance to requirements for the pressure transducers. The LabTech software and PCL-818 analog-digital converter card were also suited to temperature reading that may be involved with subsequent testing.

Micro Gage Model P-102 linear gain pressure transducers were chosen to read pressures, based on their reliability during similar testing programs. The transducers and LabTech data acquisition system were calibrated with a dead-load calibration apparatus supplied by the University of Manitoba geotechnical engineering group. For calibration, signals from the pressure transducers were shown against the known supply pressure on the dead-load calibration apparatus, the data was fitted using linear

regression techniques, and the slope and offset were calculated and used to convert the signal (mV) to engineering units for pressure (kPa or MPa). Set-up of the LabTech software is further discussed in Section 4.4.

Each pressure transducer was calibrated before the test program began (Figure 3.9) and after the tests were completed (Figure 3.10). These figures show the dead-load on the calibration apparatus in psi and kPa and the corresponding mV signal from the pressure transducers. The linear regression calculations for these data are given and pressure readings in kPa that are based on the mV signal and the regression coefficients ('scale factor' and 'offset constant') are also shown in Figures 3.9 and 3.10. A comparison of the calibration curves before and after testing is shown in Figure 3.11. In the upper range of pressure, say 5 to 10 MPa, the pressure readings differed less than 1.5 percent for a given transducer mV signal based on calibration data from before and after testing. In the lower range of pressure, say less than 1 MPa, the pressure readings differed by up to 13 percent, but were generally less than 5 percent. All three pressure transducers from a test board were calibrated simultaneously. The most important test data reported in this document were obtained at relatively high pressures, however, and so the differences between the calibration data used would not significantly affect results. Test results are based on data obtained from calibration done before testing (Figure 3.9).

4. TESTING PROGRAM AND TEST PROCEDURES

4.1 INTRODUCTION

This chapter first describes the soils that were tested. Next, the general test program and the types of tests are discussed. Finally, the test procedures are explained with a full description of the use of the different components mentioned in Chapter 3. In the context of the latter, the author is not aware of any universally accepted standard methods for measuring the gas-breakthrough characteristics of compacted clay materials. The procedures adopted for the testing program described were based on those used by other researchers (Pusch and Forsberg, 1983; Lineham, 1989; Volckaert et. al., 1993), which were modified to meet the specific requirements of this test program. The procedures for specimen preparation and specimen saturation followed procedures used in past testing at AECL Research and the University of Manitoba. For reference, each step of specimen preparation and testing is described and the purpose of the various steps is explained. The procedures are also shown in Appendix B in a checklist format which can be used as an operational manual for the new equipment developed for the program.

4.2 TEST MATERIALS

Tests were completed to measure the differential gas pressure across compacted clay

specimens at which gas rapidly permeated through the specimens (gas-breakthrough pressure). Forty six such tests were conducted on hydrous mica clay, known as illite, while six tests were completed with mixtures of sodium-bentonite and sand, known as buffer. Illite was chosen as a test material because its geotechnical properties are relatively easy to characterize and it thus serves as a good starting point for studies of more complex materials, such as buffer, which was chosen because it is being proposed for use in a program by AECL Research for disposal of nuclear fuel waste (AECL EIS, 1994).

4.2.1 Illite

The illite used was a commercially available crushed illitic shale plasticizer known as Sealbond, manufactured by Canada Brick. It originates from a Dundas shale member of the Georgian Bay Formation (Ordovician) with a stratigraphy that has been described as "soft, grey, illite-bearing shale with moderate chlorite and no detectable expanding minerals, containing narrow, discontinuous limey and sandy interlayers" (Dixon and Woodcock, 1986). The Sealbond illite was available as a fine, grey powder and was packaged in 22.7 kg (50 lb.) bags. The moisture content of the illite as stored in the bags was approximately 1.3%. Testing yielded a value of 2.76 for specific gravity. This value is similar to that used by Dixon et. al. (1985). ASTM Modified Proctor compaction tests showed a maximum dry density of 2.04 Mg/m^3 at an optimum moisture content of 12.0% whereas Dixon et. al. (1985) found optimum compaction conditions at approximately 1.93 Mg/m^3 and 13.0% moisture content. Table 4.1 summarizes the physical and engineering properties of illite (Dixon and Woodcock,

1986).

4.2.2 Buffer

The buffer was prepared from a dry powder sodium-bentonite and silica sand. The sodium-bentonite (Avonseal) originates from Avonlea Mineral Industries Limited (Saskatchewan) and is mined from the middle seam of the Bearpaw Formation (Upper Cretaceous) which has been described as "greenish grey bentonite" (Dixon and Woodcock, 1986). The silica sand, a crushed quartzite, originates from Indusmin Limited. The clay and sand constituents were prepared and mixed to a 1:1 dry mass ratio as described by Dixon et. al. (1994). The classification and associated properties of the buffer are described extensively by Dixon et. al. (1985). Typical values for physical and engineering properties of the clay and sand constituents of the buffer material are shown in Table 4.1 (Dixon and Woodcock, 1986).

4.3 TEST PROGRAM

As mentioned earlier, the focus of this test program was illite clay, on which the majority of testing was completed. Forty-six tests were performed on illite while six tests were performed on buffer material. The buffer tests were completed to provide an indication of the suitability of the apparatus for testing buffer and to provide guidance for future research. Gas-breakthrough pressures for the illite specimens were measured: (1) on compacted specimens that were saturated with water, and (2)

on unsaturated specimens immediately after compaction. The gas-breakthrough pressures of the buffer material were only measured for specimens after compaction, unsaturated, with specimens which varied in their degrees of saturation. In addition to testing the different materials and the effects of moisture content, dry density and degree of saturation, series of tests were conducted to assess different testing techniques. Some effects of test duration and repeated testing were also measured. A small number of tests were carried out to ensure uniform moisture content and dry density in compacted specimens. These latter tests are referred to as the quality control (QC) tests.

Yarechewski (1993) studied the effects of varied lift height on density in buffer specimens compacted using the same compaction equipment used in this test program. He found the effects significant, and formulated a method for appropriate correction of the effects of lift height variation. The effects were neglected in this test program because test specimens were approximately one-quarter the height of those tested by Yarechewski (1993), and so the effects should decrease by a factor of four. Furthermore, Yarechewski (1993) studied bentonite clay and clay-sand mixtures which would be much more active than illite, and so the effects of lift height variation should be more noteable in the bentonite. The QC test specimens were statically compacted using the same procedures used for the specimens tested for gas-breakthrough, except the QC test specimens were extruded before undergoing a saturation or gas-breakthrough test stage.

It is difficult in practice to compact a specimen at or near full (100%) saturation.

Moreover, the structure of clay compacted at 100% saturation will vary from that in clay compacted at, say, 85% saturation and then brought to 100% saturation by the uptake of water. Hence, the specimens for the tests on saturated clay were compacted to a specified density and degree of saturation at a known moisture content and were brought to full saturation through exposure to a source of water at a specified backpressure. Water for saturating specimens was supplied from both ends of the specimen. Once a specimen was determined to be at the desired degree of saturation, the supply of water was shut off and the gas-breakthrough stage of testing was initiated. At this point, the water supply on either side of the specimen was replaced by a gas supply at the same pressure as the maximum water pressure used to saturate the specimen. The gas pressure on the inflow side of the specimen was then increased incrementally until gas was able to pass through the specimen, as indicated by an increase in gas pressure on the gas-collection side of the specimen. For the tests on unsaturated clay, the saturation stage was omitted.

The saturation stage of testing typically lasted 1 day and was deemed to be complete when flow of water into the specimen ceased. At this point, the volume measurement from the flow meter was compared to the theoretical specimen pore-air volume to verify the degree of saturation of the specimen. For the gas-breakthrough stage of testing, the time period for each incremental increase in inflow gas pressure was arbitrarily chosen as five minutes. Therefore, gas-breakthrough tests lasted from several minutes to a few hours, depending on the magnitude of the gas-breakthrough pressure for the given specimen.

Targeted initial test conditions for specimens were based on three control variables - dry density (ρ_d), moisture content (w) and degree of saturation (S). The three variables are related such that if any two are known, the third can be determined mathematically. The relationship can be derived from a fundamental soil phase diagram, as shown in Figure 4.1 (Craig, 1989). The ranges of ρ_d, w and S studied with illite specimens are shown in Figure 4.2 (test identification numbers are given) and were set to coincide with the likely conditions that similar materials would experience if implemented as a barrier material in a nuclear waste repository. Test conditions were similar to those in previous related tests (Dixon et. al., 1985).

The property ranges for the illite were set as:

$$1.80 < \rho_d < 2.15 \text{ (Mg/m}^3\text{)},$$

$$10.0 < w < 17.0 \text{ (\%), and}$$

$$55 < S < 100 \text{ (\%)}.$$

Buffer specimen conditions were based on the proposed buffer conditions in a nuclear waste repository scheme and on previous buffer tests. The targeted dry density for buffer specimens was 1.67 Mg/m^3 and the targeted moisture contents ranged from 11.4% to 20.4%. The relationships derived in Figure 4.1 were used to prepare groups of tests so that one of the three control variables remained constant while the others varied, making it possible to study the effects of each individual variable on gas-breakthrough pressure. Table 4.2 shows the target data for tests which are based on these control variables. The as-compacted data, based on moisture content tests on

material that specimens were taken from, is also given for comparison. Data for percent difference between targeted and compacted moisture contents given in Table 4.2 show that, on average, compacted illite specimens had moisture contents 2.68% lower than the targeted values. (The percent difference is calculated as the difference between one measurement and the mean measurement, divided by the mean measurement.) The buffer specimens were, on average, 1.42% drier upon compaction than targeted values. Data for percent difference between targeted and compacted moisture contents for individual tests show relatively high deviations, but because it was not imperative that the targeted values be achieved, the degree of accuracy is acceptable.

The compacted moisture contents and measured inflow data were combined to calculate the moisture content for specimens after the saturation stages of testing and before they were tested for gas-breakthrough. Moisture contents were also measured for specimens that had undergone gas-breakthrough testing and had been extruded from the cell. These data are presented and discussed in Chapter 5 as part of the test results.

4.4 DATA ACQUISITION

The flow of water into specimens during the saturation stage of testing was recorded manually, while pressure changes were recorded using the automated data acquisition system described in Chapter 3. The LabTech Notebook software was set up so that

all data collection could be done in a single workspace, the on-screen area where a data acquisition system is programmed - the Labtech equivalent to a DOS file. A schematic of the workspace and the computer screen layout are shown in Figure 4.3. LabTech interrogated and transmitted the transducer signals every 0.1 seconds. The software then took the last 10 readings and calculated an average. In other words, every second the software calculated the average of the 10 readings taken within the last second. This method of averaging a number of readings and only reporting the averaged reading decreased the amount of noise in the data. The averaged pressure transducer reading was automatically linearized, based on calibration data for that pressure transducer, so that the information relayed to the screen and to the file was in engineering units for pressure rather than voltage. The linearized data were sent to the computer screen every second so that updated information was displayed. The data were written to the screen rapidly enough that the displayed information could be used to monitor the pressure settings as valves were adjusted. The same data were stored in an electronic file. Data for saturation tests were compiled and stored every 4 minutes while gas-breakthrough data were compiled and stored every 10 seconds.

The computer screen showed a reading (in kPa) for each pressure transducer used and plotted the data as pressure versus elapsed time. Elapsed time and the excitation voltage from the power supply were also displayed. Bourdon gauges on the test board were used as a backup to the pressure transducer readings. Data files were set up in MS-DOS .TXT format and included a heading to identify the test followed by columns of data for the elapsed time and for each of the pressure transducers. The data were then imported into a spreadsheet (Quattro-Pro 5.0 for Windows, by Borland

International, Inc.) for analysis and finally imported into a graphics software package (SlideWrite Plus for Windows, by Advanced Graphics Software, Inc.) for plotting.

4.5 SPECIMEN PREPARATION

4.5.1 Mixing

Mixing techniques for the specimens were similar to those used by other researchers at the University of Manitoba (for example, Yarechewski, 1993). Once the clay and sand constituents of the buffer had been mixed, the specimen preparation procedures for the illite tests and buffer tests were similar, and so the following sections describe the preparation of both materials.

Allowing for losses and material required for moisture content tests, approximately 150 g of bulk material was required for each compacted gas-breakthrough specimen. The clay powder, assumed to have 0% moisture content, and distilled, de-aired water (DDW) were weighed out in portions that, when mixed, would yield the target moisture content with approximately 150 g of mixed material for each specimen that would be prepared from the mixed batch. Material for any number of specimens could be mixed at one time.

Water was gradually stirred manually, with a spoon, into the clay powder in a medium sized steel mixing bowl. To limit evaporation, material was mixed in a curing room set

at approximately 4°C. The material was typically mixed for 5 to 10 minutes until the majority of large peds had been broken up. The mixture was then sealed in two bags, one inside the other, and stored in the curing room for at least 1 day. Prior to use, the mixture in the bag was shaken and kneaded at room temperature (approximately 22°C) to break up any remaining large peds. The mixture was allowed to stabilize at room temperature before the bags were opened.

4.5.2 Compaction and cell assembly

Immediately prior to use, the moisture content of the material was tested. Because the results of the moisture content tests were not available at the time of compaction, material being compacted was assumed to be exactly at the targeted moisture content. Moisture content specimens were taken at the same time that a specimen was compacted to minimize the discrepancy between actual and calculated moisture contents. Four equal portions of the material were weighed out for compaction to a known volume in the cell specimen chamber, to the predetermined target dry density at the assumed moisture content. Because results of the moisture content test usually deviated slightly from the assumed value, the dry density and degree of saturation achieved were also slightly different than the targeted values (Table 4.2). The deviations in moisture content were usually minimal, however, and only contributed to minor deviations in dry density and degree of saturation . Moreover, it was not essential to the test program to have specimens at an exact density, moisture content or degree of saturation because ranges of these parameters were tested.

The four equal portions of material weighed out were statically compacted as four separate layers directly in the cell. The cell sleeve and one flange were secured by the four Allen bolts and a filter was placed in the cell as shown in Figure 4.4. The rubber O-rings on the flange were lightly greased to both improve their seal and to ease the subsequent cell dismantling process. The cell was positioned below the hydraulic compaction ram. The ram was then extended to the top of the filter on the flange in the sleeve. The reading on the displacement gauge was noted.

The ram was extracted and using the ram, the first layer of material was pressed in the cell to one-quarter of the desired specimen height. Taking into account the geometry of the cell and the filters, the total specimen height for the constant volume cells was approximately 24 mm. The ram was retracted so that the surface of the compacted lift could be scarified with a knife, and the second lift was added. The second and third layers were compacted to the same thickness as the first and their surfaces were similarly scarified. The fourth layer was similarly compacted, but its top surface was not scarified. A filter was placed on the top lift and the top flange of the cell was fastened to the cell sleeve using four Allen bolts. The six safety bolts around the cell were then tightened in star formation to ensure that the flanges remained properly seated in the sleeve. The cell was attached to the test board immediately after it was assembled. This operation required the procedure described in Section 4.8.1.

4.6 PRELIMINARY TEST PROCEDURES

Testing was controlled by the various valves on the test board, and so the procedure description is based on the use of these valves. Figure 3.4 shows the different components of the test board and can be used as a key for the procedures. The valves in Figure 3.4 are numbered from 1 to 24 for identification. Figure 3.5 shows a detailed drawing of the flow meter and how it is connected to the test board. Figure 3.6 shows how the 4-way valve on the flow meter can be used for setting the direction of flow through the flow meter.

The following description of procedures assumes that the test apparatus is built as shown in Figure 3.4 and that the apparatus has passed an approved safety pressure test. Furthermore, it is assumed that all components of the test board are set at atmospheric pressure and contain no fluid and that all valves are in the closed position.

Several preliminary procedures had to be undertaken to prepare the equipment. Once these steps were completed, as described in Sections 4.6.1 to 4.6.7, several specimens could be tested using the test board with minimal preparation between tests. This section describes these preliminary steps of gas-breakthrough testing. It is appreciated that the following sections are presented in considerable detail. This has been done to facilitate learning of test technologies by subsequent researchers.

4.6.1 **Saturating the flow meter**

The flow meter on the test board worked on the principle of conservation of mass with displacement of a column of oil set in water. During flow measurement, pressure in the

flow meter was constant apart from minor changes in head due to density differences between the oil and water, and so the fluids in the system could be assumed to be incompressible. Therefore, a fixed volume of water flowing into a specimen was reflected by the displacement of that same volume of fluid in the flow meter. The flow of fluid in the flow meter was monitored as a displacement of the oil/water interface along a buret that was graduated in units of volume.

To minimize possible effects of compressibility of water or oil on measured flows, the flow meter was de-aired prior to use. To achieve this, the flow meter was first removed from the board. The bottom inner nut on the flow meter and the junction near valve 8 were then unfastened to separate the flow meter from the system lines. The various screws and clamps holding the flow meter against the test board were also removed. The flow meter was filled with DDW.

A source water bottle with a flexible tube nozzle was used to fill the flow meter under syphon flow. All ports on the flow meter (valves 7 and 8, the four nuts on the ends of the flow meter and the open port on the junction) were closed. Water was flushed through the source bottle to expel any existing bubbles in the nozzle. The bottle was then attached at valve 7, allowing flow to continue from the bottle to ensure that minimal air was trapped at the connection. The source bottle was positioned higher than the flow meter at all times to ensure that air-free syphon flow was maintained. Once the lid on the source bottle was tightened, the bottom-inner nut on the flow meter was opened and hand pressure was applied to the source bottle to initiate syphon flow. When water appeared to flow freely out the bottom-inner nut, the lid on the source

bottle was loosened and the hand pressure on the bottle was relieved. The bottom-inner nut was then closed once a steady flow of water was allowed to pass from the source bottle. Similarly, the bottom-outer nut, the top-outer nut, the top-inner nut, valve 8 and then the temporary nut on the junction were opened then closed, leaving the flow meter fully saturated. The buret was monitored to detect the movement of any air with the water while the top openings were flushed. As well, the flow meter was gently tapped, rotated and tilted to dislodge any air bubbles attached to the inner walls. Once the flow meter was properly filled, valve 7 was closed to seal the system.

4.6.2 Saturating the lines leading to the flow meter

The next preliminary step was saturating the water lines in the system other than those in the flow meter. This was done by providing a supply of DDW through valve 10, using a source bottle similar to that used to saturate the flow meter. The water supply was again positioned above the test apparatus to provide syphon flow of water through the lines. Note that the flow meter was still detached from the board.

Any air bubbles in the flexible rubber tubing between the water source bottle and valve 10 were removed. Next, the tubing was attached at valve 10, ensuring there was a good seal between the flexible tubing and the stainless steel tubing. Valve 10 was finally opened.

Valves 6 then 4 were opened with the 4-way valve in the downward position until water flowed out the junction near valve 8. The 4-way valve was then switched into the

horizontal position until water flowed out the open port where the bottom-inner nut of the flow meter was detached. Valves 4 then 6 were then closed.

Valve 5 was opened with the 4-way valve still in the horizontal position until water flowed out the junction near valve 8. The 4-way valve was then switched to the downward position and water was allowed to flow out the bottom-inner port on the flow meter. Valves 5 then 10 were closed. The lines directly upstream and downstream of the flow meter were now saturated.

4.6.3 **Flooding the accumulator**

The accumulator discussed in this section is the one shown in Figure 3.4 as the 'gas-water interface accumulator'. It is the larger of the two accumulators on the test board and acts as the source of water that flows into the specimen and as a gas-water interface. Although there is no physical barrier to prevent the diffusion of gas in water at the interface, the relatively low solubility of argon in water aids in separating the two phases.

Valves 10, 6, 3 then 2 were opened in sequence and water was allowed to enter the lines until the accumulator was full, as indicated by flow of water out of valve 2.

To check that the accumulator was filling, a small amount of a commercially available soapy solution gas leak detector was used on the nozzle at valve 2. Valves 2, 3, 6 then 10 were closed in sequence once the accumulator was filled.

4.6.4 Flooding pressure transducer TB

Pressure transducer TB is used to detect water pressure, and so its housing had to be flooded. Because it is attached to a dead-end line, however, the transducer had to be detached to ensure no air was trapped in the transducer housing while flooding it. To do this, valve 10 was opened slightly, and transducer TB was detached from the lines. Having valve 10 slightly open maintained a slow stream of water out the open port at TB so no air could enter into the lines. A syringe was used to carefully inject water into the transducer which was then re-attached to the line while carefully ensuring that no air was trapped either in the transducer or the open port when tightening the nut. Valve 10 was then closed.

4.6.5 Saturating the leads to the cell

The lines leading to the cell also had to be saturated so that an accurate measurement of water inflow could be achieved.

Valves 10 then 9 were opened. Valve 17 was opened and then closed once a full stream of water flowed out the port. Valve 18 was similarly opened and closed. Next, valves 9 then 10 were closed, leaving all water lines in the system fully saturated.

4.6.6 Re-attaching the flow meter

The flow meter had to be attached to the test board without the introduction of any air

into the system. It was transported to the test board fully sealed. Valve 10 was opened slightly (with the water source bottle still attached). Valve 5 was then opened and a slow stream of water was allowed to flow through it with the 4-way valve in the downward position and out the open bottom-inner port where the flow meter was detached.

The bottom-inner nut on the flow meter was then opened. (No water should escape if this is the only open port on the flow meter.) The flow meter was attached to the test board at the bottom-inner nut. Having valve 10 slightly open and allowing a slow stream of the water through the open port when tightening the nut prevented air from entering the system during this step.

The temporary nut on the flow meter at the junction near valve 8 was then opened. Water automatically flowed up through the flow meter buret from the source bottle and out of this open port. The flow meter was attached at the junction in the same manner that it was attached at the bottom-inner nut. Finally, the flow meter was secured to the test board and valve 10 was closed. To further ensure that the flow meter was fully saturated, water was cycled from the source bottle, through the flow meter and into the accumulator. The 4-way valve was placed in the horizontal position and valves 10, 5, 4, 3 then 2 were opened in sequence. Water was allowed to flow out of valve 2 for the period of time required for the volume of an entire bottle of water to be cycled through the system. During this process, the flow direction through the flow meter was periodically reversed by switching the position of the 4-way valve between the downward and the horizontal positions to dislodge any small air bubbles attached to

the inner walls of the flow meter.

Valves 2, 3, 4, 5, then 10 were closed in sequence when this procedure was completed.

The possible presence of air in the system was continuously monitored in the flow meter buret during the progress of tests. If air was detected, some or all of the previous steps were repeated.

4.6.7 **Charging the flow meter with oil**

With the system filled with DDW, the buret in the flow meter was charged with oil. The following procedures were used to install a clean, uniform column of oil in the flow meter. The procedures were best completed by two people.

The coloured oil was placed in a source bottle with a rubber tubing nozzle and positioned above the test board when being introduced into the flow meter. The oil source bottle was attached at valve 8 with a proper seal between the flexible tubing and the stainless steel tubing.

The lid on the source bottle was tightened and, maintaining constant hand pressure on the bottle, valve 8 was opened slightly, followed by the top-inner nut on the flow meter. A slow, steady flow of water was maintained to expel fluid from the open port. Eventually, oil from the source bottle reached the top-inner nut and began to flow out

the open port. This was allowed to continue until a steady flow of oil, uncontaminated by droplets of water, flowed out the open port. At this point, the open port on the flow meter was closed, valve 8 was closed, the lid on the source bottle was loosened and the pressure on the bottle was released. Similarly, the top-outer nut was opened then closed when clean oil flowed out the open port. Next, the source bottle was again pressurized and valve 8 was opened. This time, valve 7 was opened slightly, as well. Water was allowed to flow out at valve 7 until the oil was drawn approximately half way down the buret. Valves 7 then 8 were then closed and the source bottle was removed.

If the oil column in the buret was not continuous with a uniform meniscus, the entire procedure of flooding the flow meter and charging it with oil was repeated.

4.7 MAINTENANCE

Some routine maintenance was required to ensure that the test board remained in proper working order between tests. For instance, all connections were monitored for leaks using a commercially available leak detector. Leaks could occur at any fitting but were most frequent at fittings that were often adjusted, such as at the leads to the cell at valves 17 through 22. All venting nozzles (at valves 2, 10, 16, 23, and 24) were checked for leaks as well to ensure that they were fully closed. While most routine maintenance was straight forward, two of the more intricate maintenance operations require description.

4.7.1 Cleaning the flow meter

An error in adjusting the valves could cause a surge of flow through the flow meter. This caused the oil column to break up into discrete sections making it difficult to read flow volumes accurately. In this event, the flow meter had to be dismantled and cleaned. To do so, the flow meter was detached from the test board and flooded largely as described in Section 4.6.1. At this point, however, the flow meter was full of water and oil and a modified procedure was required. All valves were closed and, as in Section 4.6.1, the flow meter was first detached from the test board at the bottom-inner nut. Once the nut was opened, a temporary cap was placed on the open port on the flow meter. Then, the flow meter was detached at the junction near valve 8 and the open port was closed off with a temporary cap. With the flow meter fully detached from the test board, the temporary caps were removed and the water and oil was allowed to flow out of the flow meter and was disposed of.

In order to fill the flow meter with water and to install an uncontaminated column of oil, all the oil adhering to the inner surfaces of the flow meter had to be removed. To do this, first ordinary tap water was injected into the flow meter at a high rate through valve 7. The water was flushed out the rest of the ports on the flow meter, one at a time. Extra care was taken to ensure that the sight buret was free of oil by opening the top-outer and bottom-outer nuts on the flow meter and flushing a strong stream of water through the buret. This was repeated several times with the direction of flow being reversed. Methyl hydrate, which aids in breaking up the oil, was also flushed through the flow meter. Water was again flushed from valve 7 and out each of the

ports to remove the methyl hydrate and any remaining oil.

Once the oil and methyl hydrate were removed, the flow meter was flooded with DDW. Before the flow meter was re-attached to the test board, the lines directly downstream of the flow meter on the test board were checked to be free of oil contamination. To do this, a water source bottle was attached at valve 10 and, with the 4-way valve in the downward position, water was allowed to flow slowly from the source bottle through valve 5 and out the bottom-inner cap. If no oil was detected, the flow meter was re-attached as described in Section 4.6.6. If oil had contaminated these lines, more extensive cleaning of the flow meter and the possible replacement of lines was required.

4.7.2 **Recharging the accumulator**

The water level in the gas-water interface accumulator was monitored to ensure that there was always an ample supply of water for testing. The water level in the accumulator was determined by attaching a manometer to valve 10. With no pressure in the system, a section of transparent tubing was attached at valve 10 with its free end positioned above the height of valve 2, open to the atmosphere. Valves 10, 6, 3 then 2 were opened in sequence with all other valves closed. The level of the water in the section of tubing coincided with the level of water resting in the accumulator. If the level was far from the top of the accumulator, it was recharged using the following steps.

With all valves closed, the water source bottle was attached at valve 10 in sequence and positioned above the test board. Valves 10, 6, 3 then 2 were opened in sequence. Water was allowed to flow into the apparatus until it began flowing out of valve 2. At this point, the accumulator was full and valves 2, 3, 6 then 10 were closed.

4.8 SATURATION

Once all preliminary steps were completed for the preparation of the test board, and a specimen was properly installed in a test cell, the actual testing portion of the program could begin. For those tests which required the specimen to be saturated the following procedure was used.

4.8.1 Flushing the cell leads at atmospheric pressure

To begin the saturation of specimens, all valves were closed, there was no pressure in the system and the cell was connected to the test board by connecting valves 17 through 22 to the cell leads.

The flow of water into the specimen was measured using the flow meter. In order to get an accurate reading of the inflow of water into the specimen, the flow of water into the filters and the cell leads had to be factored out of the inflow measurement. To do so, these areas were separately flushed and saturated before reading water inflow to the specimen. Valves 2, 3, 6 then 9 were opened in sequence to give a supply of

water to the cell leads. Valve 18 was then opened, followed quickly by valve 22 so that water could flow out of valve 22. Valve 22 was rapidly opened and closed several times to dislodge any air bubbles attached to surfaces. Note that valve 18 was not opened with valve 22 closed for an extensive period of time as this would allow water to enter the specimen rather than being flushed over the filter. Valves 22 then 18 were closed when only water (no air) flowed out of valve 22.

Similarly, the bottom leads were flushed using valves 17 and 21. Valves 9, 6, 3 then 2 were closed in sequence when the leads were properly flushed and flooded.

4.8.2 Raising the pressure in the water lines to backpressure

Water had to be maintained at a suitable backpressure in order to have the specimen take in water at a rate that would allow saturation of the specimen within an acceptable period of time. Experience showed that a backpressure of 200 kPa was generally sufficient. The following steps were completed to establish the water lines at the desired backpressure.

First, the LabTech data acquisition system was started so that pressures could be monitored on the computer screen. Next, the gas source tank was opened and pressure regulator RA was set near the test board capacity. Valves 1, 3 then 6 were then opened in sequence, with all other valves closed. The pressure through pressure regulator RB was set to the desired backpressure (as read by pressure transducer TB). Note that valve 23 could be used to help set the pressure through RB by allowing

gas to be bled from the system if the target pressure was exceeded.

The likelihood of introducing discontinuities in the oil column in the flow meter have been observed by other operators to be less when the column is set to move downwards through the buret. For this reason, the 4-way valve was always in the downward position when valves 4 or 5 were adjusted.

Next, valve 6 was closed. Valve 4 was then carefully opened, watching the oil level in the flow meter sight buret. If the oil level moved suddenly, valve 4 was closed and the procedure was attempted again. If valve 4 could not be opened without excessive movement of the oil column then there was likely some air trapped in the system that would need to be removed. This could require re-saturating the flow meter in a manner similar to that discussed in Section 4.7.1.

If valve 4 could be opened without damage to the oil column in the flow meter, then valve 5 was carefully opened, again monitoring the oil column. Valves 5 then 4 were then closed to protect the flow meter from pressure surges during the next steps. At this point the flow meter and all water lines leading up to the cell leads were set to the desired backpressure.

4.8.3 **Flushing the cell leads at backpressure**

Next, the cell leads were flushed at the backpressure. This procedure was similar to the procedure for flushing the leads at atmospheric pressure, discussed in Section

4.8.1. Valves 6 then 9 were opened. As in Section 4.8.1, the top leads were flushed using valves 18 and 22 and the bottom leads were flushed using valves 17 and 21. On occasion, this process caused the pressure through RB to dip below the target value. In this instance, all valves except 1, 3, 6 and 9 were closed and the pressure through RB was reset to the backpressure. Valve 4 was carefully opened to stabilize the pressure in the flow meter and then closed. Valves 17 and 18 were quickly opened and closed to stabilize the pressures in the cell. Valves 6 then 9 were then closed.

4.8.4 **Specimen saturation**

Saturation of the specimen could commence once all the water lines in the system, including the filters adjacent to the specimen, were set at the desired backpressure. First, the pressure in the water lines was again stabilized to minimize any surge in flow that might occur when the specimen saturation stage began. Valves 6, 17 and 18 were opened. Valve 9 was quickly opened then closed to stabilize the pressures while allowing minimal water inflow into the cell. Valve 6 was then closed. With the 4-way valve on the flow meter in the downward position, valve 4 was carefully opened, watching that the oil column in the flow meter did not move excessively. Valve 5 was then carefully opened, again monitoring the oil column.

The position of the oil column in the flow meter was recorded. This was taken as the initial reading for 'zero inflow'. Valve 9 was then slowly opened, watching the movement of the oil column. On occasion, for example when testing drier, less dense specimens, there was an initial surge of flow when opening valve 9 and the initial

movement of the oil column was rapid. This surge ended within a few seconds. The position of the oil column when this initial surge stopped was then recorded. For some specimens, the initial flow surge was clearly due to improper flushing of the leads or compression of air in the system, rather than to saturation of the specimen. In this situation, the initial surge was not incorporated into the measurement of water flow into the specimen. The flow of water into the specimen was measured with time and as the oil/water interface approached either end of the sight buret, the direction of flow could be reversed using the 4-way valve. Readings were taken immediately before and after reversing the position of the 4-way valve, thereby avoiding meniscus errors in the flow measurements.

When the saturation process was completed valves 9, 17, 18, 5, 4, 3, then 1 were closed in sequence. Saturation was assumed to be complete once the rate of water inflow into the specimen was negligible. Saturation was checked by comparing the flow meter inflow volume measurement to the theoretical pore-air volume of the specimen.

4.9 GAS-BREAKTHROUGH

With the specimen at the desired saturation state, the gas-breakthrough stage of testing was carried out with the following steps.

4.9.1 Setting the system to backpressure

The water lines in the system and the test cell were set at the desired backpressure during the saturation stage. The rest of the lines, including the outflow section of the system were first set to the backpressure as a starting point for the gas-breakthrough stage as follows:

Valves 14, 15, 11, 12 and 13 were opened in sequence. The pressure through RC (read by TC) was set to the backpressure and the pressure through RB (read by TA) was checked and adjusted to ensure that it was also at the backpressure. Note that valves 23 and 24 could be used to adjust the pressure through RB and RC, respectively.

4.9.2 Flushing the leads with gas

Using valves 19 to 22, the cell leads and filters were flushed with gas and de-watered. At the bottom of the cell, valves 19 then 21 were opened. Valve 21 was opened and closed several times to flush the water out of the bottom leads and filter. Valves 21 then 19 were closed when finished. Similarly, valves 20 then 22 were used to flush and de-water the top leads and filter.

TA and TC were checked to ensure that the pressure through RB and RC was still set at the backpressure. If not, the pressures were reset and the lines were stabilized at the backpressure. The gas pressure at the top and bottom of the specimen were now

set at the backpressure and the gas-breakthrough stage could begin.

4.9.3 Setting the gas inflow pressure

The gas pressure at the base of the specimen was incrementally increased until gas-breakthrough occurred. The standard incremental increase in inflow pressure was 200 kPa and the increment duration was 5 minutes. Gas-breakthrough was deemed to occur when the pressure at the top of the specimen increased, as detected by transducer TC.

All valves were closed at the start of gas-breakthrough stage. The pressure through RB was set to the backpressure plus the preset gas pressure increment. Valves 11 then 13 were opened. Next, valves 19 and 20 were opened simultaneously. TB was monitored to detect any pressure response caused by the increased inflow pressure. If no pressure response was apparent during the set incremental time period, another increment of inflow pressure was added through RB. Again, TB was monitored for a pressure response. This step was repeated until a pressure response was seen in TC, indicating that the gas-breakthrough pressure had been exceeded.

4.10 DISMANTLING THE CELL

Once gas-breakthrough was achieved, or if the test reached the limiting pressure of the apparatus, the cell and apparatus were depressurized so the cell could be

dismantled.

Valves 19 then 20 were closed. Pressure regulators RB and RC were closed. Valves 23 and 24 were used to bleed the regulators and with valve 24 open, valves 14 then 15 were opened to depressurize the outflow circuit. Valve 23 was opened to depressurize the inflow circuit. Valves 21 and 22 were opened to depressurize the cell.

Valves 9, 3 then 2 were opened to relieve the pressure in the water lines and with the 4-way valve in the downward position valve 5 was carefully opened to relieve the pressure in the flow meter, monitoring for excess oil column movement. Thus, the entire system was returned to atmospheric pressure and all valves were then closed.

The cell was then removed from the apparatus at valves 17 through 22 and dismantled so that the specimen could be retrieved for moisture content measurement and other analysis.

5. TEST RESULTS AND DISCUSSION

5.1 INTRODUCTION

Data from the testing program are presented and discussed in this Chapter beginning with the quality control (QC) tests and followed by the gas-breakthrough tests. A complete discussion of the illite and buffer gas-breakthrough tests explains the results based on theory of gas migration and other topics. The buffer experiments were of secondary importance to the scope of this research program and are presented minimally for the sake of completeness.

5.2 QUALITY CONTROL PROGRAM

A quality control (QC) program was completed in conjunction with the gas-breakthrough test program to ensure that specimen conditions were fully understood throughout testing. A series of eight illite specimens (QC1 through QC8) were compacted to determine the range of variability to be expected in specimens and to evaluate the repeatability of specimen conditions. A QC program was not included for the buffer specimens. The QC specimens were prepared largely in the same manner as gas-breakthrough test specimens, as described in Chapter 4, but were extruded and tested for their moisture content and dry density without undergoing saturation or gas-breakthrough testing. The top flange of a test cell was not placed on QC

specimens after compaction, so QC specimens were not fully sealed in the test cell for any time. Except for QC4 which was compacted on a dry filter, the QC specimens were compacted on water-saturated filters to be consistent with the procedures proposed for preparation of gas-breakthrough test specimens.

In this context, 'target' data refers to the specimen conditions (ρ_d, w and S) proposed for a test. 'Compacted' data refers to specimen conditions based on moisture content measurements from mixed material immediately before being compacted in a test cell and the mass of material compacted. 'Final' data refers to specimen conditions based on the moisture content and mass of specimens extruded from a test cell after testing.

The following Sections describe trends in specimen conditions brought on by compacting and extruding specimens through a comparison of target, compacted and final conditions.

5.2.1 Moisture content

Moisture contents were mapped in the extruded QC specimens by sampling from various regions to study spatial variations in moisture content and to compare the final conditions to those present at the time of compaction. Typically, four smaller specimens were taken from each extruded QC specimen and moisture content tests were determined by oven-drying. Moisture content specimens were cut away from a QC specimen with a knife typically from the top (last layer compacted), bottom (first layer compacted), outer and inner regions of a specimen (Table 5.1). Moisture

contents varied from the top to the bottom by 104.31% to 99.40% of the mean values (shown in Table 5.1 as percent differences of 4.31% for QC2 and -0.60% for QC8). For example, QC2 had average top and bottom moisture contents of 17.18% and 15.76%, respectively, a greater difference than in any other QC specimen. The percent difference was calculated as the difference between the top value and the mean of the top and bottom values, divided by the mean value. In other words:

$$\frac{(15.76\% + 17.18\%)}{2} = 16.47\% \ (\textit{mean})$$

$$\frac{(17.18\% - 16.47\%)}{(16.47\%)} = 0.0431 = 4.31\% \ \textit{difference}$$

This should not be confused with the actual change in moisture content, which would be (17.18% - 15.76%) = 1.42% moisture content. Using the same method of analysis, moisture contents ranged laterally by 100.03% to 99.33% of their mean values. ASTM (1993) standards specify that results from two oven-dried moisture content tests completed by the same operator with the same equipment should differ from their mean by less than 7.8%. ASTM standards also specify that a minimum of 20 g of wet soil be used for an oven-dried moisture content test. Taking 4 moisture content specimens from one test specimen brings the mass of each specimen close to, if not below, this lower limit. Therefore, the reliability of the moisture content distribution measurements are somewhat speculative. Nevertheless, the variation in moisture content over specimen height and laterally were well within the ASTM specified limit for variations, hence the moisture content of specimens could be considered uniform. This should be the case because the material the specimens were formed from was

carefully prepared and premixed to ensure homogeneity.

The percent differences for moisture contents between the target values and the compacted values shown in Table 5.2 are less than 4%. Again, this should not be confused with the direct difference in moisture content between the two values. For example, the target value of moisture content for QC1 is shown in Table 5.2 as 12.3%. After being mixed, however, the material had a compacted moisture content of 12.39%. The difference between the compacted value and the mean of the two divided by the mean [(12.39% - 12.345%) / 12.345%] yields a percent difference of 0.36%. The actual difference in moisture contents, on the other hand, is 0.09% moisture (12.39% - 12.3%). The data show that the materials were mixed reasonably close to the targeted moisture content. The moisture contents of six of the eight specimens were mixed to within ±1% difference from their targeted value. Differences in the test procedures or final conditions of the specimens tested accounted for the outlying data points. It was concluded that using the developed mixing procedures, specimens of illitic clay could be prepared to moisture contents within ±1% of the targeted values. That is, for a target moisture content of 15%, for example, the material could be compacted to a moisture content of 15±0.15%.

Seven of the eight QC specimens increased in moisture content by less than 7% difference while in the test cells (from compacted to final conditions). These relatively small increases could be considered insignificant, according to the ASTM standards, but because the QC specimens consistently increased in moisture content (except QC4) it could be concluded that the moisture contents are indeed changing during the time that they are held within the test cells. The most likely source of moisture would

be the wet filter that specimens were compacted on. An indication of this is that QC4, which was compacted on a dry filter, did not increase in moisture content during the compaction stage while all other QC specimens did. These observations are significant since the effects of the interaction between filters and a specimen could affect test results. It may be necessary in the future to determine the consequences of these effects.

5.2.2 **Dry density**

The compacted dry density of the QC specimens was calculated based on the known test cell specimen chamber dimensions (24 mm height and 50.7 mm diameter), the moisture content and the mass of compacted material. The final dry density of QC specimens (excluding QC2 which crumbled upon extrusion from the cell) was calculated from the final bulk density determined from caliper readings of specimen dimensions and the bulk mass of each extruded specimen (Table 5.2). These bulk densities were combined with moisture content test results from the extruded specimens to give final dry densities. For example, the mean compacted moisture content for QC1 was 12.39%. Based on this reading, the known specimen dimensions and the known mass of compacted material, the compacted dry density was calculated as 2.03 Mg/m^3. The final dry density calculated from actual specimen height, specimen diameter and final moisture content measurements taken after the specimen was extruded was 1.95 Mg/m^3, a difference of -2.01%, or 97.99% of the mean of the two values. Final dry densities were consistently lower than the compacted values by between 0.27% and 2.56%. Several sources could be attributed to this relatively high

range in values. The assumed specimen dimensions of 24 mm height and 50.7 mm diameter were taken directly from the cell design drawings, but, the height measurement depended on the thickness of filters, the degree of accuracy that could be achieved with the compaction equipment and variations in the seating of the cell flanges in the sleeve. Any degree of expansion of the specimen or loss of material upon extrusion could also lead to error in the dry density calculation.

It became clear that for the equipment developed and the techniques employed, the dry density of the specimens could only be warranted to within an error of ±3%. That is, a specimen with a target dry density of 2.00 Mg/m^3 could have a dry density in the range of 2.06 Mg/m^3 to 1.94 Mg/m^3.

5.3 GAS-BREAKTHROUGH TESTS

Gas-breakthrough testing was initially to be completed on specimens brought to saturation by uptake of water and on unsaturated specimens. In the 'saturated' tests, specimens were to be placed in a test cell between saturated filters. To keep the procedures consistent, saturated filters were used also in tests on unsaturated specimens. Variations in final moisture content results in the unsaturated tests indicated that interaction between saturated filters and unsaturated specimens may have been significant. Hence, several tests on unsaturated specimens were completed with dry filters. The tests can be grouped as follows:

- *illitic clay*
  - T1 through T21 excluding T2 - saturated tests,
  - T22 through T29 excluding T28 - unsaturated tests with wet filters,
  - T2, T28 and T30 through T46 - unsaturated tests with dry filters, and

- *sand/bentonite mixtures (buffer)*
  - BT1 through BT6 - unsaturated tests with dry filters.

As in the QC specimens, 'target' data refers to the desired moisture content, dry density and saturation state for a mixed specimen. 'Compacted' data is calculated from the measured moisture content of the mixed material immediately before compaction and the mass of material compacted. 'Final' data is calculated from moisture content measured in extruded specimens and the mass of material that was compacted. 'Saturated' data refers to the state of specimens between the saturation stage and gas-breakthrough stage of testing and considers water inflow measured through the flow meter during the saturation stage. For the unsaturated tests, the saturated data are not available because the saturation stage of testing was omitted.

Specimen moisture content and dry density variations are first described and explained. A representative sample of individual gas-breakthrough test results is then discussed to highlight key trends and observations. Finally, a synthesis of the test data is presented and data are described with respect to pertinent theories discussed in the Review of Literature.

5.3.1 Moisture content

Moisture contents in illite gas-breakthrough specimens were traced throughout testing.

At the end of some gas-breakthrough tests, moisture content specimens were taken from different locations in an extruded test specimen in order to achieve some understanding of the pore-water distribution and how it relates to test procedures. Table 5.3 shows final moisture contents for several representative gas-breakthrough specimens, sampled spatially much like those in the QC program. Specimens were sampled after they were extruded from the test cell with three to five moisture content specimens being measured from each test specimen. The mean value for each specimen is given in Table 5.3. For example, the mean final moisture content for T4 was calculated from 5 individual specimens as 14.6% ± 0.44%. The maximum and minimum results from the five specimens differed by 1.4% moisture. Moisture contents in T4 varied over specimen height and laterally from their mean values by 104.71% difference and 99.49% difference, respectively.

5.3.1.1 *Lateral variation in moisture content*

In general, lateral variations in moisture content were sufficiently low that statistically, no detectable lateral trends were present. The small variations calculated can be attributed to errors in measurement associated with the small mass of the moisture content specimens. Data presented in Table 5.3 show moisture contents in the saturated gas-breakthrough specimens varying laterally by 100.51% to 102.38% of their mean values. The unsaturated gas-breakthrough specimens with wet filters varied by 98.60% to 103.24% of their mean values. The unsaturated breakthrough specimens with dry filters varied from 100.14% to 101.11% of their mean values.

Theoretically, gas flow along the cell walls would decrease moisture contents in a

specimen at its perimeter. It would therefore be expected that if gas bypassed the specimen pore-structure by leaking along the cell walls, there would be relatively large lateral variations in specimen moisture contents. There were no such moisture content variations observed. However, due to the errors associated with using small specimens for moisture content tests, as described above, the results do not allow for any positive statements in this regard.

5.3.1.2 *Variation in moisture content over specimen height*

Moisture contents in the illite gas-breakthrough specimens varied over specimen height significantly more than they did laterally (Table 5.3), but the differences, typically less than 5%, are still relatively small. The results generally show lower moisture contents on the bottom (inflow) face of specimens than the gas collection (top) face after gas-breakthrough tests. Height variations were not investigated in the unsaturated specimens with wet filters. The variations in moisture content over height, coupled with direct visual observations, indicate that 2-phase flow of gas may have occurred through specimens, resulting in migration of a significant quantity of water as a slug in front of the invading gas. Visual evidence of this included a drier appearance of bottom filters than top filters, a drier appearance of soil near the bottom of specimens than at the top (marked by a difference in colour) and accumulation of water in the top cell leads and gas collection circuit. A definitive conclusion cannot be made in this regard due to errors in measurement associated with the small mass of moisture content specimens and because the volume of displaced water was not measured. Testing larger specimens and more thorough monitoring of the mass balance of moisture and gas through specimens may offer a more acceptable statistical basis for

such conclusions. Observations indicating 2-phase flow differ from those of other researchers (Pusch et. al., 1985, for example) who noted very little change in the moisture content regime and saturations and concluded, therefore, that gas migrated primarily through discrete 'finger-like' passages in only a small number of pores within a specimen. The data shown in Tables 5.4(a) and 5.4(b) do not clarify this matter because they were likely influenced by interaction between filters and a specimen and, thus, give little information regarding the effects of moisture migration due to gas flow alone.

5.3.2 **Gas-breakthrough test results for illite material**

Gas-breakthrough pressures are summarized in Tables 5.4(a) and 5.4(b), and a detailed description of the test data for the entire set of gas-breakthrough tests on illite specimens (T1 through T46), buffer specimens (BT1 through BT6) and several specialized specimens is shown in Appendix C. A representative subset of the test data is given in Figure 5.1, and the more prominent trends are explained in the following Sections.

5.3.2.1 *Repeatability of tests*

Figure 5.1(a) shows the gas-breakthrough test results for T5 which was saturated at 200 kPa backpressure for approximately one day before the start of the gas-breakthrough test stage. The gas inflow (bottom) and gas collection (top) test cell leads and filters were flushed with gas after the saturation stage, leaving them

presumably dry for the gas-breakthrough stage. Gas-breakthrough testing began once this was complete by opening the leads and exposing the specimen to 200 kPa of gas inflow pressure at the bottom and 200 kPa gas pressure in the collection circuit at the top. The gas inflow pressure was increased approximately 200 kPa every 5 minutes, hence the stepwise slope to the gas inflow data in Figure 5.1(a). This was continued until a response was observed in the gas collection circuit, marked by a change in pressure, indicating that gas from the inflow circuit was able to pass through the specimen pore-structure and accumulate in the gas collection circuit. These conditions were met at approximately 55 minutes into the gas-breakthrough test, when the gas inflow pressure was at 2.2 MPa. The gas inflow pressure corresponding to the point when a response is seen in the gas collection circuit is referred to as the gas-breakthrough pressure. Hence, the gas-breakthrough pressure for specimen T5 was 2.2 MPa. In this test, the response seen in the gas collection circuit at gas-breakthrough was very sudden.

Specimen T11, in Figure 5.1(b), showed results similar to T5, as would be expected because the test and specimen conditions were similar. Both T5 and T11 were compacted to a dry density of 1.90 Mg/m^3. After the saturation stage, T5 was 97% saturated (16.1% moisture content) and T11 was 100% saturated (16.6% moisture content). The same backpressure was used in both tests and the gas inflow pressure was increased at the same rate. A comparison of the results from T5 and T11 show a high degree of repeatability for similar tests. Gas-breakthrough similarly occurred in T11 at 2.2 MPa, and the response was equally sudden. This relatively high degree of repeatability is typical of the majority of tests throughout the entire tested ranges of moisture content and dry density.

When different procedures were used, however, this high degree of repeatability was not always achieved. For example, specimens T10 and T45, shown in Figures 5.1(c) and 5.1(d), were established at nearly the same specimen conditions for gas-breakthrough testing, but T10 had been saturated by uptake of water before gas-breakthrough testing and T45 had simply been compacted to the gas-breakthrough test conditions. Also, the filters in test T10 were wet while those in T45 were dry. Resistance to gas-breakthrough shown by specimen T10 was approximately double that of T45, indicating that the test procedures could affect test results. Another example of discrepancies in test results due to procedural differences can be seen by comparing results from T30, T34 and T35 with those from T26 (Appendix C), the prior three tests being unsaturated tests with dry filters and the latter being an unsaturated test with wet filters. On the other hand, results from T17 and T44 were very similar, although T17 was a saturated test and T44 was unsaturated with dry filters.

In general, the tests showed a relatively high degree of repeatability throughout the full test ranges for moisture content and dry density.

5.3.2.2 *Magnitude of gas-breakthrough responses*

Specimens T14, in Figure 5.1(e), and T16, in Figure 5.1(f), both underwent an initial saturation stage. Specimen T14 was compacted to 2.06 Mg/m^3 and was at 11.6% moisture content after saturation. T16 was compacted to 1.93 Mg/m^3 and was at 14.7% moisture content after saturation. The two specimens were saturated to nearly the same degree. In T16, the gas-breakthrough pressure is marked at a point where the gas collection pressure response was very sudden and the pressure increase in

the collection circuit was significant. In T14, on the other hand, the initial pressure response in the collection circuit at 2.0 hours was not nearly as significant or as abrupt as that in T16. Although the gas collection curve in Figure 5.1(e) appears to remain unchanged at 2.0 hours, a closer look at the data shows a small response on the order of tens of kPa. At the end of each pressure increment thereafter, the gas collection circuit was brought back to 200 kPa. Upon addition of another 200 kPa pressure increment in the gas inflow circuit, a similarly small response was noted in the gas collection circuit. Gas was obviously seeping through the soil specimen, though not in the unrestricted manner that it flowed through specimen T16 at the gas-breakthrough pressure. Additional pressure increments were added to T14 approximately up to the 2.6 hour point. The pressure response in Figure 5.1(e) at this point is much more noticeable, yet still not as sudden as the response in Figure 5.1(f) at approximately 1.25 hours.

In other tests with a gas-breakthrough response similar to that in T14, a considerable amount of water had collected in the cell leads and filter on the gas collection (top) side of the specimen, though water had been flushed from this area before starting the gas-breakthrough stage of the test. This indicates that gas had pushed water from pore-spaces in the specimen into the gas collection leads and filter during gas-breakthrough testing. The accumulation of water in the gas collection cell leads and filter was typically less when more sudden gas-breakthrough responses were observed.

The distinction between the pressure responses in T14 and T16 is important because it could be indicative of different gas flow mechanisms. The shape of the gas collection pressure curve in Figure 5.1(e), or the 'magnitude' of the gas-breakthrough response

in T14, is described hereafter as 'restricted'. The response shown by T16 is described as 'sudden'. A restricted response was typically found in specimens compacted at or above the Modified Proctor maximum dry density and near 100% saturation. Sudden responses were more often evident at lower dry densities and degrees of saturation. An explanation for the differing responses could relate to the geotechnical properties of specimens and the gas flow mechanism, or factors related to the procedures or equipment design. This is discussed below.

It was mentioned in Chapter 2 that the mechanism for gas migration in compacted clay materials could involve 2-phase gas flow where invading gas pushes water through existing pores in a specimen, possibly resulting in face-wise migration of gas. This would likely be a time-dependant process and could exhibit a response similar to the gas-breakthrough response seen in tests such as T14. Further to this, visual evidence suggesting the occurrence of 2-phase gas flow included presence of water in the gas collection cell leads and filters and the drier appearance of the inflow filter and soil near the inflow side of a specimen. A sudden gas-breakthrough response, as seen in tests such as T16, could involve a flow mechanism involving dilation of existing pores or creation of new pores (fissuring) due to a local increase in total stress brought on by increased gas pressure. The resulting alteration of the soil fabric could allow nearly unrestricted flow of gas, which would explain the sudden gas-breakthrough response in T16.

The difference in magnitude of gas-breakthrough responses could also be caused by factors related to the equipment design and test procedures. The filters and cell leads were flushed with gas at the start of gas-breakthrough tests and were, therefore,

assumed to be dry. If water were only partly removed, however, passage of gas may have been restricted because it would have to displace accumulated water before passing into the gas collection chamber. This may explain why the magnitude of a restricted gas-breakthrough response could be increased, at times, by stopping a test and re-flushing the gas collection leads and filter. It is difficult to determine if the accumulated water in the filter and leads actually had an affect on gas flow or if the gas was able to percolate through it with little restriction. It is possible that gas flow restriction was caused by contamination of the filters brought on by movement of a small quantity of clay into the filters. The filters were chosen with this consideration in mind, however, and there was no visible evidence of this.

5.3.2.3 *Effects of dry density*

An increase in dry density generally appears to increase the gas-breakthrough resistance of a specimen. Three specimens that show this relationship well are T30, T36 and T37. The three specimens were compacted to between 11.2% and 11.4% moisture content and to dry densities of 1.90 Mg/m^3, 2.02 Mg/m^3 and 2.08 Mg/m^3, respectively. The least dense specimen, T30, shown in Figure 5.1(g), exhibited 0.4 MPa of gas-breakthrough resistance. Specimen T36, with medium dry density, showed a gas-breakthrough pressure of 1.6 MPa. Specimen T37, shown in Figure 5.1(h), had the highest dry density of the three specimens and showed the highest gas-breakthrough resistance, 4.0 MPa. All else the same, an increase in dry density would require a decrease in porosity of a soil. Particle rearrangement would occur to accommodate this reduction in porosity, resulting in smaller pore-spaces. The capillary pressure equation (presented in Section 2.4) states that the pressure at which

gas will pass through a pore-throat is inversely proportional to the pore-size, and the general observation of increased gas-breakthrough resistance with increased dry density is consistent with this theory.

5.3.2.4 *Effects of moisture content*

An increase in specimen moisture content generally resulted in an increase in gas-breakthrough pressure. Although not nearly as marked as the dry density effects, a transition from the test conditions from T38 to T1 to T9 provide a clear example of this trend. These three tests were compacted between 1.89 Mg/m^3 and 1.90 Mg/m^3 and to moisture contents of 12.6%, 13.8% and 17.0%, respectively. The gas-breakthrough pressures respectively increased from 0.4 MPa in T38, shown in Figure 5.1(i), to 2.2 MPa in T1 to 2.6 MPa in T9, shown in Figure 5.1(j). An explanation of this could be that at higher moisture contents, a volume of invading gas would need to displace more water to the sides and in front of the gas in order to advance through a pore. Increased moisture content would provide a higher degree of resistance to gas flow, thus requiring higher gas pressures before initiation of gas-breakthrough.

5.3.2.5 *Effects of degree of saturation*

Gas-breakthrough pressures decreased at a moderate rate with decreased degree of saturation from S=100% down to approximately S=80%. Below S=80%, gas-breakthrough resistance dropped at a higher rate. The general decrease in gas-breakthrough resistance with decreased degree of saturation can be explained in

terms of the associated decrease in dry density and/or moisture content, as described in the previous two Sections. The increase in the rate of decrease of gas-breakthrough resistance below S=80%, however, is more complicated than this and is better explained by looking at the entire illite data set, rather than just a few test results. This is investigated in Section 5.4.1

5.3.2.6 *Effects of gas pressure gradient*

The slope of the gas collection pressure curves in Figure 5.1 usually decreased over time because the gas collection pressure became closer to the gas inflow pressure and thus the pressure gradient across a specimen constantly decreased. If the pore-structure of a specimen was unaffected by gas migration, then theoretically the gas collection pressure should continue to increase until the pressure is equal on either side of a specimen and the pressure gradient, the driving force for gas migration, tends toward zero. An important observation from the tests is that, no matter how sudden and marked the gas-breakthrough response, the gas collection pressure did not reach the same level as the inflow pressure. This could possibly indicate that alteration of the pore-structure occurred during a gas-breakthrough test. It is possible that pores dilated at higher pressure gradients to allow for the movement of gas but retracted or 'healed' when the pressure gradient decreased due to accumulation of gas in the gas collection circuit. This observation is consistent with results of the repeated tests on T17 and T21. Related to this phenomenon, Horseman and Harrington (1994) observed unstable intermittent or 'burst-like' gas flow at gas-breakthrough which they similarly attributed to structural changes within the soil. The pressure detection system associated with the equipment in this research program was likely not sensitive enough

to detect this intermittent gas flow, however.

5.3.3 Gas-breakthrough test results for buffer material

A gas-breakthrough response was seen in only one of the buffer tests (BT3). All other buffer tests were taken to the limiting pressure of the equipment with no gas-breakthrough response. Inflow pressure was difficult to maintain above 9.0 MPa because the safety relief valve would open intermittently to relieve pressure. Pressure data above 9.0 MPa are therefore erratic. Tests BT1 and BT1A were completed on the same specimen using two different rates of gas inflow pressure increase. The same was done for specimens BT2 and BT2A. In each instance, the gas-breakthrough pressure was not reached.

Gas-breakthrough resistance was overcome in specimen BT3, shown in Figure 5.1(k), at approximately 9.4 MPa. Specimen BT3 was compacted to a very low degree of saturation (S=49.2%), indicating that the trend of decreased gas-breakthrough resistance with decreased degree of saturation seen in illite may also occur in the buffer material. The response was much more restricted than the response in illite specimens at low degrees of saturation, however.

The buffer material clearly offers greater resistance to gas-breakthrough than the illite material, even though the buffer was compacted much looser than the illite specimens and had porosities approximately 25 percent higher than those of illite. The reason for this discrepancy is explained in terms of capillarity in Section 5.4.5.

5.3.4 Specialized gas-breakthrough tests

Some specialized tests were completed in conjunction with the above tests. Illite test T29, shown in Figure 5.1(l), involved a gas inflow pressure loading rate of approximately 500 kPa every 5 minutes. Specimen T29 showed gas-breakthrough at 3.5 MPa which is similar to the response shown by specimens compacted to similar conditions but tested with a gas inflow pressure loading rate of 200 kPa every 5 minutes. Gelmich (1994) studied the effects of pressure loading rates in more detail by comparing results of tests with pressure increments of 200 kPa increased every 1 minute and every 5 minutes. Slightly higher resistance to gas-breakthrough was observed in the tests with higher loading rates, indicating the possibility of a time dependency in the gas flow mechanism. The number of tests completed in this study was insufficient to draw any definite conclusions regarding these effects. This relationship will likely require further investigation in the future.

Test T17 was followed by a series of 3 additional gas-breakthrough tests with a saturation stage before each test. The results, shown in Figure 5.1(m), show that there may have been some permanent damage to specimen T17 after the initial breakthrough test, as marked by a reduction in resistance to breakthrough in the latter tests. On the other hand, the pathway that permitted relatively unrestricted gas flow in the first test seemed to 'heal' to some extent before the subsequent tests. Had the soil not healed, the subsequent tests would have had very little or no resistance to gas flow because gas would likely flow through existing pathways with minimal restriction. A similar study on specimen T21, Figure 5.1(n), with seven consecutive gas-

breakthrough tests showed similar results.

5.4 SYNTHESIS OF GAS-BREAKTHROUGH TEST RESULTS

Tables 5.4(a) and 5.4(b) show gas-breakthrough pressures for tests, grouped, as before, in terms of procedural differences. The compacted moisture content, degree of saturation and dry density are also given, followed by inflow data (Q) obtained during the saturation stage. In the case of the saturated tests, the inflow data are used to calculate the moisture content and degree of saturation after the saturation stage. The unsaturated tests did not include a saturation stage, so inflow was zero and the specimen conditions after the saturation stage remained the same as the compacted conditions. Next, the final moisture content and degree of saturation are shown (based on moisture content tests on extruded specimens). Finally, a percent change in moisture content during the gas-breakthrough test stage is given, followed by a value for gas-breakthrough pressure for each test. Data reported in Tables 5.4(a) and 5.4(b) usually included the initial surge of water that flowed into the test cell at the beginning of the saturation stage. As discussed in Section 4.8.4, an initial flow surge could be caused by improperly flooding cell leads and filters or by flow of water into a specimen, though it is difficult to determine the actual cause. Similar data were calculated based on inflow measurements that exclude the initial flow surge. These data are not included herein because they did not fit the remaining data as well. For the purpose of this test program, therefore, the data shown in Tables 5.4(a) and 5.4(b) are assumed to be the correct inflow data and are used in subsequent data analysis.

Figure 5.2 shows the illite gas-breakthrough test conditions and corresponding gas-breakthrough pressures in moisture content - dry density space with the theoretical 100% saturation line (dashed) and the Modified Proctor compaction curve (solid) superimposed. Figure 5.3 shows the same data set generalized as contour intervals, showing gas-breakthrough pressures for the dry density and moisture content ranges tested. Resistance to gas-breakthrough pressure appears to increase along the 100% saturation line as the soil gets drier and denser (to the left and up in Figures 5.2 and 5.3). As the degree of saturation is decreased and conditions fall further away from the 100% saturation line (to the left and down in Figures 5.2 and 5.3) gas-breakthrough resistance decreases.

Based on the theory of capillarity, pore-size and capillary pressure are inversely proportional, and gas-breakthrough pressure can be defined as the capillary pressure required to overcome surface tension in the smallest pore-throats in a continuous pathway so that gas can invade pore-space and migrate through the porous medium. Clays compacted at higher dry densities will have lower porosity and smaller pore-sizes, and should, therefore, correspond to higher resistance to gas-breakthrough. This trend is indeed shown in Figures 5.2 and 5.3 for the illitic clay specimens. At a constant dry density, increased moisture content should cause a decrease in soil suction as forces retaining moisture within the soil decrease. Based on this alone, gas-breakthrough pressures should theoretically decrease with increased moisture content. Figures 5.2 or 5.3 show an opposite trend, in fact. Similarly, a drop in degree of saturation should increase suction or gas-breakthrough pressure, but specimens with low saturations had relatively little resistance to gas-breakthrough. A likely explanation for this is that as moisture content increased, invading gas had to displace

more water to advance through pore-space, thus the process required more energy, manifested as a higher gas-breakthrough pressure gradient. As well, the effects of compacted moisture content on soil fabric arrangement described by Garcia-Bengochea et. al. (1979) could also contribute to the these effects. Particle arrangement in soils compacted at or greater than the optimum moisture content (12.0%) may tend to be dispersed while materials compacted with lower moisture contents may have a flocculated particle arrangement which would more readily accommodate gas flow.

5.4.1 Gas-breakthrough / saturation relationship

The summary of illite gas-breakthrough test results shown as a function of dry density for ranges of degree of saturation in Figure 5.4 shows an interesting trend to the gas-breakthrough data. There seems to be a large rift between the gas-breakthrough pressures for illite specimens with degrees of saturation above and below 80%, independent of the compacted dry density. The 11 illite tests below 80% saturation and 35 illite tests above 80% saturation are fitted to exponential curves, as defined in Figure 5.4. Of the 11 tests with degrees of saturation below 80%, only 2 data points (corresponding to T25 and T26) unexplainably do not fit the rest of the data. All but one (T36) of the 35 tests above 80% saturation fit the general trend for these tests. The degree of saturation for T36 was 85% which is relatively close to the 'critical' degree of saturation of 80% which seems to separate the data. Both Corey (1990) and Wheeler (1988) noted a similar critical degree of saturation in soils between 80% and 90% saturation, below which a continuous gas phase may exist and above which the

gas phase would be discontinuous, broken up into discrete pockets and separated by water. This could offer an explanation for the rift at approximately 80% saturation seen in the gas-breakthrough test results in this research program. Below S=80%, the gas phase in the compacted clay specimens may have been continuous so that gas would not need to displace a significant quantity of water to migrate through the pore-space, thus a considerable degree of gas migration could occur at a relatively low pressure gradient. For gas to enter pore-space above S=80%, it would likely have to force significantly more water from the pores either to the sides or ahead of the invading gas phase. The additional work required for the gas phase to displace water would likely require a greater pressure gradient for gas flow to occur. Hence, specimens compacted above this critical degree of saturation would offer higher resistance to gas-breakthrough. Moreover, it is possible that the critical degree of saturation may involve a switch in dominant gas flow mechanisms from 2-phase flow to pathway dilatancy, though this is only speculative.

This relationship could also explain the restricted gas-breakthrough response in some specimens compacted with degrees of saturation near 100%. With saturation above S=80%, a relatively large quantity of water must be displaced to permit gas flow, but with the discontinuous gas phase in specimens with saturation less than S=80%, significantly less water would need to be displaced because much of the pore-space is already in the gas phase. It would likely take more time and energy for gas to move a given distance through water-saturated pore-spaces than it would to travel through the same pore-spaces if they were gas-filled, because the pressure transfer through the gas-filled pore-spaces would be direct and virtually instantaneous.

5.4.2 Swelling pressure

Swedish researchers such as Pusch et al. (1985) and Pusch (1993) contend that gas-breakthrough pressures are on the order of 50 to 90% of the clay swelling pressure. Results presented in this study give no indication of this empirical relationship. A relatively inactive clay such as illite would likely develop minimal, if any, swelling pressure, especially when only partially saturated. Yet gas-breakthrough pressures up to 6.4 MPa were observed in the test ranges of moisture content and dry density. The buffer specimens were compacted between degrees of saturation of 48.8% and 92.6%. The swelling pressure in fully saturated buffer compacted to 1.67 Mg/m^3 would likely be less than 2 MPa (Wan, 1987). Swelling pressure would be even lower for partially saturated buffer. Other than BT3 which showed indications of gas-breakthrough at approximately 9.4 MPa, the buffer specimens were taken to the upper pressure limit of the test equipment without gas-breakthrough. This indicates that, at least for the equipment and procedures developed for this program, the relationship between swelling pressure and gas-breakthrough pressure suggested by the Swedish researchers appears to be invalid for both compacted illite and buffer materials.

5.4.3 Capillarity

Based on pore-size distributions, gas-breakthrough test results are related to capillarity by two means in the following Section. Firstly, the pore-size distribution of materials that have undergone gas-breakthrough testing is measured by MIP to determine the range of pore-sizes present in such material. Secondly, the pore-size theoretically

corresponding to gas-breakthrough is determined from the capillary pressure equation by equating the gas-breakthrough pressure to capillary pressure. For a good correlation of the data, the pore-size determined from this second method of analysis (taking into account the DDL effects) should lie within the pore-size distribution determined by MIP.

5.4.3.1 *Mercury intrusion tests*

A limited number of MIP tests were conducted on illite specimens to give an indication of the pore-size distribution (PSD) of specimens prepared in the manner described in this study. A series of MIP tests were completed on illite specimens prepared at various moisture contents and dry densities, but not tested for gas-breakthrough pressure. These results (reported by Gelmich, 1994) provide a basis for comparison to specimens that were tested for gas-breakthrough, to study the effects of gas-breakthrough testing on pore-structure. Four specimens were compacted to approximately 2.04 Mg/m^3, ranging in moisture content from 10.0% to 13.0% (Figure 5.5). In general, the results show that pore-sizes ranged from 0.005 μm to 2 μm. The results also show that the smaller pores (0.005 μm to 0.1 μm) were not affected by moisture content at the time of compaction, mid-sized pores (0.1 μm to 0.5 μm) increased in frequency with increased moisture content, and the larger pores (0.5 μm to 2 μm) decreased in frequency with increased moisture content. In other words, there was a shift in the distribution from larger pores to mid-sized pores with increased moisture content, especially below the Modified Proctor optimum moisture content (w = 12%). This trend is consistent with those observed by Garcia-Bengochea et. al. (1979) and others who predicted that clays compacted dynamically below the optimum

moisture content will have a flocculated particle arrangement while those compacted at or above the optimum moisture content will have a dispersed particle arrangement.

Another series of MIP tests were completed on specimens that had been tested for gas-breakthrough (Figure 5.6). The PSD for specimens T11 (w=16.6%, ρ_d=1.90 Mg/m^3) and T15 (w=13.0%, ρ_d=2.03 Mg/m^3) were very similar, despite the difference in their compacted conditions. The PSD for specimen T17 showed a relatively high frequency of mid-sized pores (0.1 μm to 0.2 μm) which may have arisen from the repeated gas-breakthrough tests that the specimen was subjected to. Gas-breakthrough testing does not appear to have significantly affected the shape of the PSD.

The PSD for buffer material typically shows two distinct concentrations of pore-sizes from 0.003 to 0.007 μm and 5 to 50 μm, as shown by Wan in parallel studies at AECL Research. The minimum pore-size of 0.003 μm is an imposed value, governed by the MIP equipment. MIP tests were not completed on the buffer material prepared in this program.

Figure 5.7(a) shows PSD data for two similar specimens; one that underwent gas-breakthrough testing, and one that did not. The solid line in Figure 5.7(a) shows MIP data for T2 which was tested for gas-breakthrough pressure, and the dashed line shows data for specimen T2A which was compacted at the same moisture content and dry density and at the same time as T2, but was not tested for gas-breakthrough pressure. Data for the two specimens show similar PSD's, except for a difference between 1 μm and 5 μm where specimen T2A has a greater frequency of pores. One

might expect this greater frequency of relatively large pores in specimen T2 which underwent gas-breakthrough testing rather than in specimen T2A, because of the possible effects of gas-breakthrough testing. Figure 5.7(b) shows data for specimens T46 and T46A in a similar comparison of a specimen that underwent gas-breakthrough testing and one that did not. There is little difference between the PSD's of these two specimens, suggesting that gas-breakthrough testing has little affect on PSD and pore-structure of specimens. This might indicate that gas flow occurred as a 2-phase mechanism rather than by dilation of pores or by fissuring. However, because of the limited number of tests completed in this comparison, no definite conclusions can be drawn in regards to the effects of gas-breakthrough testing on pore-structure. A more thorough study using MIP to investigate gas-breakthrough specimens could be of value to future investigations.

5.4.3.2 *Pore-size determined from the capillary pressure equation*

Figure 5.8 shows sample calculations for determining the theoretical pore-size corresponding to gas-breakthrough for specimen T2, based on DDL theory, the observed gas-breakthrough pressure, and the capillary pressure equation. The DDL thickness is assumed to be 0.5 nm (0.5×10^{-9} m) which is the approximate thickness of the Stern layer (EDL) alone. This minimal DDL thickness is chosen because the extent of the effects of a DL cation cloud would likely be minimal in an inactive clay such as illite. The DDL in buffer material is assumed to be only 0.5 nm as well, although this value could be as high as 10 nm. Based on DDL theory and the phase equations for illite, the mean pore-diameter in specimen T2 was calculated as 1.13 times the effective pore-diameter (1.13 times the diameter of pores that actually

contribute to flow within the soil). The effective pore-diameter was also back-calculated using the capillary pressure equation, with the capillary pressure equated to the observed gas-breakthrough pressure. The pore-size determined by this method of analysis is considered an 'effective' pore-size because the effects of the DDL are accounted for. The MIP tests, on the other hand, yield the 'total' pore-size because the extent of the DDL effects cannot be determined or accounted for. The surface tension at the gas-water interface was assumed to be 0.073 N/m, which is similar to the value used by various researchers in similar studies (Wheeler et. al., 1990, Fredlund and Rahardjo, 1993, for example). The effective pore-diameter determined for specimen T2 at gas-breakthrough was 0.097 μm, so the total pore-diameter was (1.13 x 0.097 μm) = 0.11 μm. This value is near the peak-frequency for pore-size (0.15 μm) shown in the MIP data for specimen T2 in Figure 5.7(a). With this information in mind, it should be noted that pores contributing to gas flow in specimen T2 are those larger than 0.15 μm in Figure 5.7(a). The gas-breakthrough pressure predicted from this work was 2.9 MPa while the observed gas-breakthrough pressure was 3.0 MPa.

Similar calculations for T46 and BT3 are also shown in Figure 5.8. The theoretical value for the pore-size corresponding to gas-breakthrough in specimen T46 (0.23 μm) fits similarly well within the PSD shown in Figure 5.7(b) for that specimen. The predicted gas-breakthrough pressure for T46 was 1.5 MPa while the observed gas-breakthrough pressure was 1.4 MPa. The value calculated for buffer specimen BT3 (0.47 μm) appears to be relatively low when compared to typical PSD data for buffer. The predicted gas-breakthrough pressure for BT3 was 0.01 MPa while the observed gas-breakthrough pressure was 9.4 MPa. One would expect the pores within the large pore mode (5 to 50 μm) to be interconnected so that gas could pass through a

specimen without entering the smaller pore mode which contains the pores of 0.18 μm diameter.

The calculations shown in Figure 5.8 offer an explanation for higher gas-breakthrough pressures in buffer specimens than in illite specimens when the illite was compacted to higher dry densities. The basis of the explanation is that the sodium-bentonite constituent of buffer material has approximately ten times the specific surface area of illite, so buffer contains a much larger volume of bound water, all else equal. Therefore, although the porosity in buffer is approximately 30 times that of illite, its effective porosity is much less than that of illite, even neglecting the effects of a DL. In other words, the pore-space available for flow to occur in buffer is much less than in illite, so the effective pore-diameters in buffer are smaller than in illite. Therefore, higher gas pressures are required to overcome the higher capillary pressure associated with pore-space in buffer.

Numerous assumptions were made in comparing the PSD and gas-breakthrough pressure of the test materials. With these assumptions in mind, the theoretical values of gas-breakthrough pore-size calculated herein appear to correspond well to available PSD information for the test materials, especially in the illitic clay specimens. This conclusion gives merit to the postulation that gas-breakthrough pressure and capillary pressure are intimately linked.

6. CONCLUSIONS AND RECOMMENDATIONS

6.1 CONCLUSIONS

The research described in this thesis had three primary objectives. Stated in the Scope of Research in Chapter 2, these were:

1) to review and explain the mechanism for gas migration through compacted clay media,
2) to design, construct, qualify, install and demonstrate the suitability of a new testing system to measure the gas pressure differential across compacted clay specimens at which gas-breakthrough occurs, and
3) using the new testing system, to complete an initial series of tests on selected compacted engineered clay barrier materials to define gas-breakthrough pressure differentials and provide explanations for the phenomena observed.

These three objectives have been achieved.

The following detailed conclusions are drawn with respect to the testing system.

- An apparatus is now available for the safe measurement of gas-breakthrough pressures and one-dimensional gas flows through specimens of compacted clay

at gas pressures of up to 10 MPa.

- Procedures are in place for testing saturated and unsaturated materials. The procedures defined for the safe use of the new apparatus are understandable and transferrable to inexperienced operators by means of a testing manual.

- Due to effects on the pore size distribution at the interface between the compacted clay specimen and the inner test cell wall, the measured gas-breakthrough pressures may be less than those of a semi-infinite mass of the compacted clay.

The following detailed conclusions are drawn with respect to gas-breakthrough differential pressures in compacted illitic clay soils.

- For the compacted illitic clays tested, under the given test conditions, there is a critical degree of saturation (S = 80%) below which gas-breakthrough resistance decreases to a small fraction of that of equivalent, saturated materials. This can be explained by the hypothesis given by Wheeler (1988) and Corey (1990) that below the critical degree of saturation pore-space will contain a number of continuous gas-filled pathways.

- Gas-breakthrough pressure for the illite specimens ranged from 0.2 MPa to 6.4 MPa. The resistance of compacted illitic clay to gas-breakthrough increases directly and curvilinearly with increasing dry density and degree of saturation. The following equations describe the gas-breakthrough / dry density relationship for illite clays

compacted to degrees of saturation above and below S = 80%:

$$P_{BT} = 3.57 \times 10^{-4} \, e \, \wedge \, (4.58 \, \rho_d), \quad \text{for } S > 80\%, \text{ and}$$

$$P_{BT} = 1.30 \times 10^{-3} \, e \, \wedge \, (3.00 \, \rho_d), \quad \text{for } S < 80\%,$$

where P_{BT} = Gas-breakthrough pressure (MPa)

ρ_d = Dry-density (Mg/m^3).

The existence of separate gas-breakthrough / dry density relationships for clays compacted above and below S = 80% reflects the hypothesis of Corey (1990) and Wheeler (1988) mentioned above.

- The equations may not apply outside the given test conditions. Gas-breakthrough pressures may depend on test conditions such as specimen length, test duration and type of gas. Moreover, in common with other engineering properties of compacted clays, it is likely that gas-breakthrough pressures will be affected by scale which influences clay structure.

- Based on reasonable assumptions regarding illitic clay microstructure, the measured gas-breakthrough pressures, and the measured pore-size distributions based on mercury intrusion testing, gas-breakthrough resistance can be explained in terms of capillary theory and is related to porosity.

- Observations indicate the occurrence of a variety of gas flow mechanisms and flow paths at gas-breakthrough. The exact nature of the flow mechanism involved remains unclear and the effects of gas-breakthrough on clay microstructure are unclear.

For sand-bentonite (buffer) mixtures the following conclusions are drawn.

- The new equipment is not suitable for measuring gas-breakthrough pressures in buffer at the specified minimum dry density of 1.67 Mg/m^3. Only one of the buffer specimens reached its gas-breakthrough pressure (9.4 MPa) before the limiting pressure of the equipment was reached. Equipment with capacity greater than 10 MPa gas pressure will likely be required.

- In contrast with compacted illitic clay, under the test conditions used, the gas-breakthrough pressures of buffer are not directly related to either porosity or the maximum pore size measured using mercury intrusion testing. It is possible that microstructural factors such as decreased apparent porosity due to structured water could influence the gas-breakthrough process.

- Pusch (1993) suggests that the swelling pressure of bentonite materials such as MX-80 bentonite and the gas-breakthrough pressure are related such that gas-breakthrough will occur at 50% to 90% of the swelling pressure. This relationship between swelling pressure and gas-breakthrough pressure does not appear to hold for the buffer material specified for the Canadian nuclear fuel waste disposal concept.

6.2 RECOMMENDATIONS FOR FURTHER RESEARCH

Upon completion of the test program reported here, a number of issues remain unclear regarding gas-breakthrough testing in general and, more specifically, gas-breakthrough testing of illitic clay and buffer. The following are recommendations for future research that will clarify some aspects of the gas-breakthrough research program.

- Specimen size effects should be investigated. More specifically, specimens with larger diameter and with greater length should be tested. This will require the manufacturing of larger test cells.

- Gas pressure load rates should be varied to determine the effects of test duration on testing. The size of the pressure increment and its frequency should be varied separately.

- Specimens of differing lengths should be tested at different backpressures to de-couple the effects of pressure difference and pressure gradient on test results.

- The type of permeating gas should be varied to determine its effects on gas-breakthrough pressures.

- The actual pathway of permeating gases should be determined to ensure that gases are not bypassing specimens along the inner test cell wall and to determine the specific gas migration mechanisms involved with gas-breakthrough.

Technologies such as the use of radioactive gases, mercury intrusion testing, and electron microscopy may prove useful for this analysis.

- Test equipment for future studies should be capable of measuring gas flow directly in units of volume so that, for completeness, a mass balance of pore-fluids within specimens can be achieved.

- Future test equipment may require the addition of a gas saturation device in the gas inflow circuit, as described and used by researchers such as Volkaert et. al. (1993), to more completely separate the gas and water phases within a specimen. This may simplify analysis and lead to a better understanding of the gas-breakthrough mechanism.

	Sealbond	Sodium-bentonite
Specific gravity, Gs	2.76	2.75
Grain size distribution % Clay % Silt % Sand	 28 71 1	 66 33.5 0.5
Dominant mineral(s)	illite, kaolin	smectite/montmorillonite
Atterberg limits (in DDW) Liquid limit, wL Plastic limit, wP Plasticity index, I	 20 31 11	 49 257 208
Specific surface area (m^2/g)	60 (approx.)	600 (approx.)
Cation exchange capacity, CEC (meq/100 g)	15 (approx.)	60 (approx.)

Table 4.1: Summary of illite and buffer test specimen properties (after Dixon and Woodcock, 1986).

Test ID	TARGET			COMPACTED			Moisture change (%)
	Moisture (%)	Dry density (Mg/m^3)	Saturation (%)	Moisture (%)	Dry density (Mg/m^3)	Saturation (%)	
T1	13.0	1.90	79.3	12.90	1.90	78.9	-0.39
T2	12.0	2.04	93.0	12.79	2.02	96.5	3.19
T3	14.0	1.93	89.8	14.50	1.92	90.9	1.75
T4	14.0	1.95	93.0	14.50	1.94	95.0	1.75
T5	15.0	1.90	91.5	15.27	1.90	92.5	0.89
T6	15.0	1.93	96.3	15.21	1.92	96.3	0.70
T7	15.0	1.95	99.7	15.20	1.95	100.4	0.66
T8	14.0	1.90	85.4	14.38	1.89	86.8	1.34
T9	15.0	1.90	91.5	14.74	1.90	90.6	-0.87
T10	16.0	1.90	97.6	16.15	1.90	98.1	0.47
T11	16.0	1.90	97.6	16.19	1.90	98.3	0.59
T12	16.0	1.87	92.8	16.20	1.87	93.5	0.62
T13	11.0	2.11	98.6	11.47	2.10	100.8	2.09
T14	11.0	2.07	91.1	11.28	2.06	91.8	1.26
T15	11.0	2.03	84.4	10.99	2.03	84.3	-0.05
T16	14.0	1.93	89.8	13.97	1.93	89.7	-0.11
T17	11.0	2.00	79.9	12.05	2.00	87.4	4.56
T18	12.0	2.00	87.2	12.05	1.98	84.6	0.21
T19	11.0	1.95	73.1	13.80	1.95	91.5	11.29
T20	13.5	1.99	96.3	13.64	1.99	97.8	0.52
T21	13.8	1.99	98.4	13.64	1.99	97.8	-0.58
T22	13.8	1.99	98.4	13.70	1.99	98.0	-0.36
T23	13.8	2.00	100.2	12.06	2.00	87.4	-6.73
T24	13.8	2.00	100.2	10.92	2.00	79.5	-11.65
T25	12.0	1.95	79.7	11.13	1.95	73.7	-3.76
T26	11.0	1.90	67.1	11.13	1.90	67.7	0.59
T27	11.0	2.10	96.6	11.11	2.10	97.2	0.50
T28	12.0	1.90	73.2	11.62	1.91	71.7	-1.61
T29	13.5	1.95	89.7	13.93	1.94	91.4	1.57
T30	11.0	1.90	67.1	11.22	1.90	68.0	0.99
T31	10.0	1.85	56.1	10.11	1.85	56.6	0.55
T32	10.0	1.97	68.8	10.12	1.97	69.4	0.60
T33	10.0	1.97	68.8	10.11	1.97	69.4	0.55
T34	11.0	1.90	67.1	11.03	1.90	67.2	0.14
T35	11.0	1.90	67.1	11.03	1.90	67.2	0.14
T36	11.0	2.03	84.4	11.35	2.02	86.0	1.57
T37	11.0	2.09	94.7	11.35	2.08	96.5	1.57
T38	12.0	1.90	73.2	12.57	1.89	75.5	2.32
T39	12.0	2.04	93.8	12.57	2.03	96.5	2.32
T40	12.0	2.05	95.6	12.27	2.05	96.9	1.11
T41	13.5	1.95	89.7	13.46	1.95	89.6	-0.15
T42	13.5	1.95	89.7	13.46	1.95	89.6	-0.15
T43	10.5	2.00	76.3	10.58	2.00	76.7	0.38
T44	13.0	2.01	96.2	13.28	2.00	97.3	1.07
T45	16.0	1.91	99.2	16.75	1.90	101.8	2.29
T46	16.0	1.91	99.2	16.75	1.90	101.8	2.29
						Average	***-2.68***
B1	11.4	1.67	49.9	11.05	1.68	48.8	-1.56
B2	19.4	1.67	84.9	18.54	1.68	82.8	-2.27
B3	11.4	1.67	49.9	11.17	1.67	49.2	-1.02
B4	19.4	1.67	84.9	18.51	1.68	82.7	-2.35
B5	20.4	1.67	89.3	20.13	1.70	92.6	-0.67
B6	20.4	1.67	89.3	20.13	1.70	92.6	-0.67
						Average	***-1.42***

Table 4.2: Illite and buffer specimen preparation: targeted and compacted data.

Test ID	Final moisture contents												% difference over height	% difference lateral
	mean	range	std dev	no. of tests	mean top	no. of tests	mean bottom	no. of tests	mean outer	no. of tests	mean inner	no. of tests		
QC1	13.7	0.3	0.13	4	13.78	2	13.78	2	13.62	2	13.73	2	0.00	-0.40
QC2	16.7	1.6	0.72	4	17.18	2	15.76	2	16.36	2	16.58	2	4.31	-0.67
QC3	17.2	0.1	0.04	4	17.15	2	17.21	2	17.17	2	17.20	2	-0.17	-0.09
QC4*	15.9	0.6	0.23	4	16.03	2	15.61	2	15.80	2	15.84	2	1.33	-0.13
QC5	14.9	0.4	0.16	4	15.05	2	14.74	2	14.87	2	14.89	2	1.04	-0.07
QC6	14.5	0.9	0.36	4	14.83	2	14.13	2	14.49	2	14.48	2	2.42	0.03
QC7	15.5	0.3	0.11	4	15.53	2	15.47	2	15.47	2	15.53	2	0.19	-0.19
QC8	15.8	0.4	0.15	4	15.73	2	15.92	2	15.77	2	15.90	2	-0.60	-0.41

* Wet filters were used for all QC tests except QC4.

Table 5.1: Final moisture content spatial variations for QC specimens.

Test ID	Target	Compacted		Final					Percent difference		
	w (%)	w (%)	dry density (Mg/m^3)	mass (g)	specimen diameter (mm)	specimen height (mm)	w (%)	dry density (Mg/m^3)	w (%) target to compacted	w (%) compacted to final	dry density
QC1	12.3	12.39	2.03	112.01	51.12	24.59	13.68	1.95	0.36	4.95	-2.01
QC2	12.3	11.51	1.94	> specimen crushed upon extrusion <			16.47	---	-3.32	17.73	---
QC3	16.5	16.39	1.87	106.07	50.76	24.32	17.18	1.84	-0.33	2.35	-0.81
QC4 *	16.5	15.91	1.88	105.36	50.68	24.08	15.91	1.87	-1.82	0.00	-0.27
QC5	13.7	13.84	2.00	111.13	50.84	25.04	14.90	1.90	0.51	3.69	-2.56
QC6	13.7	13.84	2.00	111.37	50.80	25.09	14.98	1.90	0.51	3.96	-2.56
QC7	13.7	13.95	1.92	107.08	50.79	24.31	15.50	1.88	0.90	5.26	-1.05
QC8	13.7	13.95	1.92	107.39	50.82	24.50	15.83	1.87	0.90	6.31	-1.32

* Wet filters were used for all QC tests except QC4

Table 5.2: Dry density and moisture content data for QC specimens.

Test ID	Final moisture contents												% difference over height	% difference lateral
	mean	range	std dev	no. of tests	mean top	no. of tests	mean bottom	no. of tests	mean outer	no. of tests	mean inner	no. of tests		
	Saturated													
T4	14.6	1.4	0.44	5	15.23	1	13.86	1	14.69	1	14.54	1	4.71	0.51
T12	17.6	0.3	0.11	3	—*	—	—	—	17.56	1	17.43	1	—	0.37
T14	11.1	0.5	0.21	3	—	—	—	—	11.28	1	10.82	1	—	2.08
	Unsaturated, wet filters													
T22	13.2	2.9	1.04	4	—	—	—	—	14.51	1	13.60	1	—	3.24
T23	12.0	0.4	0.15	3	—	—	—	—	12.21	1	11.86	1	—	1.45
T25	13.7	0.4	0.19	3	—	—	—	—	13.41	1	13.79	1	—	-1.40
	Unsaturated, dry filters													
T30	10.9	0.1	0.04	3	—	—	—	—	10.93	1	10.83	1	—	0.46
T31	9.9	0.1	0.05	4	9.87	2	9.85	2	9.90	2	9.81	2	0.10	0.46
T34	10.8	0.4	0.17	4	11.00	2	10.67	2	10.85	2	10.82	2	1.52	0.14
T35	10.6	0.2	0.08	4	10.52	2	10.49	2	10.57	2	10.44	2	0.14	0.62
T40	11.4	1.0	0.44	3	11.85	1	10.81	1	11.55	1	11.33	2	4.59	0.96
T42	13.4	1.6	0.68	4	14.15	2	12.85	2	13.67	2	13.37	2	4.81	1.11

* Because final moisture contents were taken in different orientations, some spatial variations could not be investigate

Table 5.3: Final moisture content spatial variations for gas-breakthrough specimens.

Test ID	Compacted			After saturation			Final (after bt test)		w (%) change during bt test	Gas-breakthrough (MPa)
	w (%)	S (%)	Dry density (Mg/m^3)	Qin (mL)	w (%)	S (%)	w (%)	S (%)		
	Saturated									
T1	12.9	78.8	1.90	1.09	14.0	86.0	16.0	98.1	6.6	2.2
T3	14.5	90.9	1.92	1.13	15.7	98.6	15.5	97.1	-0.8	2.4
T4	14.5	95.0	1.94	0.51	15.0	98.5	14.6	95.6	-1.5	2.8
T5	15.3	92.5	1.90	0.75	16.1	97.4	16.1	97.7	0.2	2.2
T6	15.2	96.3	1.92	1.00	16.3	103.1	16.0	101.3	-0.9	2.6
T7	15.2	100.4	1.95	0.21	15.4	101.8	15.3	100.7	-0.6	2.8
T8	14.4	86.8	1.89	1.29	15.8	95.3	16.4	98.9	1.8	2.2
T9	14.7	90.6	1.90	1.23	16.1	98.8	15.9	97.8	-0.5	2.6
T10	16.2	98.1	1.90	0.77	17.0	103.2	16.1	97.8	-2.7	2.4
T11	16.2	98.3	1.90	0.35	16.6	100.6	16.6	100.6	0.0	2.2
T12	16.2	93.5	1.87	0.25	16.5	95.1	17.6	101.4	3.2	2.3
T13	11.5	100.8	2.10	0.14	11.6	102.0	11.0	96.7	-2.7	6.0
T14	11.3	91.8	2.06	0.42	11.7	95.2	11.1	90.4	-2.6	5.6
T15	11.0	84.3	2.03	1.99	13.0	99.9	11.9	91.2	-4.5	4.7
T16	14.0	89.7	1.93	0.64	14.7	94.1	15.2	97.6	1.8	2.6
T17	12.1	87.4	2.00	1.14	13.2	95.9	14.3	104.0	4.0	3.4
T18	12.1	84.6	1.98	0.98	13.1	91.8	13.0	91.6	-0.1	4.0
T19	13.8	91.5	1.95	0.67	14.5	96.2	15.2	101.0	2.4	2.6
T20	13.6	97.8	1.99	0.73	14.4	103.2	14.0	100.6	-1.3	3.2
T21	13.6	97.8	1.99	0.86	14.5	104.2	14.7	105.2	0.5	3.2
	Unsaturated, wet filters									
T22	13.7	98.0	1.99	0.00	13.7	98.0	13.3	95.2	-1.4	3.2
T23	12.1	87.4	2.00	0.00	12.1	87.4	12.0	87.0	-0.2	4.0
T24	10.9	79.5	2.00	0.00	10.9	79.5	11.9	86.7	4.3	3.8
T25	11.1	73.7	1.95	0.00	11.1	73.7	13.7	90.5	10.2	2.4
T26	11.1	67.7	1.90	0.00	11.1	67.7	15.1	91.8	15.1	1.6
T27	11.1	97.2	2.10	0.00	11.1	97.2	10.5	92.1	-2.7	6.4
T29	13.9	91.4	1.94	0.00	13.9	91.4	15.7	102.9	5.9	3.5

Table 5.4(a): Gas-breakthrough test specimen conditions and gas-breakthrough pressures for saturated tests and unsaturated tests with wet filters.

Test ID	Compacted			After saturation			Final (after bt test)		w (%) change during bt test	Gas-breakthrough (MPa)
	w (%)	S (%)	Dry density (Mg/m^3)	Qin (mL)	w (%)	S (%)	w (%)	S (%)		
	Unsaturated, dry filters									
T2	12.8	96.5	2.02	0.00	12.8	96.5	11.3	84.9	-6.4	3.0
T28	11.6	71.7	1.91	0.00	11.6	71.7	12.6	77.5	3.9	0.4
T30	11.2	68.0	1.90	0.00	11.2	68.0	10.9	66.1	-1.4	0.4
T31	10.1	56.6	1.85	0.00	10.1	56.6	9.9	55.2	-1.3	0.4
T32	10.1	69.4	1.97	0.00	10.1	69.4	9.6	65.8	-2.7	0.4
T33	10.1	69.4	1.97	0.00	10.1	69.4	10.0	68.7	-0.4	0.2
T34	11.0	67.2	1.90	0.00	11.0	67.2	10.8	66.0	-0.9	0.4
T35	11.0	67.2	1.90	0.00	11.0	67.2	10.5	64.0	-2.5	0.4
T36	11.4	86.0	2.02	0.00	11.4	86.0	10.9	82.5	-2.1	1.6
T37	11.4	96.5	2.08	0.00	11.4	96.5	10.0	84.7	-6.5	4.0
T38	12.6	75.5	1.89	0.00	12.6	75.5	12.0	72.2	-2.2	0.4
T39	12.6	96.5	2.03	0.00	12.6	96.5	11.3	86.8	-5.3	4.2
T40	12.3	96.9	2.05	0.00	12.3	96.9	11.4	90.0	-3.7	4.0
T41	13.5	89.6	1.95	0.00	13.5	89.6	13.9	92.6	1.7	2.4
T42	13.5	89.6	1.95	0.00	13.5	89.6	13.5	89.8	0.1	2.6
T43	10.6	76.7	2.00	0.00	10.6	76.7	10.6	77.0	0.2	0.6
T44	13.3	97.3	2.00	0.00	13.3	97.3	12.7	92.9	-2.4	3.4
T45	16.8	101.8	1.90	0.00	16.8	101.8	16.1	97.9	-1.9	1.2
T46	16.8	101.8	1.90	0.00	16.8	101.8	15.9	96.6	-2.6	1.4
	Buffer									
BT1	11.1	48.8	1.68	0.00	11.1	48.8	18.8	80.3	26.0	—
BT2	18.5	82.8	1.68	0.00	18.5	82.8	22.3	96.1	9.2	—
BT3	11.2	49.2	1.67	0.00	11.2	49.2	17.5	74.3	22.0	9.4
BT4	18.5	82.7	1.68	0.00	18.5	82.7	20.0	86.3	3.9	—
BT5	20.1	92.6	1.70	0.00	20.1	92.6	20.9	92.6	1.8	—
BT6	20.1	92.6	1.70	0.00	20.1	92.6	22.0	97.8	4.5	—

Table 5.4(b): Gas-breakthrough test specimen conditions and gas-breakthrough pressures for unsaturated tests with dry filters and buffer tests.

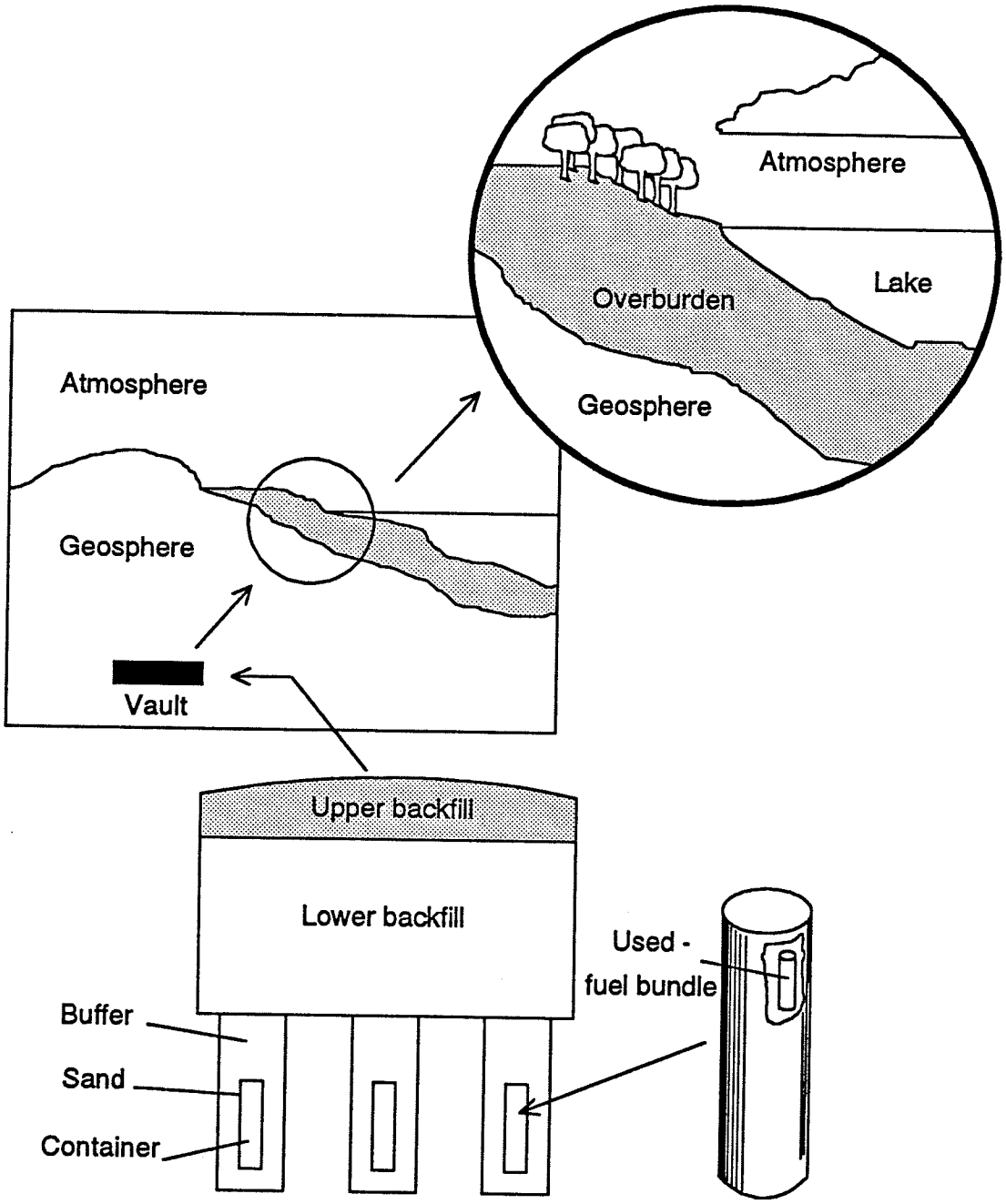

Figure 1.1: Overview of the containment barriers in the Canadian nuclear fuel waste repository scheme (from AECL EIS, 1994).

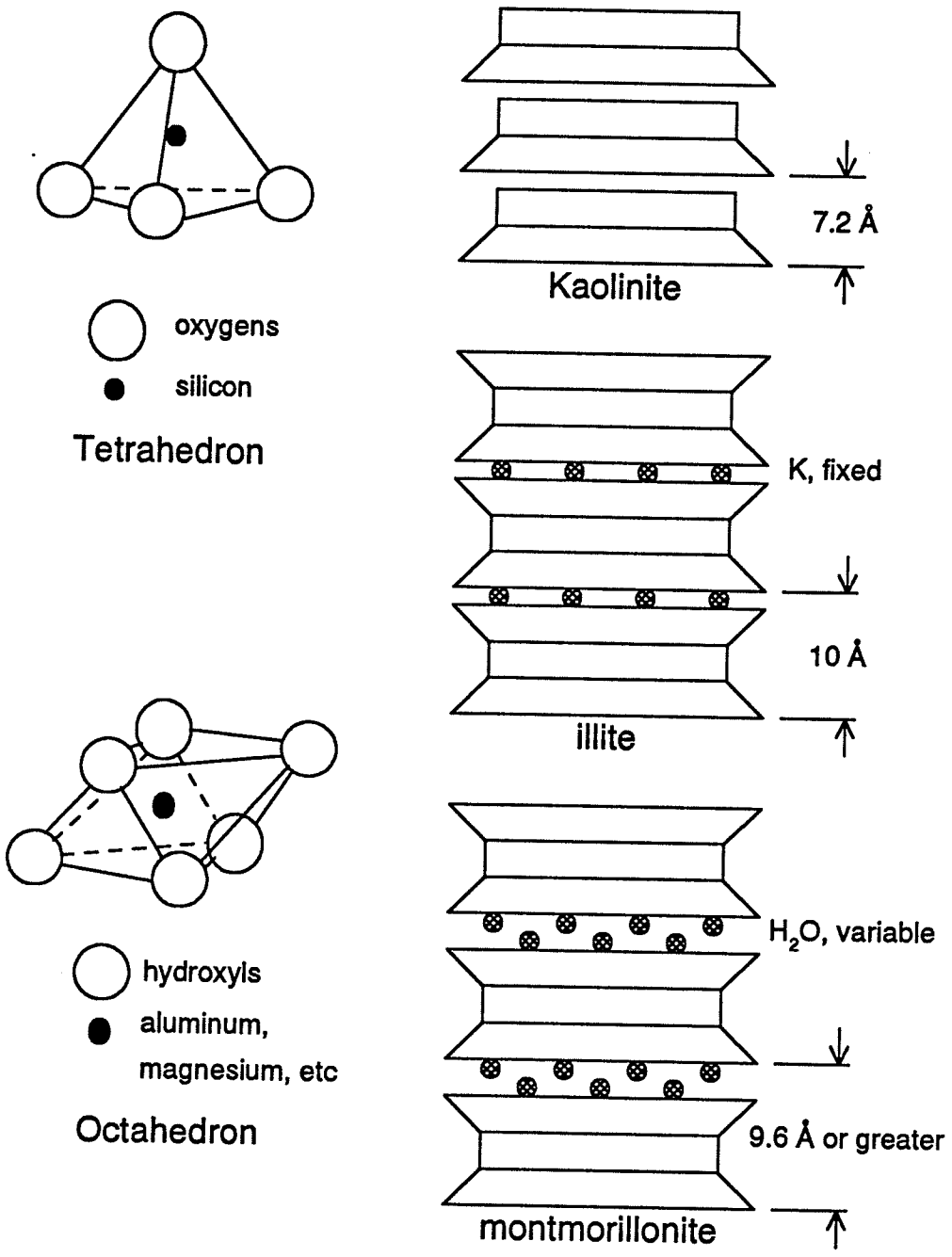

Figure 2.1: Basic microstructural unit structures and stacking arrangements (after Mitchell, 1976).

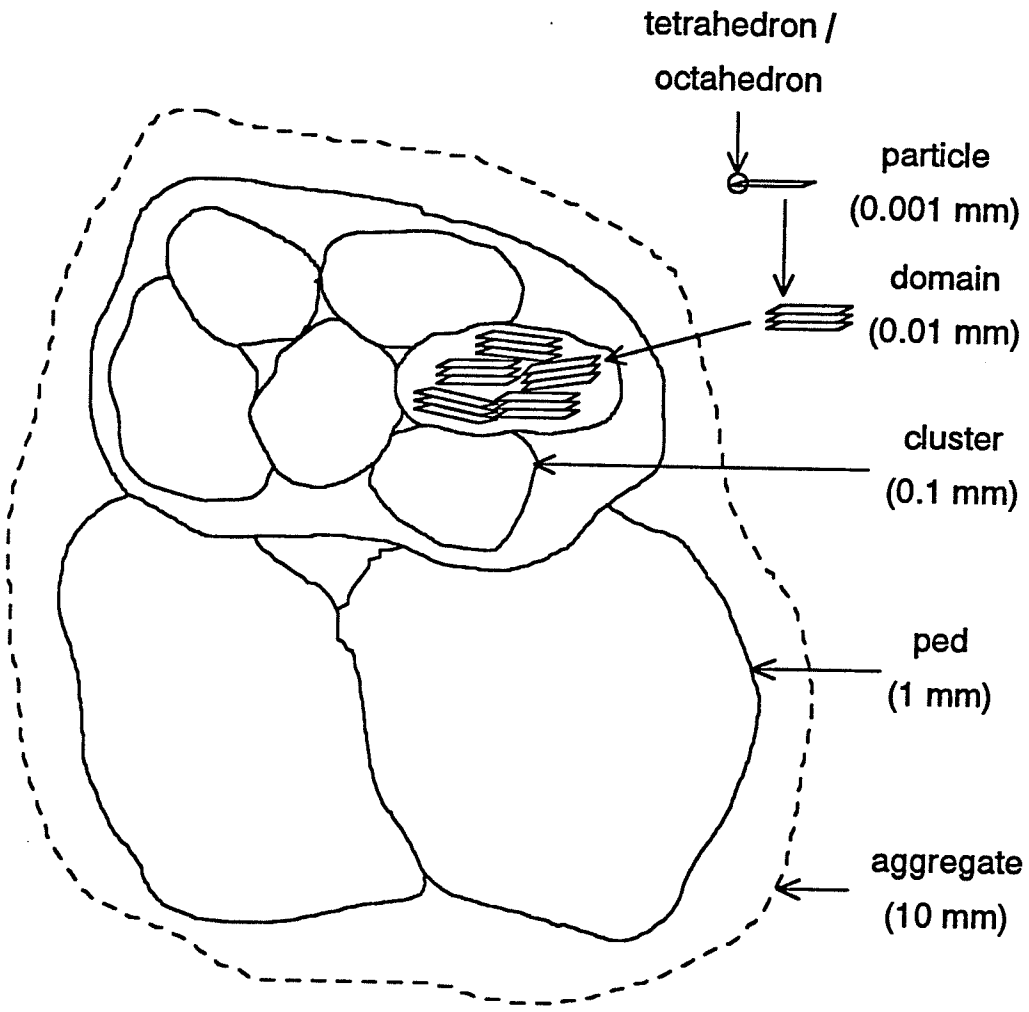

Figure 2.2: Convention for differentiation between various clay fabric structural levels.

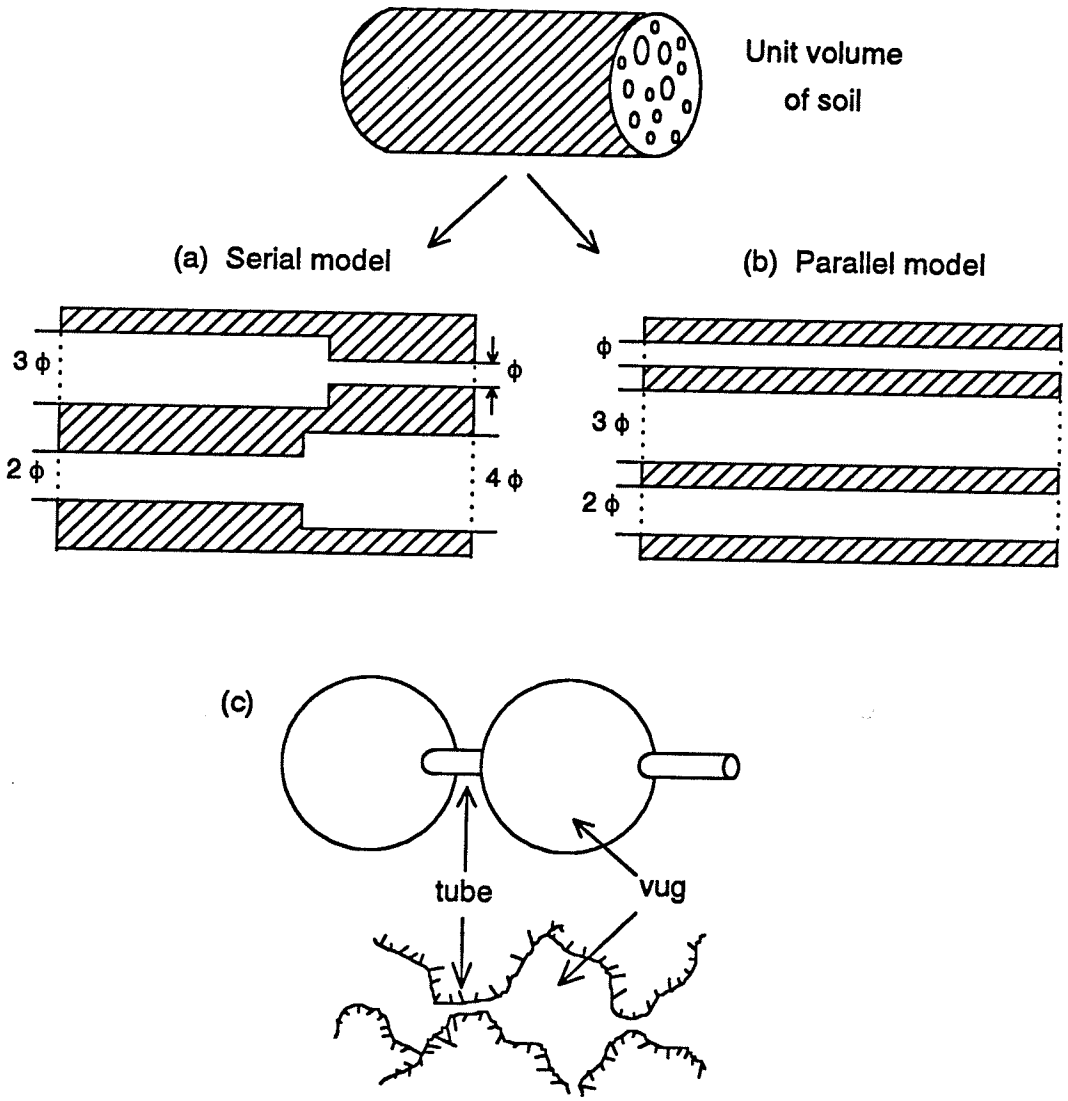

Figure 2.3: Porous media pore-structure models (after Ruth, 1993).

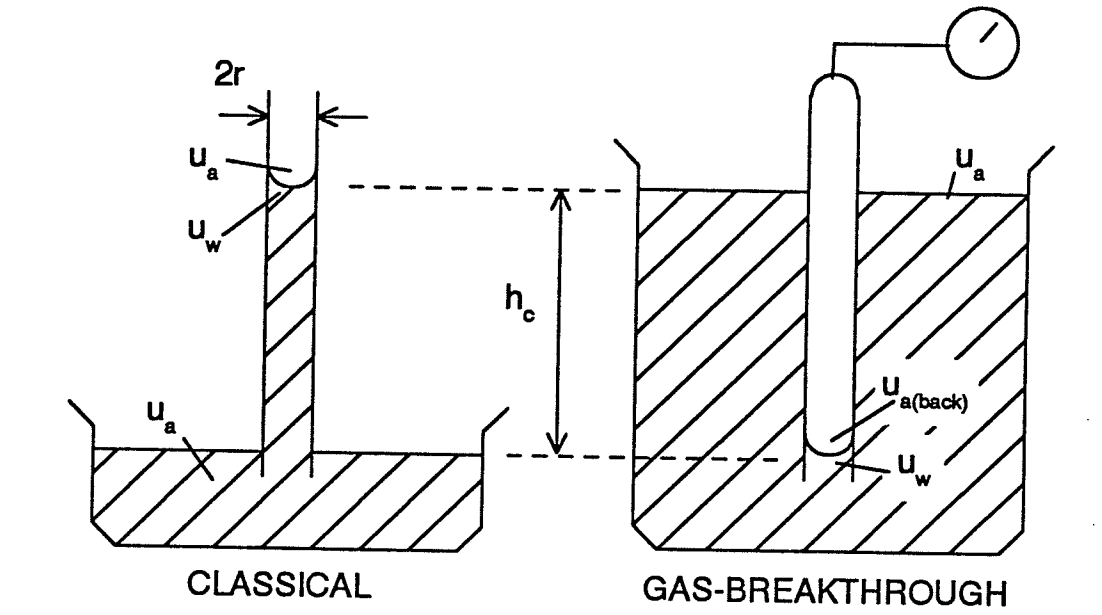

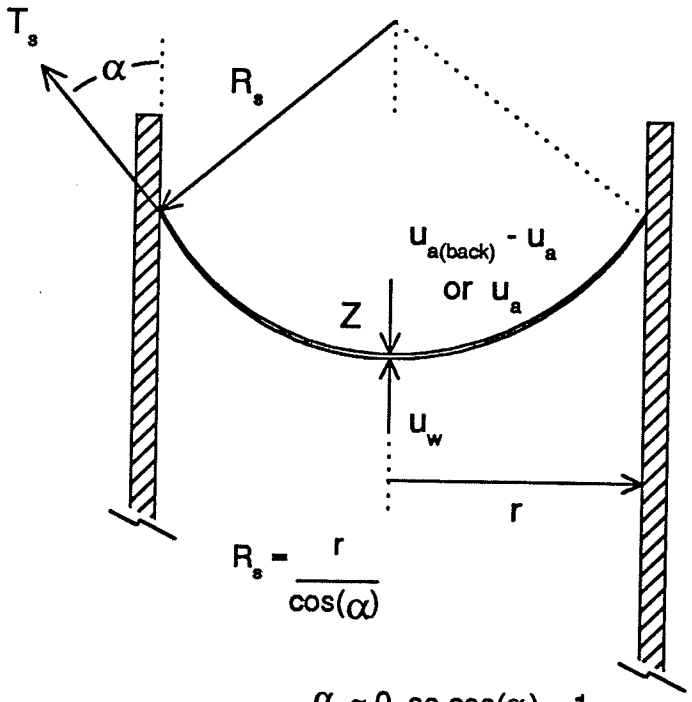

vertical force equilirium at Z:

$$2\Pi r T_s \cos(\alpha) = \Pi r^2 h_c \rho_w g$$

$$\text{or } h_c = \frac{2 T_s \cos(\alpha)}{\rho_w g r}$$

$$u_w = -\rho_w g h_c$$

$$u_a = 0 \text{ (atmospheric)}$$

$$h_c = (u_a - u_w) = \rho_w g h_c$$

$$(u_a - u_w) = \frac{2 T_s \cos(\alpha)}{r}$$

$$|h_c| = (u_a - u_w) = \frac{2 T_s}{r}$$

$$\text{or } |h_c| = (u_{a(back)} - u_a - u_w) = \frac{2 T_s}{r}$$

Figure 2.4: Capillary pressure model (after Fredlund and Rahardjo, 1993).

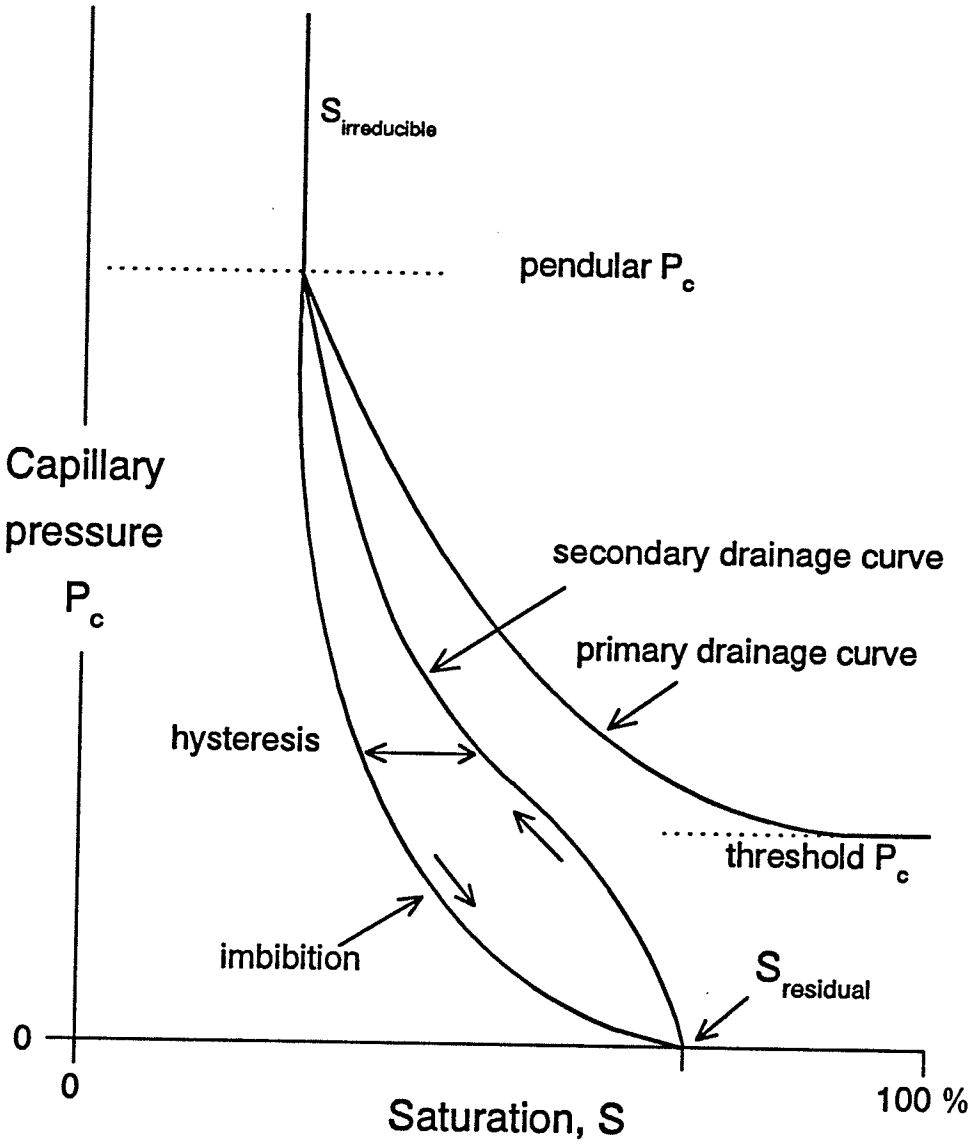

Figure 2.5: Typical capillary pressure curve (after Ruth, 1993).

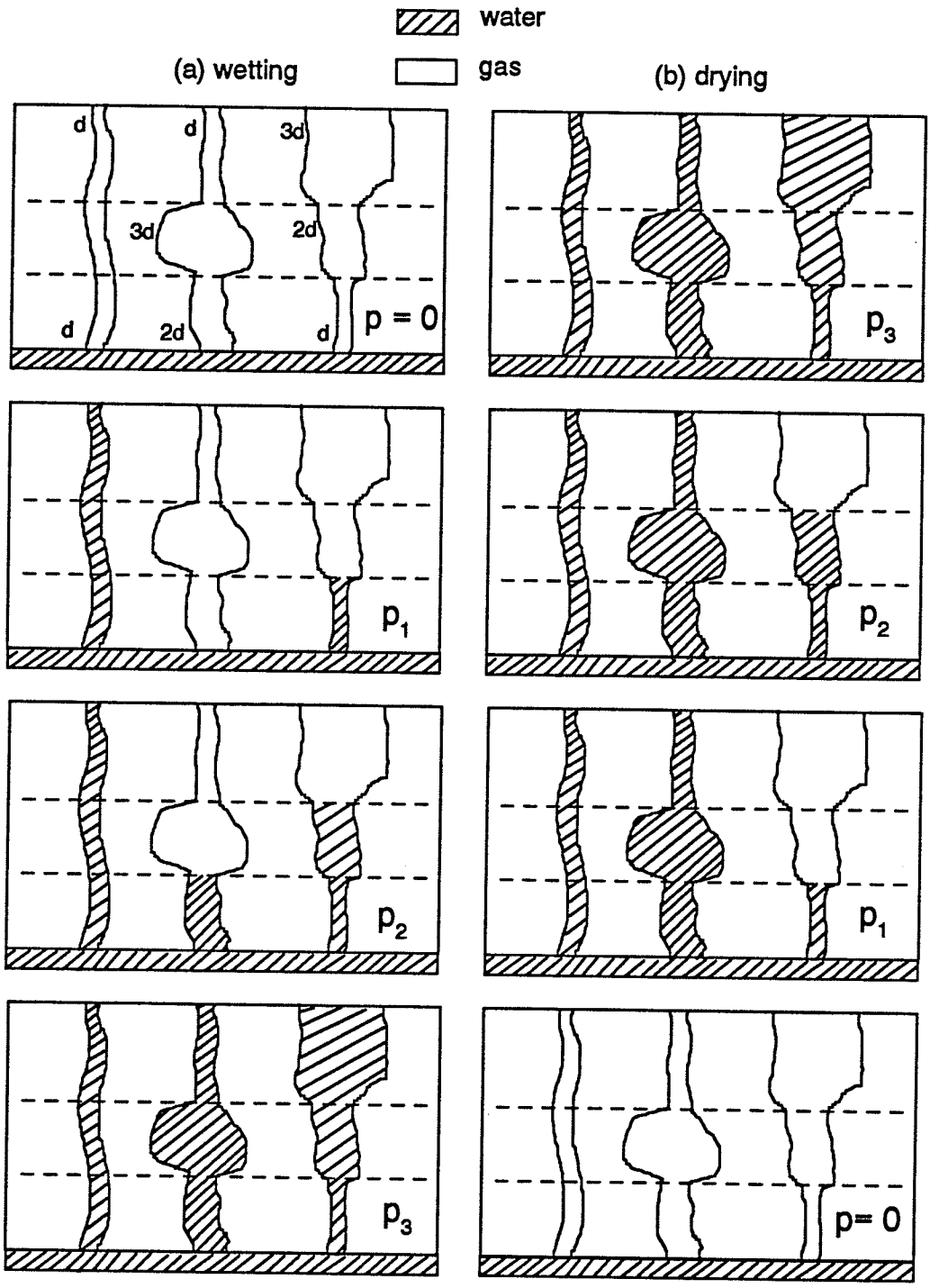

Figure 2.6: "Bottleneck" phenomenon causing hysteresis between wetting (imbibition, saturation) and drying (drainage, de-saturation) processes (after Ruth, 1993).

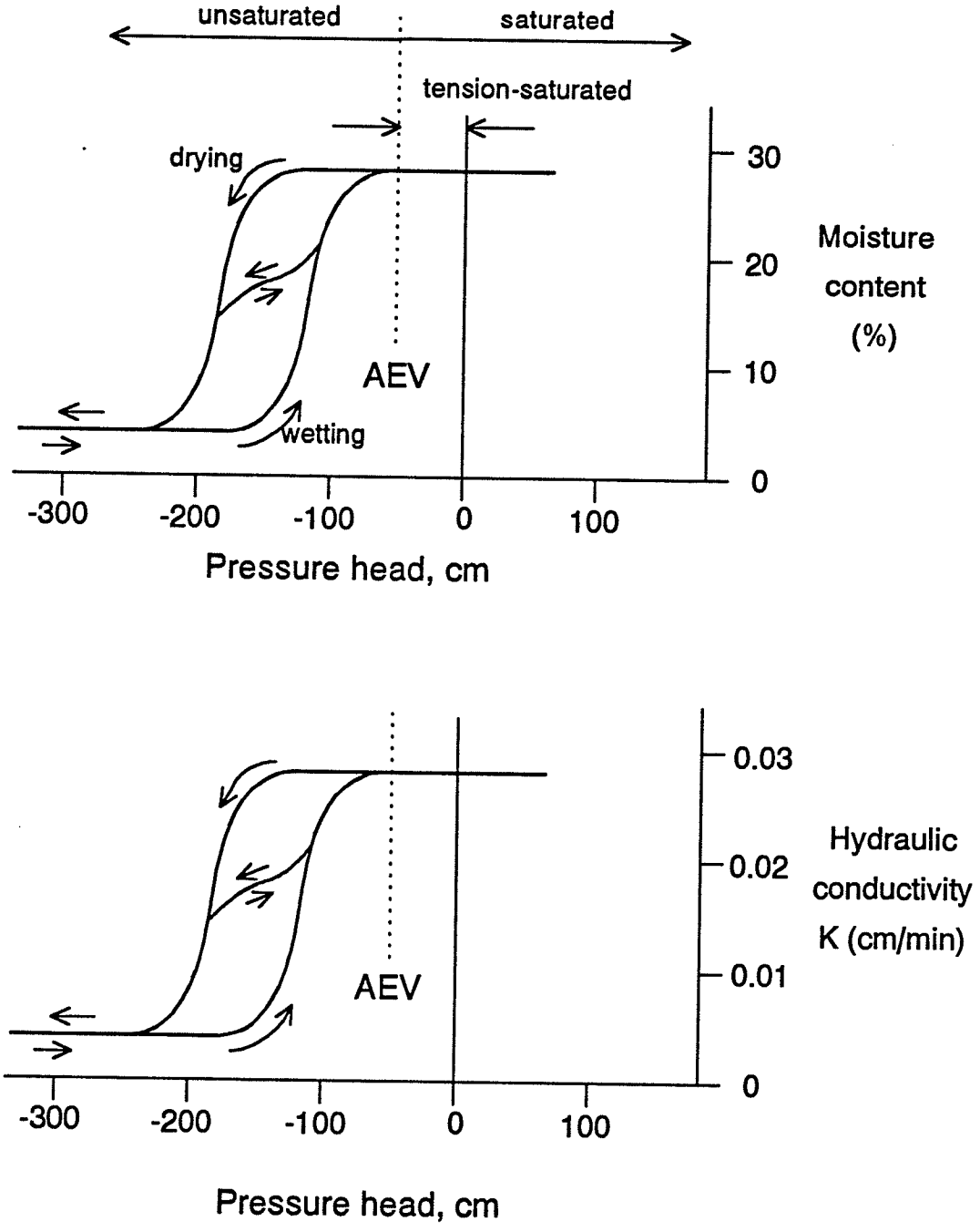

Figure 2.7: Characteristic curves for a typical soil showing moisture content and hydraulic conductivity versus pressure (after Freeze and Cherry, 1979).

Flux	Gradient			
	Hydraulic head	Temperature	Electrical	Chemical concentration
Fluid	***Hydraulic conductivity (DARCY's LAW)***	Thermo-osmosis	Electro-osmosis	Chemical osmosis
Heat	Isothermal heat transfer	***Thermal conduction (FOURIER's LAW)***	Peltier effect	Dufour effect
Current	Streaming current	Thermo-electricity: Seebeck effect	***Electric conduction (OHM's LAW)***	Diffusion & membrane potentials
Ion	Streaming current	Thermal Diffusion: Soret effect	Electro-phoresis	***Diffusion (FICK's LAW)***

Figure 2.8: Direct and coupled flow phenomena (after Mitchell, 1976). Direct flow phenomena in *italics* on diagonal from top left to bottom right.

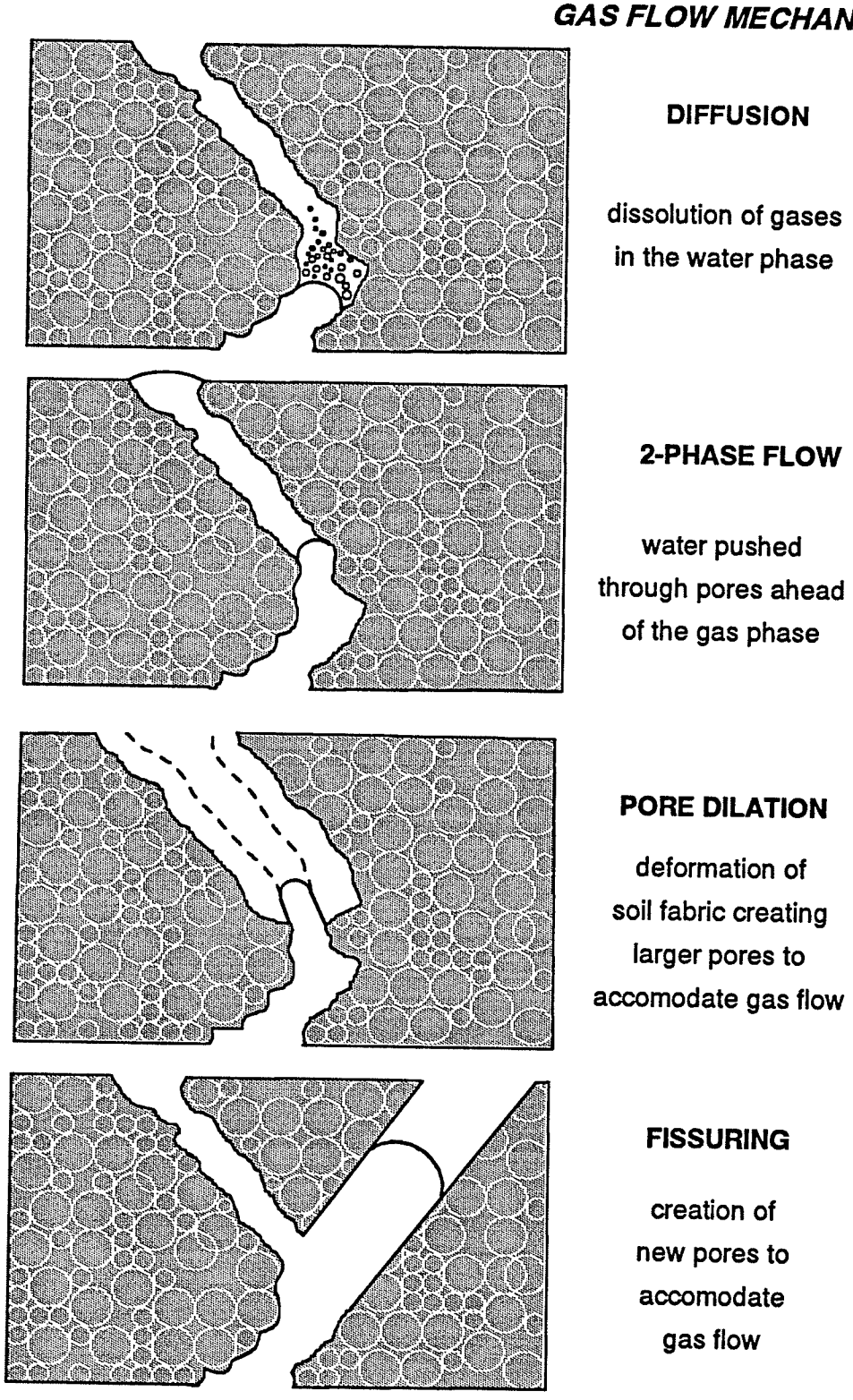

Figure 2.9: Gas flow mechanisms.

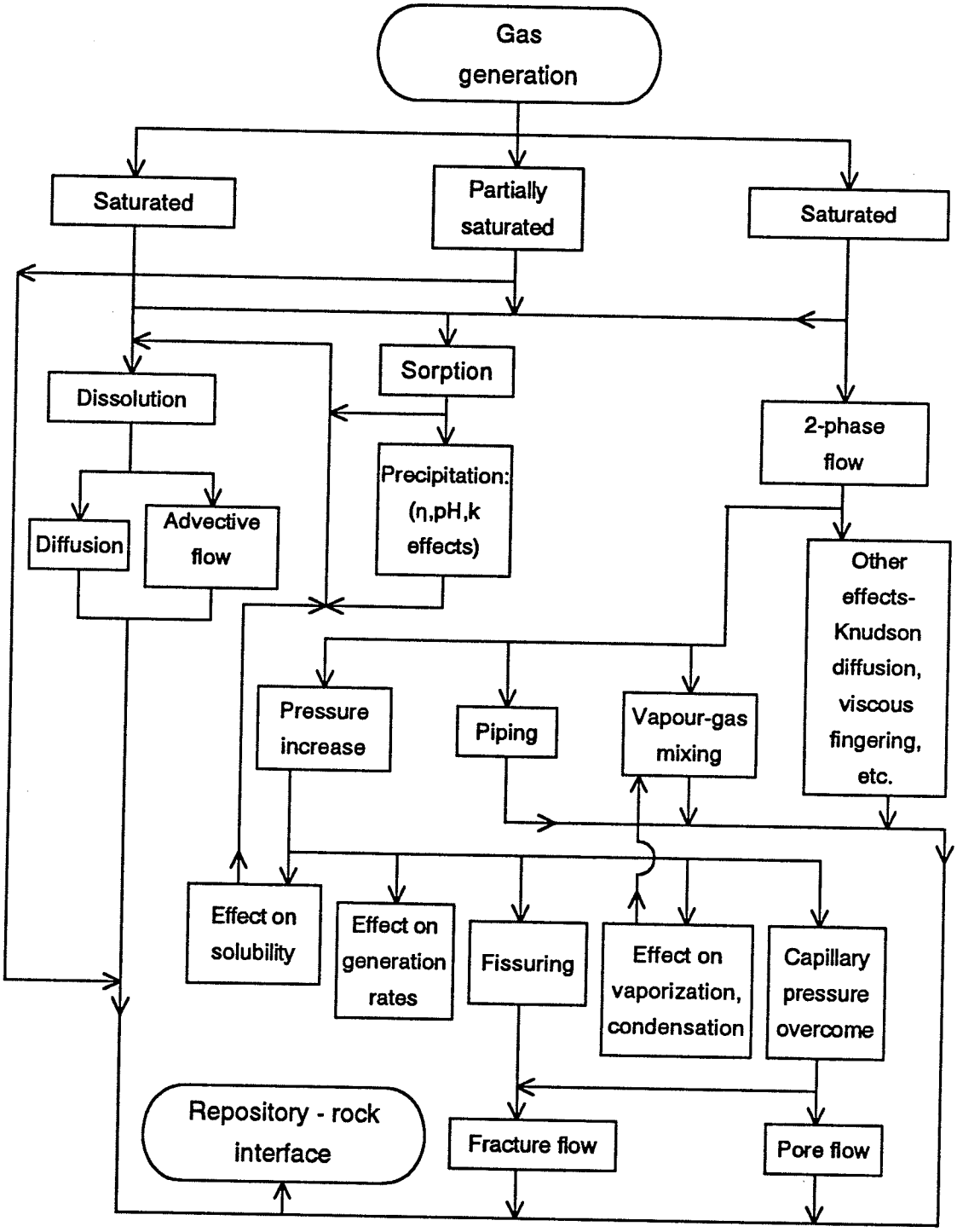

2.10: Flow chart showing possible gas flow mechanisms in a repository (after Jeffries et. al., 1991).

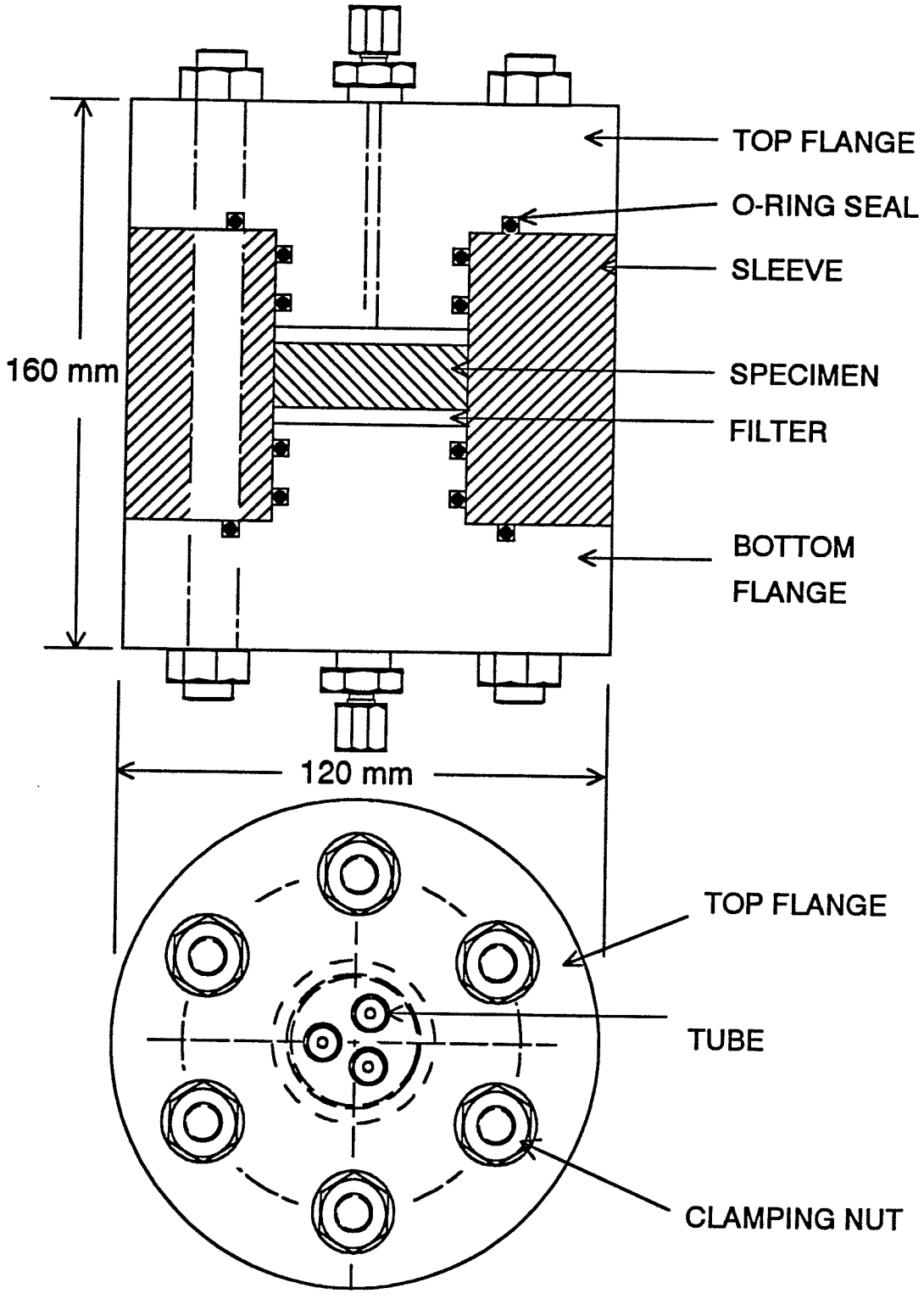

Figure 3.1: Schematic drawing of the constant volume test cell.

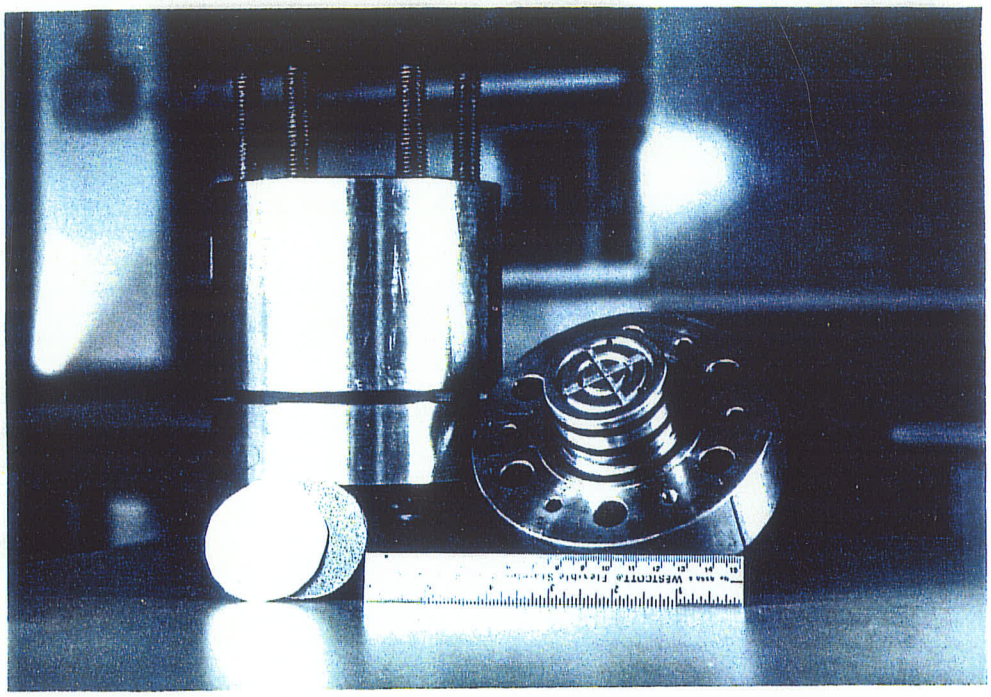

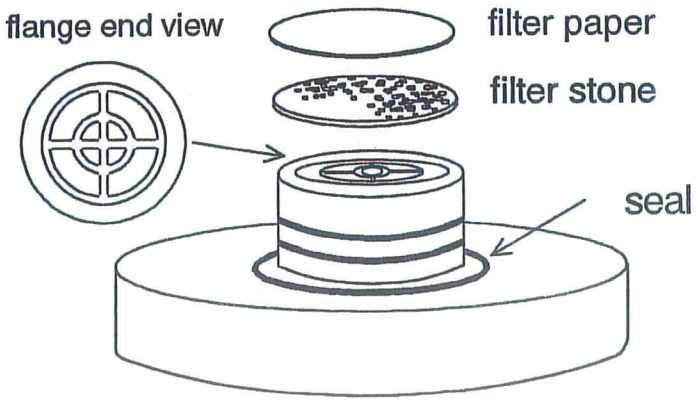

Test cell flange

Figure 3.2: Photograph of a partially assembled constant volume test cell and flange detail.

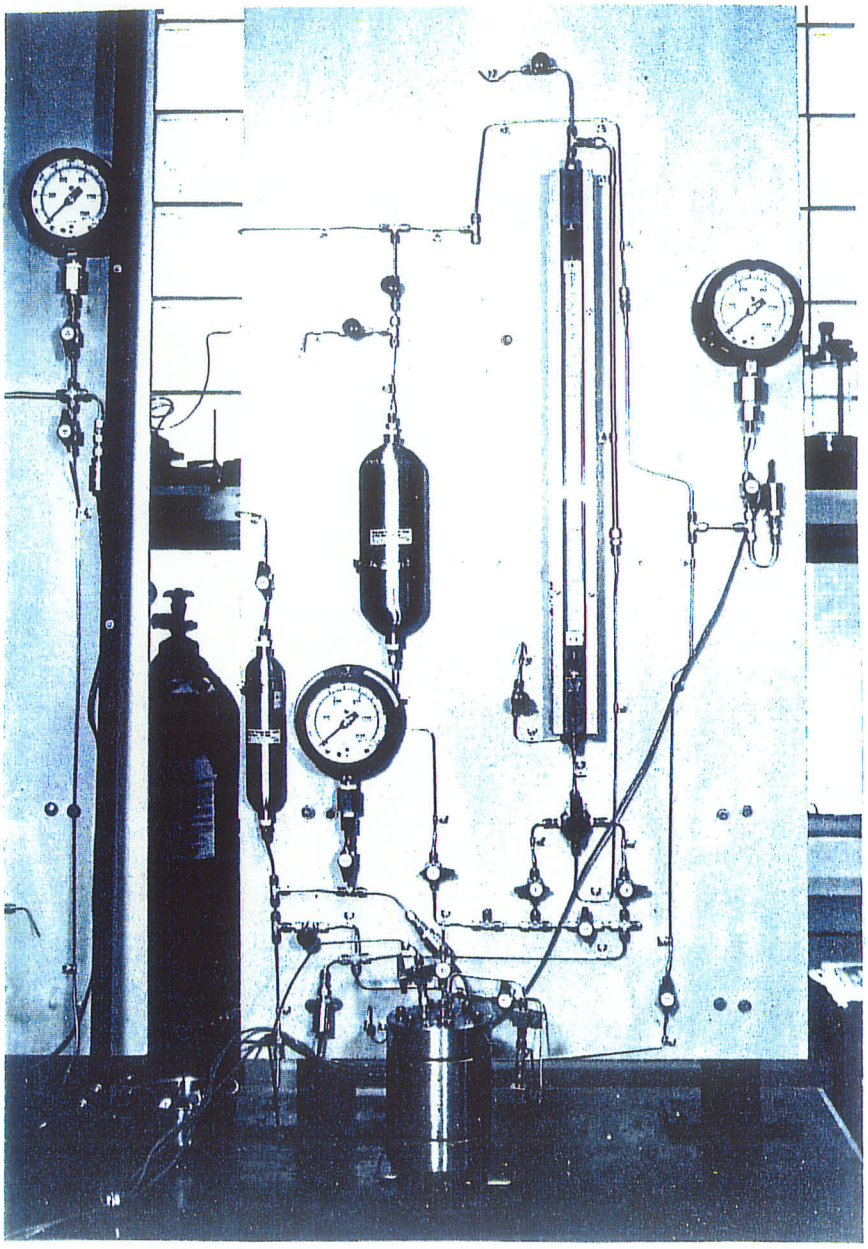

Figure 3.3: Photograph of a test board and test cell.

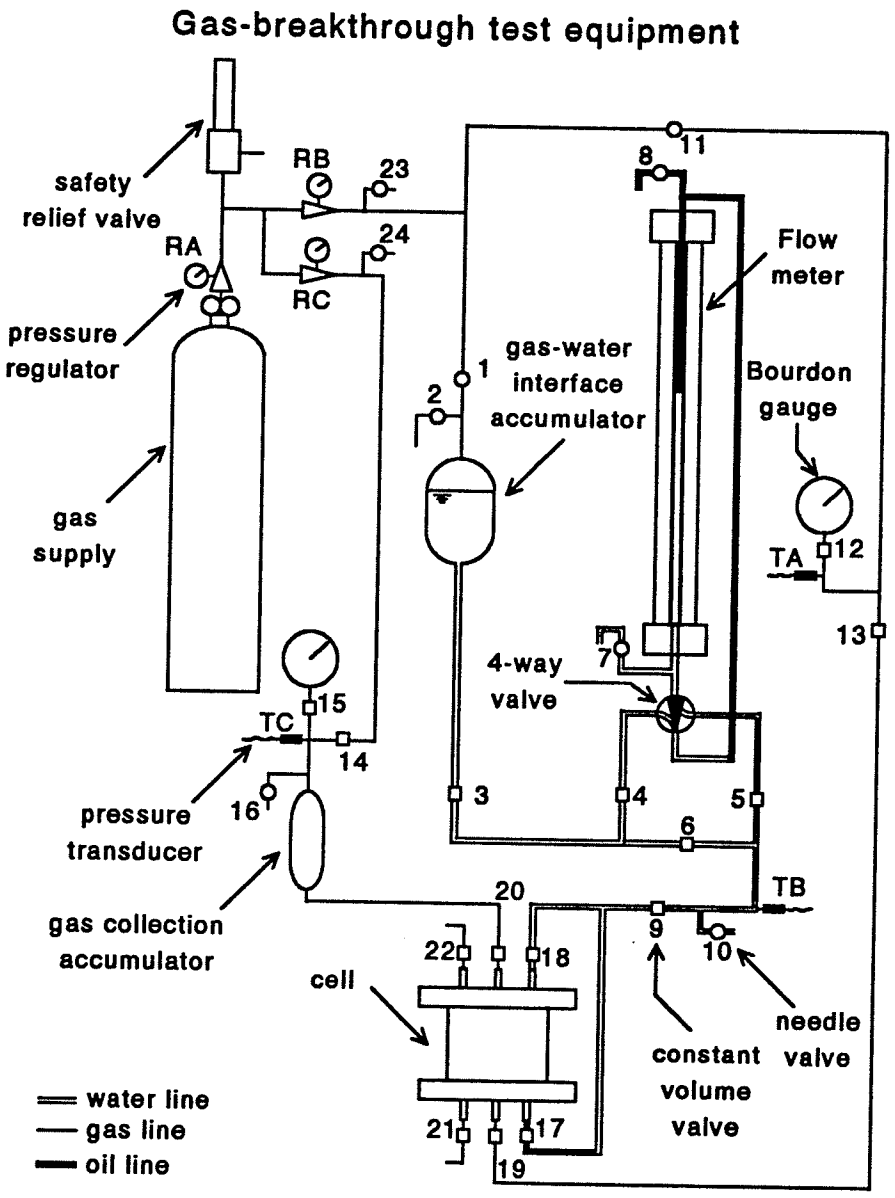

Figure 3.4: Schematic drawing of the test board.

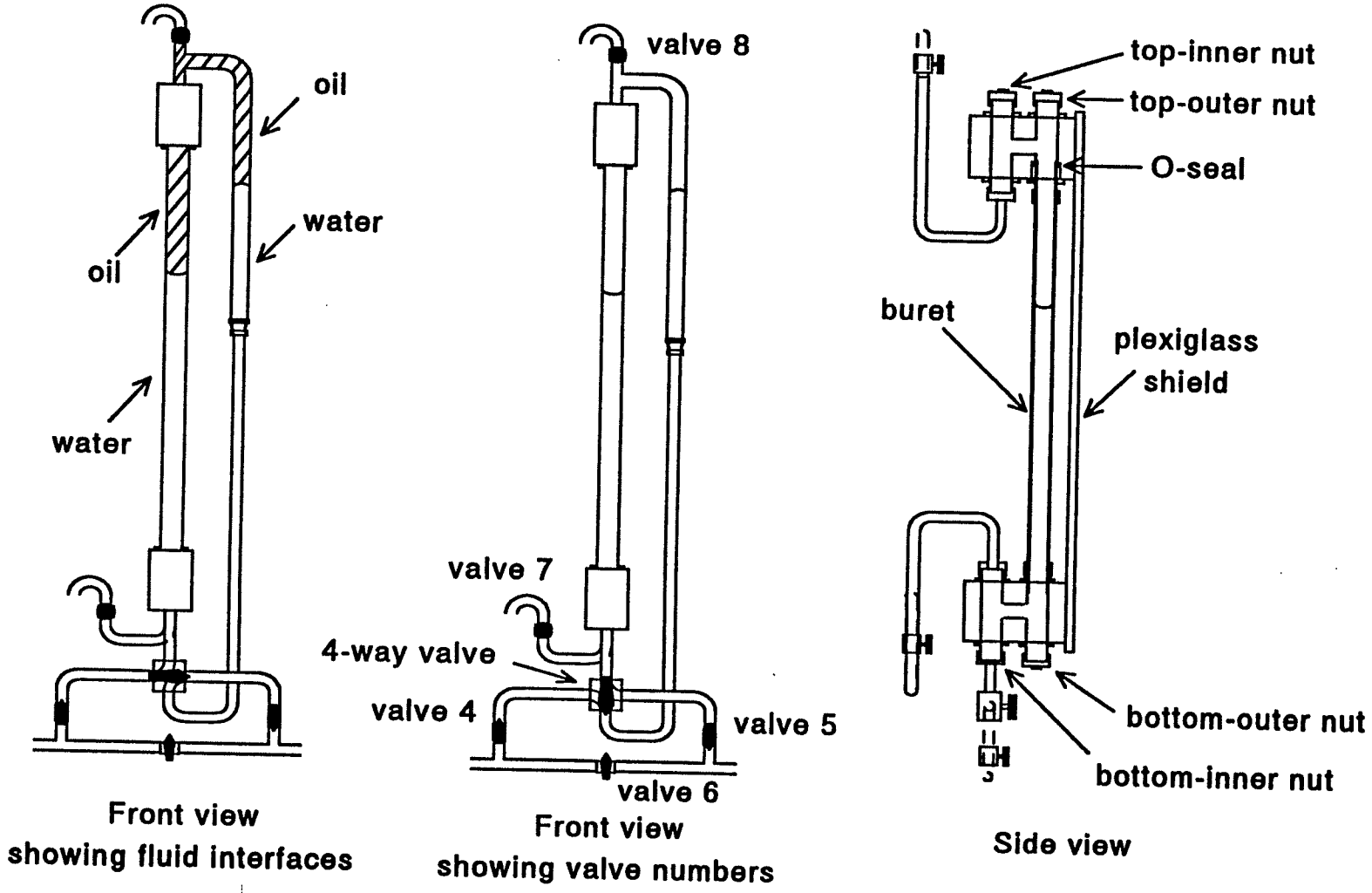

Figure 3.5: Flow meter detail.

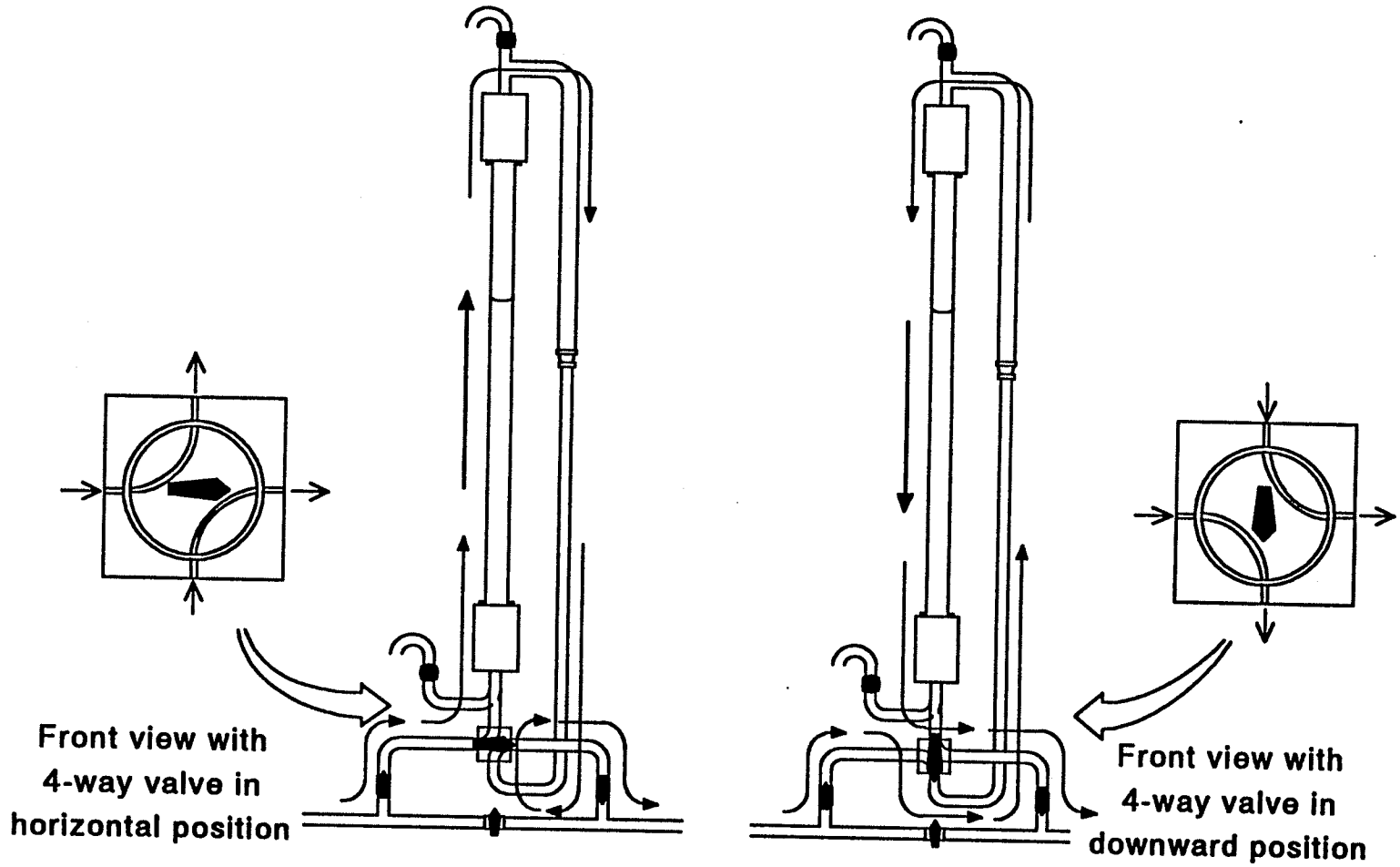

Figure 3.6: Controlling the direction of flow through the flow meter.

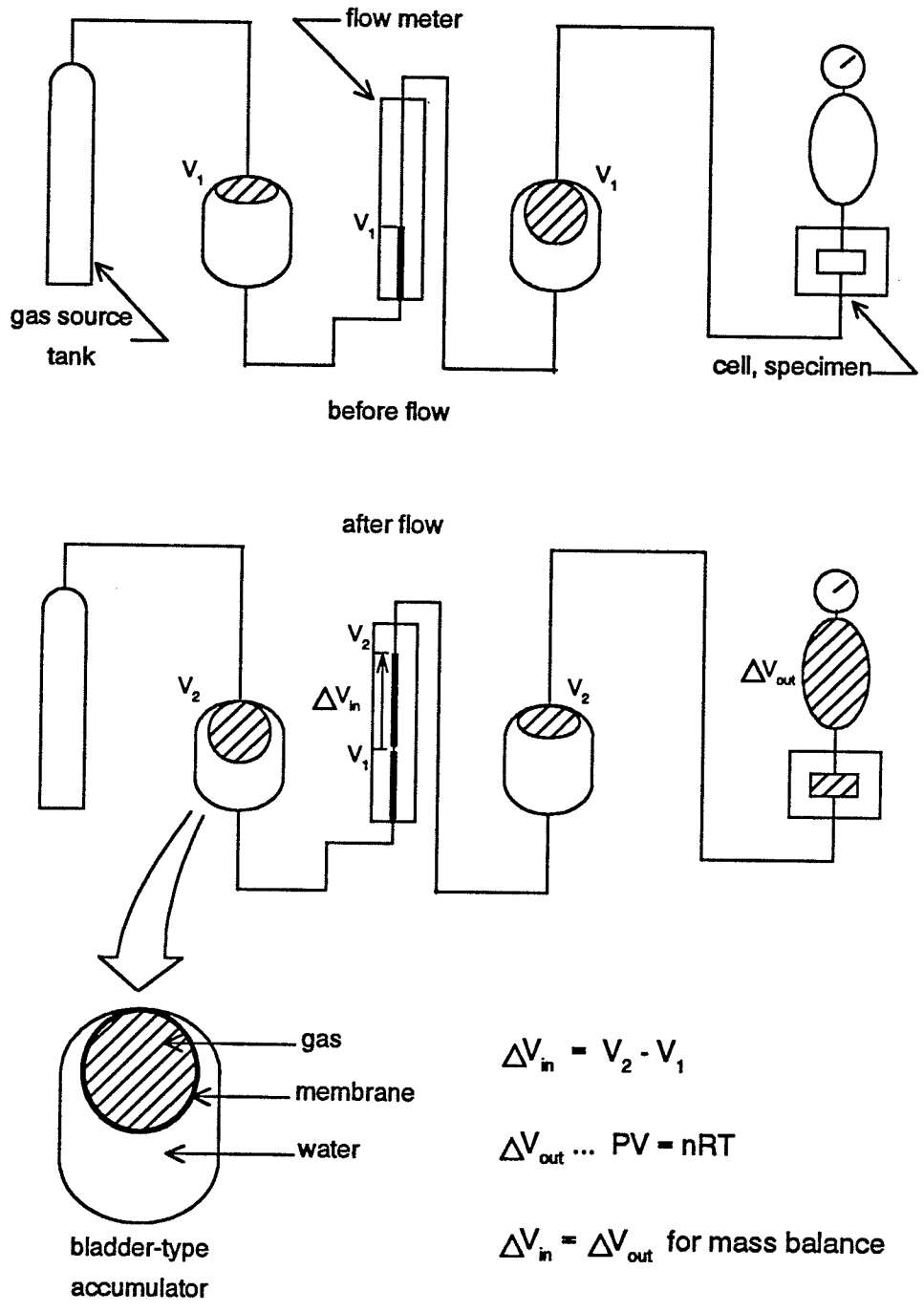

Figure 3.7: Proposed system for gas flow volume measurement using bladder-type accumulators.

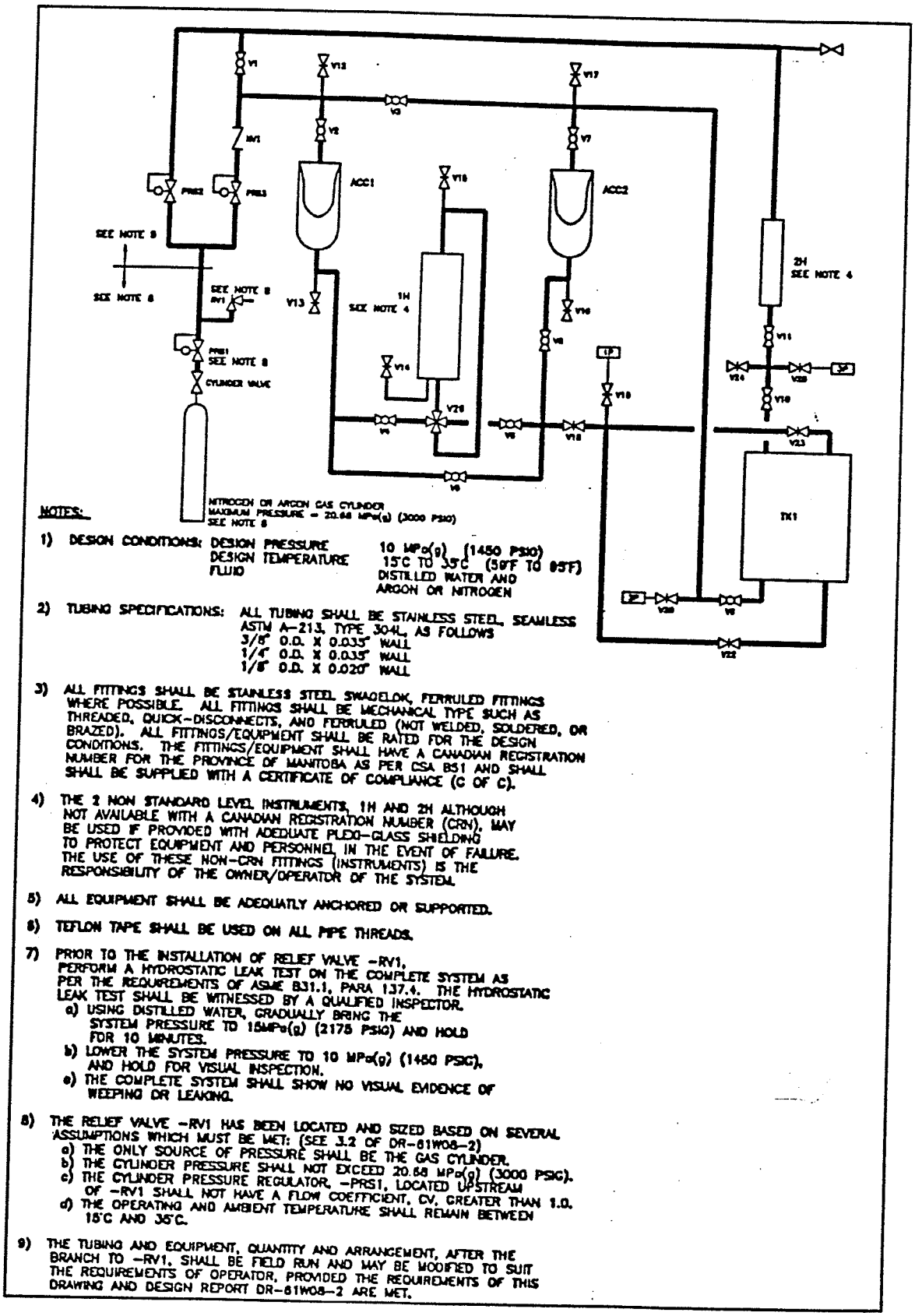

NOTES:

1) DESIGN CONDITIONS: DESIGN PRESSURE 10 MPa(g) (1450 PSIG)
DESIGN TEMPERATURE 15°C TO 35°C (59°F TO 95°F)
FLUID DISTILLED WATER AND ARGON OR NITROGEN

2) TUBING SPECIFICATIONS: ALL TUBING SHALL BE STAINLESS STEEL, SEAMLESS ASTM A-213, TYPE 304L, AS FOLLOWS
3/8" O.D. X 0.035" WALL
1/4" O.D. X 0.035" WALL
1/8" O.D. X 0.020" WALL

3) ALL FITTINGS SHALL BE STAINLESS STEEL SWAGELOK, FERRULED FITTINGS WHERE POSSIBLE. ALL FITTINGS SHALL BE MECHANICAL TYPE SUCH AS THREADED, QUICK-DISCONNECTS, AND FERRULED (NOT WELDED, SOLDERED, OR BRAZED). ALL FITTINGS/EQUIPMENT SHALL BE RATED FOR THE DESIGN CONDITIONS. THE FITTINGS/EQUIPMENT SHALL HAVE A CANADIAN REGISTRATION NUMBER FOR THE PROVINCE OF MANITOBA AS PER CSA B51 AND SHALL SHALL BE SUPPLIED WITH A CERTIFICATE OF COMPLIANCE (C OF C).

4) THE 2 NON STANDARD LEVEL INSTRUMENTS, 1H AND 2H ALTHOUGH NOT AVAILABLE WITH A CANADIAN REGISTRATION NUMBER (CRN), MAY BE USED IF PROVIDED WITH ADEQUATE PLEXI-GLASS SHIELDING TO PROTECT EQUIPMENT AND PERSONNEL IN THE EVENT OF FAILURE. THE USE OF THESE NON-CRN FITTINGS (INSTRUMENTS) IS THE RESPONSIBILITY OF THE OWNER/OPERATOR OF THE SYSTEM.

5) ALL EQUIPMENT SHALL BE ADEQUATLY ANCHORED OR SUPPORTED.

6) TEFLON TAPE SHALL BE USED ON ALL PIPE THREADS.

7) PRIOR TO THE INSTALLATION OF RELIEF VALVE -RV1, PERFORM A HYDROSTATIC LEAK TEST ON THE COMPLETE SYSTEM AS PER THE REQUIREMENTS OF ASME B31.1, PARA 137.4. THE HYDROSTATIC LEAK TEST SHALL BE WITNESSED BY A QUALIFIED INSPECTOR.
   a) USING DISTILLED WATER, GRADUALLY BRING THE SYSTEM PRESSURE TO 15MPa(g) (2175 PSIG) AND HOLD FOR 10 MINUTES.
   b) LOWER THE SYSTEM PRESSURE TO 10 MPa(g) (1450 PSIG), AND HOLD FOR VISUAL INSPECTION.
   c) THE COMPLETE SYSTEM SHALL SHOW NO VISUAL EVIDENCE OF WEEPING OR LEAKING.

8) THE RELIEF VALVE -RV1 HAS BEEN LOCATED AND SIZED BASED ON SEVERAL ASSUMPTIONS WHICH MUST BE MET: (SEE 3.2 OF DR-61WOB-2)
   a) THE ONLY SOURCE OF PRESSURE SHALL BE THE GAS CYLINDER.
   b) THE CYLINDER PRESSURE SHALL NOT EXCEED 20.68 MPa(g) (3000 PSIG).
   c) THE CYLINDER PRESSURE REGULATOR, -PRS1, LOCATED UPSTREAM OF -RV1 SHALL NOT HAVE A FLOW COEFFICIENT, CV, GREATER THAN 1.0.
   d) THE OPERATING AND AMBIENT TEMPERATURE SHALL REMAIN BETWEEN 15°C AND 35°C.

9) THE TUBING AND EQUIPMENT, QUANTITY AND ARRANGEMENT, AFTER THE BRANCH TO -RV1, SHALL BE FIELD RUN AND MAY BE MODIFIED TO SUIT THE REQUIREMENTS OF OPERATOR, PROVIDED THE REQUIREMENTS OF THIS DRAWING AND DESIGN REPORT DR-61WOB-2 ARE MET.

Figure 3.8: Apparatus safety notes from AECL Research drawing A1-61WOB-F1.

March 23, 1994
Pressure Transducer Calibrations
using LABTECH NOTEBOOK
using new power supply set at 9.99 V (+/- 0.01 V)
MAR23.WB1

LABTECH REGRESSION
kPa = Scale factor (mV + Offset constant)

psi	kPa	PT 65841 mV	LABTECH Regression kPa
0	0.0	0.66	-0.3
10	68.9	1.69	70.4
60	413.7	6.66	411.4
135	930.8	14.18	927.5
185	1275.5	19.27	1276.7
260	1792.6	26.83	1795.5
510	3516.3	51.95	3519.3
635	4378.2	64.45	4377.0
745	5136.6	75.51	5136.0
995	6860.3	100.63	6859.7

Regression Output:

Constant		-45.5863
Std Err of Y Est		2.199899
R Squared		0.999999
No. of Observations		10
Degrees of Freedom		8
X Coefficient(s)	68.62057	
Std Err of Coef.	0.021044	

Scale factor	68.62057
Offset constant	-0.66432
PT 65841	

PT 65842		
0.0	0.73	1.3
68.9	1.72	69.5
413.7	6.67	410.3
930.8	14.18	927.4
1275.5	19.27	1277.8
1792.6	26.83	1798.4
3516.3	51.76	3514.8
4378.2	64.25	4374.8
5136.6	75.32	5137.0
6860.3	100.37	6861.7

Regression Output:

Constant		-48.9228
Std Err of Y Est		3.142666
R Squared		0.999998
No. of Observations		10
Degrees of Freedom		8
X Coefficient(s)	68.85169	
Std Err of Coef.	0.030163	

Scale factor	68.85169
Offset constant	-0.71055
PT 65842	

PT 65843		
0.0	0.73	-5.6
68.9	1.84	70.5
413.7	6.84	413.3
930.8	14.4	931.7
1275.5	19.48	1280.0
1792.6	26.95	1792.2
3516.3	52.09	3516.0
4378.2	64.7	4380.7
5136.6	75.7	5134.9
6860.3	100.85	6859.4

Regression Output:

Constant		-55.6677
Std Err of Y Est		2.855662
R Squared		0.999999
No. of Observations		10
Degrees of Freedom		8
X Coefficient(s)	68.56756	
Std Err of Coef.	0.027295	

Scale factor	68.56756
Offset constant	-0.81187
PT 65843	

Figure 3.9(a): Initial calibration data for pressure transducers (S/N 65841, 65842, 65843).

April 13, 1994
Pressure Transducer Calibrations
using LABTECH NOTEBOOK
using new power supply set at 9.98 V (+/- 0.01 V)
APR13.WB1

LABTECH REGRESSION
kPa = Scale factor (mV + Offset constant)

psi	kPa	PT 66542 mV	LABTECH Regression kPa
0	0.0	1.6	-4.8
10	68.9	2.9	85.1
35	241.3	5.1	237.4
85	586.1	10.1	583.6
135	930.8	15.1	929.7
185	1275.5	20.0	1268.9
235	1620.3	25.1	1621.9
260	1792.6	27.6	1795.0
385	2654.5	40.0	2653.4
510	3516.3	52.5	3518.7
636	4385.1	64.9	4377.1
685	4722.9	69.9	4723.2
760	5240.0	77.4	5242.4
960	6619.0	97.3	6620.0
995	6860.3	100.8	6862.3

Regression Output:

Constant	-115.604
Std Err of Y Est	5.830444
R Squared	0.999994
No. of Observations	15
Degrees of Freedom	13
X Coefficient(s)	69.22482
Std Err of Coef.	0.045527

Scale factor	69.22482
Offset constant	-1.66998
PT 66542	

PT 66543		LABTECH Regression kPa
0.0	-0.4	-4.4
68.9	1.0	93.1
241.3	3.1	239.3
586.1	8.0	580.5
930.8	13.0	928.7
1275.5	17.9	1269.8
1620.3	22.9	1618.0
1792.6	25.4	1792.0
2654.5	37.8	2655.4
3516.3	50.1	3511.9
4385.1	62.5	4375.2
4722.9	67.5	4723.4
5240.0	75.0	5245.6
6619.0	94.7	6617.3
6860.3	98.3	6867.9

Regression Output:

Constant	23.49577
Std Err of Y Est	8.27665
R Squared	0.999989
No. of Observations	15
Degrees of Freedom	13
X Coefficient(s)	69.62796
Std Err of Coef.	0.065005

Scale factor	69.62796
Offset constant	0.337447
PT 66543	

PT 66544		LABTECH Regression kPa
0.0	1.0	-0.1
68.9	2.2	83.0
241.3	4.4	235.2
586.1	9.5	588.2
930.8	14.4	927.3
1275.5	19.4	1273.4
1620.3	24.4	1619.4
1792.6	26.9	1792.4
2654.5	39.3	2650.6
3516.3	51.8	3515.8
4385.1	64.2	4374.0
4722.9	69.3	4726.9
5240.0	76.8	5246.0
6619.0	96.6	6616.3
6860.3	100.2	6865.5

Regression Output:

Constant	-69.3095
Std Err of Y Est	6.077297
R Squared	0.999994
No. of Observations	15
Degrees of Freedom	13
X Coefficient(s)	69.20967
Std Err of Coef.	0.047444

Scale factor	69.20967
Offset constant	-1.00144
PT 66544	

Figure 3.9(b): Initial calibration data for pressure transducers (S/N 66542, 66543, 66544).

November 24, 1994
Pressure Transducer Calibrations
using LABTECH NOTEBOOK
using new power supply set at 9.99 V (+/- 0.01 V)
NOV24-1.WB1

LABTECH REGRESSION
kPa = Scale factor (mV + Offset constant)

psi	kPa	PT 65841 mV	LABTECH Regression kPa
0	0.0	1	-7.4
25	172.4	3.6	169.6
50	344.7	6.2	346.5
60	413.7	7.6	441.7
100	689.5	11.2	686.7
260	1792.6	27.3	1782.3
385	2654.5	40.3	2666.9
510	3516.3	52.7	3510.6
610	4205.8	62.7	4191.1
760	5240.0	77.9	5225.4
860	5929.5	87.9	5905.9
985	6791.4	101.5	6831.3

Regression Output:

Constant		-75.4169
Std Err of Y Est		19.3344
R Squared		0.999943
No. of Observations		12
Degrees of Freedom		10
X Coefficient(s)	68.04659	
Std Err of Coef.	0.162144	

Scale factor	68.04659
Offset constant	-1.10831
PT 65841	

	PT 65842	
0.0	0.7	2.7
172.4	3.2	174.0
344.7	5.8	352.2
413.7	6.8	420.7
689.5	10.7	687.9
1792.6	26.9	1797.9
2654.5	39.3	2647.6
3516.3	51.8	3504.1
4205.8	61.9	4196.1
5240.0	76.9	5223.9
5929.5	86.9	5909.1
6791.4	100.4	6834.1

Regression Output:

Constant		-45.2318
Std Err of Y Est		17.15244
R Squared		0.999955
No. of Observations		12
Degrees of Freedom		10
X Coefficient(s)	68.5197	
Std Err of Coef.	0.144845	

Scale factor	68.5197
Offset constant	-0.66013
PT 65842	

	PT 65843	
0.0	1	9.4
172.4	3.4	173.2
344.7	6	350.7
413.7	7	419.0
689.5	11	692.1
1792.6	27.1	1791.3
2654.5	39.6	2644.7
3516.3	52.2	3505.0
4205.8	62.3	4194.6
5240.0	77.4	5225.5
5929.5	87.4	5908.3
6791.4	101	6836.8

Regression Output:

Constant		-58.9238
Std Err of Y Est		17.99249
R Squared		0.999951
No. of Observations		12
Degrees of Freedom		10
X Coefficient(s)	68.27438	
Std Err of Coef.	0.151395	

Scale factor	68.27438
Offset constant	-0.86304
PT 65843	

Figure 3.10(a): Final calibration data for pressure transducers (S/N 65841, 65842, 65843).

November 24, 1994
Pressure Transducer Calibrations
using LABTECH NOTEBOOK
using new power supply set at 9.99 V (+/- 0.01 V)
NOV24-2.WB1

LABTECH REGRESSION
kPa = Scale factor (mV + Offset constant)

psi	kPa	PT 66542 mV	LABTECH Regression kPa
0	0.0	0.7	8.0
10	68.9	1.6	70.4
60	413.7	6.5	409.9
110	758.4	11.5	756.4
135	930.8	14	929.6
235	1620.3	23.9	1615.6
385	2654.5	38.9	2655.0
485	3344.0	48.9	3347.9
635	4378.2	63.7	4373.4
735	5067.7	73.7	5066.3
885	6101.9	88.7	6105.7
985	6791.4	98.6	6791.7

Regression Output: PT 66542

Constant		-40.4914
Std Err of Y Est		4.038869
R Squared		0.999997
No. of Observations		12
Degrees of Freedom		10
X Coefficient(s)	69.29183	
Std Err of Coef.	0.034806	

Scale factor	69.29183
Offset constant	-0.58436
PT 66542	

PT 66543		LABTECH Regression kPa
0.0	0.7	54.0
68.9	0.7	54.0
413.7	5.6	395.9
758.4	10.7	751.7
930.8	13.2	926.1
1620.3	23	1609.9
2654.5	37.9	2649.6
3344.0	47.9	3347.3
4378.2	62.6	4373.0
5067.7	72.5	5063.8
6101.9	87.4	6103.4
6791.4	97.4	6801.1

Regression Output: PT 66543

Constant		5.130476
Std Err of Y Est		19.5034
R Squared		0.999941
No. of Observations		12
Degrees of Freedom		10
X Coefficient(s)	69.77416	
Std Err of Coef.	0.169251	

Scale factor	69.77416
Offset constant	0.07353
PT 66543	

PT 66544		LABTECH Regression kPa
0.0	0.8	-27.1
68.9	2.3	76.5
413.7	7.3	421.7
758.4	12.2	760.0
930.8	14.8	939.5
1620.3	24.7	1622.9
2654.5	39.7	2658.5
3344.0	49.6	3342.0
4378.2	64.6	4377.5
5067.7	74.6	5067.9
6101.9	89.6	6103.5
6791.4	99.5	6786.9

Regression Output: PT 66544

Constant		-82.2995
Std Err of Y Est		9.901485
R Squared		0.999985
No. of Observations		12
Degrees of Freedom		10
X Coefficient(s)	69.03765	
Std Err of Coef.	0.085017	

Scale factor	69.03765
Offset constant	-1.1921
PT 66544	

Figure 3.10(b): Final calibration data for pressure transducers (S/N 66542, 66543, 66544).

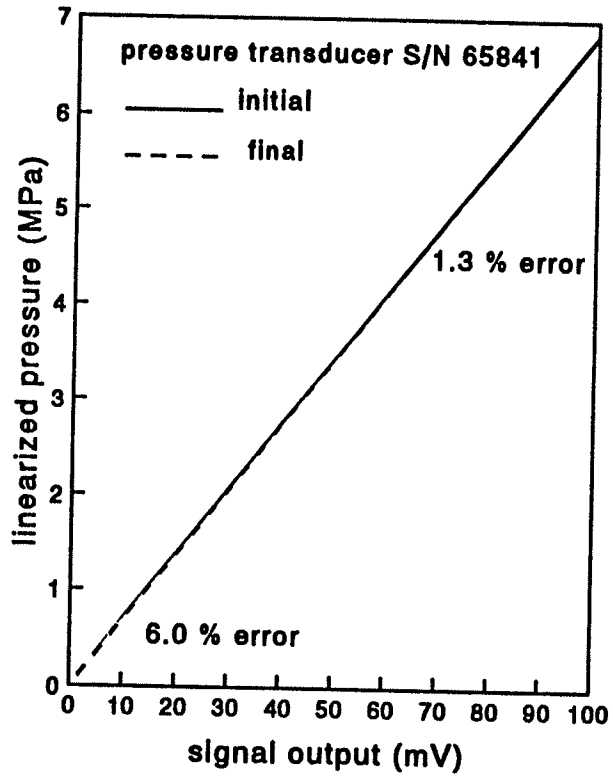

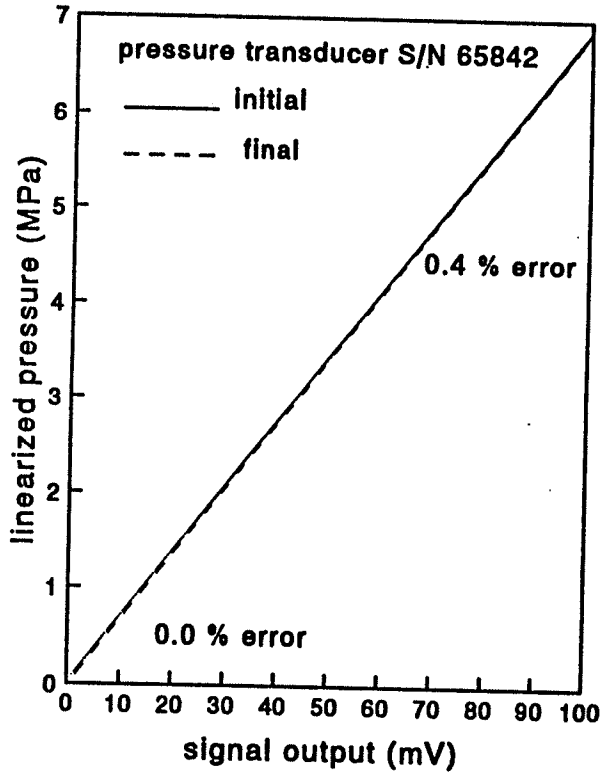

Figure 3.11(a): Comparison of initial and final calibration data for pressure transducers S/N 65841 and 65842.

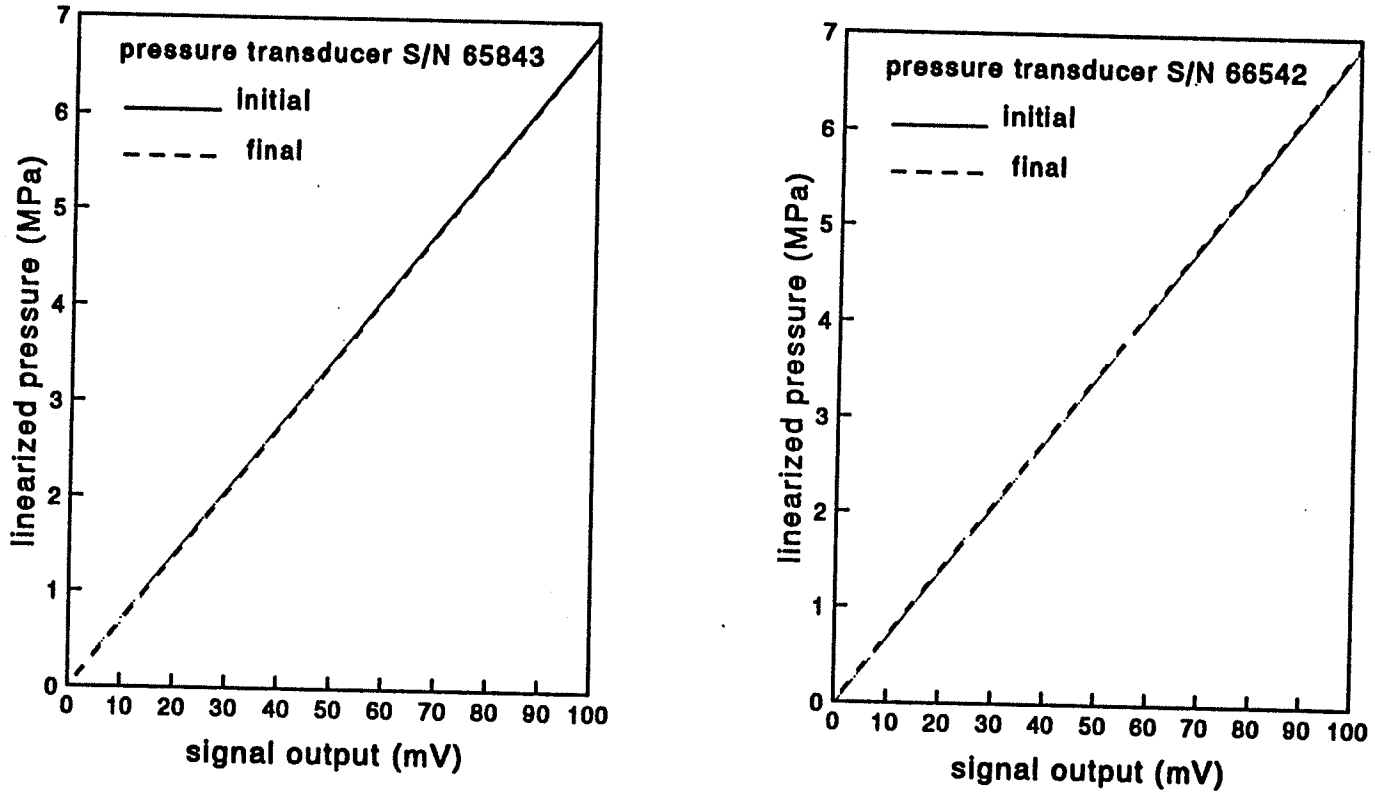

Figure 3.11(b): Comparison of initial and final calibration data for pressure transducers S/N 65843 and 66542.

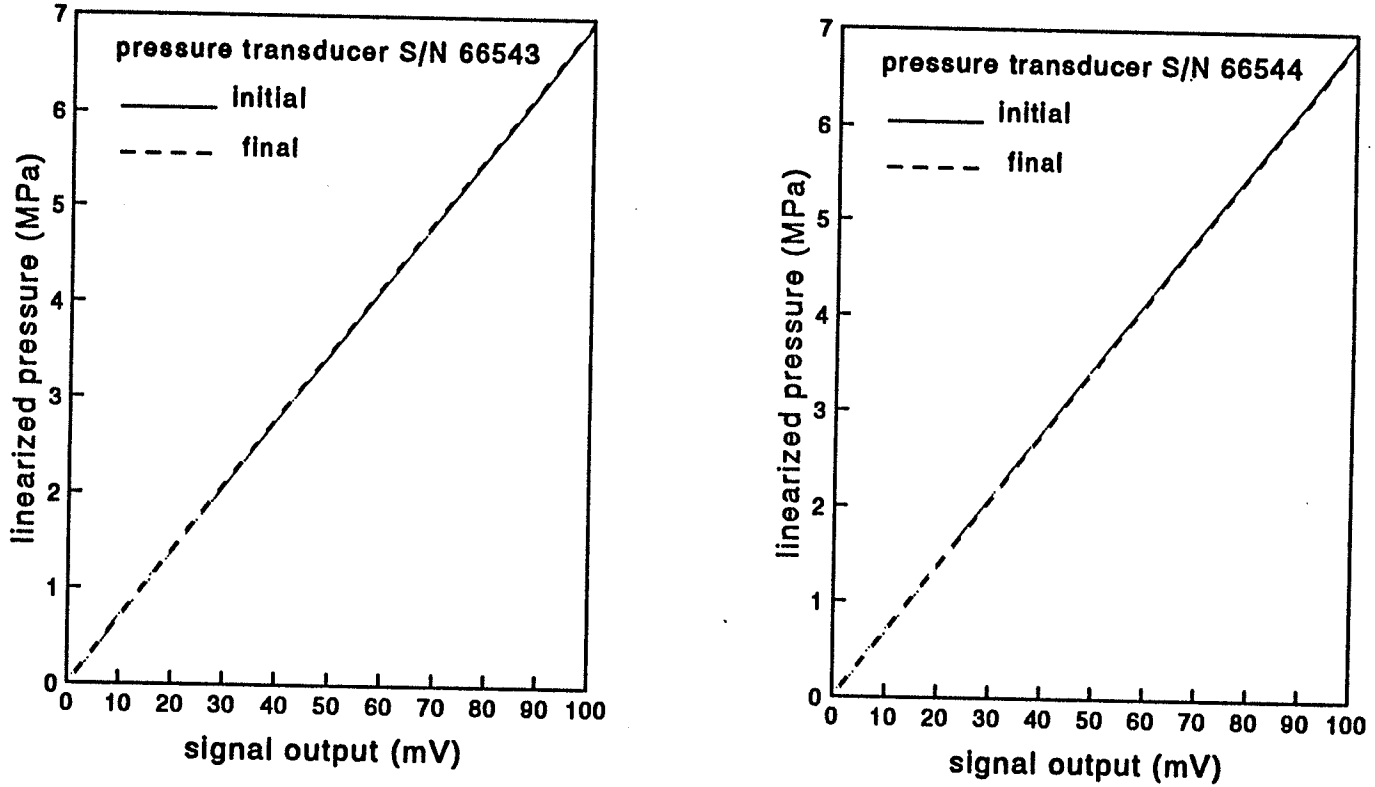

Figure 3.11(c): Comparison of initial and final calibration data for pressure transducers S/N 66543 and 66544.

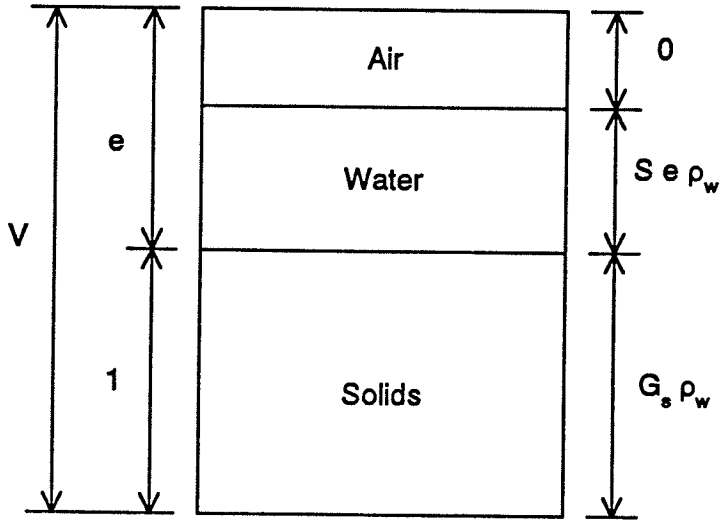

$$w = \frac{M_w}{M_s} = \frac{S\,e\,\rho_w}{G_s\,\rho_w} = \frac{S\,e}{G_s} \quad \text{or} \quad e = \frac{w\,G_s}{S}$$

$$\rho_d = \frac{M_s}{V} = \frac{G_s\,\rho_w}{1+e} = \text{or} \quad \rho_d = \left(\frac{G_s\,\rho_w}{1 + \frac{w\,G_s}{S}} \right)$$

$$\text{Rearranging, } S = w\,G_s \left(\frac{\rho_d}{G_s\,\rho_w - \rho_d} \right) \quad \text{and} \quad w = S \left(\frac{\rho_w}{\rho_d} - \frac{1}{G_s} \right)$$

where:

w = moisture content
M = mass
G_s = specific gravity
e = void ratio
ρ_w = density of water
ρ_d = dry density
S = saturation

Figure 4.1: Phase diagram for deriving control equations for specimen preparation.

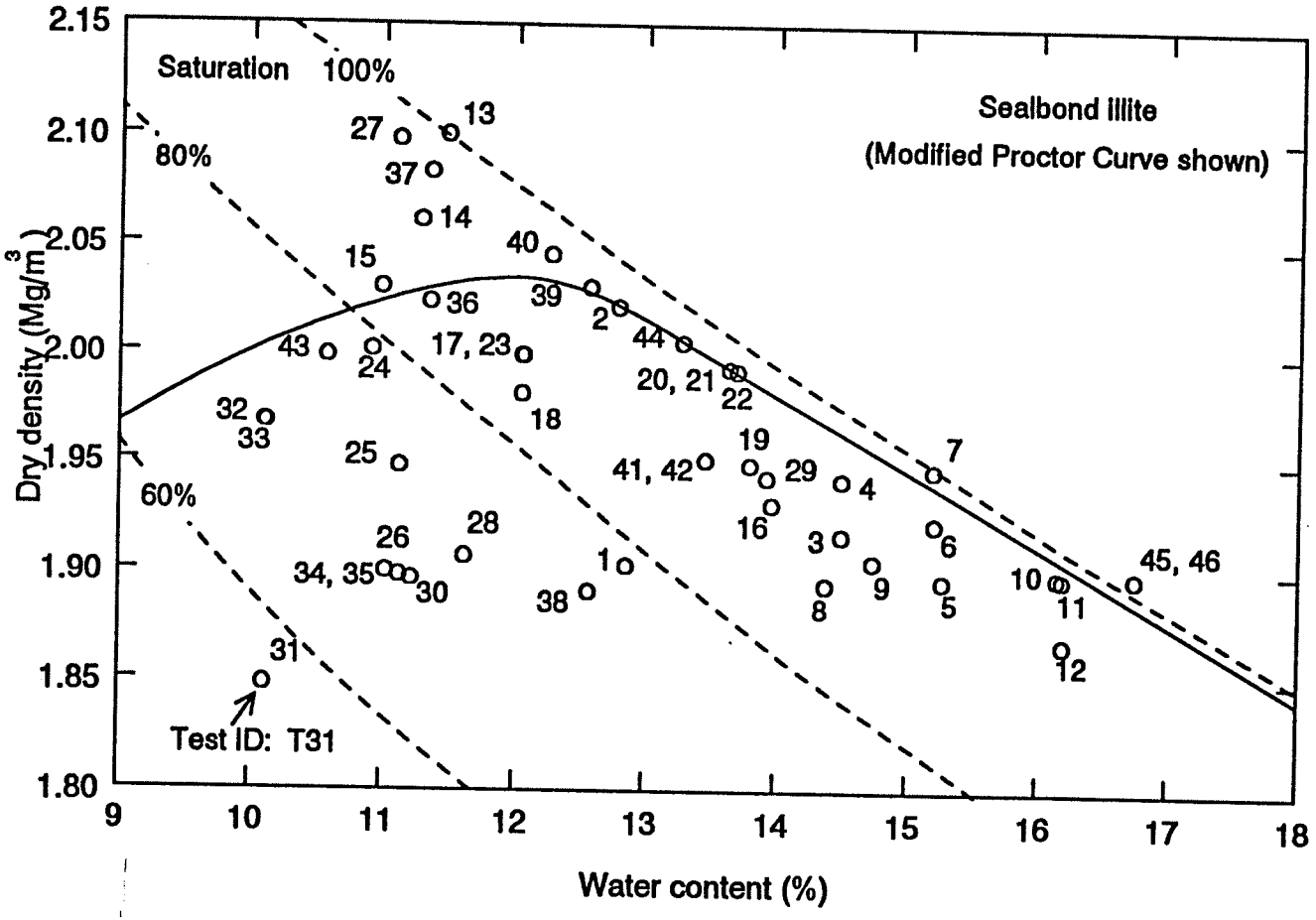

Figure 4.2: Targeted dry density, moisture content and saturation ranges for illite tests.

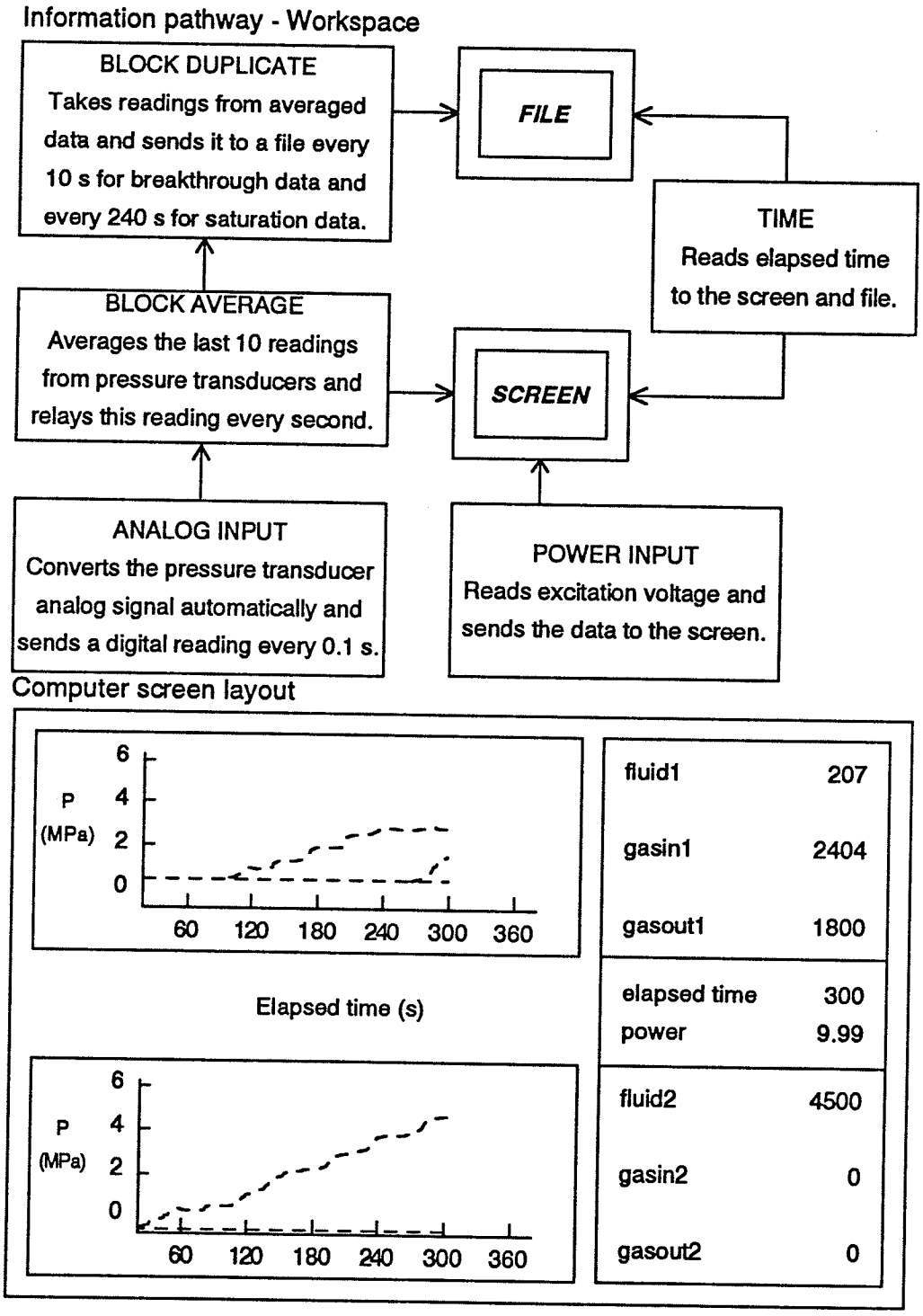

Figure 4.3: Automated data acquisition software configuration and presentation.

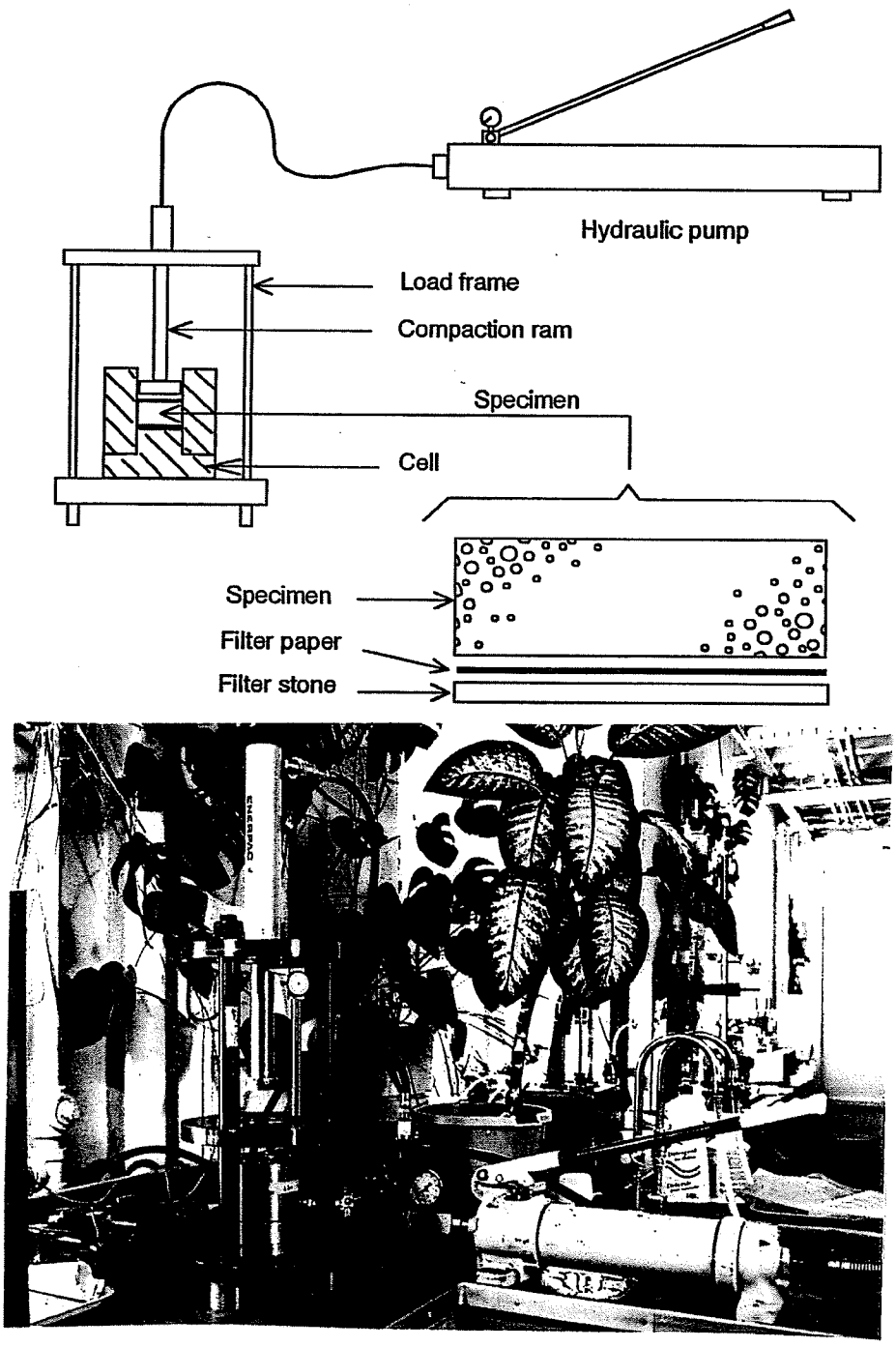

Figure 4.4: Compaction equipment.

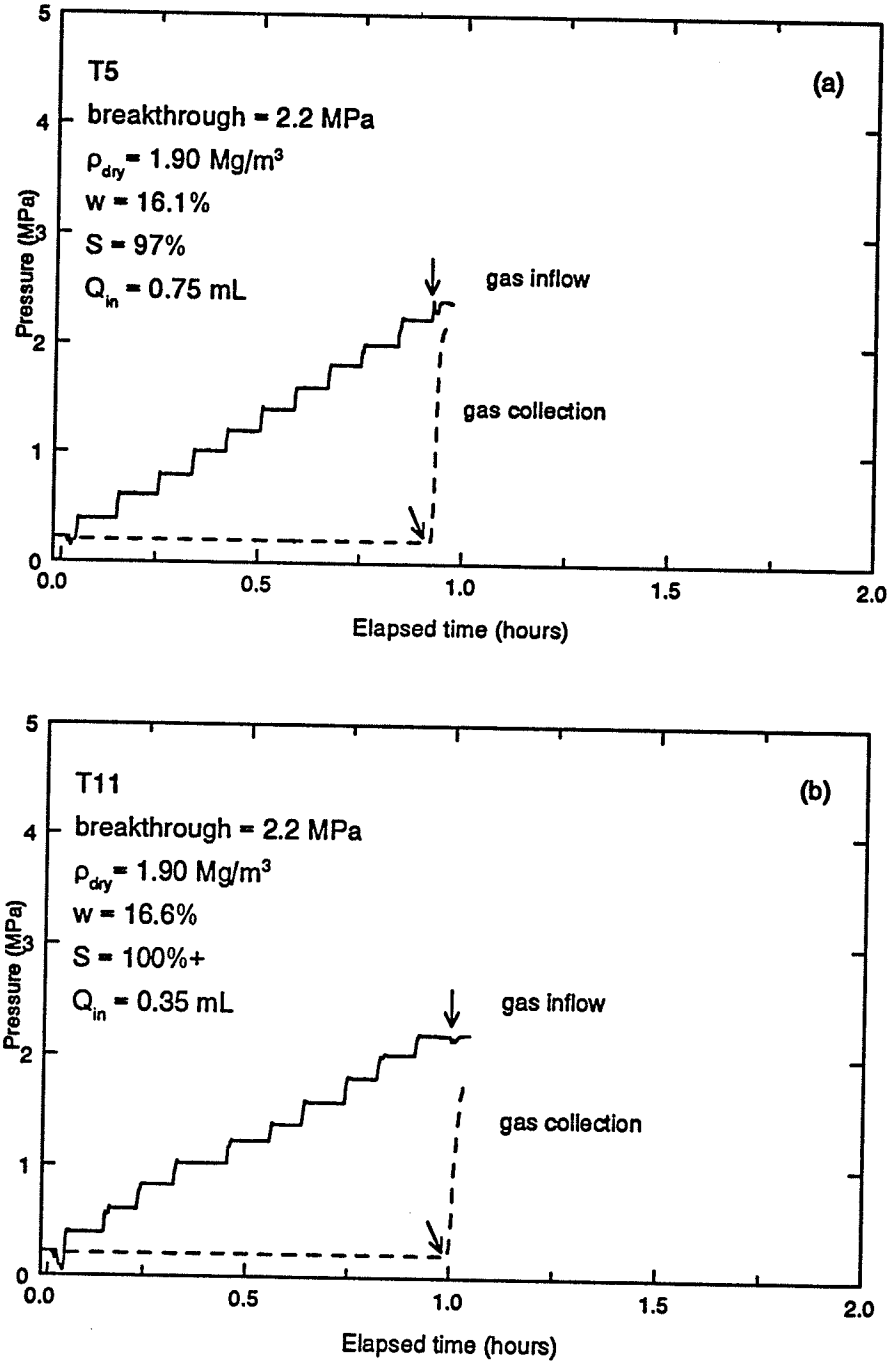

Figure 5.1(a): Gas-breakthrough test results for T5,
(b): Gas-breakthrough test results for T11.

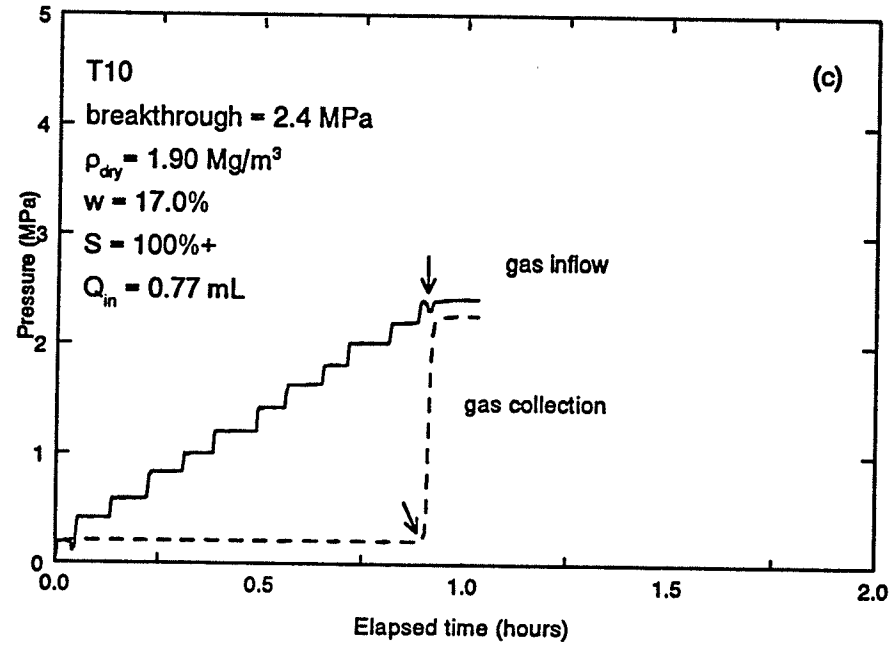

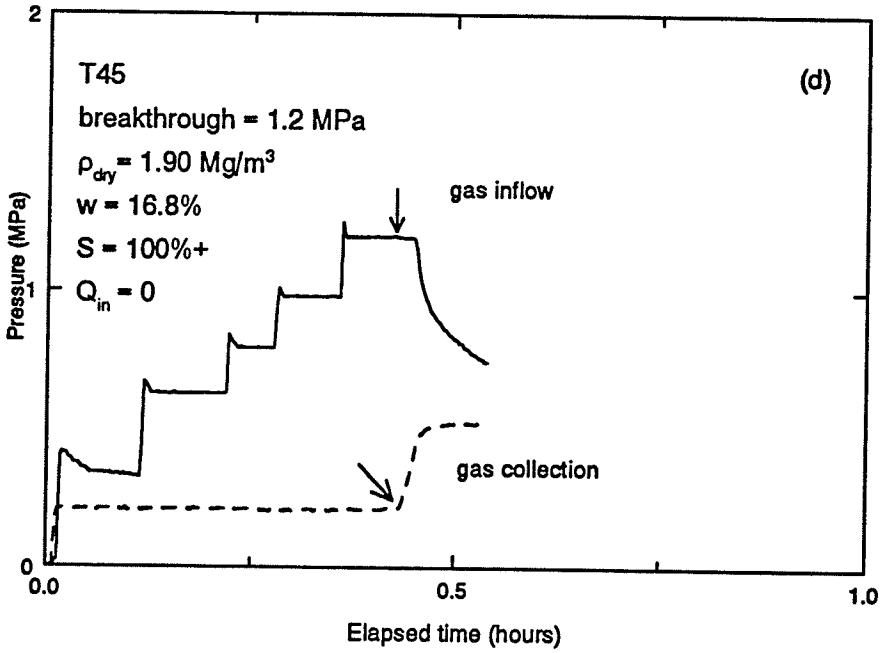

Figure 5.1(c): Gas-breakthrough test results for T10,
(d): Gas-breakthrough test results for T45.

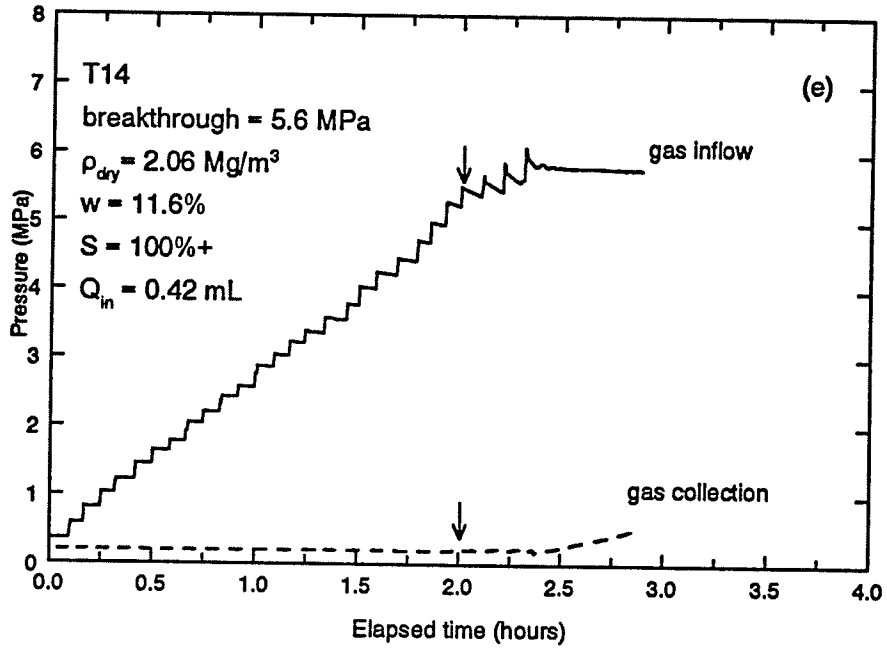

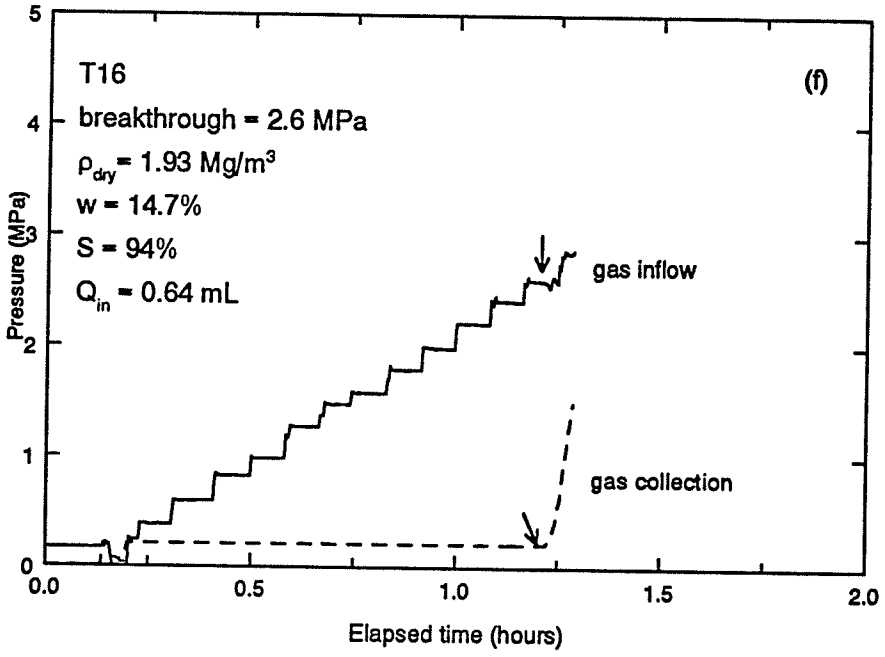

Figure 5.1(e): Gas-breakthrough test results for T14,
(f): Gas-breakthrough test results for T16.

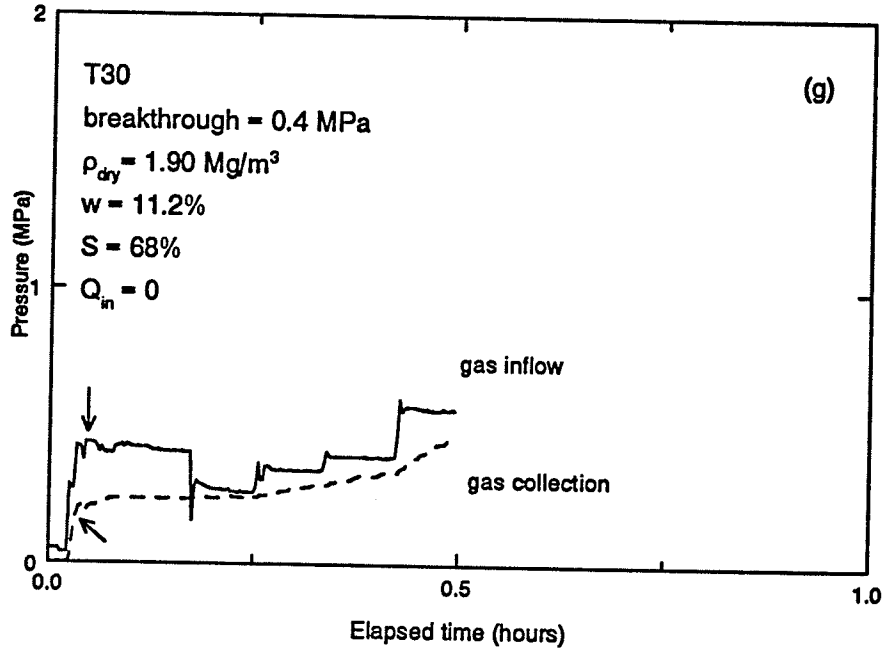

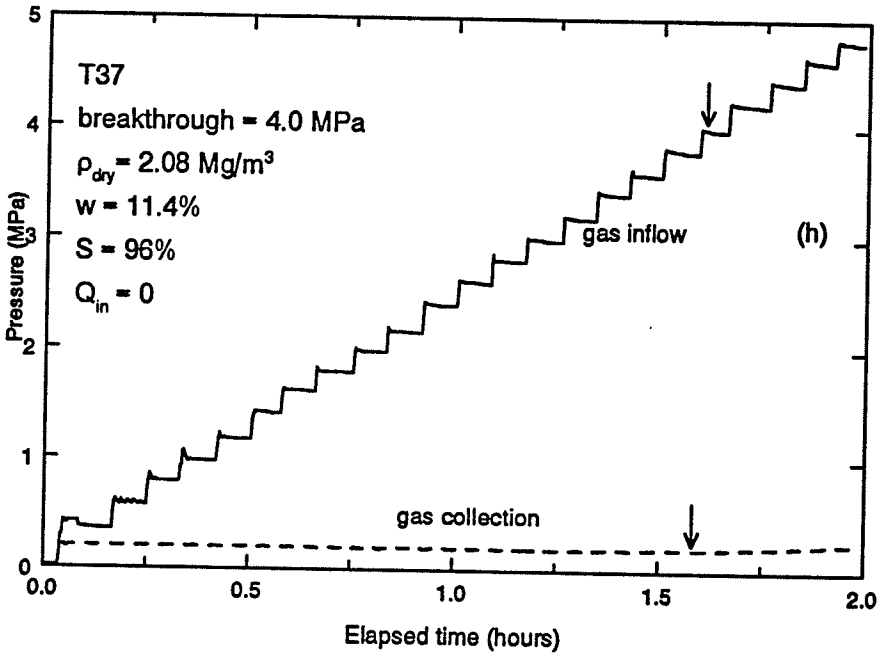

Figure 5.1(g): Gas-breakthrough test results for T30,
(h): Gas-breakthrough test results for T37.

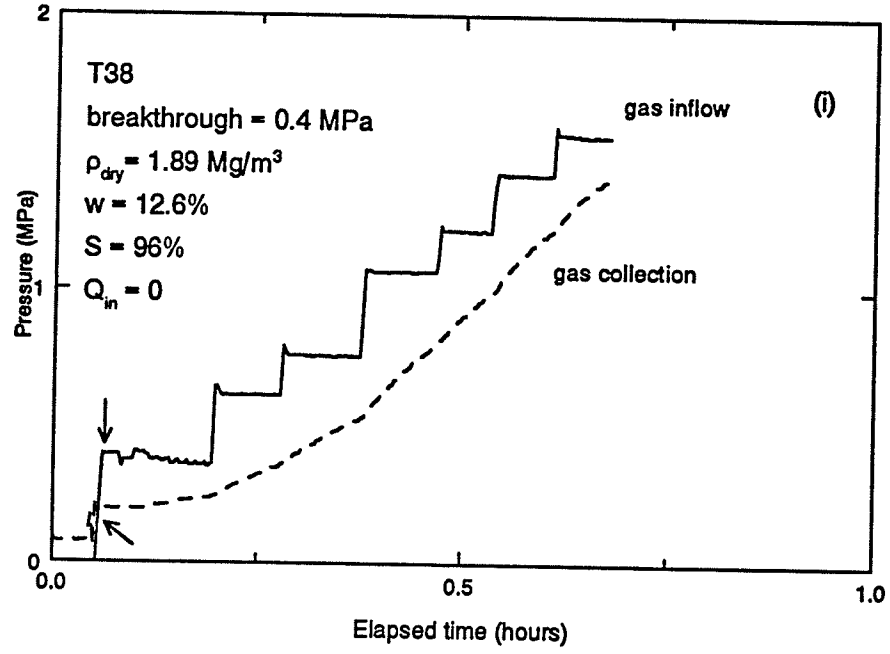

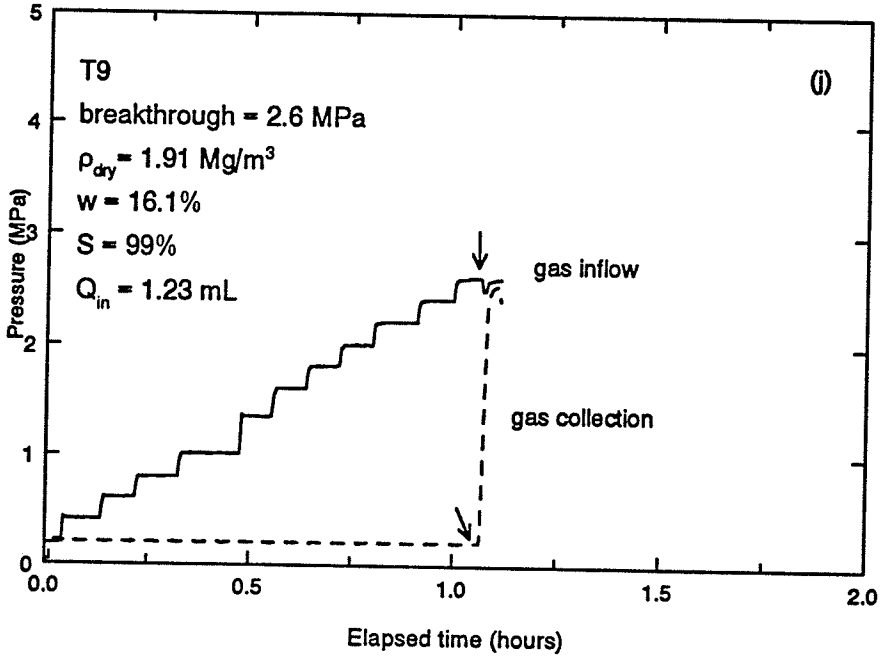

Figure 5.1(i): Gas-breakthrough test results for T38,
(j): Gas-breakthrough test results for T9.

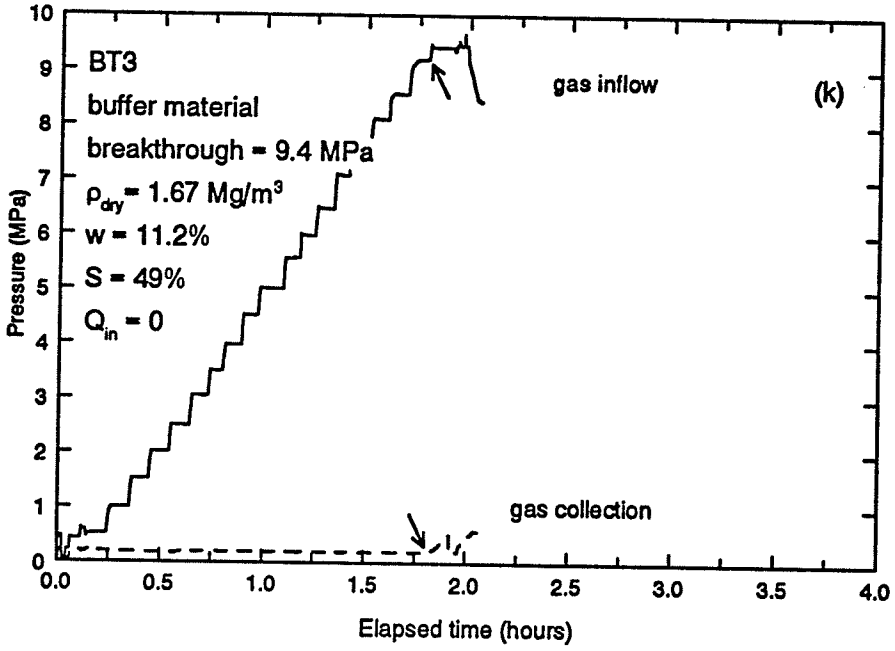

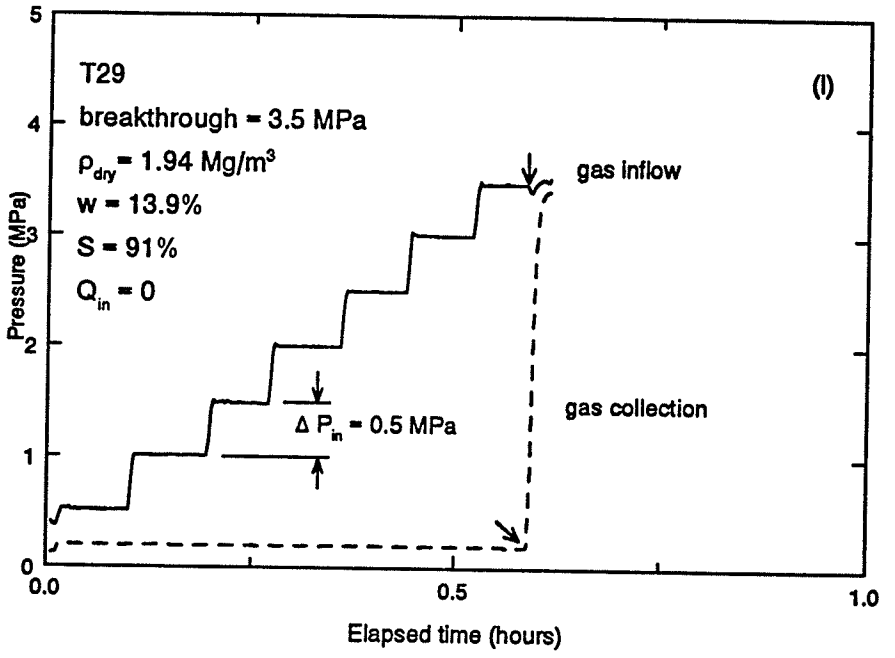

Figure 5.1(k): Gas-breakthrough test results for BT3,
(l): Gas-breakthrough test results for T29.

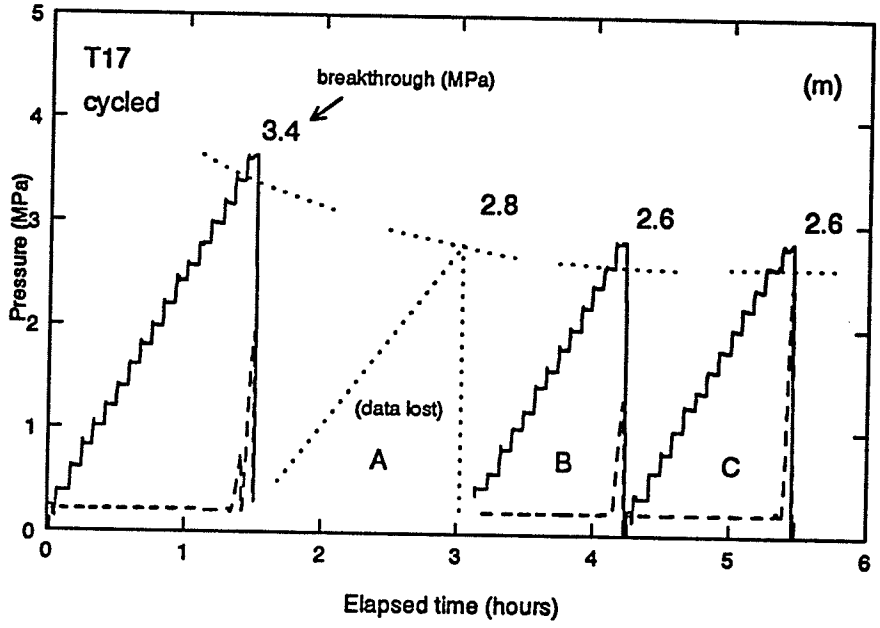

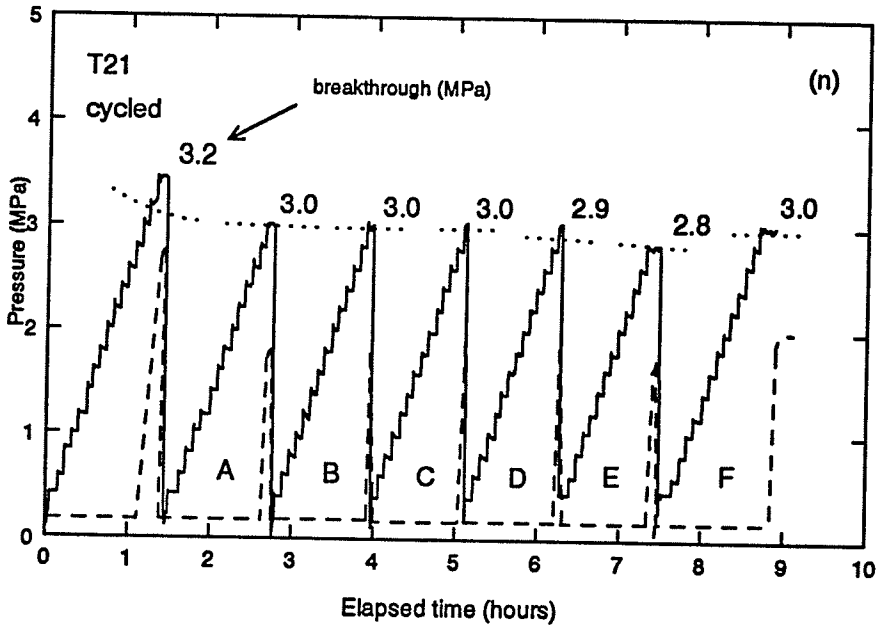

Figure 5.1(m): Gas-breakthrough test results for T17, cycled,
(n): Gas-breakthrough test results for T21, cycled.

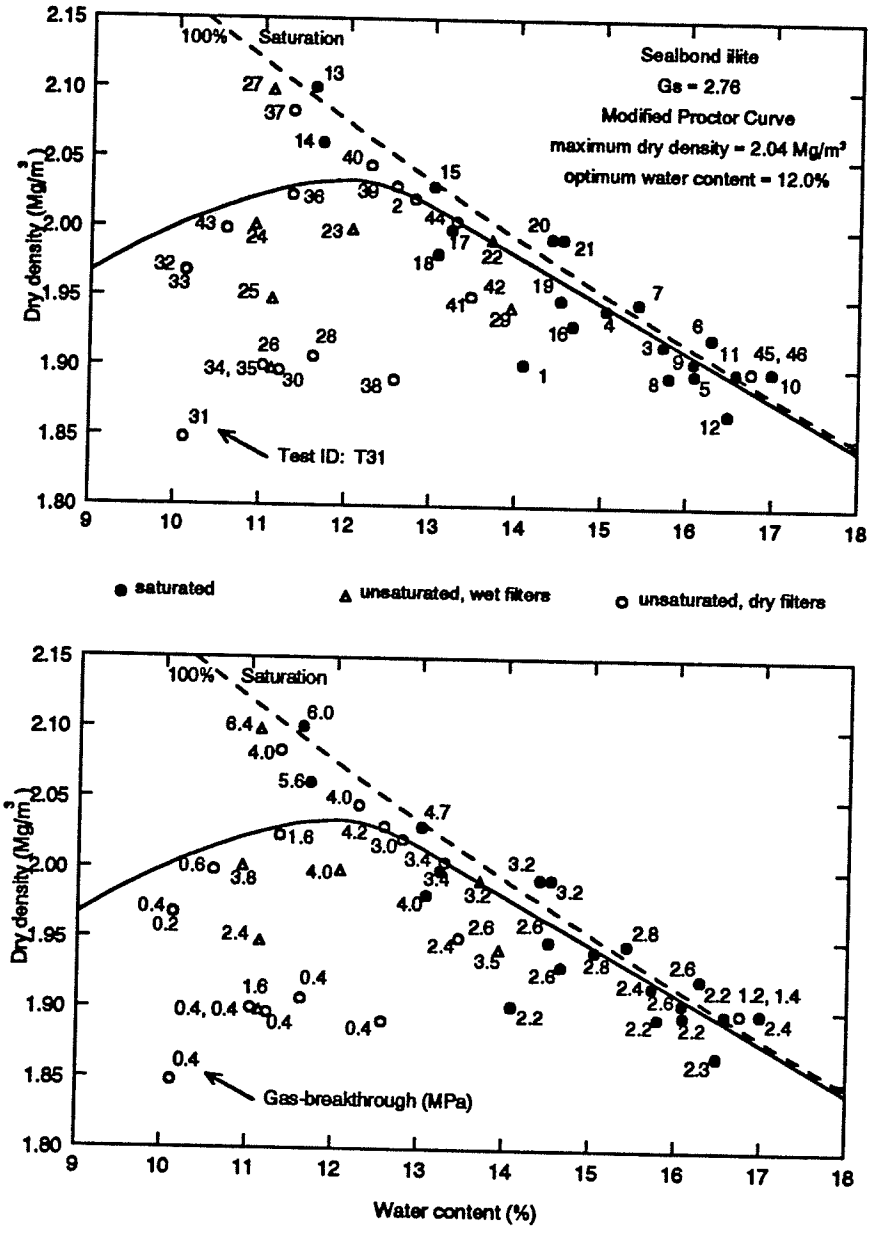

Figure 5.2: Summary of illite gas-breakthrough test conditions with test ID given in the top figure and gas-breakthrough pressures given below.

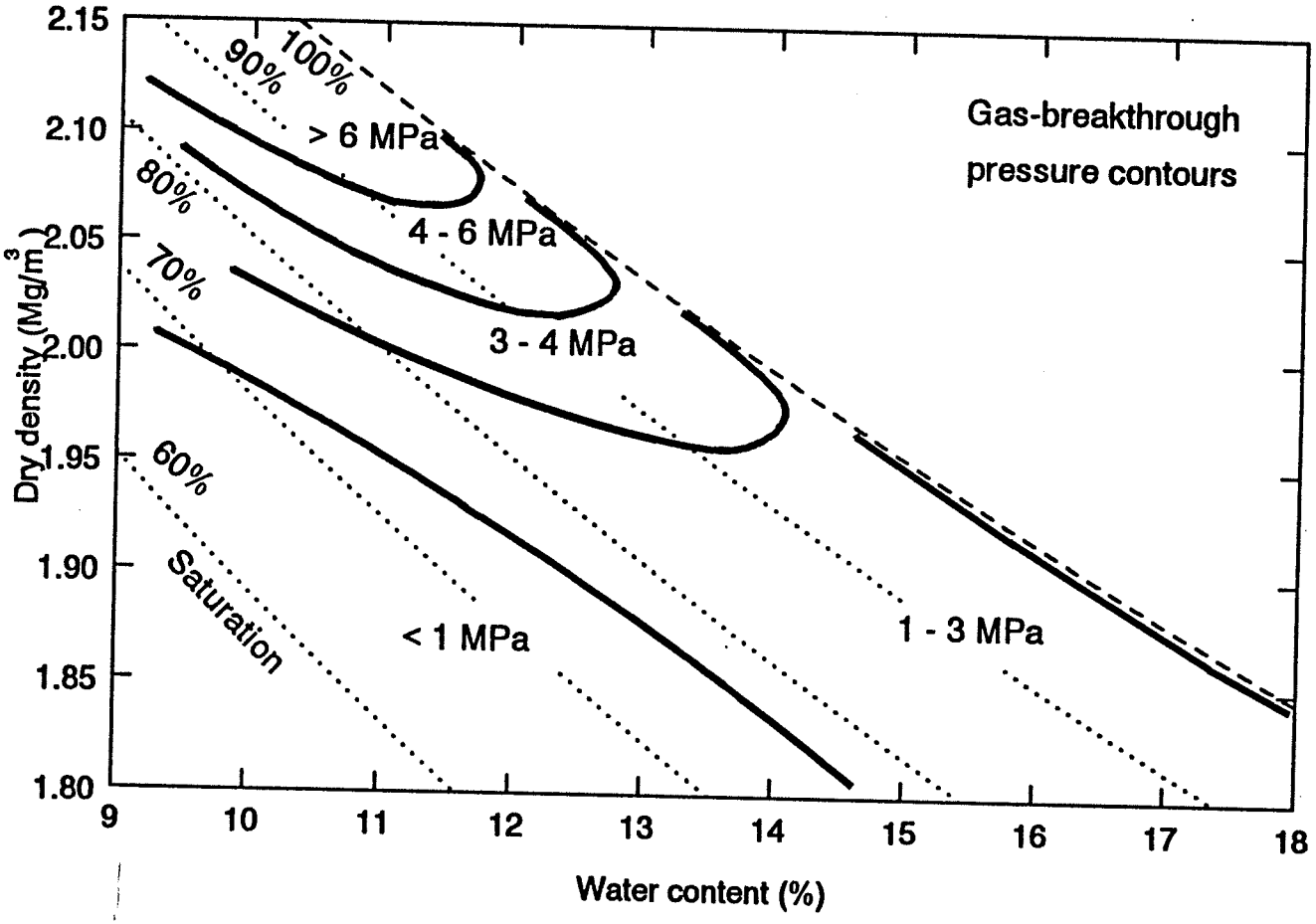

Figure 5.3: Gas-breakthrough pressure contours.

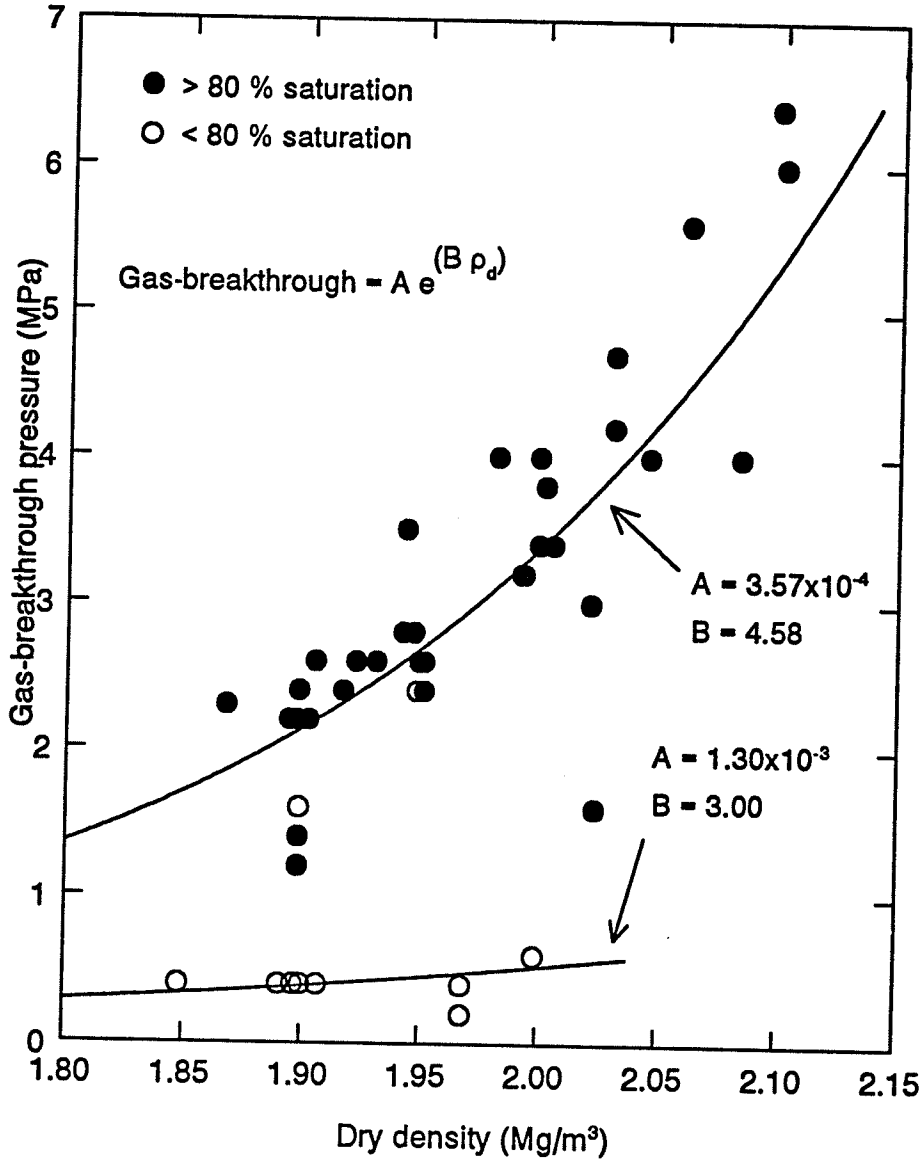

Figure 5.4: Gas-breakthrough pressure - dry density relationship for saturations above and below S = 80%.

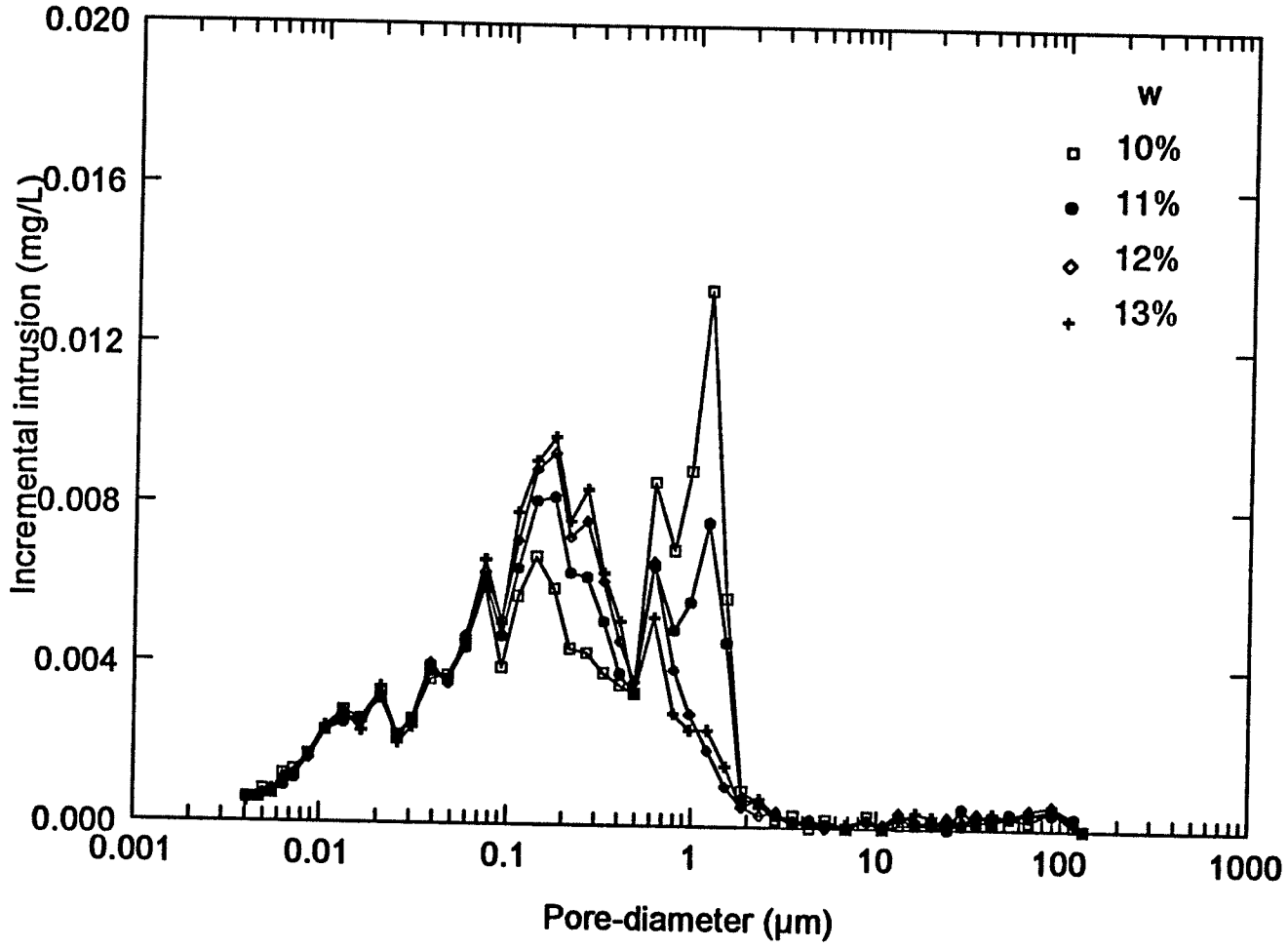

Figure 5.5: MIP data for specimens compacted to 2.04 Mg/m^3 with varying moisture contents (after Gelmich, 1994).

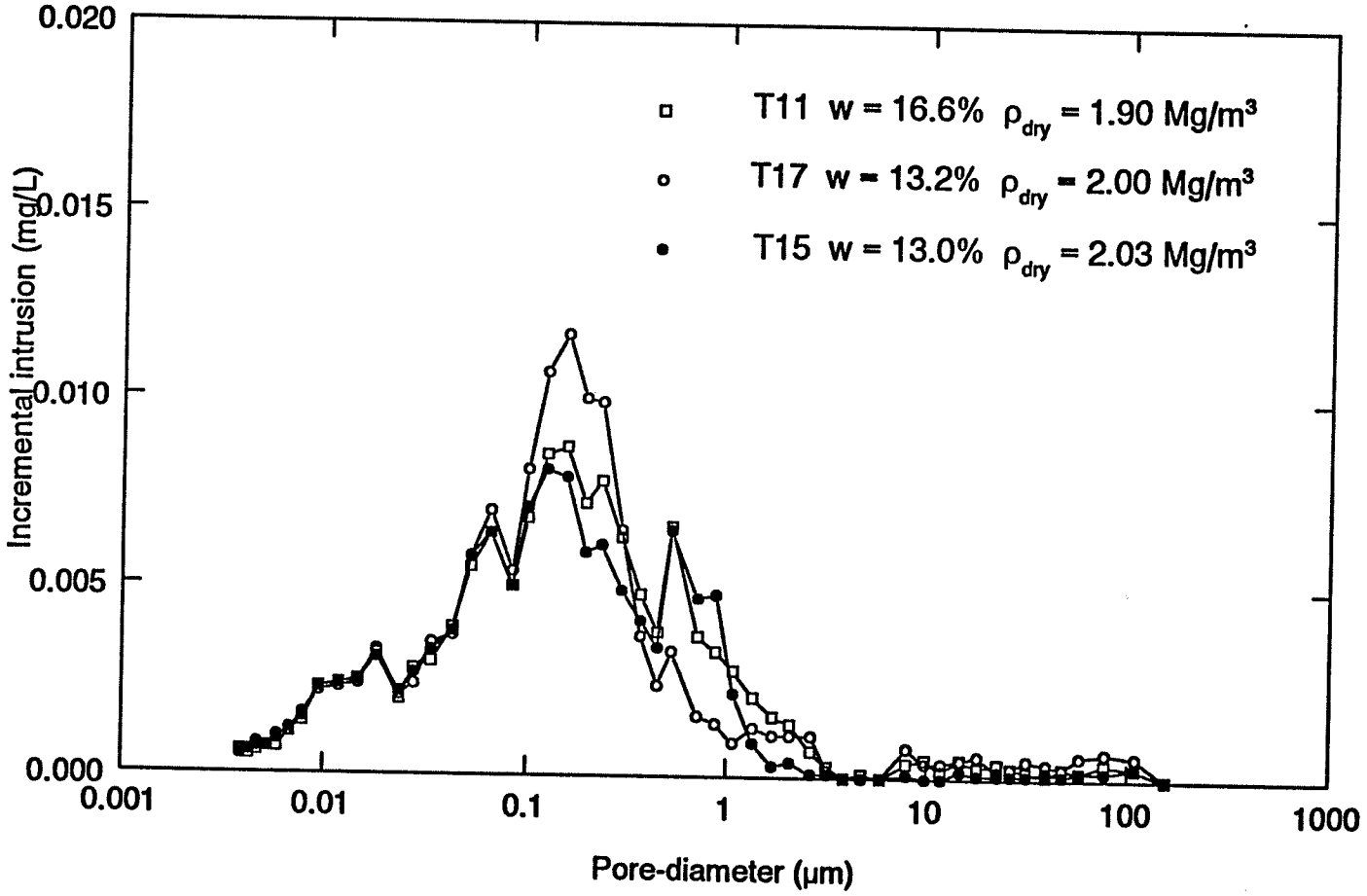

Figure 5.6: MIP data for gas-breakthrough test specimens T11, T15 and T17.

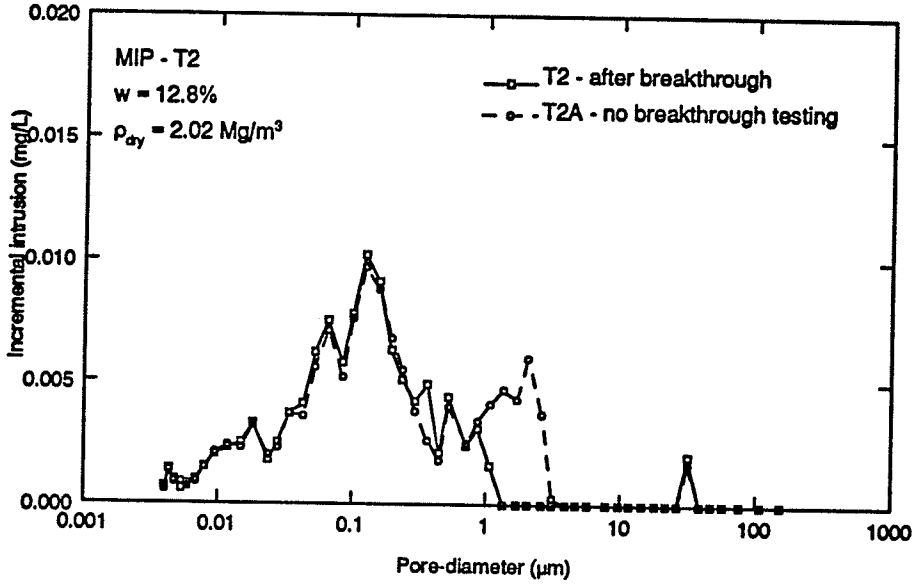

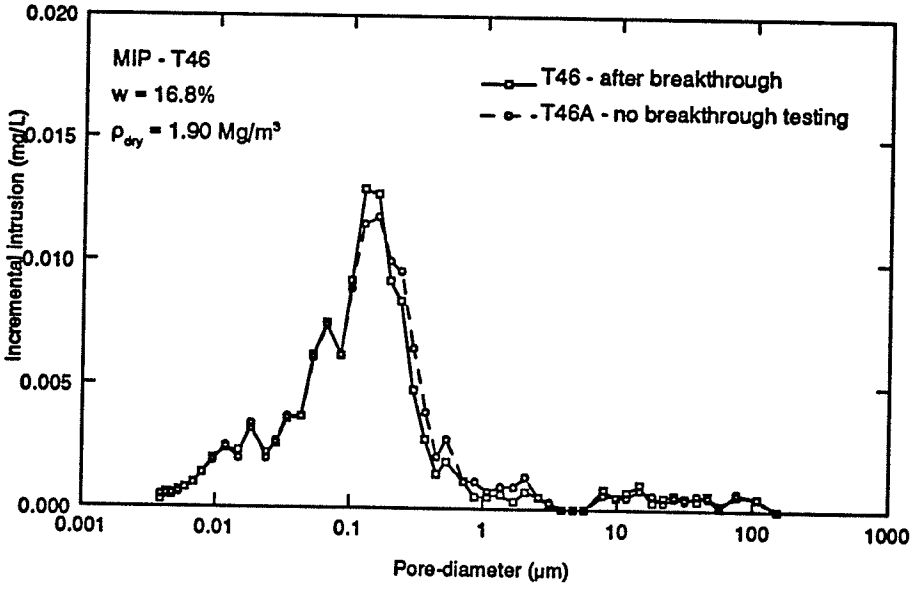

Figure 5.7(a): MIP data for specimen T2,
(b): MIP data for specimen T46.

❑ ***For illite specimen T2***

Based on phase equations and DDL theory:

- Specific surface area $S_o = 60\ m^2/g$ for illite
- Total surface area $S_T = S_o \times V_c$ where V_c = volume of clay = $\rho_c \times V$
  ρ_c = clay dry density
  V = total specimen volume

$$S_T = (60\ m^2/g) \times (2.02\ Mg/m^3) \times (48.45\ cm^3) = 5872\ m^2$$

- Volume of bound water $V_{bw} = w_{DDL} \times S_T$ w_{DDL} = width of DDL

$$V_{bw} = (5872\ m^2) \times (0.5\ nm) = 2.94 \times 10^{-6}\ m^3$$

- Porosity $\eta = V_V/V = 0.27$ V_V = volume of voids = ηV

- Effective porosity $\eta_{eff} = (V_V - V_{bw})/V$ $V_V = 12.97\ mL$
  = porosity contributing to flow phenomena.

$$\eta_{eff} = [(12.97 \times 10^{-6} - 2.94 \times 10^{-6})/48.45 \times 10^{-6}] = 0.21$$

$$\eta/\eta_{eff} = 1.29 \text{ and } \eta = \eta(\phi^2) \text{ so } \phi = (1.29)^{1/2}\ \phi_{eff} = 1.13\ \phi_{eff}$$

- Gas-breakthrough pressure = $P_c = 4T/\phi_{eff}$

T = surface tension at gas-water interface = 0.073 N/m
Gas-breakthrough pressure = 3.0 MPa

$$\text{so } \phi_{eff} = 4T/P_c = 4\ (0.073\ N/m)/(3.0 \times 10^6\ N/m^2) = 0.097\ um$$

$$\phi = 1.13\ (0.097\ um) = 0.11\ um$$

ϕ = 0.11 um (theoretical)
Predicted gas-breakthrough pressure = 2.9 MPa
Observed gas-breakthrough pressure = 3.0 MPa

❑ ***For illite specimen T46***

$\rho_c = 1.90\ Mg/m^3$, $\eta = 0.31$, Gas-breakthrough = 1.4 MPa

ϕ = 0.23 um (theoretical)
Predicted gas-breakthrough pressure = 1.5 MPa
Observed gas-breakthrough pressure = 1.4 MPa

❑ ***For buffer specimen BT3***

$\rho_{dry} = 1.68\ Mg/m^3$ so $\rho_c = 1.23\ Mg/m^3$, $\eta = 0.38$, $w_{DDL} = 0.5\ nm$
Gas-breakthrough = 9.5 MPa, $S_o = 600\ m^2/g$ for Na-bentonite

ϕ = 0.47 um (theoretical)
Predicted gas-breakthrough pressure = 0.01 MPa
Observed gas-breakthrough pressure = 9.4 MPa

Figure 5.8: Sample calculations for determining theoretical gas-breakthrough pore-size.

REFERENCES

AECL EIS, (1994). Environmental Impact Statement on the Concept for Disposal of Canada's Nuclear Fuel Waste. AECL Research document no. AECL-10711, COG-93-1.

Alonso, E.E., Gens, A., Josa, A., (1990). A Constitutive Model For Partially Saturated Soils. Géotechnique, vol. 40, no. 3, pp. 405-430.

ASTM, (1993). Annual Book of ASTM Standards. Vol. 04.08. Moisture content test standard D2216.

Barden, L., Sides, G.R., (1970). Engineering Behavior and Structure of Compacted Clay. ASCE Journal of the Soil Mechanics and Foundations Division, vol. 96, no. SM4, pp. 1171-1200.

Bishop, A.W., (1959). The Principle of Effective Stress. Teknisk Ukeblad, vol. 106, no. 39, pp. 859-863.

Bohn, McNeal, O'Connor, (1985). Soil Chemistry (2nd Ed.). John Wiley & Sons, Inc. New York, NY.

Cheung, S.C.H., (1989). Methods to Measure Apparent Diffusion Coefficients in Compacted Bentonite Clays and Data Interpretation. Canadian Journal of Civil Engineering, vol. 16, pp. 434-443.

Cheung, S.C.H., Chan. T., (1983). Computer Simulation of Contaminant Transport. Proceedings of 1983 Summer Computer Simulation Conference, Vancouver, BC, Canada, vol. I, pp. 470-475.

Corey, A.T., (1990). Mechanics of Immiscible Fluids in Porous Media. Water Resource Publications. Littleton, Colorado.

Couture, R.A., (1985). Rapid Increase in Permeability and Porosity of Bentonite-Sand Mixtures Due to Alteration by Water Vapour. Scientific Basis for Nuclear Waste Management VIII (eds. Jantzen, C.M., Stone, J.A., Ewing, R.C.). Materials Research Society, Pittsburg, PA, USA, pp. 515-522.

Craig, R.F., (1989). Soil Mechanics. (4th edition). Van Nostrand Reinhold (International) Co. Ltd. Wokingham, UK.

Diamond, S., (1970). Pore Size Distributions in Clays. Clays and Clay Minerals, vol. 18, pp. 7-23. Pergamon Press, UK.

Diamond, S., (1971). Microstructure and Pore Structure of Impact-compacted Clays. Clays and Clay Minerals, vol. 19, pp. 239-249.

Dixon, D.A., (1995). Towards an Understanding of Water Structure and Water Movement Through Dense Clays. Doctor of Philosophy Thesis, University of Manitoba, Winnipeg, Manitoba.

Dixon, D.A., Gray, M.N., Hnatiw, D., (1992). Critical Gradients and Pressures in Dense Swelling Clays. Canadian Geotechnical Journal, vol. 29, no. 6, pp. 1113-1119.

Dixon, D.S., Hnatiw, D., Kohl, C., Walker, B., (1994). Pre-Placement Quality Control, and As-Placed Properties of the Buffer and Backfill Materials Used in Buffer Container Experiment Number 1. AECL Research Technical Record TR-618, Whiteshell Laboratories.

Dixon, D.A., Gray, M.N., Thomas, A.W., (1985). A Study of the Compaction Properties of Potential Clay-Sand Buffer Mixtures for use in Nuclear Fuel Waste Disposal. Engineering Geology, vol. 21, pp. 247-255.

Dixon, D.A., Woodcock, D.R., (1986). Physical and Engineering Properties of Candidate Buffer Materials. Internal AECL Research Technical Record TR-352, Whiteshell Laboratories.

Fredlund, D.G., Rahardjo, H., (1993). Soil Mechanics for Unsaturated Soil. John Wiley & Sons, Inc. New York, NY.

Fredlund, D.G., Morgenstern, N.R., (1977). Stress State Variables for Unsaturated Soils. ASCE Journal Geotechnical Engineering Division, vol. 103, no. GT5, pp. 447-466.

Freeze, R.A., Cherry, J.A., (1979). Groundwater. Prentice-Hall Inc. Englewood Cliffs, NJ.

Garcia-Bengochea, I., Lovell, C.W., Altschaeffl, A.G., (1979). Pore Distribution and Permeability of Silty Clays. ASCE Journal of the Geotechnical Enginnering Division, vol. 105, no. GT7, pp. 839-856.

Gelmich, K.S., (1994). Gas Breakthrough and Mercury Intrusion Porosimetry Testing on Illite. unpublished report for AECL Research, Vault Sealing Section, and the University of Manitoba Geotechnical Engineering Group, Winnipeg, Manitoba.

Gens, A., Alonso, E.E., (1992). A Framework for the Behaviour of Unsaturated Expansive Clays. Canadian Geotechnical Journal, vol. 29, pp. 1013-1032.

Grogan, H.A., Worgan, K.J., Smith, G.M., Hodkinson, D.P., (1992). Post-disposal Implications of Gas Generated from a Repository for Low and Intermediate Level Wastes. INTERA, Environmental Division, Henley-on-Thames, UK. Technical Report NAGRA-NTB-92-07.

Hensley, P.J., Schofield, A.N., (1991). Accelerated Physical Modelling of Hazardous-waste Transport. Géotechnique, vol. 41, pp. 447-465.

Horseman, S.T., Harrington, J., (1994). Migration of Repository Gases in an Overconsolidated Clay. Natural Environment Research Council, British Geological Survey, Groundwater and Geotechnical Surveys Division. Keyworth, Nottingam, UK. Technical Report WE/94/7

Jeffries, R.M., Liew, S.K., Thomas, J.B., (1991). Gas Migration in deep Radioactive Waste Repositories; A Review of Processes, Data and Models. Department of the Environment: HMIP-comissioned research. WS Atkins Engineering Sciences, Epsom, Surrey, UK., Report no. M1426.050.

Johnson, L.H., LeNeveu, D.M., Shoesmith, D.W., Oscarson, D.W., Gray, M.N., Lemire, R.J., Garisto, N.C., (1994a). The Disposal of Canada's Nuclear Fuel Waste: The Vault Model for Postclosure Assessment. AECL Research AECL-10714, COG-93-4.

Johnson, L.H., Tait, J.C., Shoesmith, D.W., Crosthwaite, J.L., Gray, M.N., (1994b). The Disposal of Canada's Nuclear Fuel Waste: Engineered Barriers Alternatives. AECL Research document no. AECL-10718, COG-93-8.

Juang, C.H., Holtz, R.D., (1986). Fabric, Pore Size Distribution, and Permeability of Sandy Soils. ASCE Journal of the Geotechnical Engineering Division, vol. 112, no. 9, pp. 855-868.

Lambe, T.W., (1958). The Structure of Compacted Clay. ASCE Journal of the Soil Mechanics and Foundations Division, Paper 1654, SM 2, pp. 1-34.

Lineham, T. R., (1989). A Laboratory Study of Gas Transport Through Intact Clay Samples. Harwell Laboratory, UKAEA, United Kingdom, NSS/R155.

Matyas, E.L., Radhakrishna, H.S., (1968). Volume Change Characteristics of Partially Saturated Soils. Geotechnique, vol. 18, no. 4, pp . 432-448.

Mitchell, J.K., (1991). Conduction Phenomena: from Theory to Geotechnical Practice. Géotechnique, vol. 41, no. 3, pp. 299-340.

Mitchell, J.K., (1976). Fundamentals of Soil Behaviour. (eds. Lambe, T.W., Whitman, R.V.). John Wiley & Sons, Inc. New York, NY.

Oscarson, D.W., Dixon, D.A., (1989). The Effect of Steam on Montmorillonite. Applied Clay Science, vol. 4, pp. 279-292.

Pusch, R., (1993). Current Status and Future Plans for R&D on Gas Penetration and Release Through Buffer Materials. Reprinted from International Workshop on Research & Development of Geological Disposal, Nov. 15-18, 1993. PNC Tokai, Japan.

Pusch, R., Forsberg, T., (1983). Gas Migration Through Bentonite Clay. University of Luleå, Sweden, SKBF/KBS Technical Report 83-71.

Pusch, R., Hökmark, H., Börgesson, L., (1987). Outline of Models of Water and Gas Flow Through Smectite Clay Buffers. Swedish Nuclear Fuel and Waste Management Co., Technical Report 87-10, Stockholm, Sweden.

Pusch, R., Ranhagen, L., Nilsson, K., (1985). Gas Migration Through MX-80 Bentonite. Swedish Geological, Lund, Sweden, Technical Report NAGRA NTB 85-36.

Richards, B.G., (1974). Behaviour of Unsaturated Soils. In: Soil Mechanics - New Horizons (ed. Lee, I,K.). Butterworth & Company (Canada) Ltd.

Rolston, D.E., (1986). In: Gas Diffusivity. American Society of Agronomy - Soil Science Society of America. Madison, WI, USA. Methods of Soil Analysis, Part 1. Physical and Mineralogical Methods - Agronomy Monograpgh no. 9 (2nd Ed.), pp. 1089-1102.

Ruth, D. (1993). The Transport Phenomena in Porous Media Notebook (version 5.0). Unpublished notes. Department of Mechanical Engineering, University of Manitoba, Winnipeg, Manitoba.

Sharland, S.M., Agg, P.J., Naish, C.C., Wikramaratna, R.S., (undated) Gas Generation by Metal Corrosion and the Implications for Near-Field Containment in Radioactive Waste Repositories. (AEA Technology, under contract to UK Nirex, Ltd). Reprinted from International Workshop on Research & Development of Geological Disposal, Nov. 15-18, 1993. PNC Tokai, Japan.

Terzaghi, K., Peck, R.B., (1948). Soil Mechanics in Engineering Practice. John Wiley & Sons, Inc. New York, NY.

Troeh, F.R., Jabro, J.D., Kirkham, D., (1982). Gaseous Diffusion Equations for Porous Materials. Geoderma, vol. 27, pp. 239-253.

van Olphen, H., (1963). An Introduction to Clay Colloid Chemistry. Interscience Publishers (John Wiley & Sons, Inc. New York, NY.).

Volckaert, G., Put, M., Ortiz, L., De Cannière, P., Horseman, S., Harrington, J., Fioravante, V., Impey, M., Worgan, K., (1993). MEGAS - Modelling and Experiments on Gas Migration in Repository Host Rocks. PEGASUS Meeting, June 1993, CRS Köln.

Wan, A.W.L., (1987). Compaction and Strength Characteristics of Sand-Clay Buffer Material Formed at Swelling Pressure - Water Content Equilibrium. Master of Science Thesis, University of Manitoba, Winnipeg, Manitoba.

Wheeler, S.J., (1988). A Coneptual Model for Soils Containing Large Gas Bubbles. Géotechnique, vol. 38, pp. 389-397.

Wheeler, S.J., Sham, W.K., Thomas, S.D., (1990). Gas Pressure in Unsaturated Offshore Soils. Canadian Geotechnical Journal, vol. 27, pp. 79-87.

Wheeler, S.J., Sivakumar, V., (1993). Development and Applications of a Critical State Model for Unsaturated Soil. In: *Predictive Soil Mechanics*. (ed. Houlsby, G.T., Schofield, A.N.) Proceedings of the Wroth Memorial Symposium held at St. Catherine's College, Oxford, 27-29 July, 1992. Thomas Telford Publishers, London, UK.

Wikramaratna, R.S., Goodfield, M., (1994). A Proposed Programme of Experimental and Theoretical Modelling Studies of Gas Migration Through Bentonite. Unclassified AEA Technology document, AEA-ESD-0033 Issue 1.

Wikramaratna, R.S., Goodfield, M., Rodwell, W.R., Nash, P.J., Agg, P.J., (1993). A Preliminary Assessment of Gas Migration from the Copper/Steel Canister. Swedish Nuclear Fuel and Waste Management Co. SKB Technical Report 93-31, Stockholm, Sweden.

Wood, D.M., (1990). Soil Behaviour and Critical State Soil Mechanics. Cambridge University Press, Cambridge, UK.

Yarechewski, D., (1993). Constant Mean Effective Stress Tests on Sand Bentonite Specimens at Elevated Temperature. Master of Science Thesis, the University of Manitoba, Winnipeg, Manitoba.

Yong, R.N., Warkentin, B.P., (1975). Soil Properties and Behavior. Elsevier Scientific Publishing Company. New York, NY.

Yong, R.N., Mohamed, A.M.O., Warkentin, B.P., (1992). Principles of Contaminant Transportation in Soils. Elsevier Scientific Publishing Company. New York, NY.

APPENDIX A

EQUIPMENT AND SAFETY DOCUMENTATION

AECL EACL

AECL Research EACL Recherche

Engineering and Design Division Design Document

Classification/ Designation _____

☐ Chalk River Laboratories
Chalk River Ontario
Canada K0J 1J0

☒ Whiteshell Laboratories
Pinawa, Manitoba
Canada R0E 1L0

DOCUMENT TITLE DESIGN REVIEW REPORT

PROJECT/JOB TITLE PERMEABILITY CELL/SYSTEM

DOCUMENT TYPE _____

Prepared By	L. HIEBERT	Date 93.6.25
Reviewed By	N/A	Date
Approved By		Date 93/06/25
Accepted By	N/A	Date
Accepted By	N/A	Date

(Signatories for Rev. 0 only)

RELEASED FOR CONSTRUCTION
NOT TO BE USED FOR CONSTRUCTION

Design Job No. 61W08

Document No. A-61W08-DR2

Revision No. 0

Alternate Document No. N/A

CRL-3554-1-Rev.2

Research
P · Laboratories
R..r, Ontario K0J 1J0

ENGINEERING CHANGE NOTICE

(1) NO. 61W08 (Project/Design Job #) -ECN- 1 (Serial #)

(2) PROJECT/JOB TITLE: GAS PERMEABILITY SYSTEM

ECN Issued by: L. HIEBERT Date: 93/11/08 Branch: D&E

REFERENCE No. A1-61W08-F1 (NCR, Field Mods, etc.)

(3) SUBJECT/PROBLEM DESCRIPTION: (a) 1 - Design 2 - Software 3 - Project 4 - Process

AT THE REQUEST OF THE REQUISITIONER, THE LEAK TEST FLUID PREVIOUSLY SPECIFIED AS DISTILLED WATER IS NOW TO BE ARGON OR NITROGEN.

☐ Attachments

(4) PROPOSED CHANGE AND JUSTIFICATION:

AN ACCEPTABLE ALTERNATIVE TO THE LEAK TEST SPECIFIED ON NOTE 7 OF A1-61W08-F1 IS GIVEN ON THE ATTACHED SHEET.

☑ Attachments

(5) CHANGE REQUEST:

(a) CATEGORY
1 - Project Scope 2 - Work Group Scope (3) - Convenience 4 - Deficiency Correction 5 - Field Mod

(b) CAUSE
(Regulatory) 1 - Safety 2 - Licensing 3 - Environmental 4 - Other _____
(Function/Group) 11 - Design 12 - Supply 13 - Contract 14 - Production 15 - Other _____
(Project Improvement) 21 - Operability 22 - Performance 23 - Reliability 24 - Maintainability 25 - Other _____
(Product Improvement) 31 - Economics 32 - Schedule 33 - Safety 34 - Standardization 35 - Other _____

(c) CLASS
1 - Major (Project or PRB Review and Acceptance) 2 - Moderate (Design/Functional Group Review and Acceptance)
(3) - Minor (Design/Engineering Review and Acceptance) 4 - Rejected (Change Requisitioner Acknowledgement)

Requisitioner Acknowledgement of Rejected ECN _____ Date _____ Project Designer/Engineering Manager _____ Date _____

(6) IMPACT ASSESSMENT: (a) By: 1 - Project Designer/Engineering Manager 2 - Project Manager
3 - Advisory Functions (DTS# ____ - ____ - ____) 4 - Project Review Board (PRB)

NO IMPACT

FOR CONSTRUCTION

☐ Attachments Summary by _____ Date 93/11/08

(7) DISPOSITION:

(a) (1 - Approved) 2 - Rejected 3 - ECN Revised

(b) 1 - Project Designer/Engineering Manager: _____ Date: 93/11/08
2 - Project Manager: _____ Date: _____
3 - Project Review Board: _____ Date: _____
4 - Owner: _____ Date: _____

(8) NOTICE OF CHANGE: (a) Change Documentation: 1 - Revision 2 - MOD 3 - Sketch (4) - Note 5 - Pink Prints

NOTE ON DWGS

94/1/27

☑ Attachments (b) _____ 93/11/08 _____ _____
1 - Change Release Approval (PD/EM) Date 2 - Update Complete (PD/EM) Date

DISTRIBUTION: WHITE: Project Designer/Engineering Manager (QA Record) BLUE - ECN Register YELLOW - ECN Requisitioner

FOR CONSTRUCTION

Divided Copy #4

7) PRIOR TO THE INSTALLATION OF RELIEF VALVE -RV1, PERFORM A PNEUMATIC LEAK TEST ON THE COMPLETE SYSTEM AS PER THE REQUIREMENTS OF ASME B31.1, PARA 137.5. THE PNEUMATIC LEAK TEST SHALL BE WITNESSED BY A QUALIFIED INSPECTOR, AND PERFORMED UNDER THE DIRECTION OF THE OPERATOR.

STEP 1 A) AS PER PARA 137.5.4 PERFORM A PRELIMINARY TEST TO 175 KPA USING ARGON OR NITROGEN GAS.

STEP 2 B) AS PER PARA 137.5.5, GRADUALLY PRESSURIZE THE SYSTEM TO 12.5 MPA USING ARGON OR NITROGEN GAS. MAINTAIN THIS PRESSURE FOR A MINIMUM OF 10 MINUTES.

STEP 3 C) LOWER THE PRESSURE TO 0.7 MPA AND EXAMIN FOR LEAKAGE BY SOAP BUBBLE OR EQUIVALENT METHOD. THE SYSTEM SHALL SHOW NO EVIDENCE OF LEAKAGE.

Leak test 1H (Glass Tube) separate as per note 7 above, except step 2 (B) shall be to 10 MPa, not 12.5 MPa

93/01/27

ATOMIC ENERGY OF CANADA LIMITED
WHITESHELL NUCLEAR RESEARCH ESTABLISHMENT

PNEUMATIC TEST REPORT

Ref. IRR No. 354

DESIGN JOB NO. - DWG.NO. 61W28-F1 ECN 61W02-1	PROJECT - JOB TITLE GAS PERMEABILITY SYSTEM
SPOOL PIECE - LINE - VESSEL NO. TUBING SYSTEM	SPEC. - CODE - ENG. STD N/A
TEST PROCEDURE NO. CMS-PROC 02	MARKED - #1-61W08 2ND SYSTEM FABRICATED

TEST DATA

TEST MEDIUM NITROGEN GAS	LOCATION OF PRESSURE GAUGE IN-LINE
PRESSURE GAUGE SERIAL NUMBER P412-42	PRESSURE GAUGE RANGE 0 TO 25mPa
PRESSURE GAUGE CALIBRATION DATE DUE FEB 10/94	APPLICATION PRESSURE 12.5mPa
PRESSURE HOLDING TIME 10 min.	EXAMINATION PRESSURE 0.7mPa

TEST RESULTS

Inspector's Findings:

1. Leakage (Soap Bubble Test) — NO [ ] YES [✓] SNOOP TEST. LEAKS RECTIFIED BY TIGHTNING.
   if Yes, give details
2. Fall in Pressure — NO [✓] YES [ ]
   If Yes, give details
3. Visible Permanent Distortion — NO [✓] YES [ ]
   If Yes, give details

Comments:if any PRESSURE WAS HELD AT 12.5mPa FOR 10 min. WITHOUT ANY DETECTABLE LEAKS.

ACCEPT [✓]

REJECT [ ]

INSPECTOR _____

DATE COMPLETED FEB 1/94

ATOMIC ENERGY OF CANADA LIMITED
WHITESHELL NUCLEAR RESEARCH ESTABLISHMENT

PNEUMATIC TEST REPORT

Ref. IRR No. 85

DESIGN JOB NO. - DWG.NO. 61WDR-F1 ECN 61WDR-1	PROJECT - JOB TITLE GAS PERMEABILITY SYSTEM
SPOOL PIECE - LINE - VESSEL NO. TUBING SYSTEM	SPEC. - CODE - ENG. STD N/A
TEST PROCEDURE NO. CMS-PROC 02	MARKED - #2-61WDR (1st SYSTEM FABRICATED)

TEST DATA

TEST MEDIUM NITROGEN GAS	LOCATION OF PRESSURE GAUGE IN-LINE
PRESSURE GAUGE SERIAL NUMBER P412-42	PRESSURE GAUGE RANGE 0 TO 25 mPa
PRESSURE GAUGE CALIBRATION DATE DUE FEB 10/94	APPLICATION PRESSURE 12.5 mPa
PRESSURE HOLDING TIME 10 min.	EXAMINATION PRESSURE 0.7 mPa

TEST RESULTS

Inspector's Findings:

1. Leakage (Soap Bubble Test) — NO [✓] YES [ ]
   If Yes, give details (SOAP TEST)
2. Fall in Pressure — NO [✓] YES [ ]
   If Yes, give details
3. Visible Permanent Distortion — NO [✓] YES [ ]
   If Yes, give details

Comments:if any PRESSURE WAS HELD AT 12.5mPa WITHOUT ANY DETECTABLE LEAKS. THE PRESSURE WAS HELD FOR 10min.

ACCEPT [✓]

REJECT [ ]

INSPECTOR _____

DATE COMPLETED 31 FEB 1/94

ATOMIC ENERGY OF CANADA LIMITED
WHITESHELL NUCLEAR RESEARCH ESTABLISHMENT

PNEUMATIC TEST REPORT

Ref. IRR No. 354

DESIGN JOB NO. - DWG.NO. 61W08-F1 ERN 61W08-1	PROJECT - JOB TITLE GAS PERMEABILITY SYSTEM
SPOOL PIECE - LINE - VESSEL NO. LEVEL INDICATOR 1H	SPEC. - CODE - ENG. STD N/A.
TEST PROCEDURE NO. CMS-PROC 02	LEVEL INDICATOR FOR SYSTEM MARKED #1-61W08. THE SECOND TUBING SYSTEM FABRICATED.

TEST DATA

TEST MEDIUM NITROGEN GAS	LOCATION OF PRESSURE GAUGE IN-LINE
PRESSURE GAUGE SERIAL NUMBER P412-42	PRESSURE GAUGE RANGE 0 TO 25 mPa
PRESSURE GAUGE CALIBRATION DATE DUE FEB 10/94	APPLICATION PRESSURE 10 mPa
PRESSURE HOLDING TIME 10 min.	EXAMINATION PRESSURE 0.7 mPa

TEST RESULTS

Inspector's Findings:

1. Leakage (Soap Bubble Test) — NO [✓] YES [ ]
   if Yes, give details _____
2. Fall in Pressure — NO [✓] YES [ ]
   If Yes, give details _____
3. Visible Permanent Distortion — NO [✓] YES [ ]
   If Yes, give details _____

Comments:if any PRESSURE WAS HELD AT 10 mPa FOR 10 min WITHOUT ANY DETECTABLE LEAKS. /AA

ACCEPT [✓]

REJECT [ ]

INSPECTOR ____

DATE COMPLETED Feb. 1/94

AECL Research
Whiteshell Laboratories
Quality Assurance Branch

INSPECTION REQUEST / REPORT

INSPECTION REQUEST

DATE 1994 February 1 NO. 13945

DESIGN ENGINEER: D. Patterson	SPEC/CODE/ENG STD: N/A	DESIGN JOB NO./DWG NO./ECN NO.: 61W08-F1 Rev. 0 ECN 61W08-1
OWNER/CONTACT: T. Kirkham	PURCHASE ORDER NO.: N/A	PROJECT/JOB TITLE: Gas Permeability System
MANUFACTURING ENGINEER: J. Harding	MANUF. WORK ORDER NO.: W9778800	
FOREMAN/TEAM LEADER: G. Buchanan	TRAVELLER NO.: N/A	ITEM DESCRIPTION (DETAILS BELOW): Tubing System
PURCHASING AGENT: N/A	CHECKLIST NO.: N/A	SPECIFIC DETAILS
REQUISITIONERS: G. Buchanan, T. Kirkham, L. Hiebert	SUPPLIER: WL	LOCATION: WL Bldg. 100 QUANTITY: 2 Ass'y MATERIAL: As Per Drawing SIZE: " SCHEDULE: " RATING: " HEAT NO.: "
JURISDICTION (IF REQUIRED): N/A	MANUFACTURER: WL	

INSPECTIONS REQUIRED

- ☐ DIMENSIONAL
- ☐ RADIOGRAPHIC
- ☐ LIQUID PENETRANT
- ☐ ULTRASONIC
- ☐ EDDY CURRENT
- ☐ OTHER (SPECIFY)
- ☐ ELECTRICAL
- ☐ MAGNETIC PARTICLE
- ☐ VISUAL INSPECTION
- ☒ PRESSURE TEST
- ☐ DOP
- ☐ RECEIVING

REQUEST DETAILS

Witness pressure tests on gas permeability tubing systems.

INSPECTION REPORT

Q.A. RECORDS FILE NO.	Q.A. WORK ORDER NO.	PROCEDURE NO.	NCR NO.	QUANTITY ACCEPTED	MAN HOURS
851	W9778800	N/A		2 Ass'y	4

RADIOGRAPHY: X-RAY NUMBERS N/A

RECEIVING INSPECTION: MATERIAL MARKINGS

N/A

INSPECTION RESULTS

A pneumatic test was performed on gas permeability tubing systems 1 & 2 as specified in ECN 61W08-1 (copy attached). There were three separate tests: Tests #1 & 2 were performed on two systems with the exception of relief valve RV1 and Level Indicator 1H. The two pressure gauges 1P & 2P to valves V19 & V20 were tested at a test pressure of 10MPa in place of the specified pressure of 12.5MPa (As discussed with L. Hiebert this pressure is acceptable). Test #3 was performed on Level Indicator 1H of the newly fabricated tubing system (marked #1-61W08). The pressure tests are acceptable as reported on attached sheets.

FINAL DISPOSITION

- ☒ ACCEPT
- ☐ REJECT

INSPECTOR R.T. Borgford

QA REPRESENTATIVE

DATE COMPLETED 1994 January 2

ATOMIC ENERGY OF CANADA LIMITED
Research Company
Chalk River Nuclear Laboratories
Chalk River, Ontario K0J 1J0

Whiteshell Laboratories
Pinawa, Manitoba R0E 1L0

DOCUMENT REVIEW RECORD FORM

DTS No.: _____ - _____ - _____
(Division/Branch) Project/ Job No. Serial No.

Issued by: L. HIEBERT Stn.: 9 Date: 93.06.25

PROJECT/JOB TITLE: PERMEABILITY CELL / SYSTEM

COMMENTS BY: DUE: RECEIVED:

Reference Document (e.g., P.O., DCR)

DOCUMENT - Title: A.1-61W08-F1, A-61W08-DL1,-DR1,-SP1 DATE: 93.06.25

NUMBER: REV:

Item No.	Reviewed by	Doc. Page / Section No.	Comment	Resolution
			A DESIGN REVIEW MEETING WAS HELD ON 93.06.23 @ 1:00 IN DESIGN CONFERENCE RM. PRESENT: S. CAMPBELL T. KIRKHAM THE DOCUMENTS REVIEWED WERE IN THE PRECHECKED STAGE. COMMENTS: 1) CAN THE SYSTEM BE MODIFIED AFTER THE RELIEF VALVE BRANCH?	YES PROVIDING THE REQUIREMENTS OF NOTE 9 ARE MET.
			2) DO WE NEED CRNs FOR THE PRESSURE INSTRUMENTS	YES.
			3) CAN 1H AND 2H BE REMOVED FOR THE HYDROSTATIC LEAK TEST?	YES.
			4) CAN THE RELIEF VALVE SET PRESSURE BE ADJUSTED DOWN FOR LOWER PRESSURE TESTS? ALL RESOLUTIONS WERE AGREED TO, DURING THE MEETING AND THEREFORE RESOLUTION ACCEPTANCE IS NOT REQUIRED BELOW.	I WOULD LEAVE THE RELIEF VALVE AT THE SET PRESSURE REQUIRED TO PROTECT THE SYSTEM. PRESSURE REGULATORS - PR1, 2, 4 3 MAY BE ADJUSTED TO SUIT.

Resolutions Accepted by: _____ Date _____ Page ____ of ____

CRNL 3539 (12/89)

SPECIFICATION FOR PRESSURE RELIEF VALVE RV1

1.0 SCOPE

This specification covers the requirements for the pressure relief valve to be installed on the discharge of the cylinder pressure regulator of the gas permeameter cell system. The valve must comply with jurisdictional codes.

2.0 APPLICABLE DOCUMENTS

The latest issue of the following documents form part of this specification unless otherwise noted.

ASME B31.1	Power Piping Code, 1992 Edition
ASME	Boiler and Pressure Vessel Code Sections II, VIII, 1992 Edition
CSA B51	Boiler, Pressure Vessel, and Pressure Piping Code, 1991 Edition

3.0 MATERIALS

Pressure boundary materials shall be selected from ASME Section II (for Section VIII) or equivalent ASTM materials.

4.0 APPLICATION

The relief valve will be located at the discharge of the cylinder pressure regulator. The valve shall protect the gas permeability cell (a registered ASME Section VIII pressure vessel) and the associated system in the event the pressure regulator were to fail.

5.0 REGISTRATION

The relief valve shall be ASME Section VIII certified and satisfy the statutory requirements of and be registered with the government regulatory body of the Province of Manitoba (Department of Labour).

The supplier shall be responsible for ensuring the relief valve is registered in accordance with CSA B51.

6.0 DOCUMENTATION

i) A Product Certificate of Compliance (C of C) shall accompany the shipment of the valve. The C of C shall identify the Canadian Registration Number(s) (CRN) for the Provinces of Manitoba, as per CSA B-51, the ASME certified approval, together with verification that the material is as called for in the Purchase Order and any tests carried out by the supplier/manufacturer have been completed and found acceptable.

ii) Descriptive literature and complete relief valve specification.

iii) Record of any concessions made by AECL at the vendors request.

AECL reserves the right to return shipments that arrive without all of the above documentation or the documentation lacks a specific statement referencing the specifications in Section 2.0 above.

7.0 MARKING AND IDENTIFICATION

The supplier shall ensure that the valve is marked and identified according to the requirements of ASME Section VIII Division 1, para UG-129 and UG-130, and are also marked with the Canadian Registration Number(s).

8.0 PRESERVATION, PACKAGING AND SHIPPING

Best commercial practice shall be applied to preserving, packaging, and shipping of this product. When more detailed instructions are required they shall be defined in the Purchase Order documents.

9.0 TECHNICAL SPECIFICATION SHEET

Tag Number	61W08-RV1
Service	Argon
Line No./Vessel No.	Gas Permeability Cell System
Full Nozzle/Semi Nozzle	Full
Safety or Relief	Safety
Conv., Bellows, Pilot Op.	Conventional
Bonnet Type	MFR. STD.
Size Inlet/Outlet	1/2" MNPT/1" FNPT
Flange Rating or Screwed	Screwed
Type of Facing	N/A
Body and Bonnet	Carbon Steel 316
Seat and Disc	Stainless Steel 316
Resilient Seat Seal	N/A
Guide and Rings	MFR. STD.
Spring	MFR. STD.
Bellows	N/A
Balance of Parts	MFR. STD.
Cap: Screwed or Bolted	Screwed
Lever: Plain or Packed	N/A
Test Gag	N/A
Code	ASME B31.1, ASME Section VIII
Fire	N/A
Fluid and State	Argon/Gas State
Required Capacity	42.76 cubic metre/min. (1510 cu. ft./min.)
Sp. Gr.	1.38
Oper. Press./Set Press.	9.3 MPa(g)/10.0 MPa(g) (1350 PSIBG/1450 PSIG
Oper. Temp./Rel. Temp	25°C/25°C (77°F/77°F)
Back Pressure Constant	0.0 MPa(g)
% Allowable Overpressure	10
Latent Heat of Vaporization	Nil
Calc. Area sq. in.	38.71 sq. mm (0.06 sq. in.)
Selected Area	38.71 sq. mm (0.06 sq. in.)
Orifice Designation	N/A
Manufacturer	FARRIS
Model No.	274OUL
Reference Drawing	

1. INTRODUCTION

The Fuel Waste Management program requires testing of different types of granular compounds used as a buffer material for nuclear waste storage. Part of the testing requires the buffer material to be checked for gas and liquid permeability. A cell was designed and constructed under job number 47W23. The cell was modified under an earlier issue of Job 61W08.

This design report will involve providing relief protection for the cell and associated system as required by applicable codes, and ensure compliance with the applicable codes on the associated system.

2. APPLICABLE REQUIREMENTS

2.1 PUBLICATIONS

ASME Section II, Boiler and Pressure Vessel Code, Material Specifications, 1992
ASME Section VIII, Division I, 1992, Boiler and Pressure Vessel Code
ASME B31.1-92 Power Piping Code
CSA B51-M1991, Boiler, Pressure Vessel, and Pressure Piping Code

2.2 DRAWINGS

A1-61W08-F1, Flow Diagram - Tubing System

2.3 SPECIFICATION SHEETS

A-61W08-SP1 Relief Valve (Equip. Code 61W08-RV1)

3. DESIGN

The design conditions for the system are as follows:

Design Pressure:	10 MPa(g) (1450 PSIG)
Design Temperature:	15°C (59°F) to 35°C (95°F)
System Fluid:	Nitrogen, Argon, or Distilled Water

The limiting factor in the design of this system is the permeability cell with a design pressure of 10 MPa(g).

3.1 SYSTEM DESIGN

The material and equipment used for the system was selected by the operator. The rated pressures have been checked for adequacy. The material is primarily stainless steel for corrosion prevention. All fittings used in the system shall be mechanical type, compression,

threaded, etc. All fittings shall have a Canadian Registration Number (CRN) as per CSA B51 for the Province of Manitoba. All fittings shall be rated for the system design pressure or higher. See Appendix A for tubing wall thickness calculations.

3.2 RELIEF VALVE DESIGN

A relief valve -RV1, provides overpressure protection as required by the applicable codes. The relief valve provides protection in the event the gas cylinder pressure regulator were to fail open. In sizing the relief valve, several assumptions were made, all noted on the flow diagram. The assumptions were:

1. The only source of pressure is the gas cylinder,
2. The worst case cylinder pressure is 20.68 MPa(g),
3. The cylinder pressure regulator must have a flow coefficient (Cv) equal to, or less than 1.0. See Appendix B for Relief Valve, -RV1, sizing, and
4. The operating/ambient temperatures will remain within the design temperature range (15°C to 35°C).

The applicable code for the permeability cell, ASME Section VIII, Division 1, allows for the installation of the pressure vessel (permeability cell) relief device to be installed in a location other than on the vessel when the source of pressure is external to the vessel and is under such positive control that the pressure in the vessel cannot exceed the maximum allowable working pressure at the operating temperature. The code also does not allow stop valves between the relief device and the pressure vessel. The location chosen for the relief device, -RV1, at the discharge of pressure regulator, -PRS1 is acceptable only if the ambient/operating temperatures remain with the design temperature 15°C to 35°C. If the pressure vessel were filled with fluid, pressurized to design pressure, isolated, and warmed up above the design temperature, the pressure within the isolated vessel could exceed the vessel design pressure.

4. CODES AND STANDARDS

The permeability cell was designed to ASME Section VIII, and registered with the Manitoba Department of Labour as per CSA B51. Therefore, the relief valve protecting the cell must also comply with ASME Section VIII.

The associated system is designed to ASME B31.1 in compliance with CSA B51. The system, although within the scope of CSA B51, will not be registered with the Manitoba Department of Labour (DOL) as agreed by DOL. The system shall meet the requirements of CSA B51 and shall be pressure tested as per ASME B31.1.

5. HAZARDS EVALUATION AND SAFETY CONSIDERATIONS

The hazards involved in this project can be categorized into two general types:

- those associated with the vessel under pressure
- those associated with the connected tubing system

The hazards involved with operating the pressure retaining vessel and system has been minimized by designing the vessel in accordance with ASME Section VIII, Division 1, and the system to ASME B31.1. In addition, the relief valve will ensure the vessel and system never exceeds the design pressure.

The two (2) level instruments, 1H and 2H, are not available with CRNs. Both components will be surrounded with plexi-glass to provide protection of equipment and personnel in the event either were to fail. Both components are connected with 1/8" O.D. x 0.020" wall tubing.

Whiteshell Research
Site Support Services
Design and Project Engineering Branch
Pinawa, MB ROE 1L0

PROJECT DR-61W08-2			
PART APPENDIX A			
DESIGNED BY	DATE	JOB NO.	PAGE NO.
L. HIEBERT	93-6-23	61W08	1 OF 2

1 DESIGN CONDITIONS:

PRESSURE: 10.0 MPa(g) (1450.3 PSIG)
TEMP.: 35°C (95°F)
MATERIAL: TUBING ASTM A213 TYPE 304L SMLS STAINLESS STEEL

CONNECTIONS: FERRULED SWAGELOK
NPT (THREADED) TO SWAGELOK FERRULED SAE STRAIGHT THREAD O-RING

2 TUBING DESIGN:

CALCULATED AS STRAIGHT PIPE UNDER INTERNAL PRESSURE IN ACCORDANCE WITH FORMULA (3) AND DEFINITIONS IN ACCORDANCE WITH PARA 104.1.2 OF ASME B31.1, POWER PIPING CODE

$$t_m = \frac{P D_o}{2(SE + Py)} + A$$

P = 1450.3 PSIG
D_o = 1/8" O.D. TUBING
SE = 15,700 PSI
y = 0.4
A = 0

$$t_m = \frac{1450.3\ (0.125)}{2(15{,}700 + 1450.3(0.4))} + 0 = 0.005"$$

Whiteshell Research
Site Support Services
Design and Project Engineering Branch
Pinawa, MB ROE 1L0

PROJECT	DR-61W08-2		
PART	APPENDIX A		
DESIGNED BY	DATE	JOB NO.	PAGE NO.
L. HIEBERT	93·6·23	61W08	2 OF 2

USING THE FORMULA ON PAGE 1, THE TABLE BELOW LISTS THE MINIMUM SELECTED WALL THICKNESSES FOR VARIOUS NOMINAL TUBE SIZES.

ASTM A213 TYPE 304L SMLS S/ST TUBING

TUBE O.D.	CALCULATED t_m	SELECTED STOCK WALL THK.	SELECTED WALL MINUS 10% TOLERANCE
1/8"	0.005"	0.020"	0.018"
1/4"	0.011"	0.035"	0.031"
3/8"	0.016"	0.035"	0.031"

Whiteshell Research
Site Support Services
Design and Project Engineering Branch
Pinawa, MB ROE 1LO

PROJECT DR-6IW08-2			
PART APPENDIX B			
DESIGNED BY	DATE	JOB NO.	PAGE NO.
L. HIEBERT	93-6-23	6IW08	1 OF 9

1. INTRODUCTION

IN THE EVENT THAT THE PRESSURE REGULATOR AT THE GAS CYLINDER WERE TO FAIL OPEN, THE PERMEABILITY CELL AND ASSOCIATED SYSTEM WOULD BE EXPOSED TO THE CYLINDER PRESSURE, TWICE THE DESIGN/MAXIMUM ALLOWABLE WORKING PRESSURE. THIS APPENDIX INCLUDES THE BASIS FOR SIZING OF THE SYSTEM/CELL RELIEF VALVE, -RV1, INCLUDING THE SIZING CALCULATIONS. THE RESULTS OF THESE CALCULATIONS ARE THE BASIS FOR -RV1 SPECIFICATION, A-6IW08-SP1.

2. DETERMINATION OF RELIEF REQUIREMENTS

2.1 PRESSURE RELIEF VALVE (-RV1)

THE APPLICABLE CODE FOR THE PERMEABILITY CELL IS ASME SECTION VIII, DIVISION 1, BOILER AND PRESSURE VESSEL CODE. THE CODE REQUIRES OVERPRESSURE PROTECTION FOR THE CELL BUT ALLOWS THE RELIEF DEVICE TO BE LOCATED AT THE SOURCE OF PRESSURE, THE PRESSURE REGULATOR. THE RELIEF DEVICE MUST MEET THE REQUIREMENTS OF ASME SECTION VIII.

THE APPLICABLE CODE FOR THE TUBING SYSTEM IS ASME B31.1, POWER PIPING CODE. PARA 122.5.1 OF ASME B31.1 STATES THAT RELIEF VALVES INSTALLED DOWNSTREAM OF PRESSURE REGULATORS MUST ENSURE THAT THE DOWNSTREAM PRESSURE (OF THE REGULATOR) WILL NOT EXCEED THE DESIGN PRESSURE IF THE REGULATOR FAILS OPEN.

Whiteshell Research
Site Support Services
Design and Project Engineering Branch
Pinawa, MB ROE 1L0

PROJECT	PR-6\W08-2		
PART	APPENDIX B		
DESIGNED BY	DATE	JOB NO.	PAGE NO.
L HIEBERT	93.6.23	6\W08	2 OF 9

THE PRESSURE REGULATOR FAILED OPEN FLOW RATE IS DEPENDENT ON THE MAXIMUM REGULATOR INLET PRESSURE (THE GAS CYLINDER FULL PRESSURE), AND THE REGULATOR FLOW COEFFICIENT (C_V).

DUE TO THE RELATIVELY LOW REQUIRED FLOW RATE AND THE UNSELECTED REGULATOR, AN ASSUMPTION HAS BEEN MADE. THE PRESSURE REGULATOR FLOW COEFFICIENT (C_V) WILL NOT EXCEED 1.0.

3 PRESSURE RELIEF VALVE SIZING

MAXIMUM FLOW TO BE VENTED = MAXIMUM PRESSURE REGULATOR FLOW RATE

ASSUMED PRESSURE REGULATOR FLOW COEFFICIENT = 1.0 (MAX

ASSUMED MAXIMUM CYLINDER PRESSURE = 20.69 MPa(g) (3000 P

CYLINDER GAS IS NITROGEN OR ARGON (USE ARGON FOR CALCULAT

SYSTEM DESIGN PRESSURE = 10 MPa(g) (1450.3 PSIG) LIMITE BY THE DESIGN OF THE PERMEABILITY CELL.

RELIEF SET PRESSURE = 10 MPa(g) (1450.3 PSIG)

Whiteshell Research
Site Support Services
Design and Project Engineering Branch
Pinawa, MB R0E 1L0

PROJECT	DR-61W08-Z		
PART	APPENDIX B		
DESIGNED BY	DATE	JOB NO.	PAGE NO.
L. HIEBERT	93.6.23	61W08	3 OF 9

FIND REQ'D -RV1 CAPACITY

SINCE THE RELIEF VALVE SET PRESSURE MAY BE SET LOWER THAN HALF THE CYLINDER PRESSURE, THE CYLINDER PRESSURE IS A CRITICAL PRESSURE.

$P_2 \leq 0.53 P_1$ THEREFORE CRITICAL PRESSURE CONDITION

$P_1 = 3015$ PSIA
$P_2 = 1465$ PSIA

UNDER A CRITICAL PRESSURE CONDITION, THE FLOW FORMULA IS AS FOLLOWS:

$$Q = 13.61 (P_1) C_v \sqrt{\frac{1}{(SG)T}}$$

$C_V = 1.0$
$SG = 1.38$
$T = 530°R$

($T_{DESIGN} = 555°R$ BUT A HIGHER FLOW RATE OCCURS WITH NORMAL OPERATING TEMP 530°R)

$$Q = 13.61 (3015) 1.0 \sqrt{\frac{1}{(1.38)530}} = 1517 \text{ SCFM}$$

Whiteshell Research
Site Support Services
Design and Project Engineering Branch
Pinawa, MB ROE 1LO

PROJECT DR-61W08-2			
PART APPENDIX B			
DESIGNED BY	DATE	JOB NO.	PAGE NO.
L. HIEBERT	93-6-23	61W08	4 OF 9

FIND REQ'D-RV1 ORIFICE AREA

$$A = \frac{V\sqrt{G}\sqrt{T}\sqrt{Z}}{1.175\,(C)\,Kd\,(P)\,Kb}$$

V = 1517 SCFM (REQ'D CAPACITY)
G = 1.38 (SPECIFIC GRAVITY)
T = 70 + 460 = 530° (INLET TEMPERATURE)
Z = 1.0 (COMPRESSIBILITY FACTOR)
C = 377.8 (GAS FLOW CONSTANT)
Kd = 0.953 (COEFFICIENT OF DISCHARGE FOR GAS)
P = 1450.3 + (1450.3 x 0.1) + 14.7 = 1610 PSI (RELIEVING PRESSURE)
Kb = 1.0 (GAS FLOW COEFFICIENT)

$$A = \frac{1517\sqrt{1.38}\sqrt{530}\sqrt{1.0}}{1.175\,(377.8)\,0.953\,(1610)\,1.0} = 0.06\ IN^2\ (38.7\ mm^2)$$

SEE THE ATTACHED PHOTOCOPIES FOR FORMULA REFERENCES.

SEE THE ATTACHED COMPUTER PRINTOUT TO CONFIRM THESE CALCULATIONS.

SIZING

General Equations

Before initiating any calculations, it is necessary to establish the general category of the pressure relief valve being considered. This section covers conventional spring-loaded types and BalanSeal spring-loaded types. Pilot operated types are covered in a separate catalog.

Given the rate of fluid flow to be relieved, the usual procedure is to first calculate the minimum area required in the valve orifice for the conditions contained in one of the following equations. In the case of steam, air or water, the selection of an orifice may be made directly from the capacity tables if so desired.

In either case, the second step is to select the specific type of valve that meets the pressure and temperature requirements.

General equations are given first, to identify the basic terms which correlate with ASME Pressure Vessel Code, Section VIII. Then, an alternate sizing method is given to provide modified equations which reduce computation.

Since these equations are conservative, it is recommended that computations of relieving loads avoid cascading of safety factors or multiple contingencies beyond the reasonable flow required to protect the pressure vessel.

Conventional Valves— constant back pressure only

The conventional valve may be used when the variation in backpressure does not exceed 10% of the set pressure, provided the corresponding variation in set pressure is acceptable.

ORIFICE AREA CALCULATIONS

VAPORS or GASES—Lbs./hr.—

$$A = \frac{W\sqrt{TZ}}{CK_dPK_b\sqrt{M}}$$

CONSTANT BACK PRESSURE
K_b = 1 when back pressure is below 55% of abs. relieving pressure.

VAPORS or GASES—S.C.F.M.—

$$A = \frac{V\sqrt{G}\sqrt{TZ}}{1.175\,CK_dPK_b}$$

CONSTANT BACK PRESSURE
K_b = 1 when back pressure is below 55% of abs. relieving pressure.

STEAM—Lbs./hr.—

$$A = \frac{W_s}{51.5\,K_dPK_bK_{sh}K_n}$$

CONSTANT BACK PRESSURE
K_b = 1 when back pressure is below 55% of abs. relieving pressure.
K_{sh} = 1 for Sat. Steam

AIR—S.C.F.M.—

$$A = \frac{V_a\sqrt{T}}{418\,K_dPK_b}$$

CONSTANT BACK PRESSURE
K_b = 1 when back pressure is below 55% of abs. relieving pressure.

LIQUIDS—G.P.M.—
ASME Code (2600L Series)

$$A = \frac{V_L\sqrt{G}}{38.0\,K_d\sqrt{\Delta P}\,K_u}$$

CONSTANT BACK PRESSURE
K_p = 1 at 25% overpressure
K_u = 1 at normal viscosities

Non-ASME Code (2600 Series)

$$A = \frac{V_L\sqrt{G}}{38.0\,K_d\sqrt{1.25\,P_1 - P_2}\,K_p\,K_u}$$

NOMENCLATURE

A = Required orifice area in square inches. This value may be compared with the effective discharge areas published in this catalog, and defined in ANSI/API Std. #526.
W = Required vapor capacity in pounds per hour.
W_s = Required steam capacity in pounds per hour.
V = Required gas capacity in S.C.F.M.
V_a = Required air capacity in S.C.F.M.
V_L = Required liquid capacity in U.S. gallons per minute.
G = Specific gravity of gas (air = 1) or specifc gravity of liquid (water = 1) at actual discharge temperature. A specific gravity at any lower temperature will obtain a safe valve size.
M = Average molecular weight of vapor.
P = Relieving pressure in pounds per square inch absolute = set pressure + overpressure + 14.7. Minimum overpressure is 3 psi.
P_1 = Set pressure at inlet, psig.
P_2 = Back pressure at outlet psig.
ΔP = Set pressure + overpressure, psig — back pressure, psig. At 10% overpressure delta P equals 1.1 $P_1 - P_2$. Below 30 psig set delta P equals $P_1 + 3 - P_2$.
T = Inlet temperature °F. absolute (°F. plus 460).
Z = Compressibility factor corresponding to T and P (if this factor is not available, compressibility correction can be safely ignored by using a value of Z = 1.0).
C = Gas or vapor flow constant. Select from table, page 41 or use the curve and table on page 39.
k = Ratio of specific heats. C_p/C_v. This value is constant for an ideal gas. If this ratio is not known, the value k = 1.001, C = 315 will result in a safe valve size. Isentropic coefficient n may be used instead of k. See curve and table page 39.
K_p = Liquid capacity correction factor for overpressures lower than 25% from curve on page 44. Non-Code equations only.
K_b = Vapor or gas flow correction factor for constant back pressures above critical pressure from curve on page 42.
K_v = Vapor or gas flow factor for variable back pressures from curve on page 42. Applies to BalanSeal valves only.
K_w = Liquid flow factor for variable back pressures from curve on page 44. Applies to BalanSeal valves only.
K_u = Liquid viscosity correction factor from chart page 45 or curve page 46.
K_{sh} = Steam superheat correction factor from table on page 43.
K_n = Napier steam correction factor for set pressures between 1500 and 2900 psig from table on page 43.
K_d = Coefficient of discharge:
0.953 for air, steam, vapors & gases;
0.724 for ASME Code liquids;
0.64 for non-ASME Code liquids.

Where the pressure relief valve is used in series with a rupture disk, a combination capacity factor of 0.8 must be applied to the denominator of the above equations. Consult the factory for higher factors based on National Board flow test results conducted with various rupture disk designs.

AIR CURVE

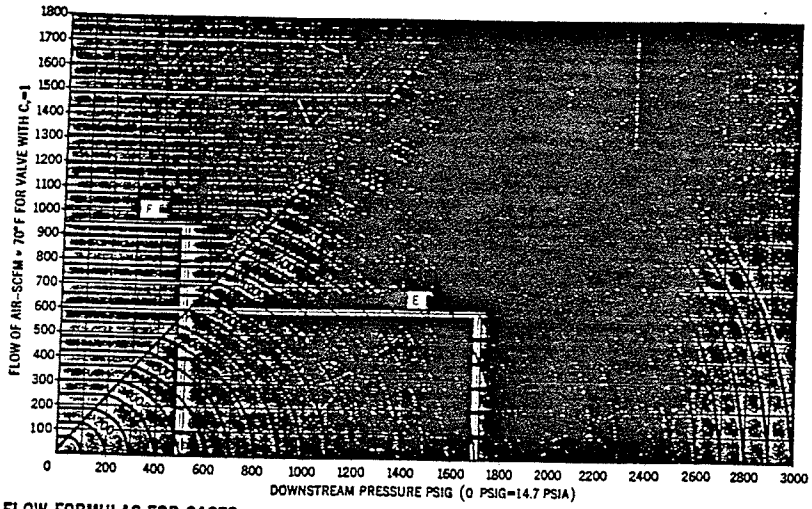

FLOW FORMULAS FOR GASES

Recommended by the Fluid Controls Institute, Inc.

(4)
$$Q = 16.05\, C_v \sqrt{\frac{(P_1^2 - P_2^2)}{(SG) \times T}}$$

(5*)
$$Q = 13.61 \times P_1 \times C_v \sqrt{\frac{1}{(SG) \times T}}$$

Where: Q = Flow in SCFM
C_v = Valve flow coefficient
SG = Specific gravity of gas (Air @ 14.7 PSIA and 70°F = 1.0)
‡T = Absolute temperature of flowing gas (°F + 460)
$\Delta P = (P_1 - P_2)$ Pressure drop (PSI)
P_1 = Inlet pressure (PSIA)
P_2 = Outlet pressure (PSIA)

‡Refer to "USEFUL CONVERSION DATA" on reverse side of "Technical Information" tab for converting °C to °F.

*When outlet pressure is approximately one half or less of the inlet pressure ($P_2 = .53P_1$) this condition becomes known as a critical pressure and then formula (5) must be used. Formula (5) is exactly the same as formula (4) except that $.53 \times P_1$ is substituted for P_2.

SPECIFIC GRAVITY TABLE FOR GASES

	Specific gravity relative to air @ 70°F
Acetylene	.907
Air	1.000
Ammonia	.587
Argon	1.38
Butane	2.07
Carbon Dioxide	1.529
Helium	.137
Hydrogen	.0695
Methane	.554
Nitrogen	.967
Oxygen	1.105
Propane	1.562
Sulfur Dioxide	2.264

Flow calculations and charts for gases differ from those for liquids due primarily to the compressibility of gases. The above chart shows the flow rates in standard cubic feet per minute (SCFM) of 70°F air flowing through a valve having a $C_v = 1$. From this chart, sizing of a valve can be readily accomplished. Corrections for gases having specific gravities other than air and flowing at temperatures other than 70°F can be made by using formulas (4) or (5).

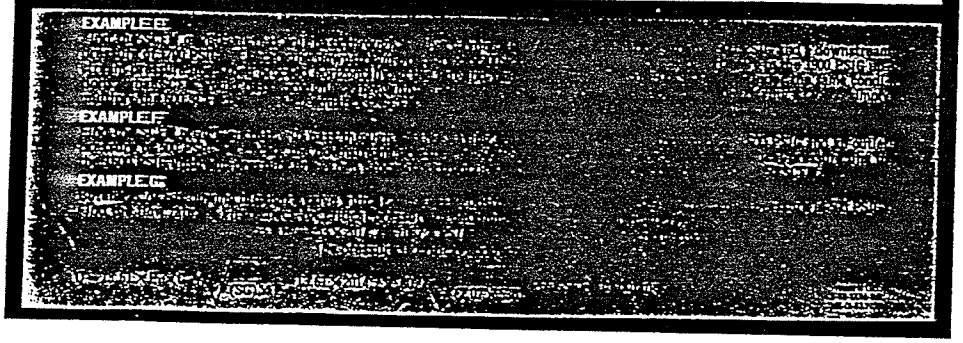

========== AREA CALCULATION SHEET ==========

1. Customer	S. CAMPBELL	2. Sheet	of
3. Inquiry #	61W03	4. Rev	
5. Plant		6. Date	06-22-93
P&ID		7. By	L.J. HIEBERT
8. Tag No.	61W03-RV1	9. Service	ARGON
10. Sizing Code	ASME SEC VIII	11. Sizing Basis	Blocked Flow
12. Fluid State	Gas - Volume	13. Rupture Disk	No

15. Fluid	Argon		
16. Set Pressure	1450.3	PSIG	
17. Back Pressure	atm	PSIG	Constant
18. Over Pressure	10	%	
19. Relieving Capacity	1510	FT3/MIN	
20. Relieving Temperature	70	F	
21. Specific Gravity	1.378		
29. Gas Constant	377.800		
30. Compressibility	1		
38. Calculated Area	0.0600	IN2	
39. Valve Type	Conventional		
40. Valve Series	2740UL		
41. Selected Area	.06	IN2	
42. Orifice Designation			
43. Maximum Relieving Capacity	1510.000	FT3/MIN	

44. Operating Temp	70	F	Cold Diff Set Press	1450.300	PSIG
45. Oper. Pressure	1350	PSIG	46. Oper/Set Press	93.084	%
47. Inlet Class	2200# WOG		5i. Facing	MNPT	
48. Outlet Class	400# WOG		52. Facing	FNPT	
49. Manufacturer	FARRIS		50. Model No.	2740UL/S2/SP	
77. Inlet size	1/2"		78. Outlet size	1"	

90. Note 1 1350 PSIG IS THE MAXIMUM RECOMMENDED OPERATING PRESSURE FOR
91. Note 2 THE SET PRESSURE OF 1450.3 PSIG SET PRESSURE. EXCEEDING
92. Note 3 1350 PSIG, AS THE CONTINUOUS OPERATING PRESSURE WILL RESULT IN
93. Note 4 DAMAGE TO THE VALVE. THIS PRINTOUT CONFIRMS THE MANUAL CALCS.

Materials have been changed from program calculated

Coefficients are:
kd = 0.9530 kv = 1.0000 kb = 1.0000 cf = 0.0000

EQUATION USED IN CALCULATION:

Gas

$$A = \frac{V * \mathrm{sqr}(G * T * Z)}{1.175 * C * Kd * P * Kb}$$

Where:

A = required orifice area	V = required gas capacity
G = specific gravity	P = relieving pressure
T = inlet temperature	Z = compressibility factor
C = gas or vapor constant	NOTE: Minimum Over Pressure is 3 psi

========== PRESSURE RELIEF VALVE SPECIFICATION SHEET ==========

1. Customer	S. CAMPBELL	2. Sheet	of
3. Job No.	61W03	4. Rev	Spec
5. Plant		6. Date	06-22-93
7. By	L.J. HIEBERT	Reqn. #	

-- INDENTIFICATION --

8. Tag No.	61W03-RV1	9. Service	ARGON
10. P & ID			

-- ACCESSORIES --

51. Valve Type	Conventional	52. Bonnet Type	Closed
53. Cap/Lever	Screwed Cap	54. Rupture Disk	No
55. Test Gag	Without Gag	56. O Ring Seat	Not Required

-- CONNECTIONS --

57. Inlet Class	2200# WOG	75. Facing	MNPT
58. Outlet Class	400# WOG	76. Facing	FNPT
77. Inlet size	1/2"	78. Outlet size	1"

-- MATERIAL --

65. Body	Carbon Steel	66. Sleeve Gd	316 SS
67. Bonnet	Carbon Steel	68. Spring	316 SS
69. Disc	316 SS	70. Bellows	N/A
71. Nozzle	Carbon Steel		

-- BASIS OF SELECTION --

73. Sizing Code	ASME SEC VIII	74. Sizing Basis	Blocked Flow

-- SERVICE CONDITIONS --

15. Fluid	Argon		
16. Set Pressure	1450.3	PSIG	
17. Back Pressure	atm	PSIG	Constant
18. Over Pressure	10	%	
19. Relieving Capacity	1510	FT3/MIN	
20. Relieving Temperature	70	F	
21. Specific Gravity	1.378		
29. Gas Constant	377.800		
30. Compressibility	1		

-- ORIFICE AREA --

61. Orifice Desig			62. Calculated	0.0600	IN2
63. Selected	.06	IN2	64. Max Rel Cap	1510.000	FT3/MIN

-- MODEL SELECTION --

59. Manufacturer	FARRIS	60. Model No.	2740UL/S2/SP
99. Valve Price			

-- NOTES --

90. Note 1 1350 PSIG IS THE MAXIMUM RECOMMENDED OPERATING PRESSURE FOR
91. Note 2 THE SET PRESSURE OF 1450.3 PSIG SET PRESSURE. EXCEEDING
92. Note 3 1350 PSIG, AS THE CONTINUOUS OPERATING PRESSURE WILL RESULT IN
93. Note 4 DAMAGE TO THE VALVE. THIS PRINTOUT CONFIRMS THE MANUAL CALCS.

==========

Materials have been changed from program calculated

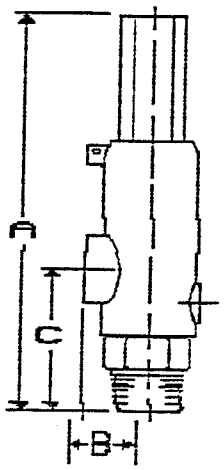

TELEDYNE FARRIS ENGINEERING OUTLINE DRAWING

2740UL SERIES

ENGLISH DIMENSIONS (INCHES)					
A	B	C	E	F	WEIGHT
10 3/4	1 3/4	3 9/16			7 1/2 LBS

	SIZE	ANSI RATING	FACING
INLET	1/2"	2200# WOG	MNPT
OUTLET	1"	400# WOG	FNPT

SELECTED ORIFICE | Area: .06 IN2 | Letter:

PART NAME	MATERIAL	PART NAME	MATERIAL
BODY	Carbon Steel	BONNET	SA-216 GR.WCB
DISC	316 SS	NOZZLE	Carbon Steel
SLEEVE GUIDE	316 SS	SPRING	316 SS
BELLOWS	N/A	'O' RING	Not Required
BODY STUD	N/A	BODY HEX NUT	N/A

FARRIS MODEL NUMBER	2740UL/S2/SP		
VALVE/DESIGN TYPE	Conventional		
SET PRESSURE	1450.3	(PSIG)	
BACK PRESSURE		(PSIG)	
COLD DIF. SET PRESS	1450.300	(PSIG)	
NOISE LEVEL	97	(dBA)	at 3FT FROM PT OF DISCHARGE
REACTIVE FORCE	173.2	(LBS)	
OPER/SET PRESSURE	93.084	(%)	

OUTLINE DRAWING DATA

CUSTOMER	S. CAMPBELL	DATE	06-22-93
JOB NUMBER	61W08	REQ'N NUMBER	
REV NUMBER		BY	L.J. HIEBERT
TAG NUMBER	61W08-RV1	P & ID	

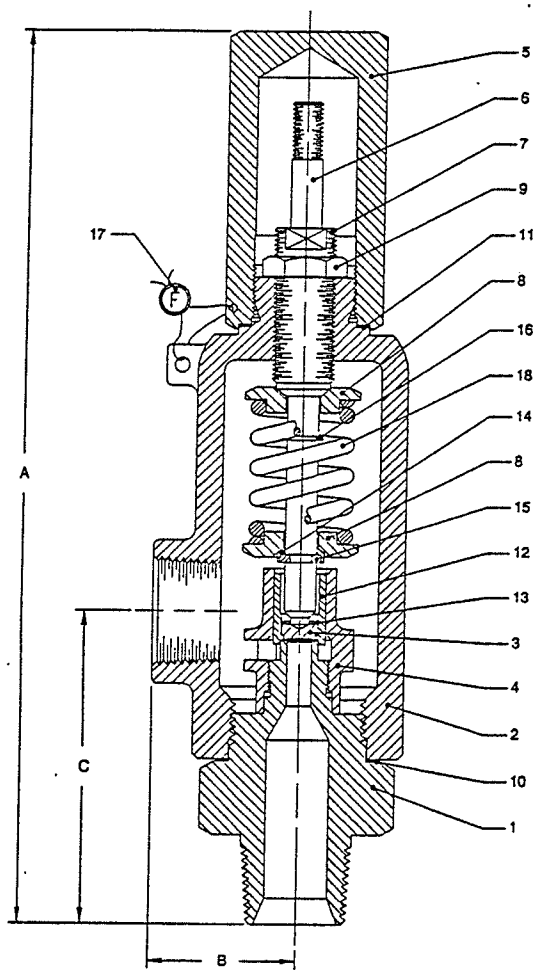

BILL OF MATERIALS

ITEM	PART NAME		MATERIALS
1	BODY		SA-351, GR. CF8M, 316 ST. ST.
2	BONNET		SA-216, GR. WCB, CARB. ST.
3	DISC		ASTM A479, TYPE 316 ST. ST.
4	GUIDE		ASTM A351, GR. CF8M, 316 ST. ST.
5	CAP PLAIN SCREWED		ASTM A105, GR. 1117, CARB. ST.
6	STEM		ASTM A479, TYPE 316 ST. ST
7	SPRING ADJUSTING SCREW		ASTM A582, TYPE 303 ST. ST
8	SPRING BUTTON		ASTM A108, GR. 1117, CARB. ST. PLTD.
9	JAM NUT (SPR. ADJ. SCREW)		ASTM A479, TYPE 316 ST. ST.
10	BODY GASKET		SOFT IRON OR STEEL
11	CAP GASKET		SOFT IRON OR STEEL
12	DISC HOLDER		ASTM A479, TYPE 316 ST. ST.
13	DISC RETAINING RING		PRECIPITATION HARDENED ST. ST.
14	STEM SHOULDER		AISI 316 ST. ST.
15	SPLIT RING		AISI 316 ST. ST.
16	LIFT STOP RING		PRECIPITATION HARDENED ST. ST.
17	WIRE SEAL		ST. ST. WIRE/LEAD SEAL
18	SPRING	2740UL	STAINLESS STEEL
		2740ULT	HIGH TEMP. ALLOY, RUST PROOFED
19	NAME PLATE (NOT SHOWN)		STAINLESS STEEL

COMPLIES WITH ASME BOILER AND PRESSURE VESSEL CODE SECTION VIII, PRESSURE VESSELS FOR PRESSURE RELIEF VALVES MARKED

UV AND NB

REQUIRING TEST LEVER FOR STEAM, AIR AND WATER SERVICE OVER 140°F PER AUXILARY DRAWING 23354-F. UNLESS OTHERWISE SPECIFIED ALL VALVES FURNISHED WITH PLAIN SCREWED CAPS.

SCREWED CONNECTIONS (MNPT INLET x FNPT OUTLET)

TYPE NO.	ORIFICE	VALVE SIZE INLET x OUTLET	A ALL CAP CONSTRUCTION	B	C	APPROX. WGT. LBS.
2740UL	.06	1/2 X 1	10-3/4	1-3/4	3-9/16	7-1/2
		3/4 X 1	10-3/4		3-9/16	7-1/2
		1 X 1	11		3-3/4	7-3/4

TAG NUMBERS AND SPECIFICATIONS

Farris Model 2740UL
1/2" Inlet X 1" Outlet
Set at 1450 PSIG (10 MPa)
Capacity at 10% Overpressure
is 1710 SCFM
Tag: 61W08-RV1

serial nos.:
CO-10417 thru 10420-KC

CRN #OG-254.1234567890TY

2740UL SERIES, SAFETY-RELIEF VALVE, SERIAL KC
SCREWED CONNECTIONS

TELEDYNE FARRIS ENGINEERING
PALISADES PARK, NEW JERSEY

DRAWING NO. 23338-F, REV. D

CUSTOMER AECL Research
PURCHASE ORDER NO. W111738
FACTORY ORDER NO. 793SS-348

BW 9

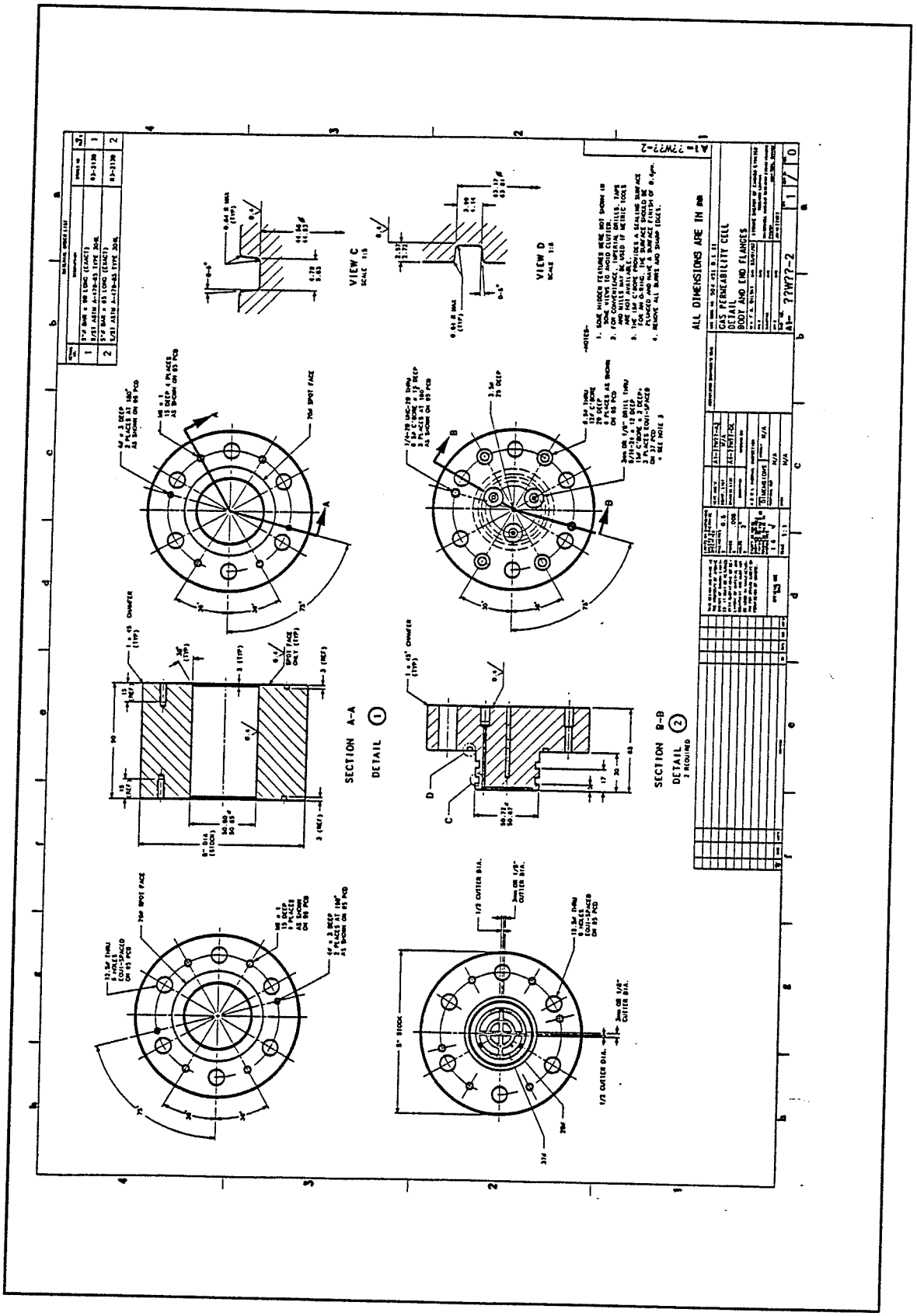

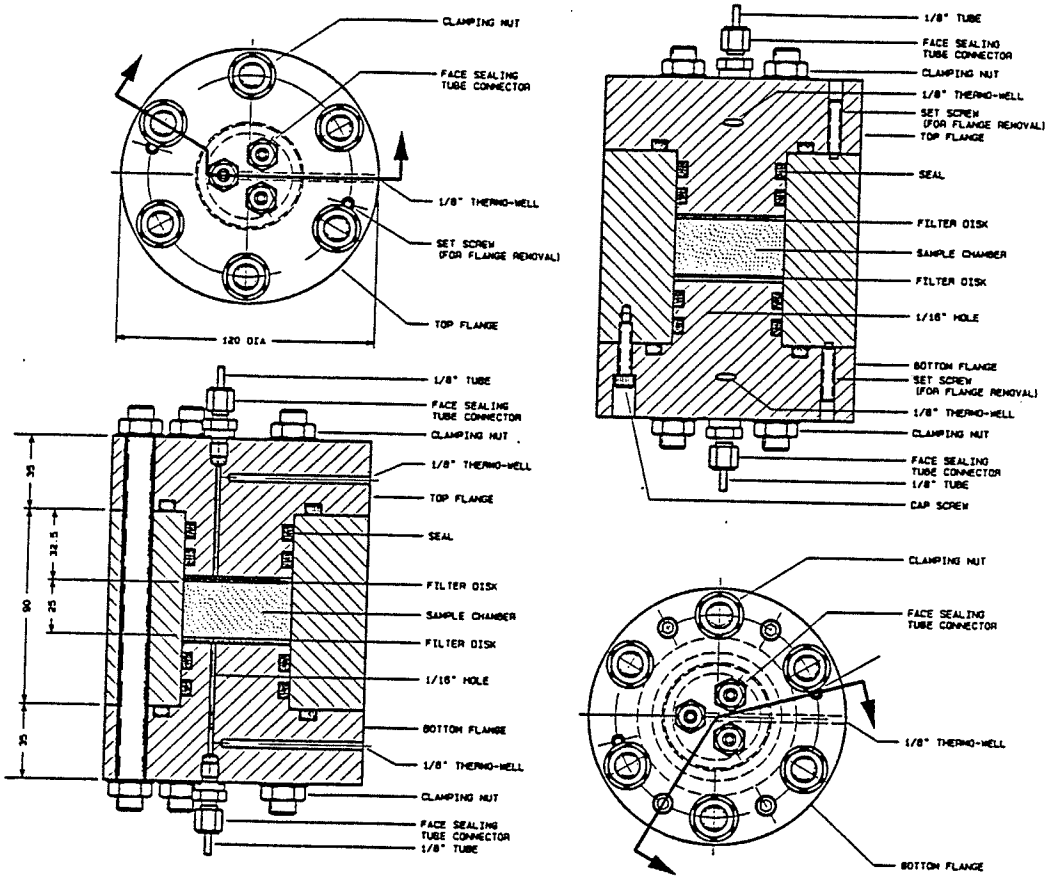

GAS PERMEABILITY CELL DESIGN

11-DEC-92
V0.2

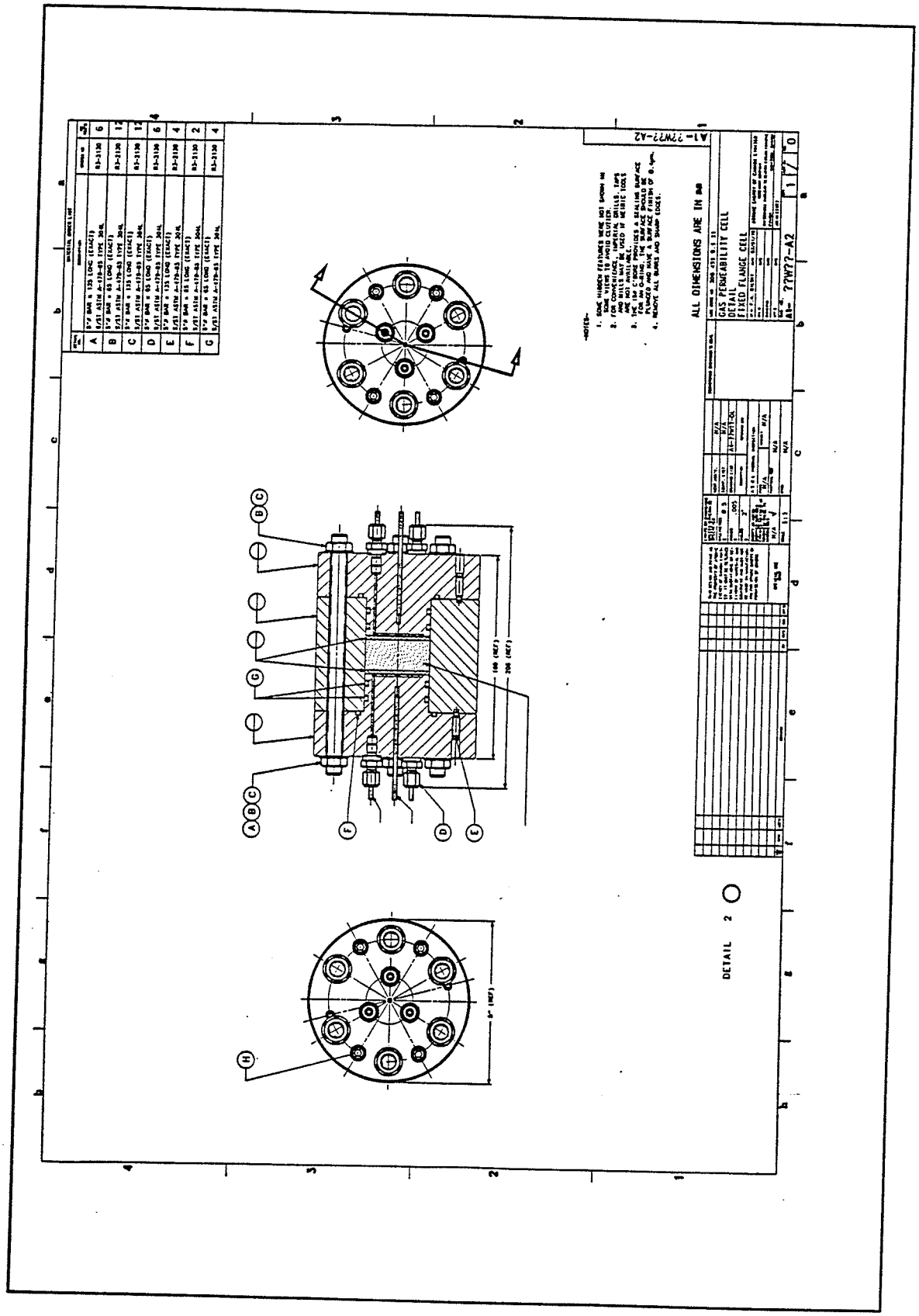
GAS PERMEABILITY CELL
DETAIL
FIXED FLANGE CELL
ALL DIMENSIONS ARE IN mm
DETAIL 2

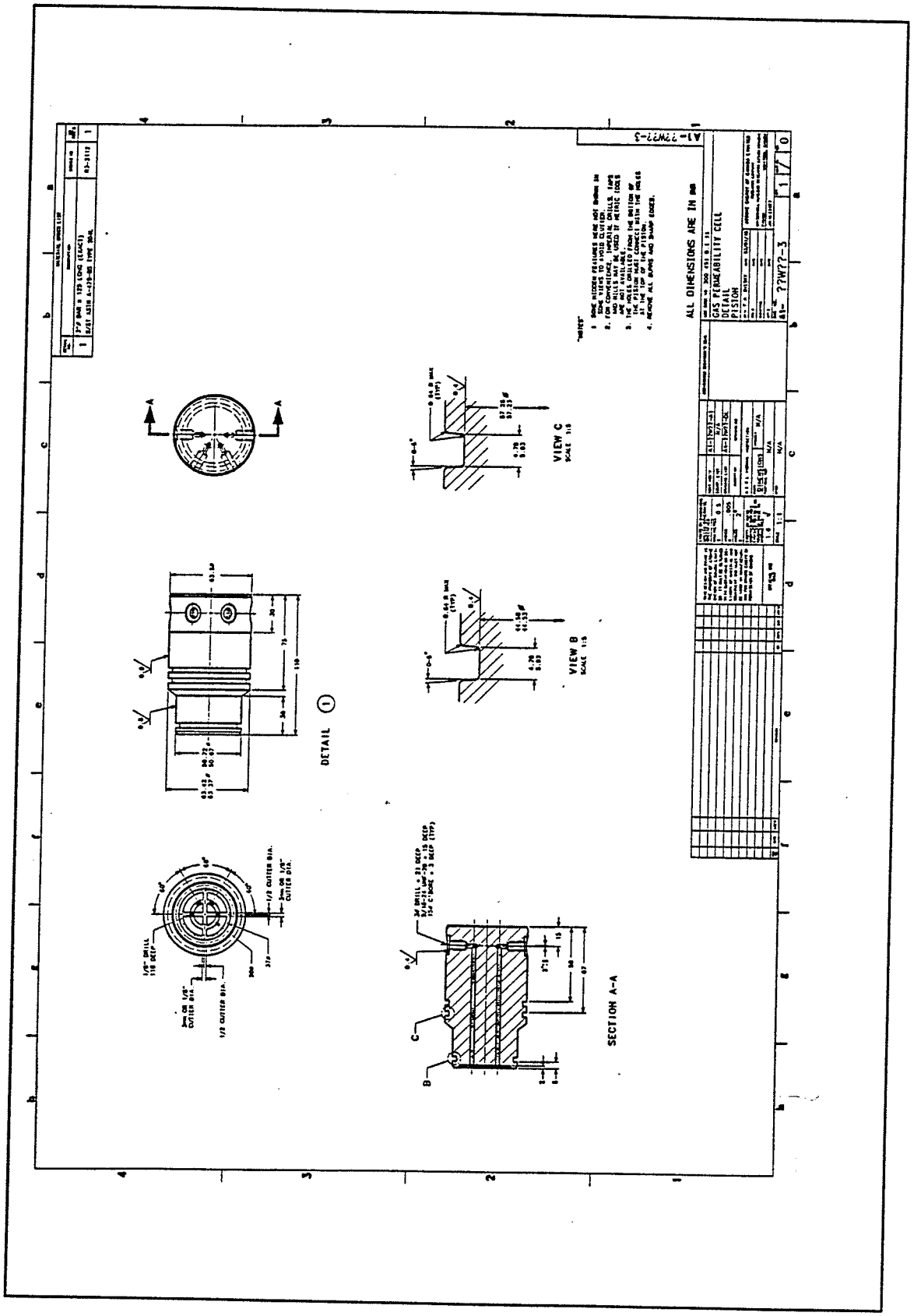
ALL DIMENSIONS ARE IN mm
GAS PERMEABILITY CELL
DETAIL
PISTON
DETAIL ①
VIEW B
SCALE 1:1
VIEW C
SCALE 1:1
SECTION A-A

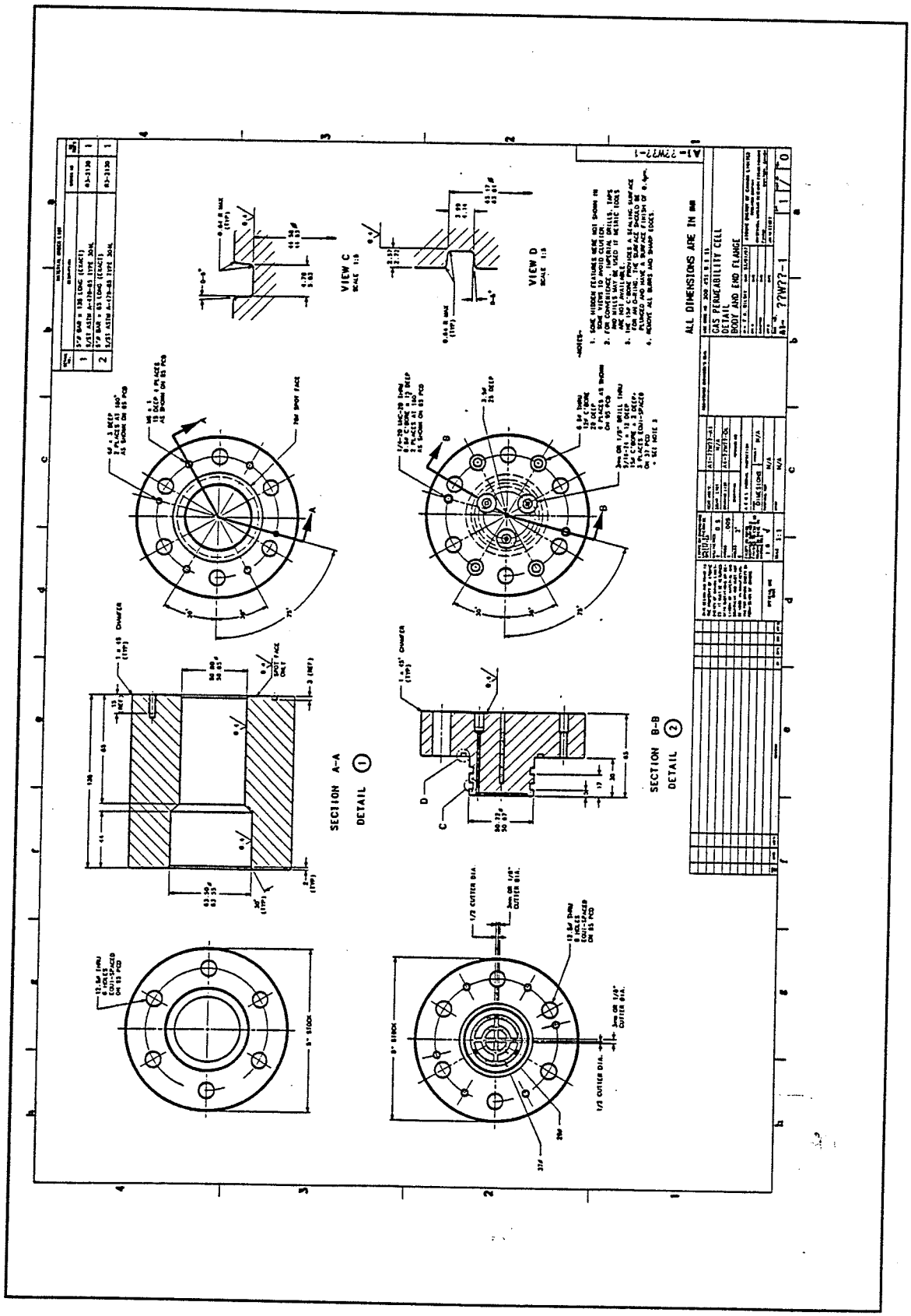
VIEW C
SCALE 1:1
VIEW D
SCALE 1:1
SECTION A-A
DETAIL (1)
SECTION B-B
DETAIL (2)
ALL DIMENSIONS ARE IN mm
GAS PERMEABILITY CELL
DETAIL
BODY AND END FLANGE

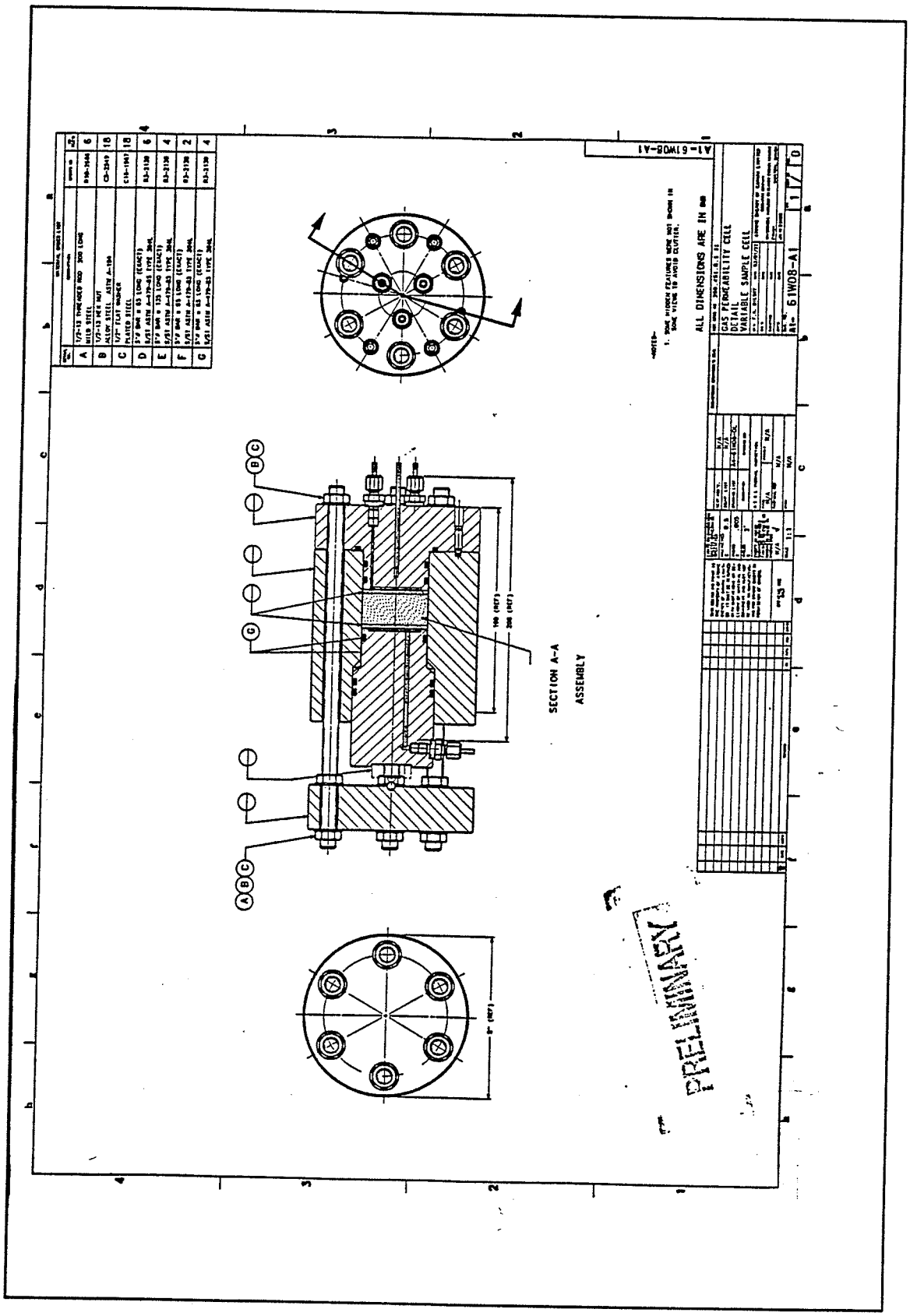
SECTION A-A
ASSEMBLY
ALL DIMENSIONS ARE IN
PRELIMINARY

APPENDIX B

PROCEDURE CHECKLIST

PROCEDURE CHECKLIST

INTRODUCTION

Testing was controlled by the various valves on the test board, and so the procedure description is based on the use of these valves. Figure B-1 shows the different components of the test board and can be used as a key for the procedures. The valves in Figure B-1 are numbered from 1 to 24 for identification. Pressure transducers are identified as TA, TB and TC and pressure regulators are identified as RA, RB and RC.

The following description of procedures assumes that:

- the test apparatus is built as shown in Figure B-1,
- the apparatus has passed an approved safety pressure test set up by the Quality Assurance Branch at AECL Research,
- all components of the test board are set at atmospheric pressure and contain no fluid, and
- all valves are in the closed position.

PRELIMINARY

Saturating the flow meter

- Remove the flow meter from the board by unfastening:
  - the bottom-inner nut,
  - the tee near valve 8, and
  - the various screws and clamps holding the flow meter against the board.
- Transport the flow meter to a waste receptacle with a water supply (a 'sink').

- Close all ports on the flow meter, including:
  - valves 7 and 8,
  - the four nuts on the ends of the flow meter, and
  - the open port on the tee near valve 8.

- Position a bottle of distilled, de-aired water above the flow meter.
  Maintain a slow flow rate from the bottle and attach the flexible tubing to valve 7.
  Ensure that the lid on the water source bottle is tight.

- Open the bottom-inner nut on the flow meter and apply hand pressure to the source bottle to initiate syphon flow out the open valve.

- Once water flows freely from the bottom-inner nut, loosen the lid and release the hand pressure on the source bottle.
  Allow water to flow from the source bottle, through the flow meter and out valve 7.

- Visually monitor the sight buret to detect movement of air within the water.
  Gently tap, rotate and tilt the flow meter during the saturation stage to help dislodge any air bubbles attached to inner walls.

- Close the bottom-inner nut once a steady flow of water passes through it from the source bottle.

- Similarly open then close the bottom-outer nut, the top-outer nut, the top-inner nut, valve 8 and then the temporary nut on the tee, leaving the flow meter fully saturated.

- Once fully saturated, ensure that valve 7 and all ports on the flow meter are closed to seal the flow meter.
  Detach the source bottle from valve 7.

Saturating the lines leading to the flow meter

- Remove all air from the flexible tubing attached to the water source bottle.

- Place the water source bottle above the test board.
  Attach the source bottle at valve 10, ensuring a complete seal between the flexible tubing and stainless steel tubing.

- Set the 4-way valve in the downward position.
  Open valve 10.
  Open valves 4 then 6 until water flows out the tee near valve 8.

- Switch the 4-way valve to the horizontal position until water flows out the open port where the bottom-inner nut of the flow meter was detached.
  Close valves 4 then 6.

- Open valve 5 (with the 4-way valve still in the horizontal position) until water flows out the tee near valve 8.

- Switch the 4-way valve to the downward position until water flows out the open port where the bottom-inner nut on the flow meter was detached.
  Close valves 5 then 10.

The lines directly upstream and downstream of where the flow meter was to be installed should now be saturated.

Saturating the accumulator

The accumulator discussed in this section is the one shown in Figure B-1 as the

"gas-water interface accumulator". It is the larger of the two accumulators on the test board.

Because the accumulator volume is greater than that of the water source bottle, at least one spare bottle of de-aired, distilled water should be kept at hand to ensure that enough water is available to complete this step without the source bottle emptying.

- Open valves 10, 6, 3 then 2.
  Allow water to enter the lines until the accumulator is full (as indicated by water flow from valve 2).

- To check that the accumulator is filling, a small amount of leak detector ('Snoop') can be poured onto the nozzle at valve 2.
  If a soap bubble forms, then air is being forced out valve 2 and the accumulator is indeed filling.

- Close valves 2, 3, 6 then 10 once the accumulator is full.

Saturating pressure transducer TB

- Pressure transducer TB has to be detached to be saturated without trapped air which would affect transducer readings.

- The water source bottle is still positioned as it was in the previous step.

- Open valve 10 slightly to maintain a slow stream of water out the open port at TB so no air can enter into the lines.

- Remove TB from the test board.

Use a syringe to carefully inject water into the transducer.
Re-attach TB, being careful not to introduce air into the lines.
Close valve 10.

Saturating the leads to the cell

- Open valves 10 then 9.
- Open valve 17 then close it once a full stream of water flows out the port.
- Similarly open and close valve 18.
- Close valves 9 then 10, leaving all water lines in the system fully saturated.

Re-attaching the flow meter

The flow meter must be re-attached to the test board without introducing air into the system.

- Transport the flow meter to the test board fully sealed.
- Open valve 10 slightly (with the water source bottle still attached, as before). With the 4-way valve in the downward position, open valve 5 to allow passage of a slow stream of water out the open port.
- Open the bottom-inner port on the flow meter the flow meter.
  (No water should escape from the flow meter if this is the only open port.)
  Attach the flow meter to the test board at the bottom-inner nut.
- Open the temporary nut at the tee near valve 8 on the flow meter.

Water should automatically flow up through the flow meter buret from the source bottle and out this open port. Attach the flow meter to the test board at the tee.

- Fully secure the flow meter to the test board.

To further ensure that the flow meter is fully saturated, water is cycled from the source bottle, through the flow meter and into the accumulator.

- Open valves 10, 5, 4, 3 then 2.
  Allow water to flow out valve 2.

- Switch the 4-way valve to the horizontal position and let more water flow out valve 2.
  Continue to allow water to flow from the source bottle and out valve 2 with the 4-way valve being switch between the horizontal and downward positions several times.
  Continue, say, until an entire source bottle of water has been cycled through the system.

- Visually inspect the flow meter sight buret for water bubbles during this step. If the flow meter was improperly de-aired or there is a leak in a fitting somewhere in the system between the flow meter and the source bottle, some or all of the previous steps may need to be repeated in order to remove the air.

- Assuming no appreciable air was detected in the sight buret, close valves 2, 3, 4, 5, then 10 to complete this procedure.

Charging the flow meter with oil

Flow is detected by movement of a coloured paraffin oil column in the flow meter sight buret. The following procedures must be performed with care because it is

important to install a clean, uniform column of oil in the flow meter and because the work involved with removing an improperly installed oil column is extensive. This procedure is best completed by two people.

- Place the oil in a source bottle with a flexible tubing nozzle above the test board.
  Attach the oil source bottle at valve 8 with a proper seal between the flexible tubing and the stainless steel tubing.
  Tighten the lid on the source bottle and apply constant hand pressure.

- Open valve 8 slightly, maintaining pressure on the bottle.
  Open the top-inner nut on the flow meter.
  Apply enough hand pressure to the source bottle to maintain a slow and steady flow of water out the top-inner port on the flow meter.
  Wipe away the water expelled from the open port as it accumulates.

- Eventually, oil from the source bottle will reach the top-inner nut and flow out the open port.
  Allow this to continue until a steady flow of pure oil (not polluted by droplets of water) is established.

- Close valve 8.
  Loosen the source bottle lid.
  Release the pressure on the source bottle.

- Similarly, tighten the source bottle lid and apply pressure.
  Open the top-outer nut on the flow meter until clean oil flows out the open port.
  Close the top-outer nut.
  Close valve 8.
  Loosen the source bottle lid.
  Release the pressure on the source bottle.

- Again, tighten the source bottle lid and pressurize.
  Open valve 8.
  Open valve 7 slightly.
  Allow water to flow out valve 7 until the oil is forced approximately half way down the sight buret.
  Close valves 7 then 8.
  Loosen the source bottle lid.
  Release the pressure on the source bottle.

- Detach the oil source bottle from valve 8.

At this point, the oil column showing in the buret should be continuous.
If the oil is broken up by pockets of water, taking flow readings will prove to be difficult, and the entire procedure of saturating the flow meter and charging it with oil may need to be repeated. (This procedure is discussed in the following sections on maintenance.)

MAINTENANCE

Some routine maintenance is required to ensure that a test board remains in proper working order between tests. For instance, leak detector ('Snoop') is used regularly to monitor for leaks at all connections. Leaks can occur at any fitting but are most frequent at fittings that are often adjusted, such as at the leads to the cell at valves 17 through 22. All venting nozzles (at valves 2, 10, 16, 23, and 24) are checked for leaks as well, to ensure that they are fully closed. While most routine maintenance is straight forward, two of the more intricate maintenance jobs are described below.

Cleaning the flow meter

It is relatively easy to open or close a valve at the wrong time during testing.

Such an error in adjusting the valves could cause a surge of flow through the flow meter, causing the oil column to break up into discrete sections making it difficult to accurately read flow volumes. If this occurs, the flow meter will have to be dismantled and cleaned. This procedure is similar that described in the preliminary steps, except at this point, the flow meter is full of water and oil.

- All valves should be closed when beginning this step.

- As in the preliminary steps, the flow meter is first detached from the test board at the bottom-inner nut.
  Once the nut is opened, a temporary cap is placed on the open port on the flow meter.

- The flow meter is detached at the tee near valve 8 and the open port is again closed off with a temporary cap.

- The flow meter is fully detached from the test board and transported to a sink. The temporary caps are removed and the water and oil is allowed to flow out of the flow meter.

The flow meter has to be completely flushed of paraffin oil before a pure column of oil can be re-installed.

- Ordinary tap water is injected into the flow meter at a high velocity through valve 7 to remove most of the oil.
  This water is flushed out the rest of the ports on the flow meter, one at a time.

- Methyl hydrate, which aids in breaking up the oil, is also flushed through the flow meter from valve 7.

- Water is again flushed out each of the ports to remove the methyl hydrate and any remaining oil.

- Once the oil and methyl hydrate are removed, the flow meter is saturated with de-aired, distilled water (as described in the preliminary steps).

- Before the flow meter is re-attached to the test board (as described in the preliminary steps), the lines directly downstream of the flow meter on the test board are checked to ensure that no oil has contaminated this area:

  - The 4-way valve is placed in the downward position.
  - A water source bottle is attached at valve 10.
  - Water is allowed to flow slowly from the source bottle through valve 5 and out the bottom-inner cap.
  - If no oil is detected, the flow meter is re-attached as described in the preliminary steps.
  - If oil has contaminated these lines, more extensive cleaning of the system and replacement of lines may be required.

Recharging the accumulator

The gas-water interface accumulator may empty after several tests or if a large volume of water escapes the lines for some reason. The water level in the accumulator can be monitored to ensure that there is always an ample supply of water for testing.

- The water level in the accumulator can be determined by attaching a manometer to valve 10:

  - With no pressure in the system, a section of transparent tubing is attached at valve 10 with its free end positioned above the height of valve 2, open to the atmosphere.
  - Valves 10, 6, 3 then 2 are opened with all other valves closed.
  - The level of the water in the section of tubing should coincide with the level of

water resting in the accumulator.

If the level is far from the top of the accumulator, it is recharged using the following steps.

- With all valves closed, attach the water source bottle at valve 10 and position it above the test board, as described in the preliminary steps.

- Open valves 10, 6, 3 then 2.
  Allow water to flow into the apparatus until it flows out valve 2.

- Close valves 2, 3, 6 then 10.

At this point, the accumulator is full.

SATURATION

Once all preliminary steps are completed for the preparation of the test board, and a specimen is properly installed in a test cell, the actual testing portion of the program can begin. Testing is completed in two stages. The first stage is a saturation stage where water is allowed to enter the specimen at a constant back pressure until a desired degree of saturation is achieved in the specimen. The second stage is the breakthrough stage where an incrementally-increased gas pressure is introduced to one end of the specimen. Specimens that are to be tested under partially saturated conditions do not undergo the saturation stage of testing.

Flushing the cell leads at atmospheric pressure

- To begin the saturation stage of testing, all valves are closed and there is no

pressure in the system.

- Attach the cell to the test board simply by connecting valves 17 through 22 to the cell leads.

Saturation and water inflow are determined by the flow meter. In order to get an accurate reading of the inflow of water into the specimen, the flow of water into the filter stones, filter papers and the cell leads has to be factored out of inflow measurements. To do so, these areas are separately saturated before reading water inflow to the specimen.

- Open valves 2, 3, 6 then 9 to give a supply of water to the cell leads at atmospheric pressure.

- Open valves 18 then 22 to flush water over the top filter.
  Rapidly open and close valve 22 several times to dislodge any air bubbles attached to surfaces.
  (Note that valve 18 is not opened with valve 22 closed for an extensive period of time as this would allow water to enter the specimen rather than being flushed over the filters.)
  Close valves 22 then 18 when only water (no air) flows out of valve 22.

- Similarly, flush the bottom leads using valves 17 and 21.

- Close valves 9, 6, 3 then 2 when the leads are properly flushed.

Establishing the water lines at back pressure

Water has to be maintained at a suitable bback pressurein order to have the specimen take on water at a rate that will saturate the specimen within an acceptable period of time. The standard bback pressurechosen for testing is 200

kPa. The following steps are completed to bring the water lines to the desired back pressure.

- Start the LabTech data acquisition system so that pressures can be monitored on the computer screen.

- Open the gas source tank.
  Carefully set pressure regulator RA to near the test board capacity.
  Open valves 1, 3 then 6, with all other valves closed.

- Set the pressure through pressure regulator RB to the desired back pressure (as read by pressure transducer TB).
  (Note that valve 23 can be used to bleed pressure when the targetted pressure is overshot.)

- Set the 4-way valve to the downward position.

The likelihood of introducing discontinuities in the oil column are less when the column is set to move downwards through the buret. For this reason, the 4-way valve is always set in the downward position when valves 4 or 5 are adjusted.

- Close valve 6.

- Open valve 4 carefully, watching the oil level in the flow meter sight buret.

  - If the oil level moves suddenly, valve 4 should be closed and the procedure should be attempted again.
  - If valve 4 cannot be opened without excessive movement of the oil column then there is likely some air trapped in the system that needs to be removed.
  - This could require re-saturating the flow meter in a manner similar to that discussed in preliminary steps.

- Assuming valve 4 can be opened without damage to the oil column in the flow meter, open valve 5 carefully.
  Again, monitor the oil column.

- Close valves 5 then 4 to protect the flow meter from pressure surges during the ensuing procedures.

At this point, the flow meter and all water lines leading up to the cell leads should be charged to the desired back pressure.

Flushing the cell leads at back pressure

Once the water lines up to the cell are set at the desired back pressure, the next step is to flush the cell leads at back pressure. This procedure is similar to the procedure for flushing the leads at atmospheric pressure, as discussed earlier.

- Open valves 6 then 9.

- Flush the top leads using valves 18 and 22.
  Flush the bottom leads using valves 17 and 21.
  Be careful not to leave valve 17 or 18 open for long with valve 22 or 21closed as this will promote uptake of water into the specimen.

- This process may cause the pressure through RB to dip below the target back pressure. If this is the case:

- Close all valves except 1, 3, 6 and 9.
- Reset the pressure through RB to the back pressure.
- Open valve 4 carefully to establish the back pressure in the flow meter.
- Close valve 4.
- Open and close valves 17 and 18 quickly to stabilize the pressures in the cell.

- Close valves 6 then 9.

Specimen saturation

Once all the water lines in the system are set at the desired back pressure and are fully saturated, saturation of the specimen can commence.

- Check again that all water lines, including the flow meter and the cell leads, are set to the desired back pressure to minimize the initial surge of flow when the specimen saturation stage begins:

- Open valves 6, 17 and 18.

- Open then immediately close valve 9 to stabilize the cell pressure.
- Close valve 6.
  Set the 4-way valve in the downward position.
  Open valve 4 carefully, visibly monitoring for excess movement of the oil column in the flow meter.
  Open valve 5 carefully, again monitoring the oil column.

- Record the position of the oil column in the flow meter as the initial reading for "zero inflow".

- Slowly open valve 9, watching the movement of the oil column.
  There may be an initial rush of flow when opening valve 9 and the movement of the oil column may initially be fast but should slow down within a few seconds.
  Record the position of the oil column when this initial surge stops.
  This initial flow surge may or may not be factored out of the inflow readings, as it may be due to improper flushing of the leads or compression of air in the system, rather than to actual saturation of the specimen.

- Periodically record readings of the oil column position (mL gradation) and elapsed time.

- If the front of the oil column moves close to either end of the sight buret, reverse the direction of flow through the flow meter simply by changing the position of the 4-way valve.
  A reading should be taken immediately before and after reversing the position of the 4-way valve so that any small jump in the oil level can be factored out of inflow measurements.

- Close valves 9, 17, 18, 5, 4, 3, then 1 when the saturation process is completed.

BREAKTHROUGH

Once the specimen is stabilized at the desired saturation state, the next portion of testing is gas breakthrough.

Setting the system to back pressure

The water lines in the system and the cell itself have been set at the back pressure as part of the preparation for the saturation stage of testing. This step sets the rest of the lines, including the outflow section of the system to the back pressure as a starting point for the breakthrough portion of testing.

- Open valves 14, 15, 11, 12 and 13.

- Set the pressure through RC (read by TC) to the back pressure.
  Set the pressure through RB (read by TA) to the back pressure.
  (Note that valves 23 and 24 can be used to adjust the pressure through RC.)

Flushing the leads with gas

The cell leads, filter stones and filter papers have to be flushed with gas so that no water can restrict the flow of gas in and out of the specimen during the breakthrough stage of testing.

- Open valve 19.
  Repeatedly open and close valve 21 to flush the water out of the bottom leads, filter paper and filter stone.
  Continue this until mostly gas flows out valve 21.
  Close valves 21 then 19 when finished.

- Open valve 20.
  Open valve 22 to similarly flush gas through the top leads, filter paper and filter stone.
  Close valves 22 then 20.

- Check TA and TC to ensure that the pressure through RB and RC is still set at the back pressure.
  If not, reset the pressures, as discussed earlier.

Setting the gas inflow pressure

In this step, an increment of gas pressure is added to the inflow (bottom) side of the specimen. This step is repeated at regular intervals until enough pressure is present on the inflow side of the specimen to initiate flow of gas through the specimen and into the outflow (top) circuit. The standard incremental increase in

inflow pressure is 200 kPa with an increment duration of 5 minutes.

- Close valve 14.

- Set the pressure through RB to the back pressure plus the preset gas pressure increment (read by TA).

- Simultaneously open valves 19 and 20.

- Monitor TB to detect any pressure response caused by the increased inflow pressure.
  If no pressure response is apparent during the allotted increment time period, add another increment of inflow pressure through RB.
  RB must be set carefully so that the target pressure is not surpassed because with valve 19 open, the specimen would be exposed to whatever pressure went through RB.

- The above steps are repeated until a pressure response is seen in TC, indicating that breakthrough has occurred.

DISMANTLING THE CELL

Once breakthrough is achieved, or if the test board reaches the limiting pressure of the test board (10 MPa), the cell and apparatus are depressurized so the cell can be dismantled.

- Close valves 19 then 20.
  Reduce the pressure through RB and RC to atmospheric.
  Open valves 23 and 24 to bleed the pressure in the lines.
  Open valves 14 and 15 to depressurize the gas collection circuit.
  Open valves 21 and 22 to depressurize the cell.

- Open valves 9, 6, 3 then 2 to relieve the pressure in the water lines.
  Set the 4-way valve in the downward position.
  Open valve 5 was carefully to relieve the pressure in the flow meter, monitoring for excess movement of the oil column.

The entire system should be at atmospheric pressure at this point.

- Close the safety valves on the gas source tank between tests.

- Close all valves on the test board.

- Remove the cell from the apparatus at valves 17 through 22.

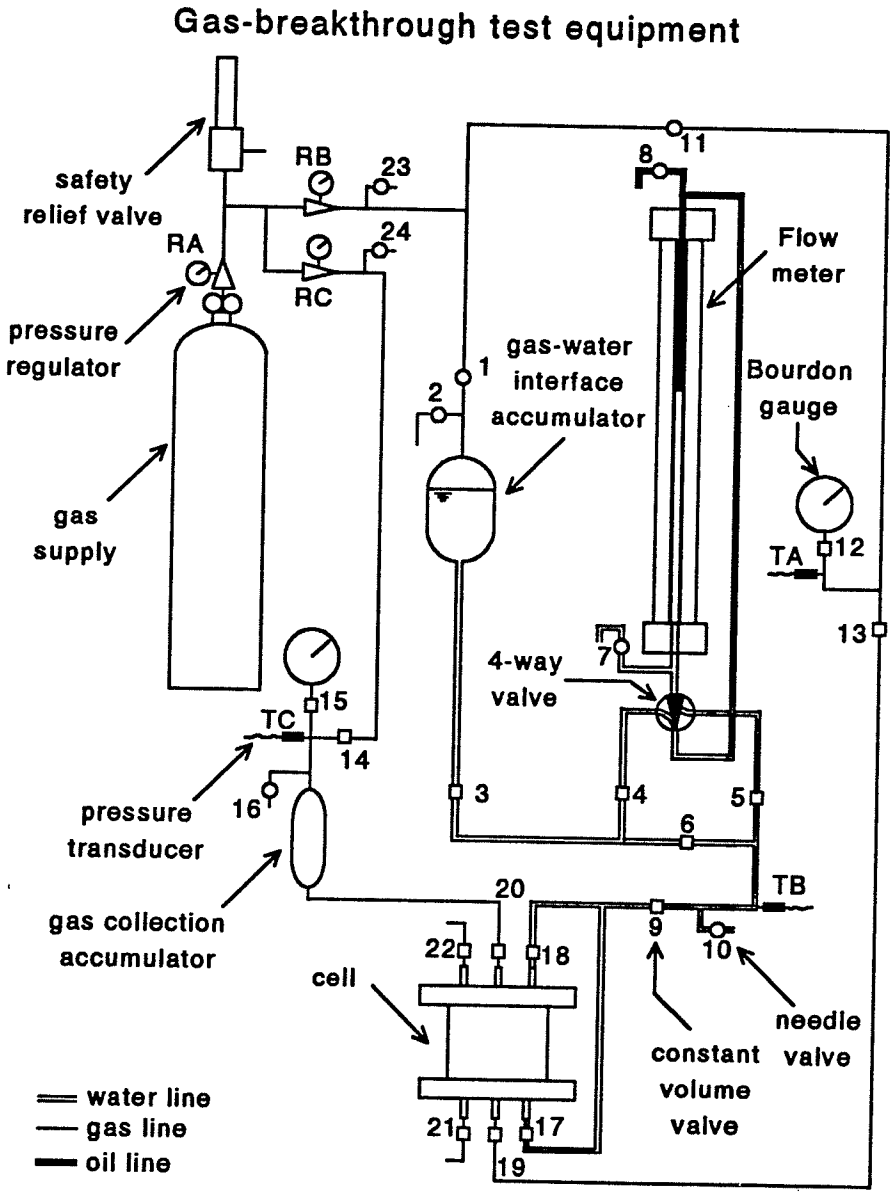

Figure B-1: Test epuipment

APPENDIX C

GAS-BREAKTHROUGH TEST DATA

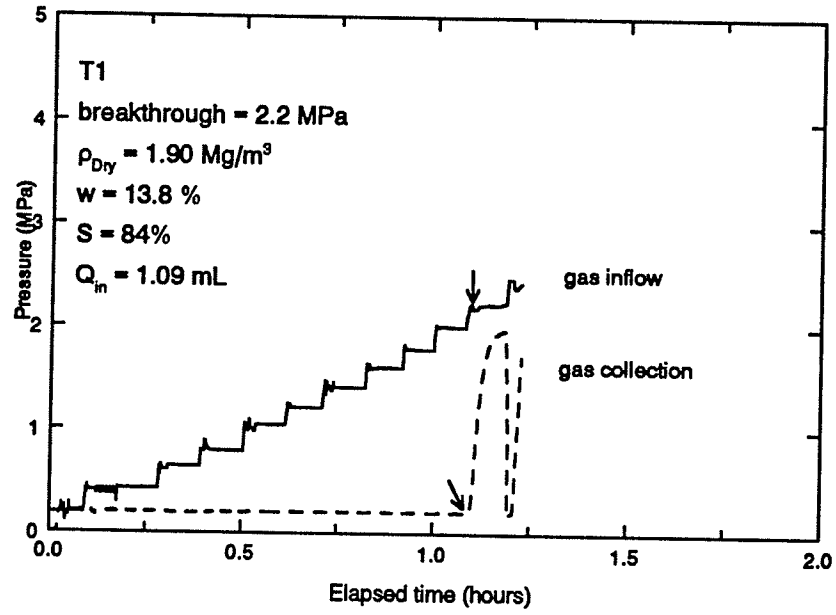
T1
breakthrough = 2.2 MPa
ρ_{Dry} = 1.90 Mg/m^3
w = 13.8 %
S = 84%
Q_{in} = 1.09 mL
gas inflow
gas collection
Pressure (MPa)
Elapsed time (hours)
0
1
2
3
4
5
0.0
0.5
1.0
1.5
2.0

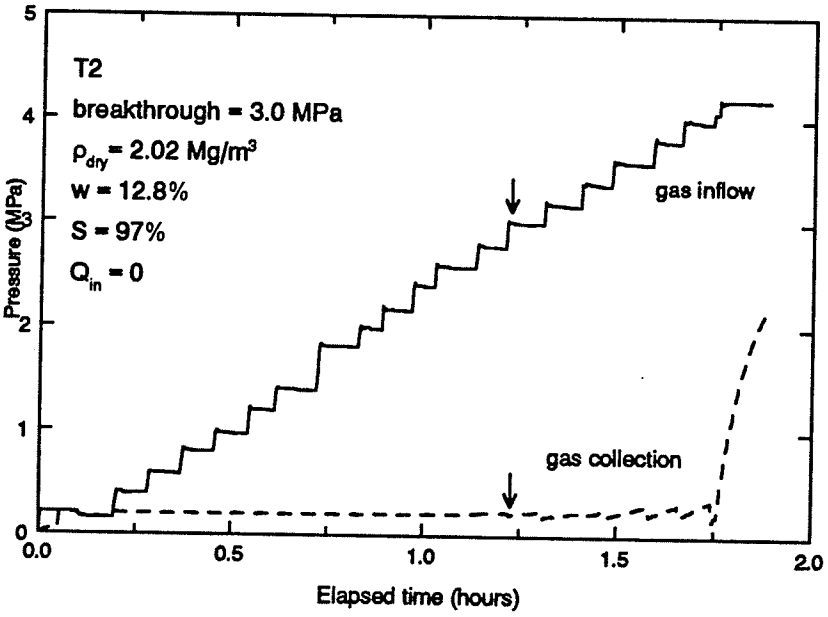
T2
breakthrough = 3.0 MPa
ρ_{dry} = 2.02 Mg/m^3
w = 12.8%
S = 97%
Q_{in} = 0
gas inflow
gas collection
Pressure (MPa)
Elapsed time (hours)
0
1
2
3
4
5
0.0
0.5
1.0
1.5
2.0

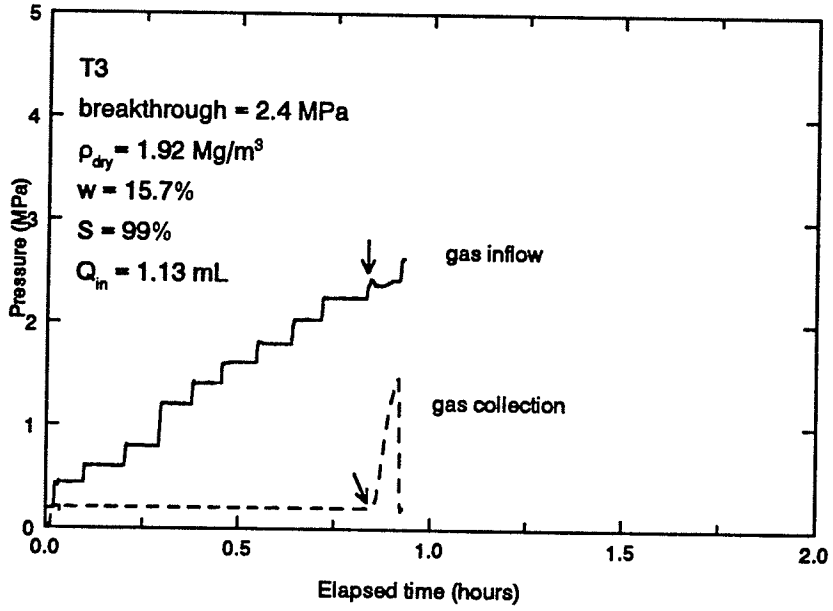
T3
breakthrough = 2.4 MPa
ρ_{dry} = 1.92 Mg/m^3
w = 15.7%
S = 99%
Q_{in} = 1.13 mL
gas inflow
gas collection
Pressure (MPa)
Elapsed time (hours)
0
1
2
3
4
5
0.0
0.5
1.0
1.5
2.0

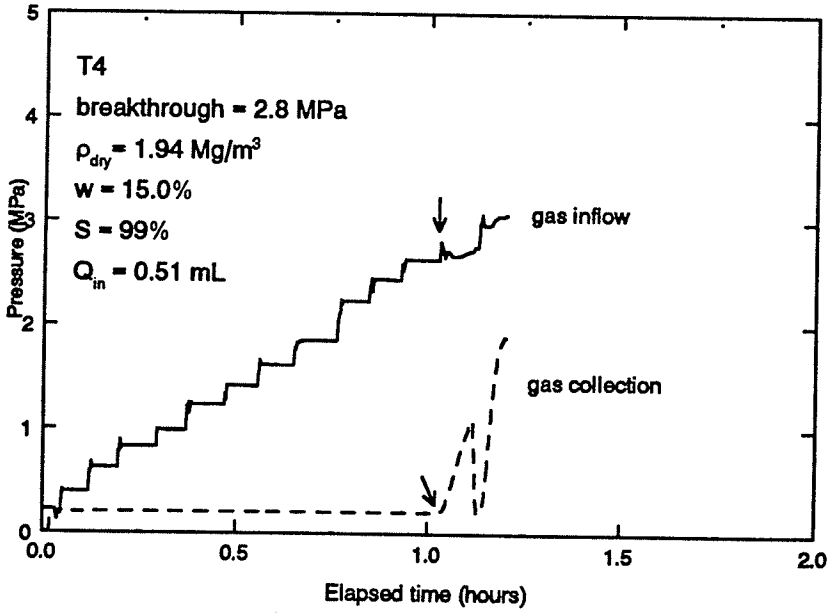
T4
breakthrough = 2.8 MPa
ρ_{dry} = 1.94 Mg/m^3
w = 15.0%
S = 99%
Q_{in} = 0.51 mL
gas inflow
gas collection
Pressure (MPa)
Elapsed time (hours)
0
1
2
3
4
5
0.0
0.5
1.0
1.5
2.0

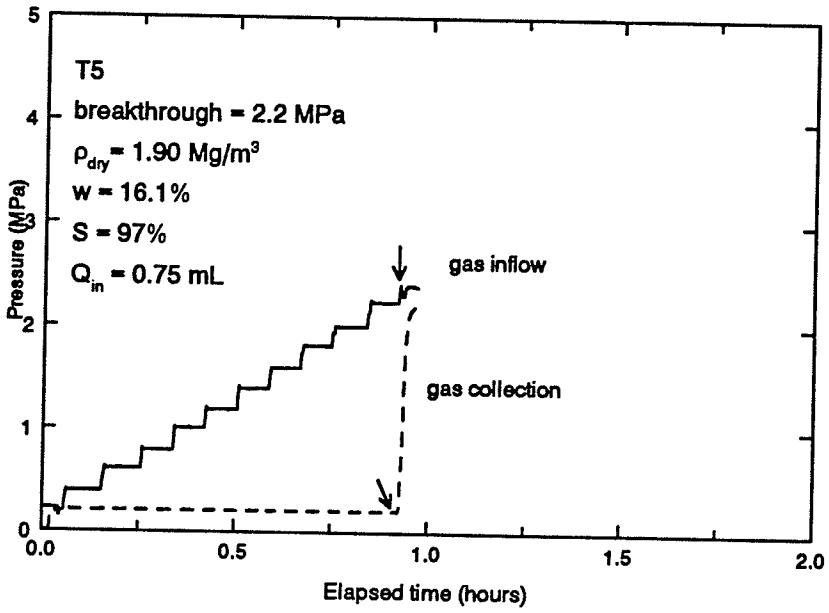
T5
breakthrough = 2.2 MPa
ρ_{dry} = 1.90 Mg/m^3
w = 16.1%
S = 97%
Q_{in} = 0.75 mL
gas inflow
gas collection
Pressure (MPa)
Elapsed time (hours)
0
1
2
3
4
5
0.0
0.5
1.0
1.5
2.0

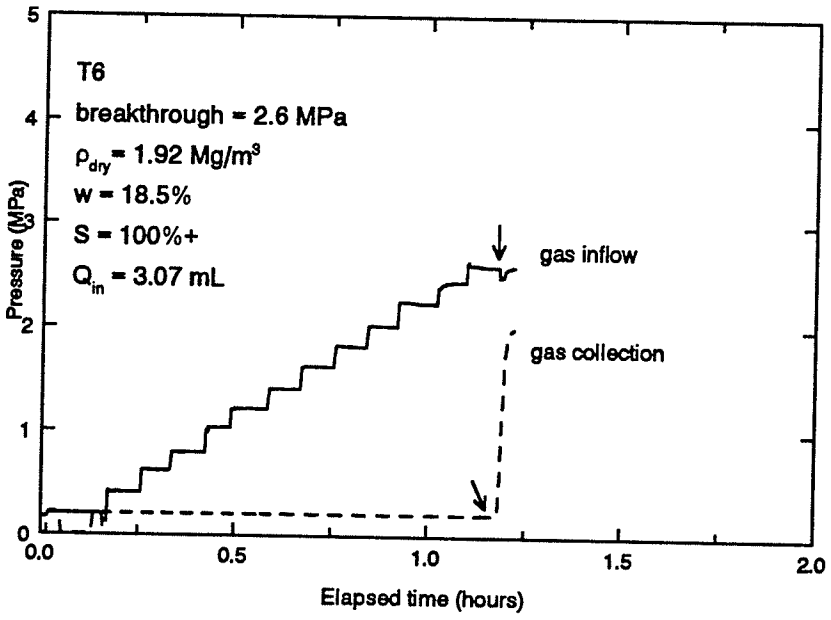
T6
breakthrough = 2.6 MPa
ρ_{dry} = 1.92 Mg/m^3
w = 18.5%
S = 100%+
Q_{in} = 3.07 mL
gas inflow
gas collection
Pressure (MPa)
Elapsed time (hours)
0
1
2
3
4
5
0.0
0.5
1.0
1.5
2.0

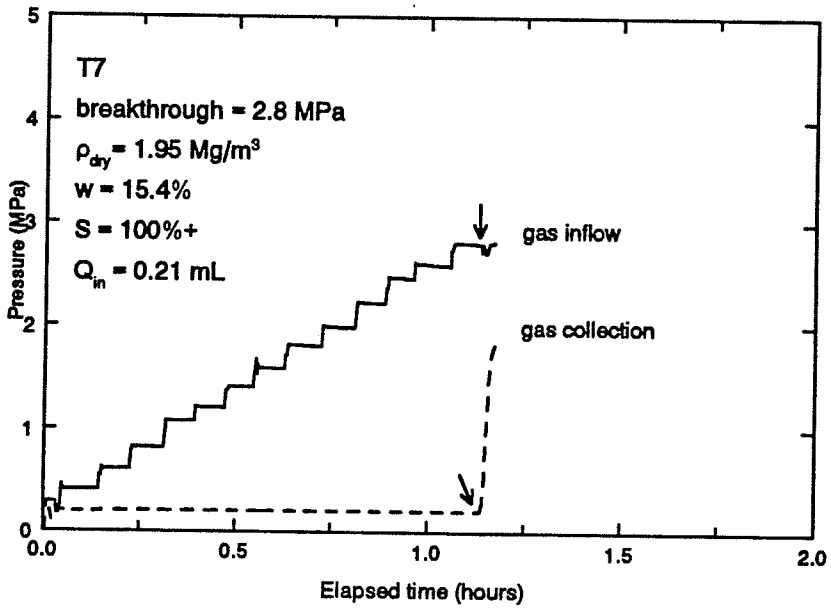
T7
breakthrough = 2.8 MPa
ρ_{dry} = 1.95 Mg/m^3
w = 15.4%
S = 100%+
Q_{in} = 0.21 mL
gas inflow
gas collection
Pressure (MPa)
Elapsed time (hours)
0
1
2
3
4
5
0.0
0.5
1.0
1.5
2.0

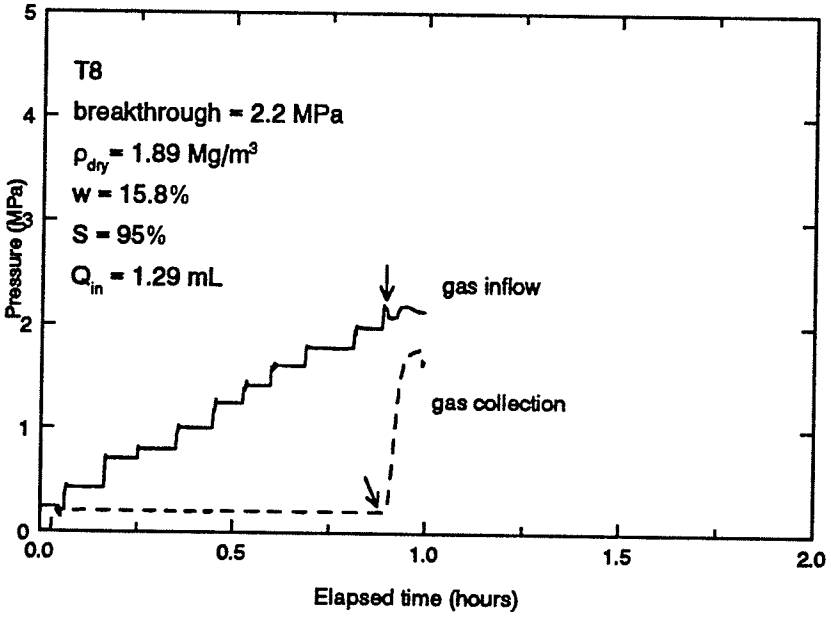
T8
breakthrough = 2.2 MPa
ρ_{dry} = 1.89 Mg/m^3
w = 15.8%
S = 95%
Q_{in} = 1.29 mL
gas inflow
gas collection
Pressure (MPa)
Elapsed time (hours)
0
1
2
3
4
5
0.0
0.5
1.0
1.5
2.0

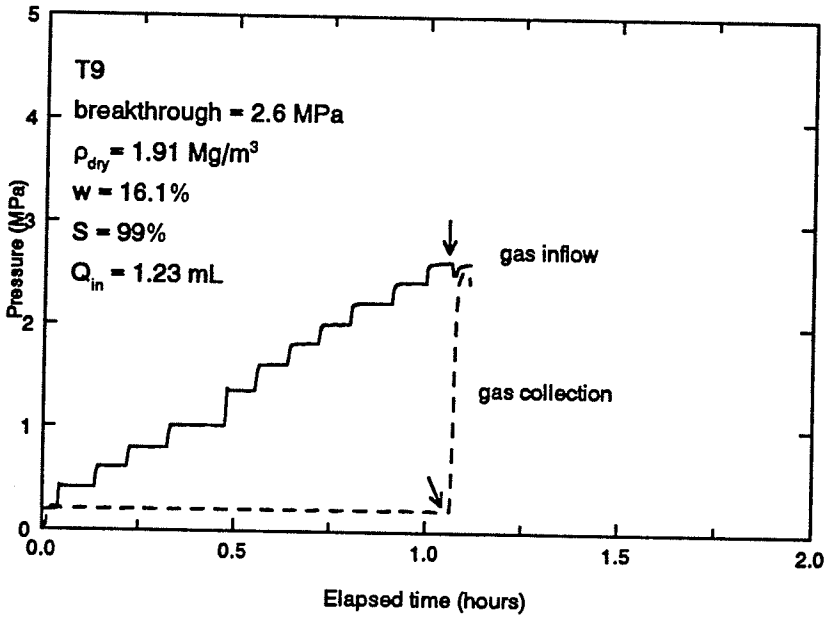
T9
breakthrough = 2.6 MPa
ρ_{dry} = 1.91 Mg/m^3
w = 16.1%
S = 99%
Q_{in} = 1.23 mL
gas inflow
gas collection
Pressure (MPa)
Elapsed time (hours)
0
1
2
3
4
5
0.0
0.5
1.0
1.5
2.0

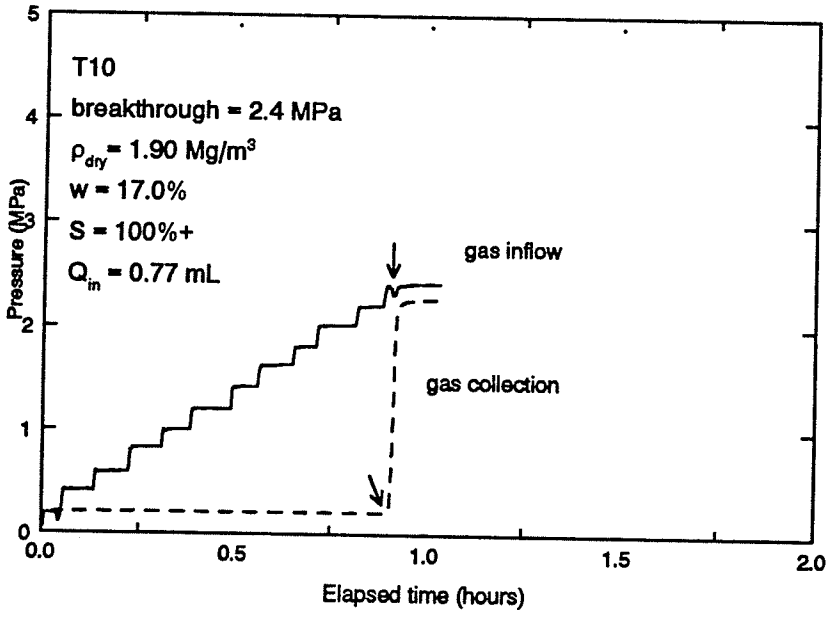
T10
breakthrough = 2.4 MPa
ρ_{dry} = 1.90 Mg/m^3
w = 17.0%
S = 100%+
Q_{in} = 0.77 mL
gas inflow
gas collection
Pressure (MPa)
Elapsed time (hours)
0
1
2
3
4
5
0.0
0.5
1.0
1.5
2.0

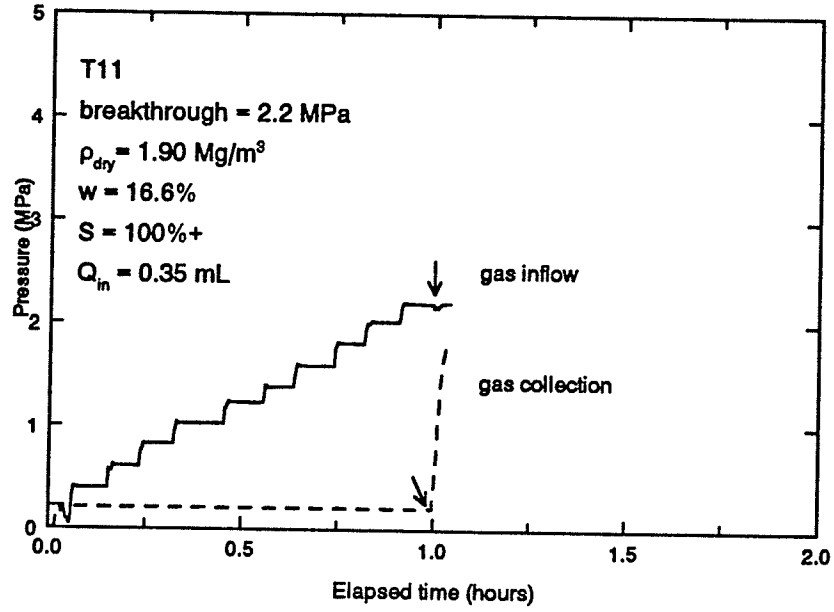
T11
breakthrough = 2.2 MPa
ρ_{dry} = 1.90 Mg/m^3
w = 16.6%
S = 100%+
Q_{in} = 0.35 mL
gas inflow
gas collection
Pressure (MPa)
Elapsed time (hours)
0
1
2
3
4
5
0.0
0.5
1.0
1.5
2.0

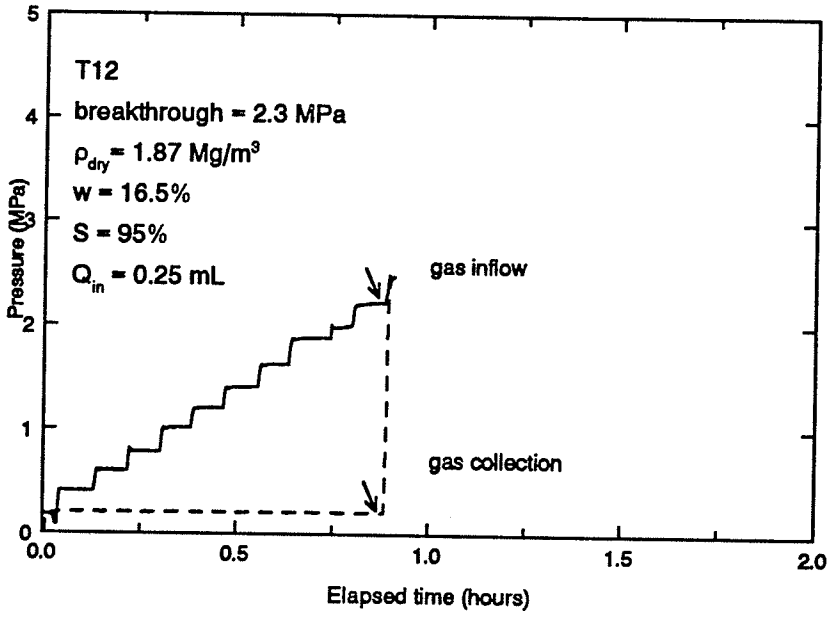
T12
breakthrough = 2.3 MPa
ρ_{dry} = 1.87 Mg/m^3
w = 16.5%
S = 95%
Q_{in} = 0.25 mL
gas inflow
gas collection
Pressure (MPa)
Elapsed time (hours)
0
1
2
3
4
5
0.0
0.5
1.0
1.5
2.0

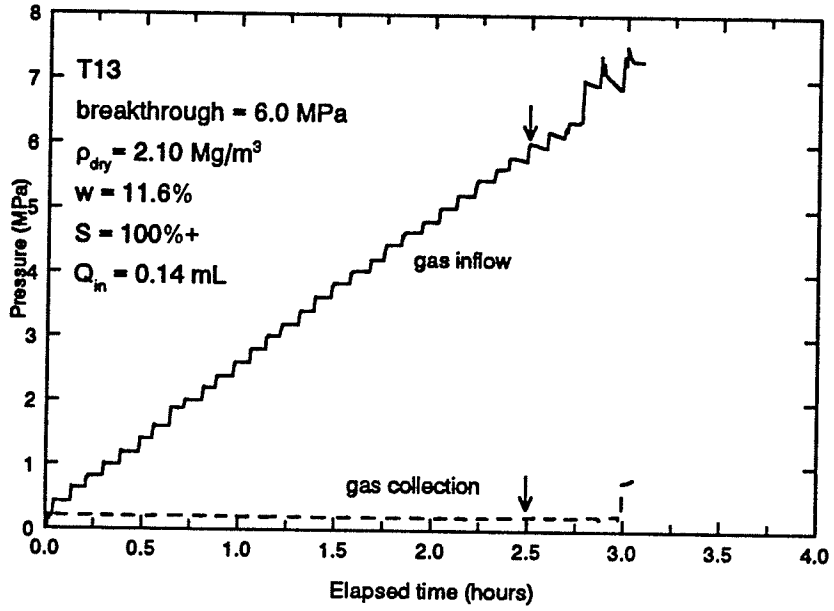
T13
breakthrough = 6.0 MPa
ρ_{dry} = 2.10 Mg/m^3
w = 11.6%
S = 100%+
Q_{in} = 0.14 mL
gas inflow
gas collection
Pressure (MPa)
Elapsed time (hours)
0
1
2
3
4
5
6
7
8
0.0
0.5
1.0
1.5
2.0
2.5
3.0
3.5
4.0

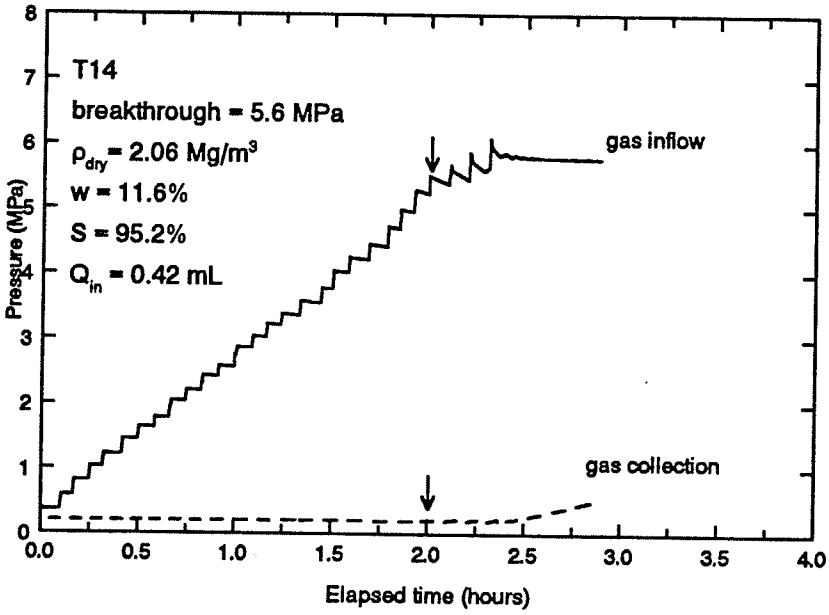
T14
breakthrough = 5.6 MPa
ρ_{dry} = 2.06 Mg/m^3
w = 11.6%
S = 95.2%
Q_{in} = 0.42 mL
gas inflow
gas collection
Pressure (MPa)
Elapsed time (hours)
0
1
2
3
4
5
6
7
8
0.0
0.5
1.0
1.5
2.0
2.5
3.0
3.5
4.0

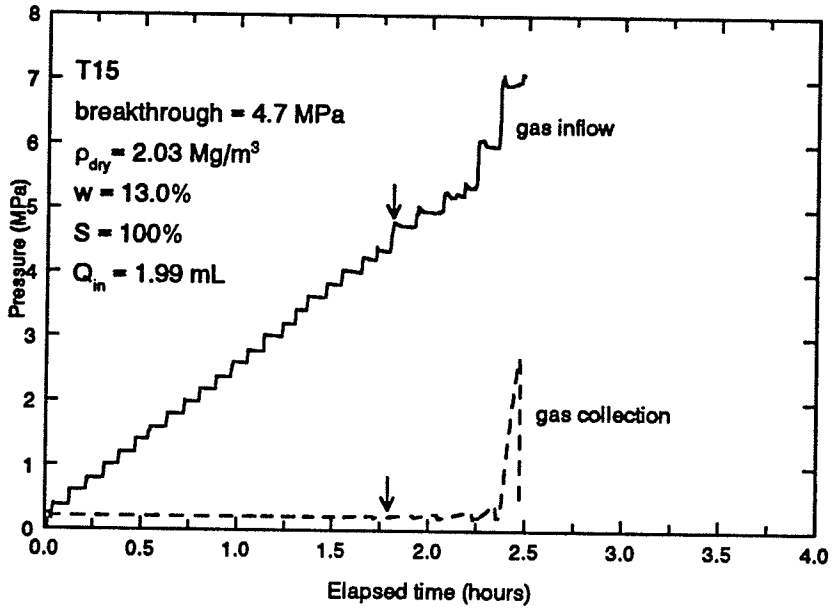
T15
breakthrough = 4.7 MPa
ρ_{dry} = 2.03 Mg/m^3
w = 13.0%
S = 100%
Q_{in} = 1.99 mL
gas inflow
gas collection
Pressure (MPa)
Elapsed time (hours)

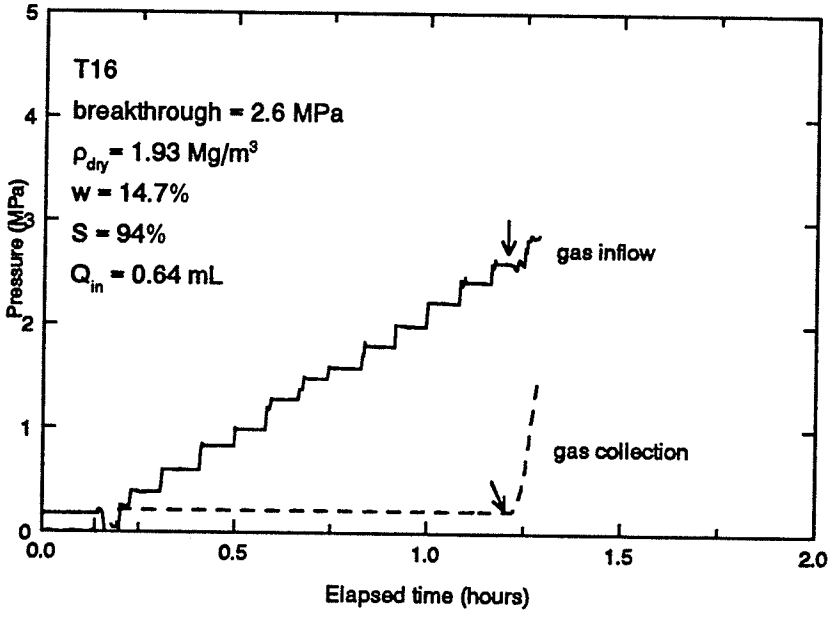
T16
breakthrough = 2.6 MPa
ρ_{dry} = 1.93 Mg/m^3
w = 14.7%
S = 94%
Q_{in} = 0.64 mL
gas inflow
gas collection
Pressure (MPa)
Elapsed time (hours)

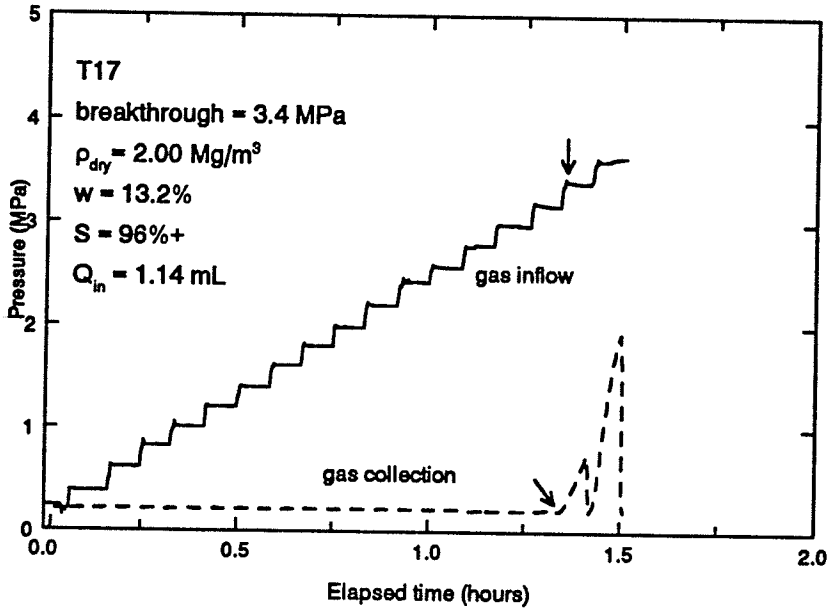
T17
breakthrough = 3.4 MPa
ρ_{dry} = 2.00 Mg/m^3
w = 13.2%
S = 96%+
Q_{in} = 1.14 mL
gas inflow
gas collection
Pressure (MPa)
Elapsed time (hours)
0
1
2
3
4
5
0.0
0.5
1.0
1.5
2.0

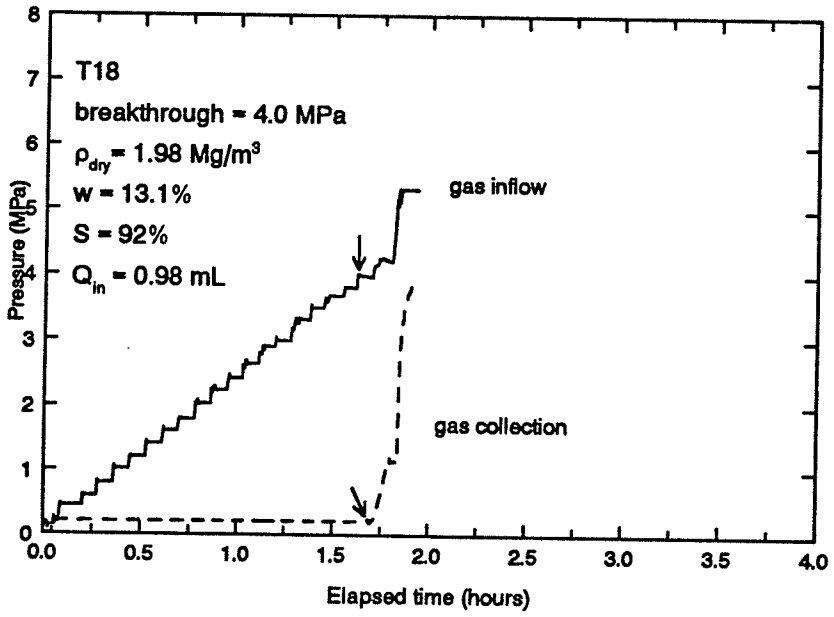
T18
breakthrough = 4.0 MPa
ρ_{dry} = 1.98 Mg/m^3
w = 13.1%
S = 92%
Q_{in} = 0.98 mL
gas inflow
gas collection
Pressure (MPa)
Elapsed time (hours)
0
1
2
3
4
5
6
7
8
0.0
0.5
1.0
1.5
2.0
2.5
3.0
3.5
4.0

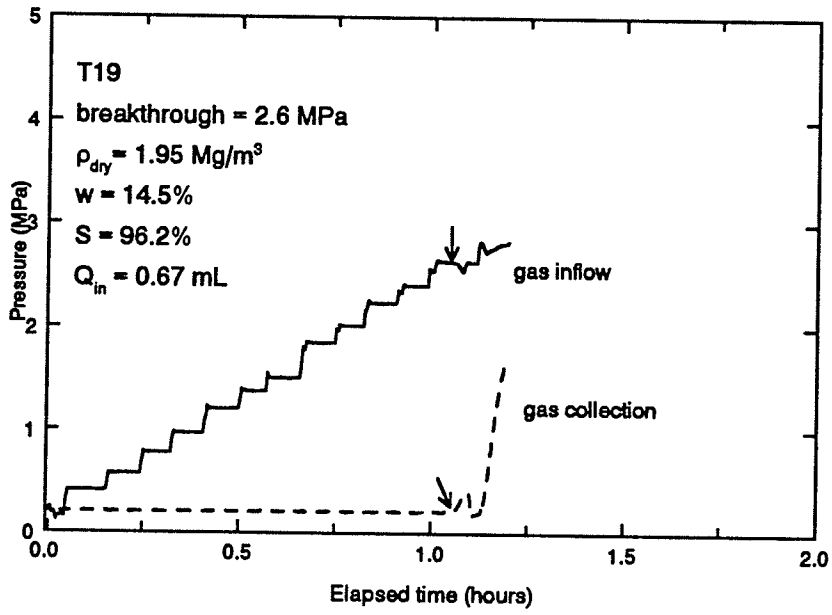
T19
breakthrough = 2.6 MPa
ρ_{dry} = 1.95 Mg/m^3
w = 14.5%
S = 96.2%
Q_{in} = 0.67 mL
gas inflow
gas collection
Pressure (MPa)
Elapsed time (hours)
0
1
2
3
4
5
0.0
0.5
1.0
1.5
2.0

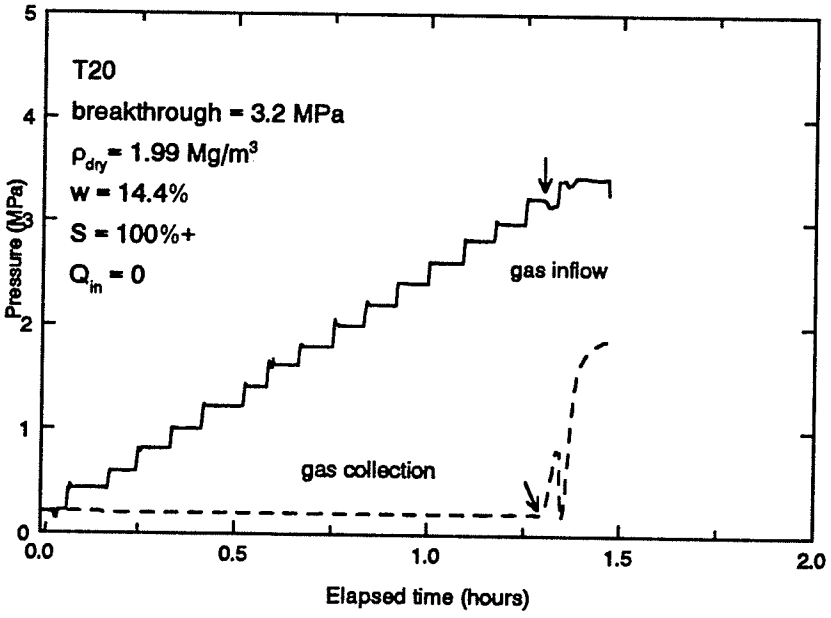
T20
breakthrough = 3.2 MPa
ρ_{dry} = 1.99 Mg/m^3
w = 14.4%
S = 100%+
Q_{in} = 0
gas inflow
gas collection
Pressure (MPa)
Elapsed time (hours)
0
1
2
3
4
5
0.0
0.5
1.0
1.5
2.0

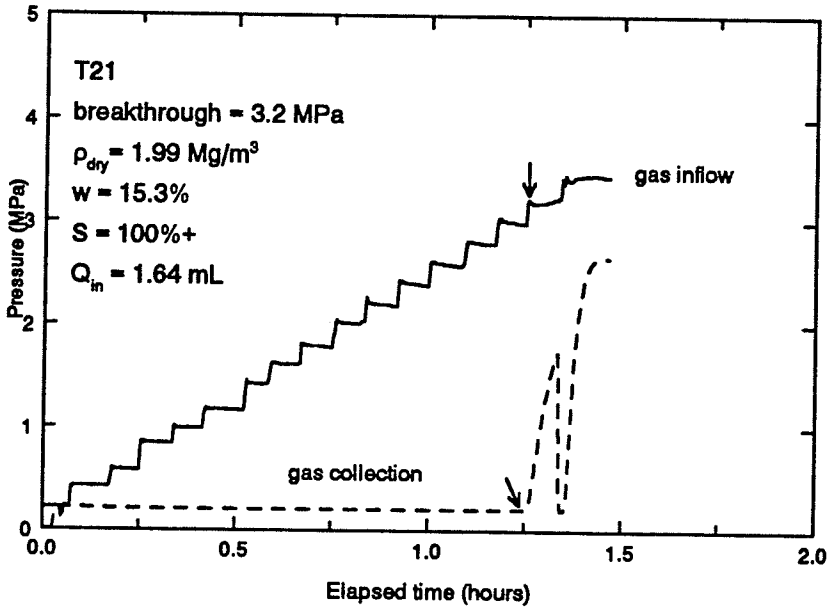
T21
breakthrough = 3.2 MPa
ρ_{dry} = 1.99 Mg/m^3
w = 15.3%
S = 100%+
Q_{in} = 1.64 mL
gas inflow
gas collection
Pressure (MPa)
Elapsed time (hours)
0
1
2
3
4
5
0.0
0.5
1.0
1.5
2.0

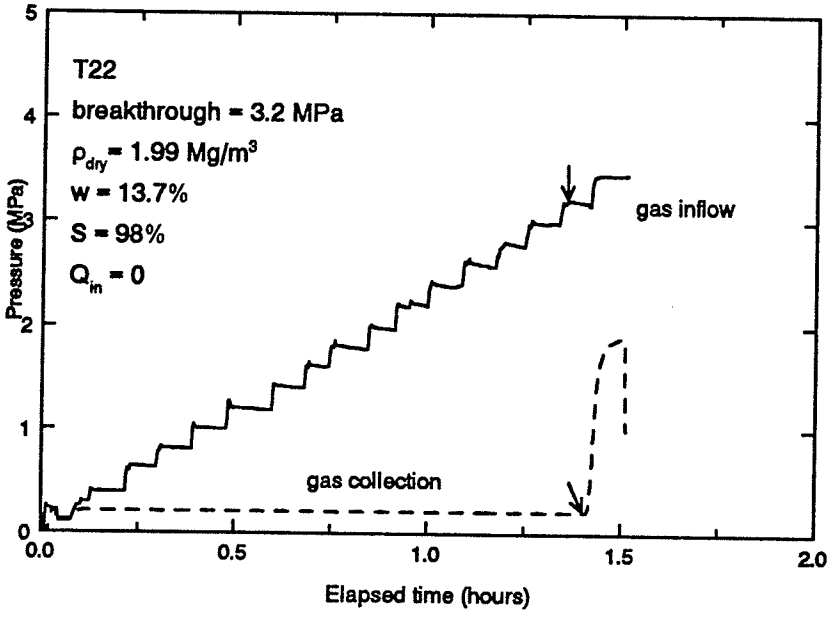
T22
breakthrough = 3.2 MPa
ρ_{dry} = 1.99 Mg/m^3
w = 13.7%
S = 98%
Q_{in} = 0
gas inflow
gas collection
Pressure (MPa)
Elapsed time (hours)
0
1
2
3
4
5
0.0
0.5
1.0
1.5
2.0

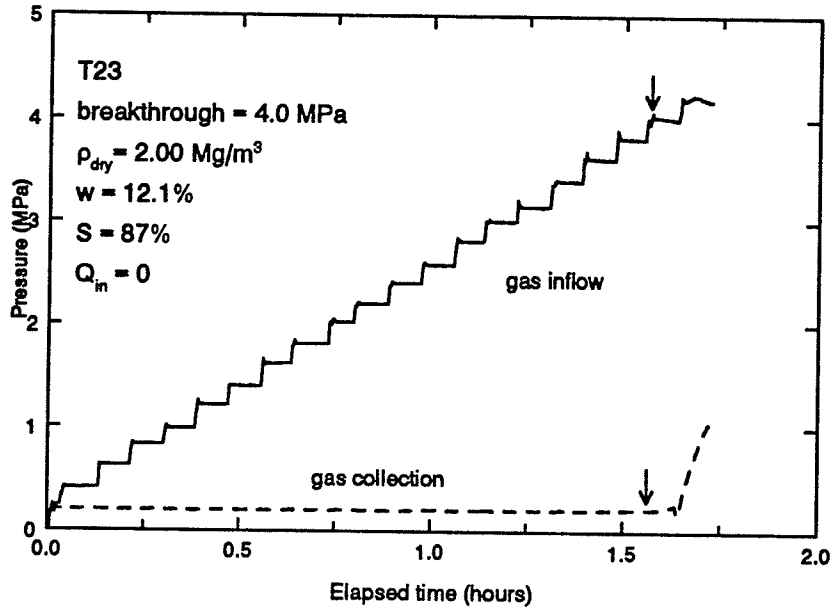
T23
breakthrough = 4.0 MPa
ρ_{dry} = 2.00 Mg/m^3
w = 12.1%
S = 87%
Q_{in} = 0
gas inflow
gas collection
Pressure (MPa)
Elapsed time (hours)
0
1
2
3
4
5
0.0
0.5
1.0
1.5
2.0

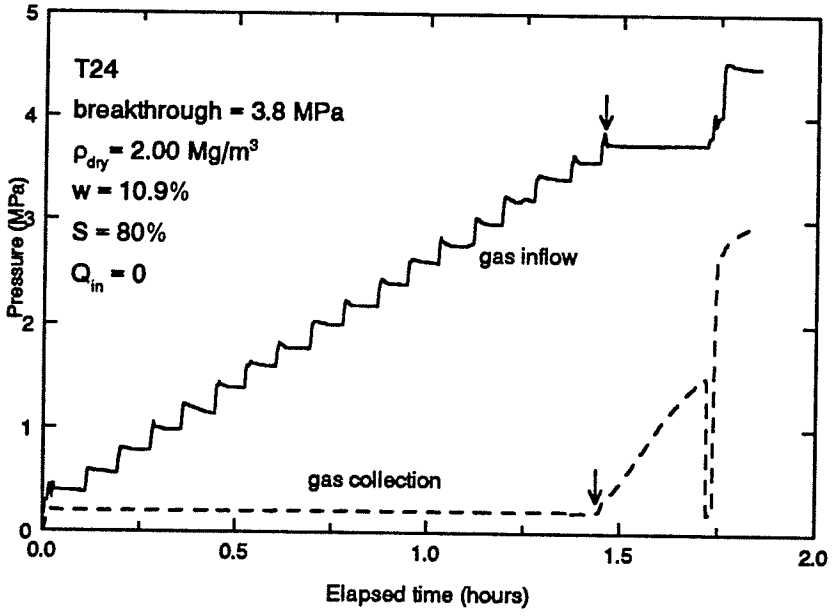
T24
breakthrough = 3.8 MPa
ρ_{dry} = 2.00 Mg/m^3
w = 10.9%
S = 80%
Q_{in} = 0
gas inflow
gas collection
Pressure (MPa)
Elapsed time (hours)
0
1
2
3
4
5
0.0
0.5
1.0
1.5
2.0

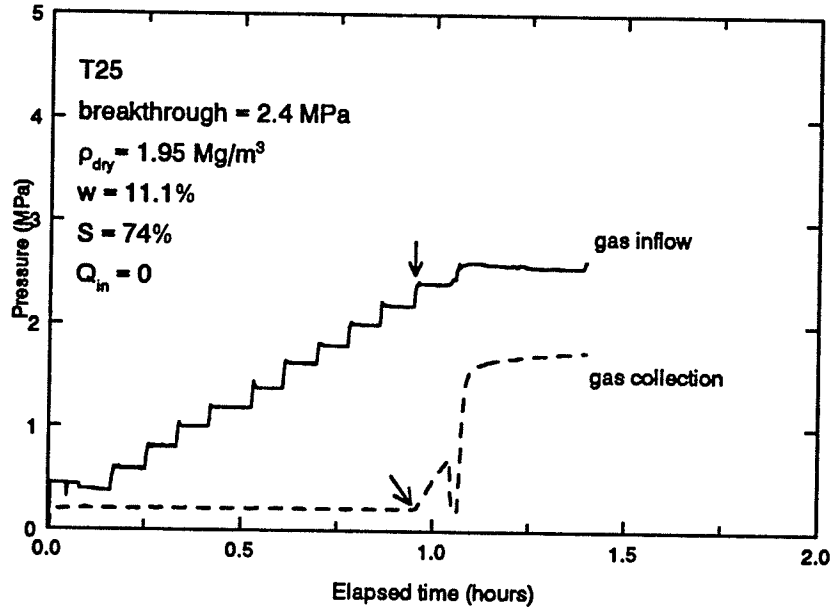
T25
breakthrough = 2.4 MPa
ρ_{dry} = 1.95 Mg/m^3
w = 11.1%
S = 74%
Q_{in} = 0
gas inflow
gas collection
Pressure (MPa)
Elapsed time (hours)
0
1
2
3
4
5
0.0
0.5
1.0
1.5
2.0

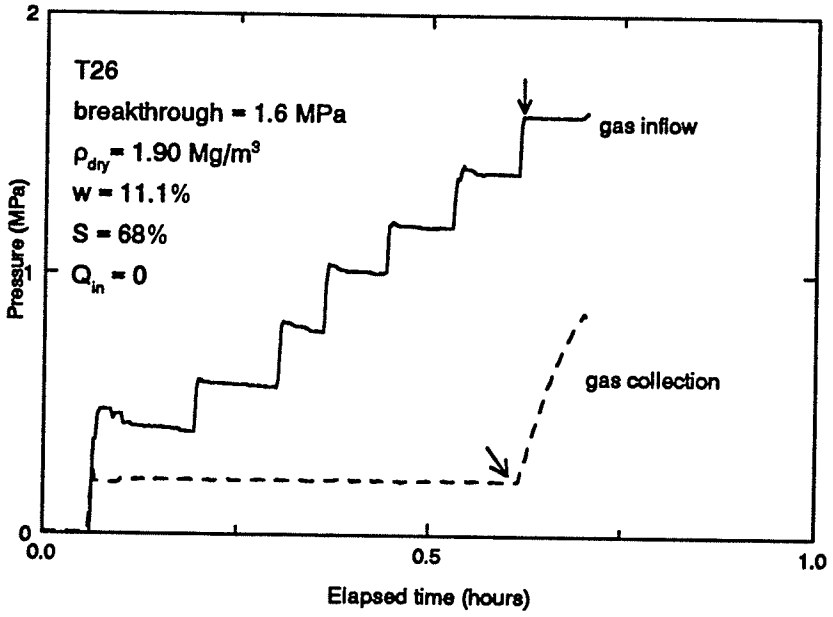
T26
breakthrough = 1.6 MPa
ρ_{dry} = 1.90 Mg/m^3
w = 11.1%
S = 68%
Q_{in} = 0
gas inflow
gas collection
Pressure (MPa)
Elapsed time (hours)
0
1
2
0.0
0.5
1.0

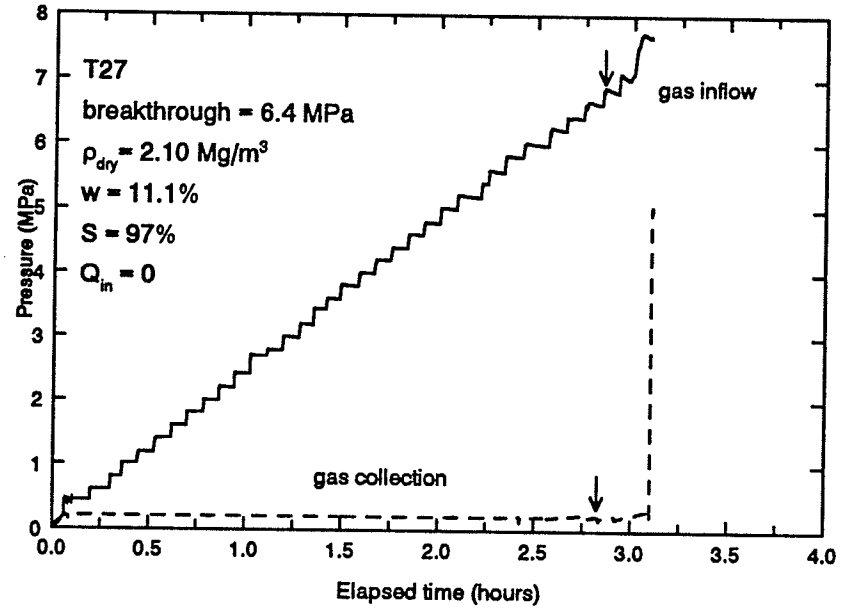
T27
breakthrough = 6.4 MPa
ρ_{dry} = 2.10 Mg/m^3
w = 11.1%
S = 97%
Q_{in} = 0
gas inflow
gas collection
Pressure (MPa)
Elapsed time (hours)
0
1
2
3
4
5
6
7
8
0.0
0.5
1.0
1.5
2.0
2.5
3.0
3.5
4.0

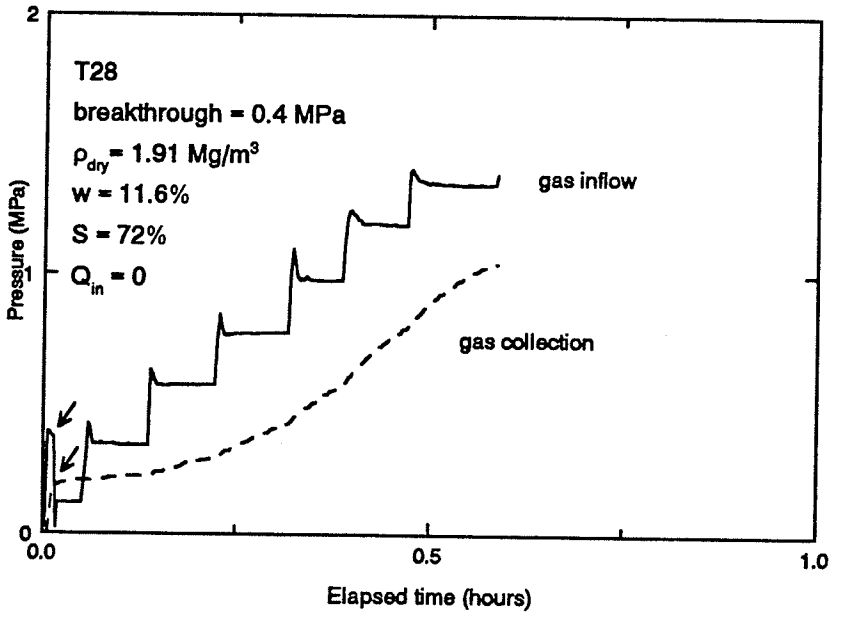
T28
breakthrough = 0.4 MPa
ρ_{dry} = 1.91 Mg/m^3
w = 11.6%
S = 72%
Q_{in} = 0
gas inflow
gas collection
Pressure (MPa)
Elapsed time (hours)
0
1
2
0.0
0.5
1.0

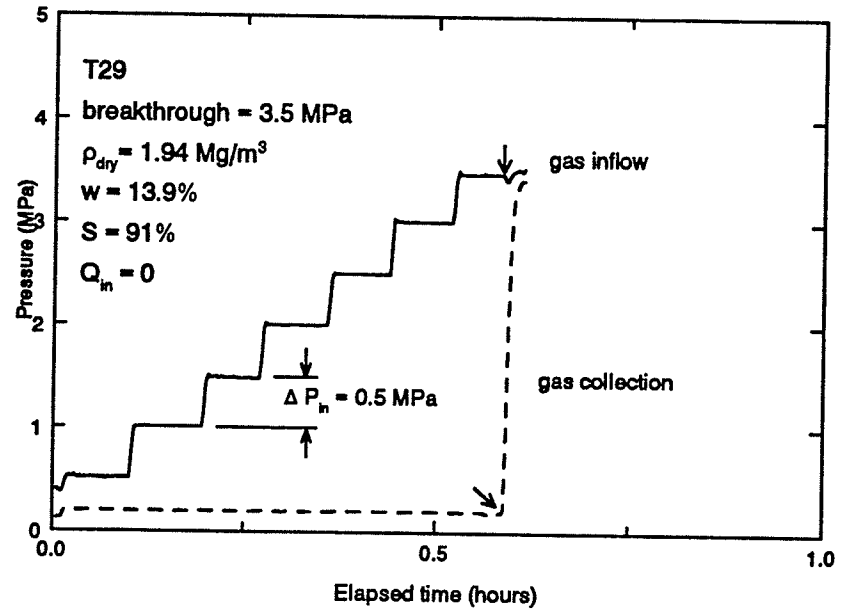
T29
breakthrough = 3.5 MPa
ρ_{dry} = 1.94 Mg/m^3
w = 13.9%
S = 91%
Q_{in} = 0
gas inflow
gas collection
ΔP_{in} = 0.5 MPa
Pressure (MPa)
Elapsed time (hours)
0
1
2
3
4
5
0.0
0.5
1.0

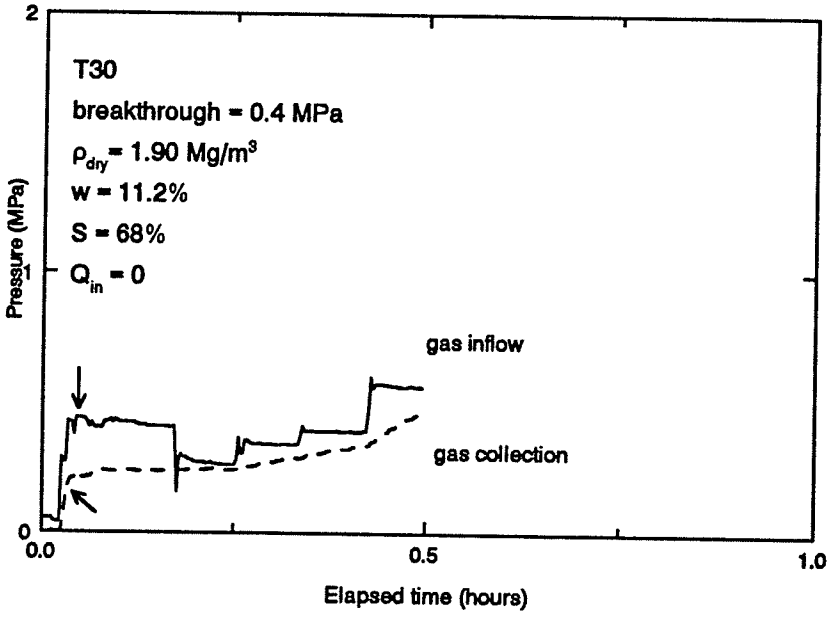
T30
breakthrough = 0.4 MPa
ρ_{dry} = 1.90 Mg/m^3
w = 11.2%
S = 68%
Q_{in} = 0
gas inflow
gas collection
Pressure (MPa)
Elapsed time (hours)
0
1
2
0.0
0.5
1.0

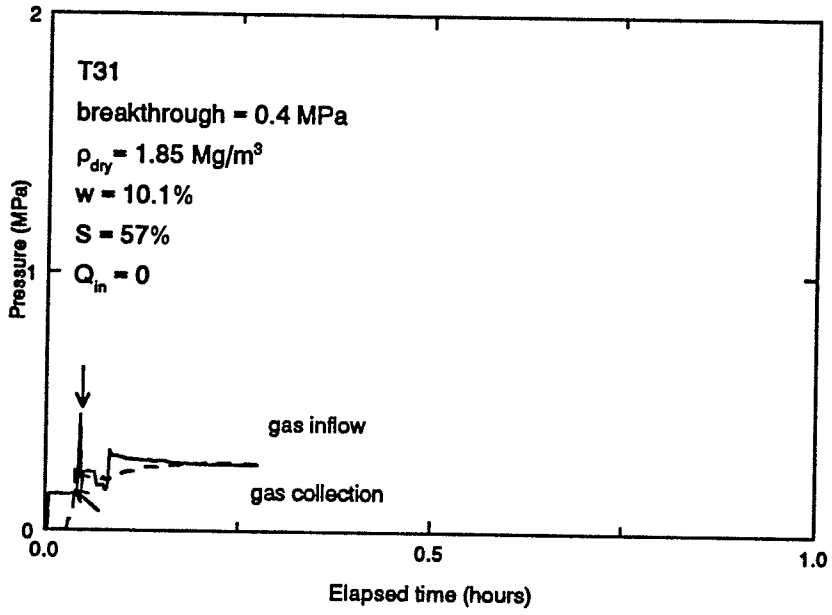
T31
breakthrough = 0.4 MPa
ρ_{dry} = 1.85 Mg/m^3
w = 10.1%
S = 57%
Q_{in} = 0
gas inflow
gas collection
Pressure (MPa)
Elapsed time (hours)
0
1
2
0.0
0.5
1.0

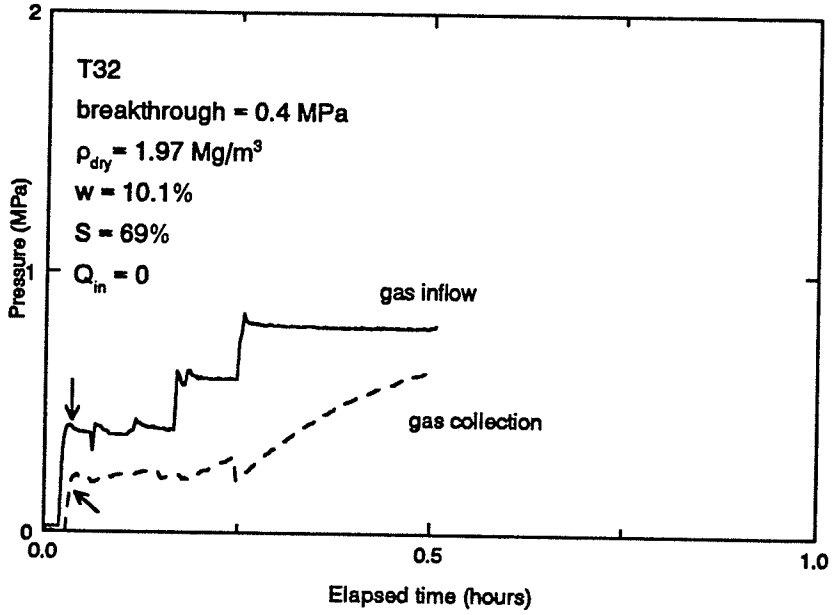
T32
breakthrough = 0.4 MPa
ρ_{dry} = 1.97 Mg/m^3
w = 10.1%
S = 69%
Q_{in} = 0
gas inflow
gas collection
Pressure (MPa)
Elapsed time (hours)
0
1
2
0.0
0.5
1.0

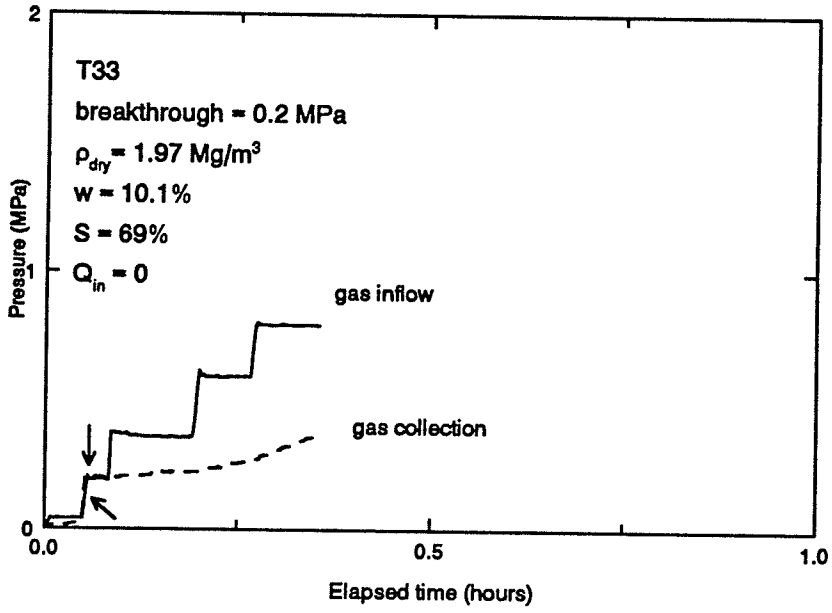
T33
breakthrough = 0.2 MPa
ρ_{dry} = 1.97 Mg/m^3
w = 10.1%
S = 69%
Q_{in} = 0
gas inflow
gas collection
Pressure (MPa)
Elapsed time (hours)
0
1
2
0.0
0.5
1.0

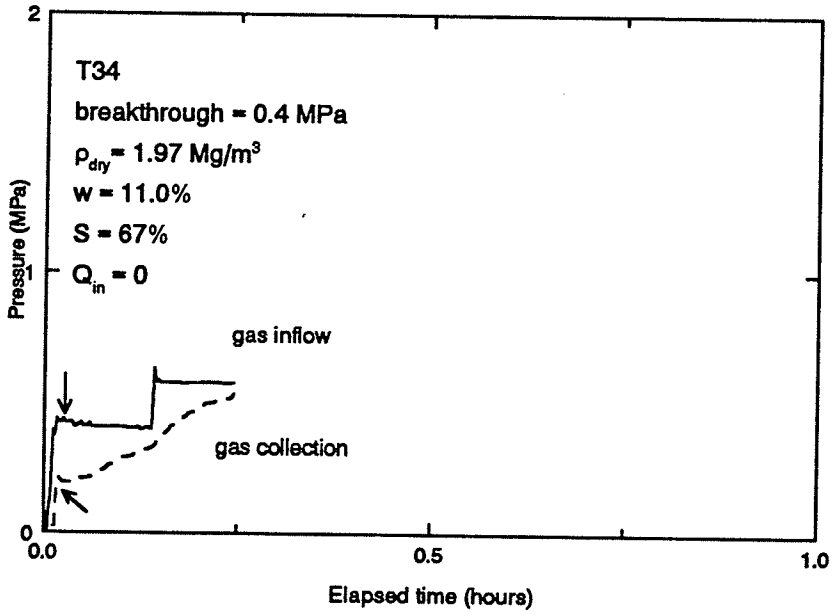
T34
breakthrough = 0.4 MPa
ρ_{dry} = 1.97 Mg/m^3
w = 11.0%
S = 67%
Q_{in} = 0
gas inflow
gas collection
Pressure (MPa)
Elapsed time (hours)
0
1
2
0.0
0.5
1.0

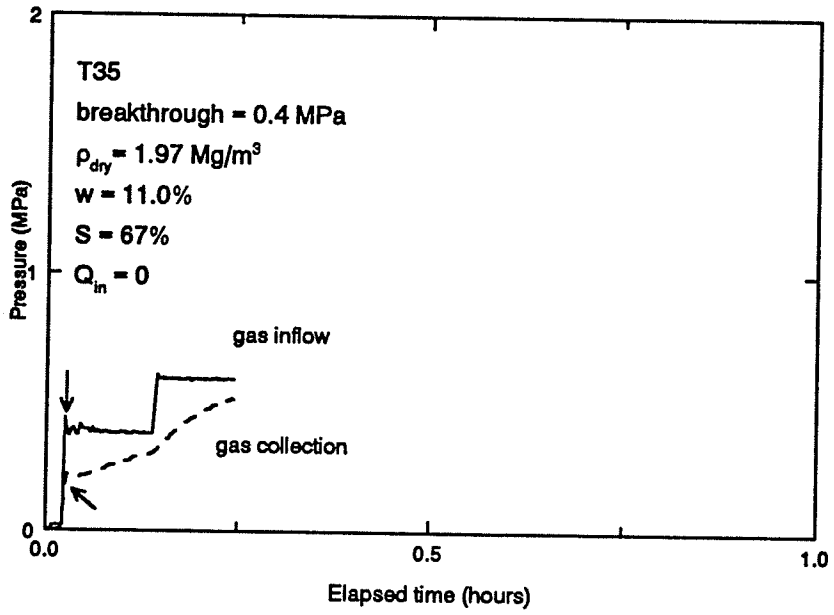
T35
breakthrough = 0.4 MPa
ρ_{dry} = 1.97 Mg/m^3
w = 11.0%
S = 67%
Q_{in} = 0
gas inflow
gas collection
Pressure (MPa)
Elapsed time (hours)
0
1
2
0.0
0.5
1.0

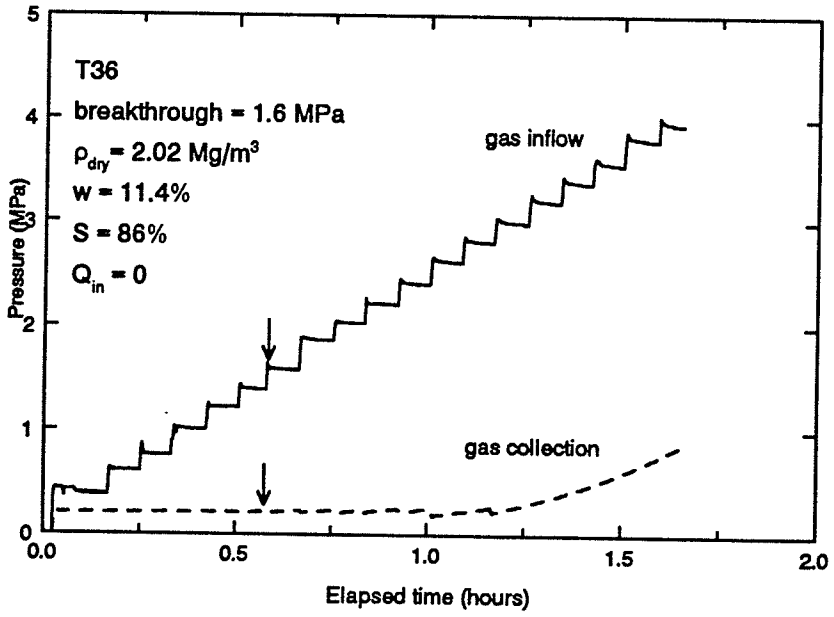
T36
breakthrough = 1.6 MPa
ρ_{dry} = 2.02 Mg/m^3
w = 11.4%
S = 86%
Q_{in} = 0
gas inflow
gas collection
Pressure (MPa)
Elapsed time (hours)
0
1
2
3
4
5
0.0
0.5
1.0
1.5
2.0

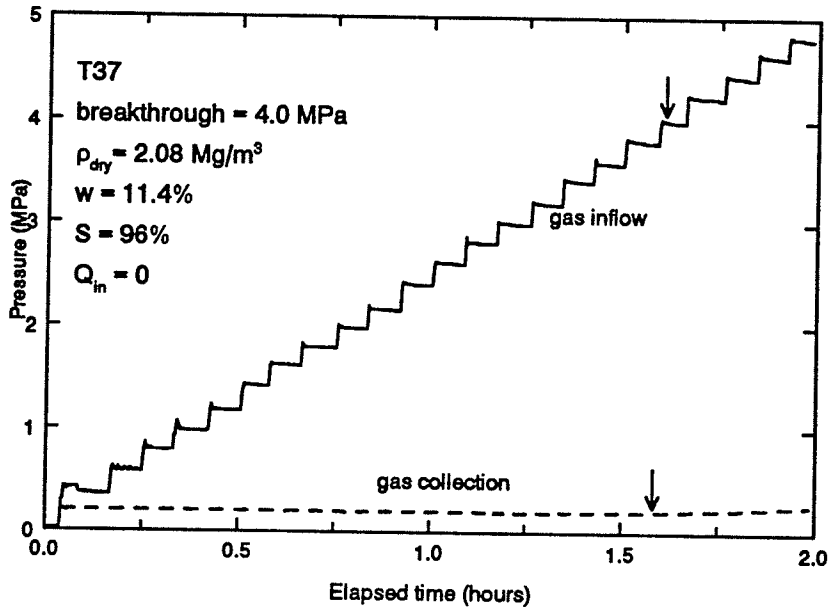
T37
breakthrough = 4.0 MPa
ρ_{dry} = 2.08 Mg/m^3
w = 11.4%
S = 96%
Q_{in} = 0
gas inflow
gas collection
Pressure (MPa)
Elapsed time (hours)
0
1
2
3
4
5
0.0
0.5
1.0
1.5
2.0

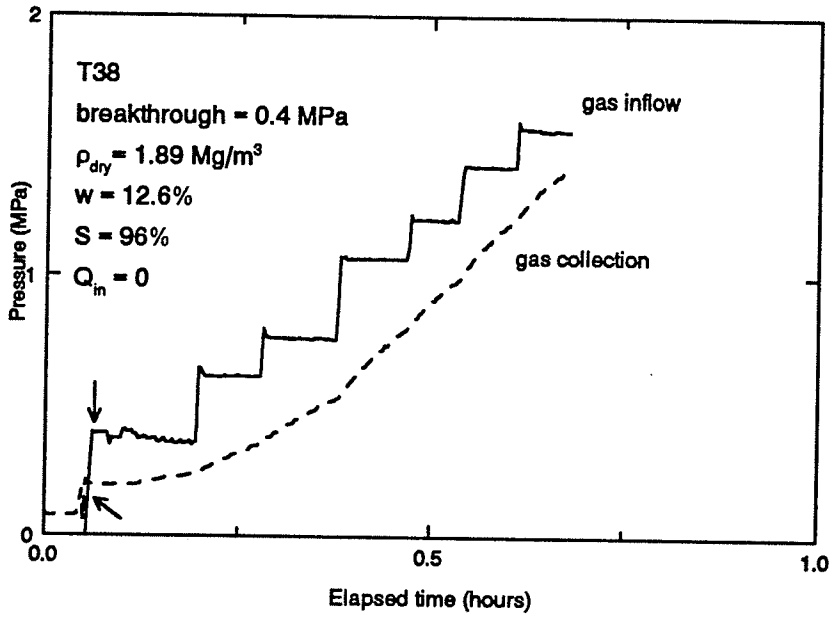
T38
breakthrough = 0.4 MPa
ρ_{dry} = 1.89 Mg/m^3
w = 12.6%
S = 96%
Q_{in} = 0
gas inflow
gas collection
Pressure (MPa)
Elapsed time (hours)
0
1
2
0.0
0.5
1.0

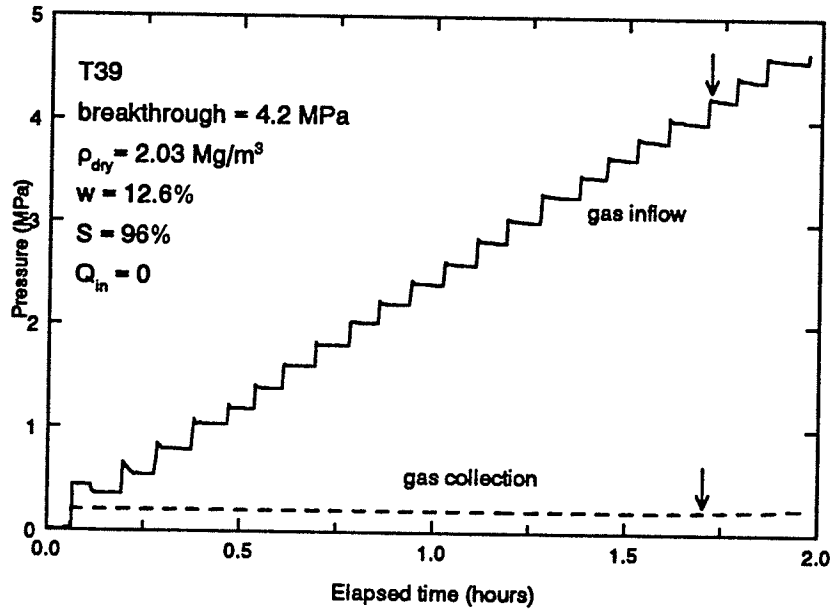
T39
breakthrough = 4.2 MPa
ρ_{dry} = 2.03 Mg/m^3
w = 12.6%
S = 96%
Q_{in} = 0
gas inflow
gas collection
Pressure (MPa)
Elapsed time (hours)
0
1
2
3
4
5
0.0
0.5
1.0
1.5
2.0

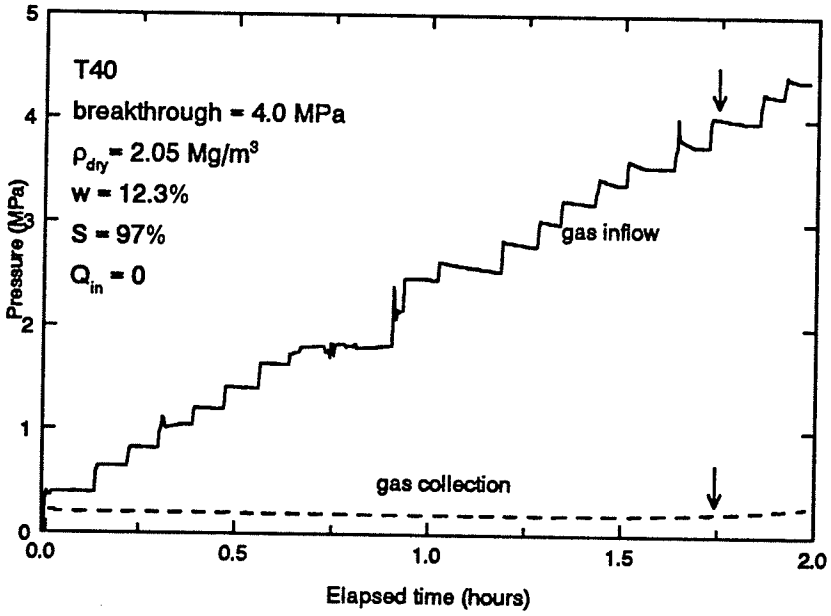
T40
breakthrough = 4.0 MPa
ρ_{dry} = 2.05 Mg/m^3
w = 12.3%
S = 97%
Q_{in} = 0
gas inflow
gas collection
Pressure (MPa)
Elapsed time (hours)
0
1
2
3
4
5
0.0
0.5
1.0
1.5
2.0

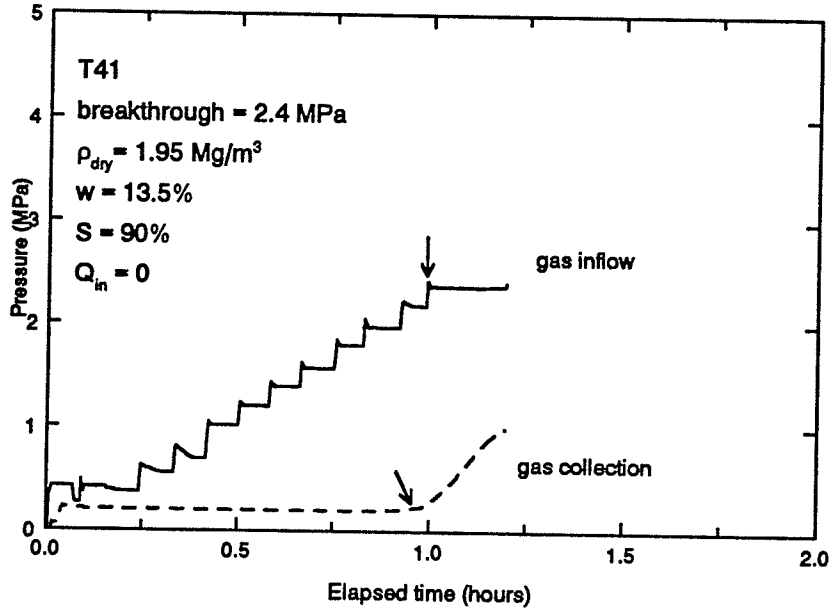
T41
breakthrough = 2.4 MPa
ρ_{dry} = 1.95 Mg/m^3
w = 13.5%
S = 90%
Q_{in} = 0
gas inflow
gas collection
Pressure (MPa)
Elapsed time (hours)
0
1
2
3
4
5
0.0
0.5
1.0
1.5
2.0

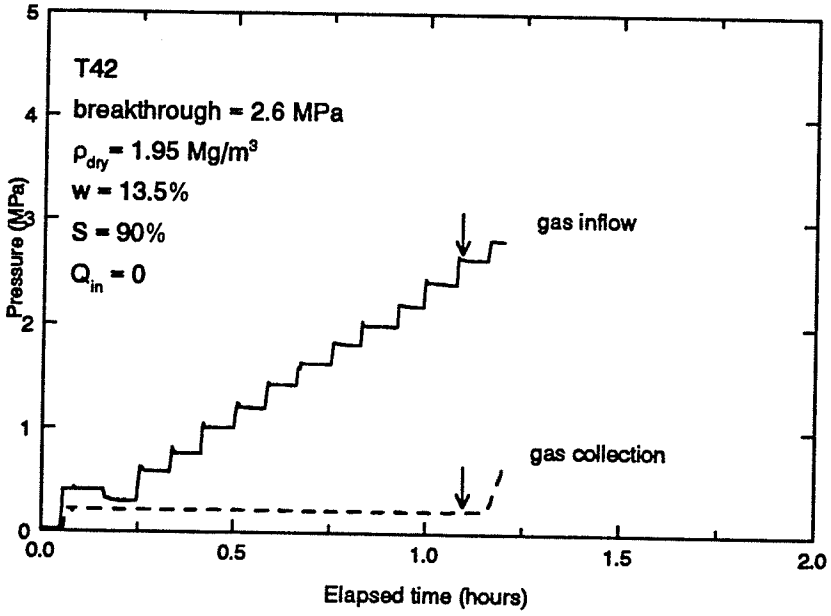
T42
breakthrough = 2.6 MPa
ρ_{dry} = 1.95 Mg/m^3
w = 13.5%
S = 90%
Q_{in} = 0
gas inflow
gas collection
Pressure (MPa)
Elapsed time (hours)
0
1
2
3
4
5
0.0
0.5
1.0
1.5
2.0

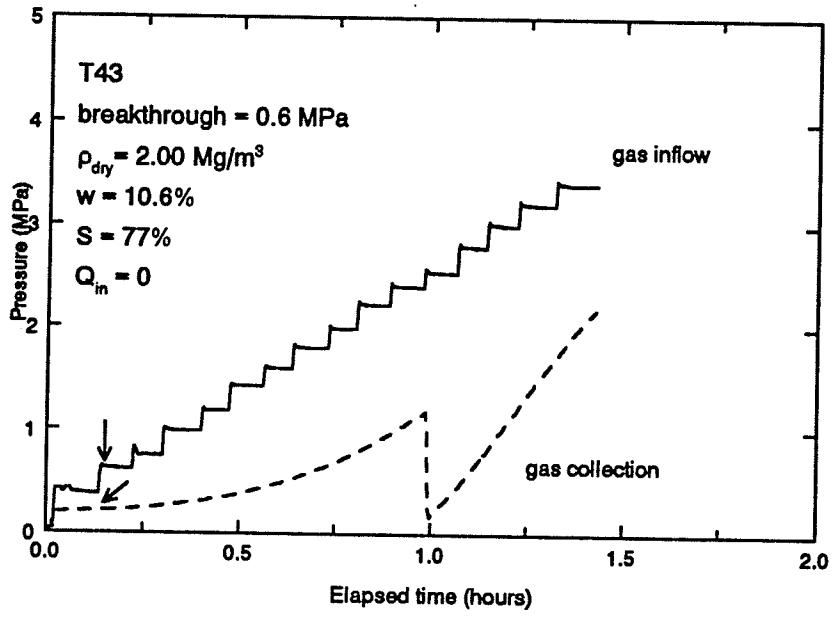
T43
breakthrough = 0.6 MPa
ρ_{dry} = 2.00 Mg/m^3
w = 10.6%
S = 77%
Q_{in} = 0
gas inflow
gas collection
Pressure (MPa)
Elapsed time (hours)
0
1
2
3
4
5
0.0
0.5
1.0
1.5
2.0

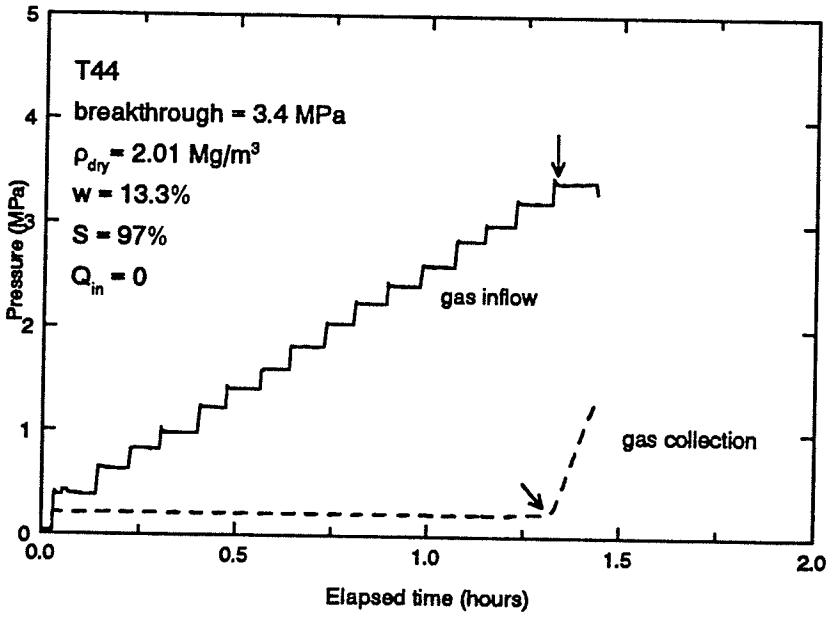
T44
breakthrough = 3.4 MPa
ρ_{dry} = 2.01 Mg/m^3
w = 13.3%
S = 97%
Q_{in} = 0
gas inflow
gas collection
Pressure (MPa)
Elapsed time (hours)
0
1
2
3
4
5
0.0
0.5
1.0
1.5
2.0

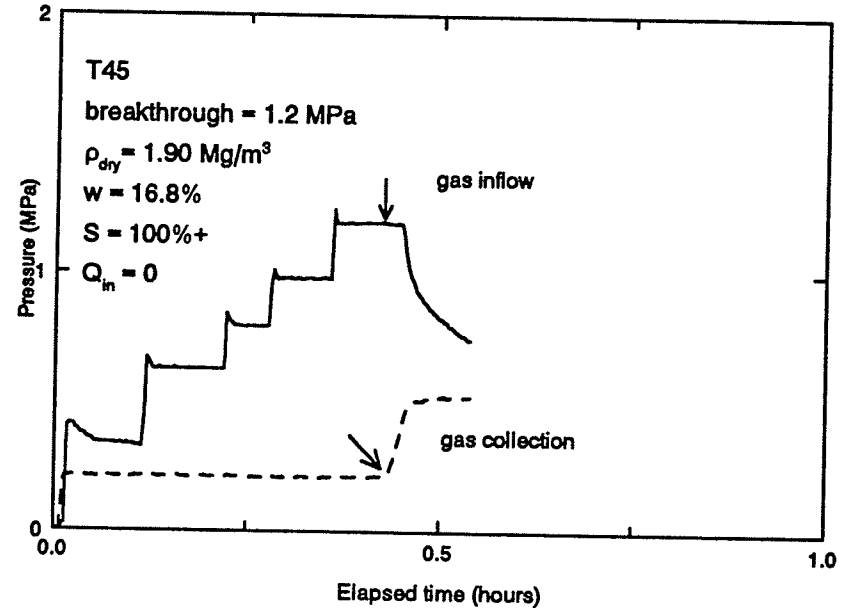
T45
breakthrough = 1.2 MPa
ρ_{dry} = 1.90 Mg/m^3
w = 16.8%
S = 100%+
Q_{in} = 0
gas inflow
gas collection
Pressure (MPa)
2
1
0
0.0
0.5
1.0
Elapsed time (hours)

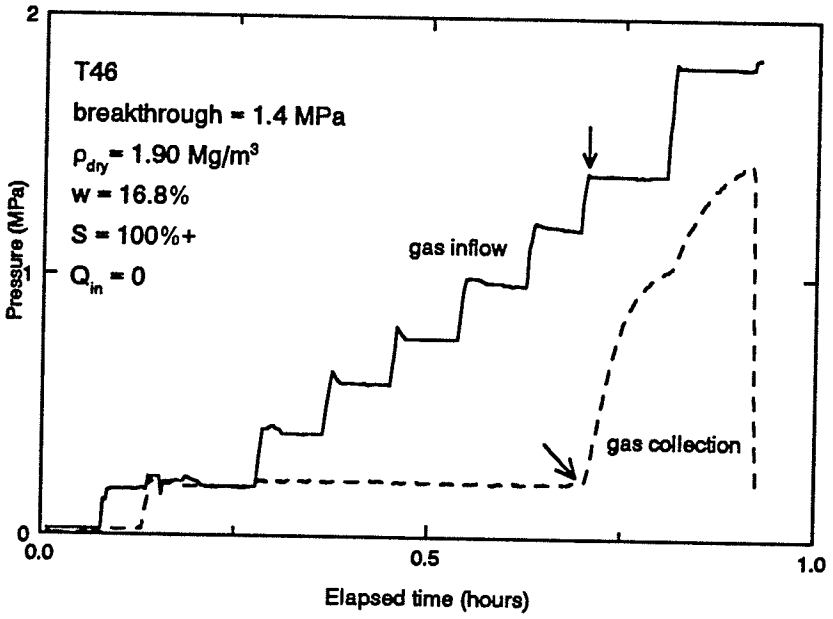
T46
breakthrough = 1.4 MPa
ρ_{dry} = 1.90 Mg/m^3
w = 16.8%
S = 100%+
Q_{in} = 0
gas inflow
gas collection
Pressure (MPa)
2
1
0
0.0
0.5
1.0
Elapsed time (hours)

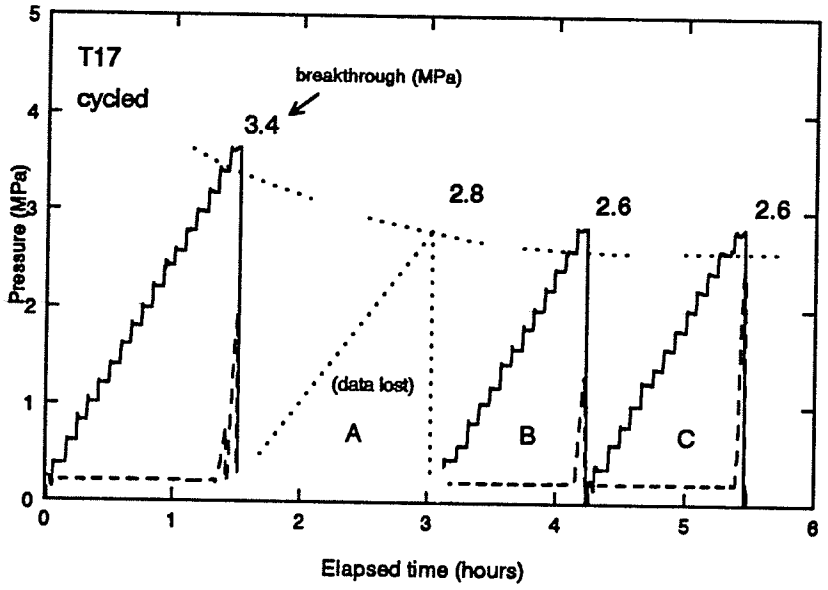
T17
cycled
breakthrough (MPa)
3.4
2.8
2.6
2.6
(data lost)
A
B
C
Pressure (MPa)
Elapsed time (hours)

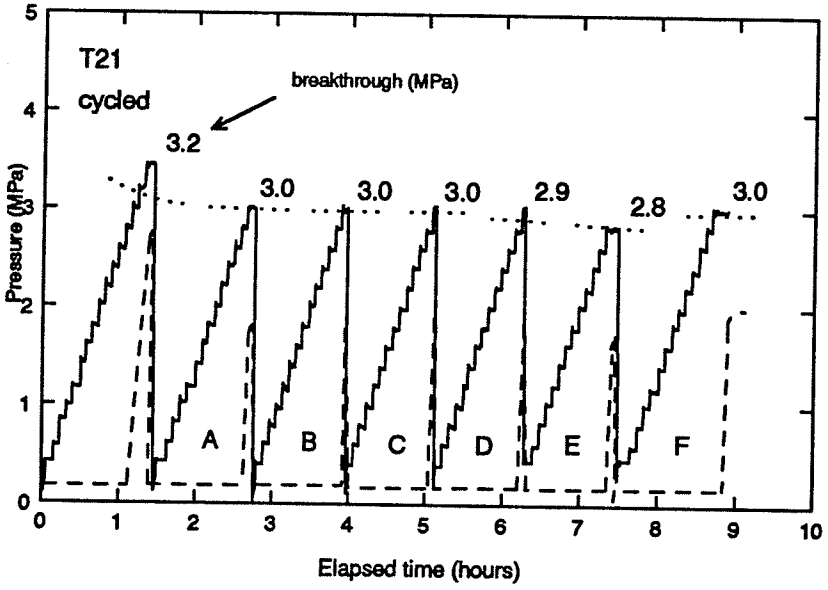
T21
cycled
breakthrough (MPa)
3.2
3.0
3.0
3.0
2.9
2.8
3.0
A
B
C
D
E
F
Pressure (MPa)
Elapsed time (hours)

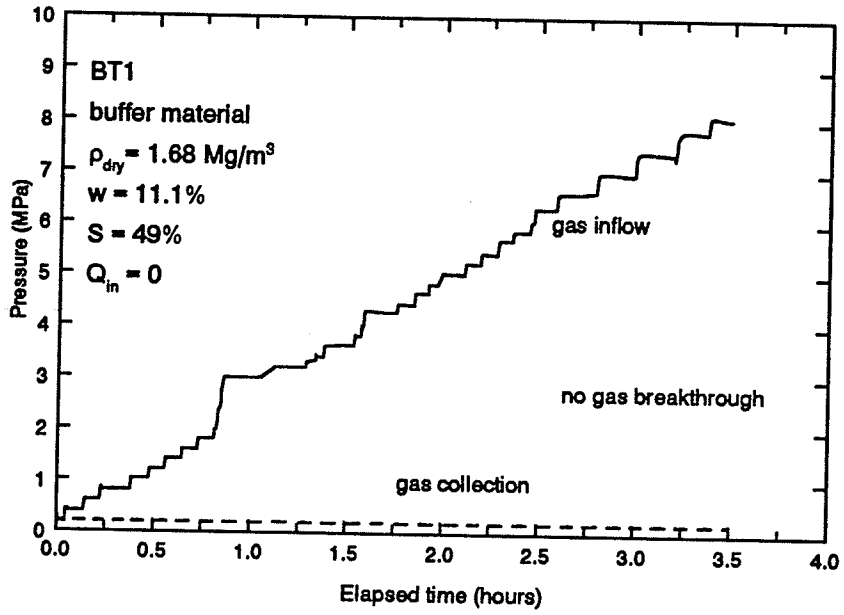
BT1
buffer material
ρ_{dry} = 1.68 Mg/m^3
w = 11.1%
S = 49%
Q_{in} = 0
gas inflow
no gas breakthrough
gas collection
Pressure (MPa)
Elapsed time (hours)
0
1
2
3
4
5
6
7
8
9
10
0.0
0.5
1.0
1.5
2.0
2.5
3.0
3.5
4.0

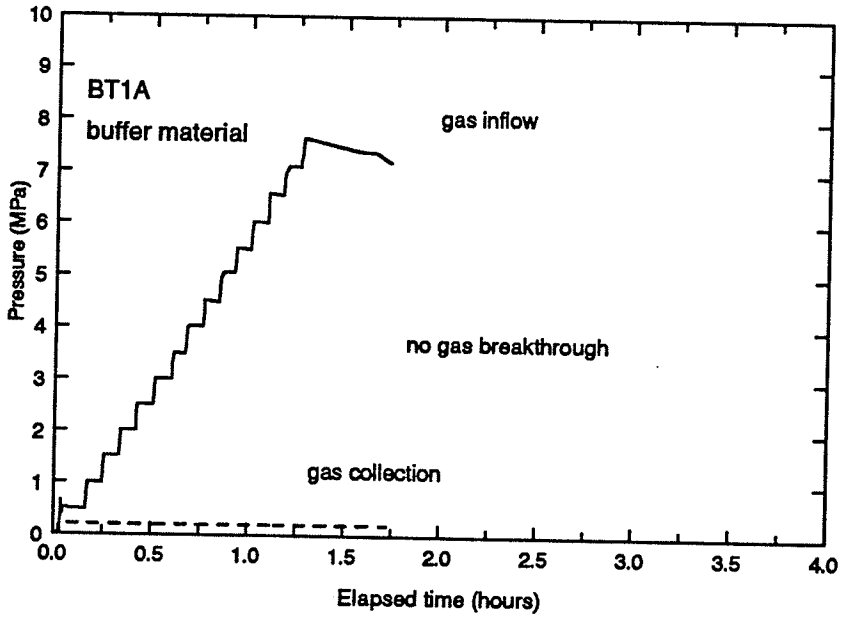
BT1A
buffer material
gas inflow
no gas breakthrough
gas collection
Pressure (MPa)
Elapsed time (hours)
0
1
2
3
4
5
6
7
8
9
10
0.0
0.5
1.0
1.5
2.0
2.5
3.0
3.5
4.0

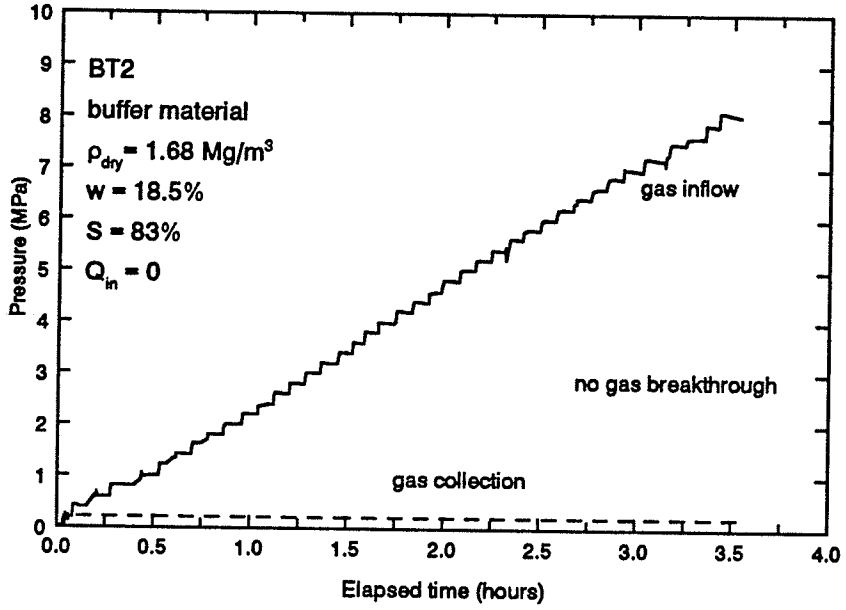
BT2
buffer material
ρ_{dry} = 1.68 Mg/m^3
w = 18.5%
S = 83%
Q_{in} = 0
gas inflow
no gas breakthrough
gas collection
Pressure (MPa)
Elapsed time (hours)

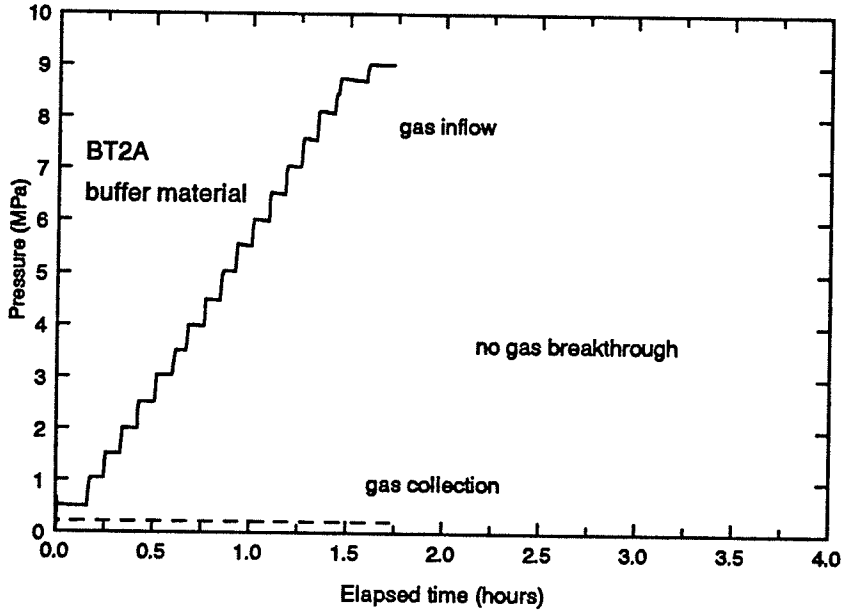
BT2A
buffer material
gas inflow
no gas breakthrough
gas collection
Pressure (MPa)
Elapsed time (hours)

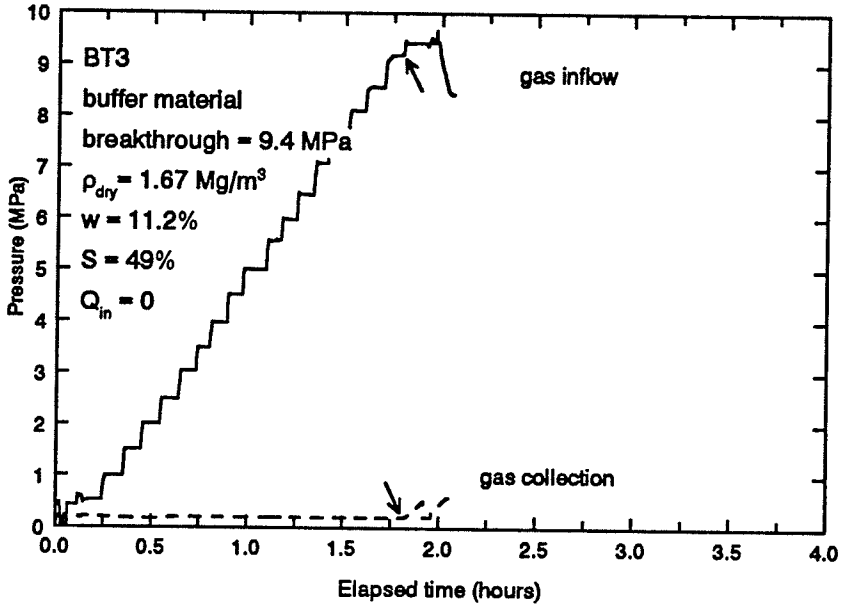
BT3
buffer material
breakthrough = 9.4 MPa
ρ_{dry} = 1.67 Mg/m^3
w = 11.2%
S = 49%
Q_{in} = 0
gas inflow
gas collection
Pressure (MPa)
Elapsed time (hours)

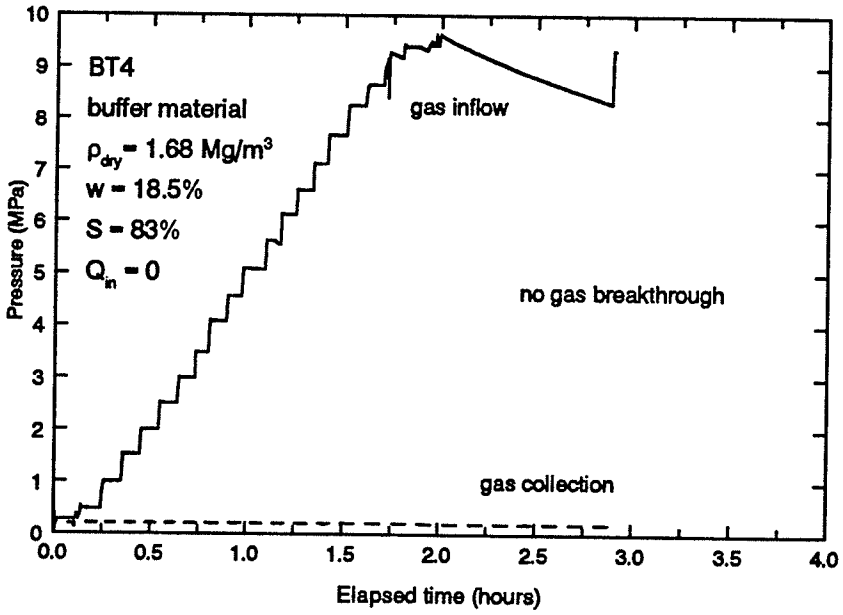
BT4
buffer material
ρ_{dry} = 1.68 Mg/m^3
w = 18.5%
S = 83%
Q_{in} = 0
gas inflow
no gas breakthrough
gas collection
Pressure (MPa)
Elapsed time (hours)

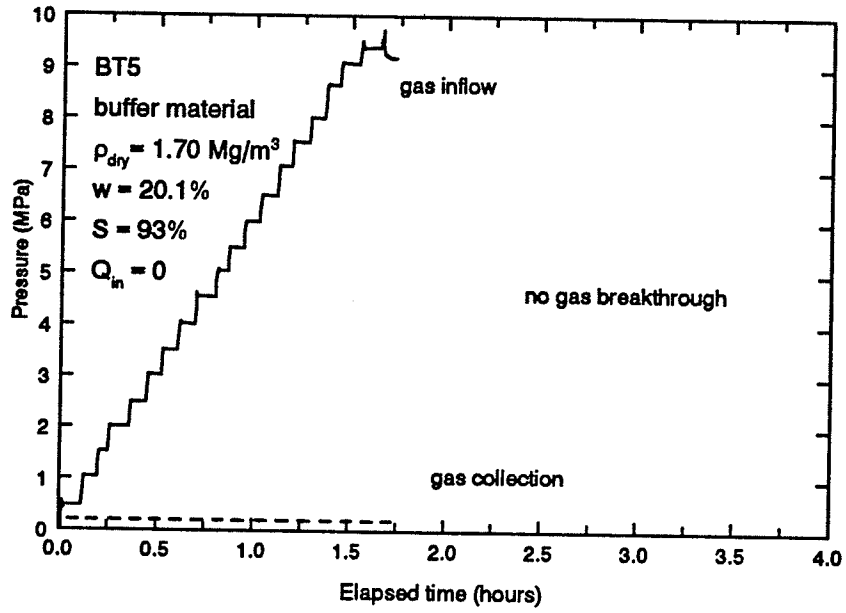
BT5
buffer material
ρ_{dry} = 1.70 Mg/m^3
w = 20.1%
S = 93%
Q_{in} = 0
gas inflow
no gas breakthrough
gas collection
Pressure (MPa)
Elapsed time (hours)
0
1
2
3
4
5
6
7
8
9
10
0.0
0.5
1.0
1.5
2.0
2.5
3.0
3.5
4.0

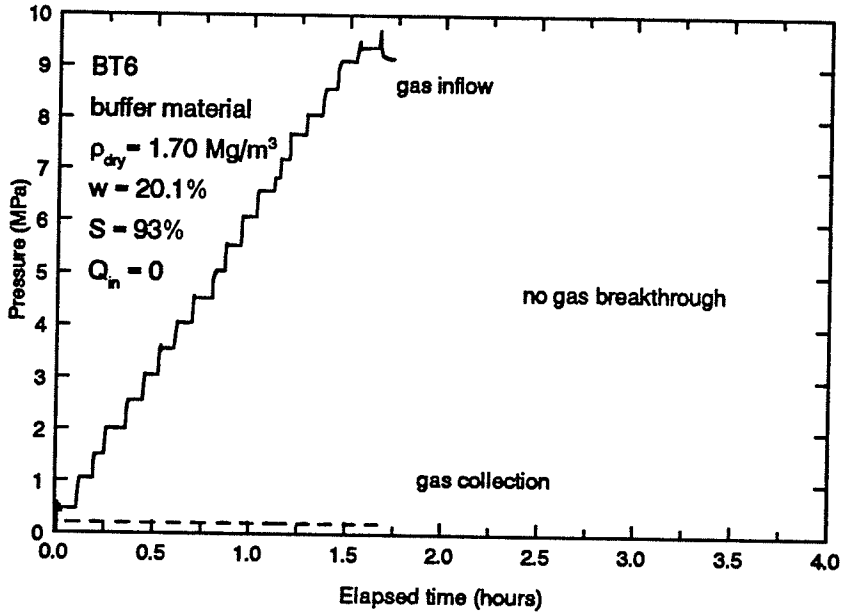
BT6
buffer material
ρ_{dry} = 1.70 Mg/m^3
w = 20.1%
S = 93%
Q_{in} = 0
gas inflow
no gas breakthrough
gas collection
Pressure (MPa)
Elapsed time (hours)
0
1
2
3
4
5
6
7
8
9
10
0.0
0.5
1.0
1.5
2.0
2.5
3.0
3.5
4.0